

MULTIDRUG RESISTANCE MECHANISMS
IN IMATINIB RESISTANT
HUMAN CHRONIC MYELOID LEUKEMIA CELLS

A THESIS SUBMITTED TO
THE GRADUATE SCHOOL OF NATURAL AND APPLIED SCIENCES
OF
MIDDLE EAST TECHNICAL UNIVERSITY

BY

YUSUF BARAN

IN PARTIAL FULFILLMENT OF THE REQUIREMENTS
FOR
THE DEGREE OF DOCTOR OF PHILOSOPHY
IN
BIOLOGY

AUGUST 2006

Approval of the Graduate School of Natural and Applied Sciences

Prof. Dr. Canan ÖZGEN

Director

I certify that this thesis satisfies all the requirements as a thesis for the degree of Doctor of Philosophy.

Prof. Dr. Semra KOCABIYIK

Head of the Department

This is to certify that we have read this thesis and that in our opinion it is fully adequate, in scope and quality, as a thesis for the degree of Doctor of Philosophy.

Prof. Dr. Ufuk GÜNDÜZ

Supervisor

Examining Committee Members

Prof. Dr. Ali Uğur URAL (GATA, HEMA) _____

Prof. Dr. Ufuk GÜNDÜZ (ODTÜ, BIO) _____

Prof. Dr. Hüseyin Avni ÖKTEM (ODTÜ, BIO) _____

Prof. Dr. Semra KOCABIYIK (ODTÜ, BIO) _____

Prof. Dr. Reyhan ÖNER (Hacettepe U, BIO) _____

I hereby declare that all information in this document has been obtained and presented in accordance with academic rules and ethical conduct. I also declare that, as required by these rules and conduct, I have fully cited and referenced all material and results that are not original to this work.

Name, Surname: Yusuf BARAN

Signature:

ABSTRACT

MULTIDRUG RESISTANCE MECHANISMS IN IMATINIB RESISTANT HUMAN CHRONIC MYELOID LEUKEMIA CELLS

BARAN, Yusuf

Ph.D., Department of Biology
Supervisor: Prof. Dr. Ufuk GÜNDÜZ

August 2006, 214 pages.

In this study, mechanisms of resistance to Imatinib-induced apoptosis in human K562 and Meg-1 chronic myeloid leukemia (CML) cells were examined. Continuous exposure of cells to step-wise increasing concentrations of Imatinib resulted in the selection of 0.2 and 1 μ M Imatinib resistant cells.

Measurement of endogenous ceramide levels showed that treatment with Imatinib increased the generation of C₁₈-ceramide significantly, which is mainly synthesized by the human longevity assurance gene 1 (hLASS1), in sensitive, but not in resistant cells. Mechanistically, analysis of mRNA and enzyme activity levels of hLASS1 in the absence or presence of Imatinib did not show any significant differences in the resistant cells when compared to its sensitive counterparts, suggesting that accumulation and/or metabolism, but not the synthesis of ceramide, might be altered in resistant cells.

Indeed, further studies demonstrated that expression levels, and enzyme activity of sphingosine kinase-1 (SK-1), increased significantly in resistant K562 or Meg-1 cells. The expression levels of glucosyl ceramide synthase (GCS) also increased in resistant cells, comparing to the sensitive counterparts, which indicates conversion of pro-apoptotic ceramide to glucosyl ceramide.

Expression analyses of BCR-ABL gene demonstrated that expression levels of BCR-ABL gene increased gradually as the cells acquired the resistance. However, Nucleotide sequence analyses of ABL kinase gene revealed that there was no mutation in Imatinib binding region of the gene in resistant cells. There was also an increase in expression levels of MDR1 gene in resistant cells, which transport the toxic substances outside of cells.

In conclusion, these data show, for the first time, a role for endogenous ceramide synthesis via hLASS1 in Imatinib-induced apoptosis, and those alterations of the balance between the levels of ceramide and S1P. Mainly the overexpression of SK-1 seems to result in resistance to Imatinib in K562 cells. The cellular resistance may also result from conversion of ceramide to glucosyl ceramide, from overexpression of BCR-ABL and MDR1 genes but not due to mutations in Imatinib binding site of ABL kinase.

Keywords: CML, Imatinib, Multidrug resistance, Ceramide Metabolism, Apoptosis

ÖZ

İMATİNİB'E DİRENÇLİ İNSAN KRONİK MYELOİD LÖSEMİ HÜCRELERİNDE ÇOKLU İLAÇ DİRENÇLİLİK MEKANİZMALARI

BARAN, Yusuf

Doktora, Biyoloji Bölümü
Tez Yöneticisi: Prof. Dr. Ufuk GÜNDÜZ

Ağustos 2006, 214 sayfa

Bu çalışmada, K562 ve Meg-01 insan kronik myeloid lösemi hücrelerinde İmatinibin yol açtığı apoptoza karşı geliştirilen direnç mekanizmaları incelenmiştir. Hücrelerin sürekli artan dozlarda İmatinibe maruz bırakılmaları ile 0.2- ve 1 μ M İmatinibe dirençli hücreler elde edilmiştir.

Hücre içi seramid düzeylerinin ölçülmesi ile, duyarlı hücrelerde İmatinibin insan longevitiy assurance geni-1 (hLASS1) tarafından sentezlenen C₁₈-seramidinin konsantrasyonunda önemli bir artış neden olduğunu ancak dirençli hücrelerde ciddi bir artış olmadığını göstermiştir. Duyarlı hücrelerle karşılaşıldığı zaman, dirençli hücrelerde hLASS1 geninin mRNA ve enzim aktivitesi düzeyinde yapılan analizleri, İmatinibin bulunup bulunmamasına göre ciddi farklılıklar göstermemiştir. Bu durum, dirençli hücrelerde seramidin sentezlenmesinin ötesinde hücre içerisinde birikiminin ve/veya metabolismasının değişmiş olabileceğini öngörmektedir.

Daha sonraki çalışmalarдан elde edilen veriler sonucunda, dirençli K562 veya Meg-1 hücrelerinde sfingozin kinaz-1 (SK-1) geninin ifade düzeyinde ve enzim aktivitesinde önemli artışlar gözlenmiştir. Glukozil seramid sentaz geninin duyarlı hücrelerle karşılaşıldığında dirençli hücrelerde daha fazla ifade edildiği belirlenmiştir. Bu durum pro-apoptotik seramidin glukozil seramide dönüştürüldüğünü göstermektedir.

BCR-ABL gen ifade analizi çalışmaları sonucunda, hücrelerin ilaca dirençliliğinin artmasına paralel olarak BCR-ABL gen ifade düzeylerinde de bir artış olduğunu göstermiştir. Ancak, ABL kinaz bölgesindeki nükleotid dizi analizleri İmatinibin bağındığı bölgelerde herhangi bir mutasyon olmadığını göstermiştir. Aynı zamanda, dirençli hücrelerde toksik maddeleri hücre dışına pompalayan MDR1 geninin ifade düzeyinde de bir artış gözlenmiştir.

Sonuç olarak, hLASS1 geni tarafından sentezlenen seramidin İmatinibin neden olduğu apoptozdaki rolü ve seramid ile SK-1'in aşırı ifadesi ile sentezlenen S1P düzeyleri arasındaki dengenin K562 hücrelerinde dirençliliğe neden olduğu ilk defa bu çalışma ile gösterilmiştir. İmatinibe karşı dirençliliğin, aynı zamanda glukozil seramide dönüştürülen seramid, BCR-ABL ve MDR1 genlerinin aşırı ifadesi sonucu olabileceği ancak İmatinibin bağındığı ABL kinaz bölgesindeki mutasyonların bu dirençlilikle bir ilgisi olmadığı belirlenmiştir.

Anahtar Kelimeler: KML, İmatinib, Çoklu İlaç Dirençliliği, Seramid Metabolizması, Apoptoz.

To BAHAR
and
to my parents

ACKNOWLEDGEMENTS

I wish to express my deepest gratitude to my supervisor Prof. Dr. Ufuk Gündüz for her guidance, advice, criticism, encouragements, critical discussions and insight throughout the research.

I would like to express my deepest gratitude to Assoc. Prof. Dr. Besim Öğretmen for accepting me to study under his supervision in Medical University of South Carolina, USA, and for his great guidance and advice.

I would like to thank Prof. Dr. Ali Uğur Ural for his helpful advices and critical suggestions throughout the research.

I would like to thank to Prof. Dr. Yusuf A. Hannun and Prof. Dr. Lina M. Obeid for their critical discussions during the study.

I would like to thanks to Dr. Jacek Bielawski for his help in LC-MS studies.

My special thank to my parents, for their great supports, understanding and encouragement throughout the study.

I am also thankful to my laboratory friends, Pelin Kaya, Kamala Sundararaj, Can Emre Şenkal, Leslie Wooten, Pengfei Song, Arelis Salas, Archana and Suriyan Ponnusamy, for their continuous help and collaboration, especially, in the laboratory work of this study.

My special thanks to my friends Aytekin Karayaka, Dr. Bengü Çobanoğlu, Dr. Necat Polat, Fatih Kürşat Fırat, Dr. Çağatay Ceylan, Sabry Ali Elneggar, Dr.

Dan-Victor Giurgiutiu, Banu Sarıcı and Osman Altun for their moral support at every stage of this study.

I am thankful to all jury members for their helpful suggestions and comments and I wish studies done for this thesis to be a helpful step for prospective studies in this field.

This study was supported by the research grants from National Institutes of Health (CA88932 and DE01657 to Dr. Besim Öğretmen and CA097132 to Dr. Yusuf Hannun), Department of Defense (Program Project phase 7, through Hollings Cancer Center to Dr. Besim Öğretmen), the National Science Foundation/EPSCoR (EPS-0132573 to Dr. Besim Öğretmen), and Middle East Technical University research project (BAP-2004-07-02-00-20 to Dr. Ufuk Gündüz). I also would like to thank to The Scientific and Technological Research Council of Turkey through NATO-A2 research grant since I was partially sponsored by a fellowship. We also would like to thank to Novartis for providing base form of Imatinib for this project.

TABLE OF CONTENTS

PLAGIARISM.....	iii
ABSTRACT.....	iv
ÖZ.....	vi
DEDICATION.....	viii
ACKNOWLEDGEMENTS.....	ix
TABLE OF CONTENTS.....	xi
LIST OF TABLES.....	xvii
LIST OF FIGURES.....	xviii
ABBREVIATIONS.....	xxv
CHAPTER	
1. INTRODUCTION.....	1
1-1 CHRONIC MYELOID LEUKEMIA.....	2
1-2 MOLECULAR BIOLOGY OF CHRONIC MYELOID LEUKEMIA.....	3
1.2.1 The Physiologic Function of the Translocation Partners.....	4
1.2.2 Molecular Anatomy of the BCR-ABL Translocation.....	6
1.3 ACTIVATED SIGNALING PATHWAYS AND BIOLOGICAL PROPERTIES OF BCR-ABL POSITIVE CELLS.....	8
1.3.1 Activation of Mitogenic Signaling.....	8
1.3.1.1 Ras and the MAP Kinase Pathways.....	8
1.3.1.2 Jak-Stat Pathway.....	10
1.3.1.3 Phosphotidyl Inositol-3 Kinase Pathway.....	11
1.3.1.4 Myc Pathway.....	11
1.3.2 BCR-ABL Mediated Protection from Apoptosis.....	12

1.4 TREATMENT STRATEGIES FOR CHRONIC MYELOID LEUKEMIA.....	14
1.4.1 Imatinib, a Molecular Targeting Approach in CML Treatment.....	14
1.5 MULTIDRUG RESISTANCE MECHANISMS IN CML.....	17
1.5.1 Molecular Mechanisms of Resistance to Imatinib.....	18
1.5.2 BCR-ABL Gene Overexpression.....	19
1.5.3 BCR-ABL Gene Mutations.....	20
1.5.4 P-glycoprotein (P-gp)	23
1.6 INVOLVEMENT OF CERAMIDE IN MULTIDRUG RESISTANCE.....	25
1.6.1 Structure and Metabolism of Ceramide.....	26
1.6.2 hLASS (Human Longevity-Assurance) Genes Regulate Synthesis of Specific Ceramides.....	30
1.6.3 Cancer-suppressing roles of ceramide.....	32
1.6.3.1 Ceramide in Apoptosis.....	33
1.6.3.2 Ceramide in Quiescence and Senescence.....	34
1.6.4 Cancer-Promoting Roles of Sphingosine 1 Phosphate (S1P).....	35
1.6.4.1 The Sphingolipid Rheostat: a Conserved Stress Regulator.....	35
1.6.4.2 Cancer-Promoting Roles of S1P.....	36
1.6.5 Targeting Ceramide Metabolism to Overcome Drug Resistance.....	38
1.7 AIM OF THE STUDY.....	39
2. MATERIALS AND METHODS.....	40
2.1 MATERIALS.....	40
2.1.1 K562 and Meg-01 Cell Lines.....	40
2.1.2 Chemicals.....	40
2.1.3 Plasmid Vectors and siRNA.....	42
2.1.4 Primers.....	42

2.2 METHODS.....	44
2.2.1 Cell Line and Culture Conditions.....	44
2.2.2 Thawing Frozen Cells.....	44
2.2.3 Maintenance of the K562 and Meg-01 Cell Culture.....	44
2.2.4 Trypan Blue Dye Exclusion Method.....	45
2.2.5 Freezing Cells.....	45
2.2.6 Generation of Resistant Sub-lines.....	46
2.2.7 Total RNA Isolation from Cells.....	46
2.2.8 Quantification of RNA.....	47
2.2.9 Agarose Gel Electrophoresis of RNA.....	48
2.2.10 cDNA Preparation from RNA.....	48
2.2.11 Nucleotide Sequence Analyses of Imatinib Binding Site of ABL Kinase Domain in Parental and Resistant human CML Cells.....	49
2.2.11.1 DNA Extraction from Agarose Gel.....	50
2.2.12 Polymerase Chain Reaction.....	50
2.2.13 Amplification Conditions of PCR.....	52
2.2.14 Agarose Gel Electrophoresis of PCR Products.....	53
2.2.15 Measurement of Cell Survival by 3-(4, 5-Dimethylthiazol-2-yl)-2-5-diphenyltetrazolium bromide (MTT).....	54
2.2.16 Transient Transfection of Suspension Cells in 60 mm dishes.....	54
2.2.17 Transfection of Cell Lines with siRNA.....	55
2.2.18 Western Blotting Analyses.....	56
2.2.18.1 Protein Isolation.....	56
2.2.18.2 Determination of Protein Concentration by Bradford Assay.....	56
2.2.18.3 SDS Polyacrylamide Gel Electrophoresis (SDS-PAGE).....	57
2.2.18.4 Transfer of Proteins from Gel to Membrane.....	58
2.2.18.5 Detection of Desired Proteins by Specific Antibodies...	58
2.2.18.6 Stripping the Membranes.....	59
2.2.19 Analysis of Cell Cycle Profiles.....	59

2.2.19.1 Fixation.....	59
2.2.19.2 Staining.....	60
2.2.20 Determination of Caspase-3 Activity.....	60
2.2.21 Detection of Mitochondrial Membrane Potential.....	61
2.2.22 Measurement of Total Endogenous Ceramide Levels by LC/MS.....	61
2.2.22-1 Determination of Inorganic Phosphate (Pi) Concentrations.....	62
2.2.23 Analysis of the Endogenous Ceramide Synthase and Sphingosine Kinase Activities by LC/MS.....	63
3. RESULTS.....	64
3.1 LONG-TERM EXPOSURE TO INCREASING CONCENTRATIONS OF IMATINIB RESULTS IN THE DEVELOPMENT OF RESISTANCE TO APOPTOSIS.....	64
3.1.1 Cell Cycle Profiles in Parental and Resistant Cells.....	67
3.1.2 Caspase-3 Activity in Parental and Resistant Cells.....	72
3.1.3 Mitochondrial Membrane Potential in Parental and Resistant Cells.....	73
3.1.4 Protein Levels of Pro-Apoptotic and Anti-Apoptotic Genes in Parental and Resistant Cells.....	74
3.1.5 Increased Ceramide Synthesis might be Involved in the Regulation of Imatinib-Induced Apoptosis.....	76
3.2 ROLE OF hLASS1, WHICH SPECIFICALLY INVOLVED IN THE GENERATION OF C ₁₈ -CERAMIDE, IN IMATINIB-INDUCED CELL DEATH.....	81
3.2.1 Overexpression of hLASS1 in Resistant K562/IMA-0.2 and -1 Cells Increased Sensitivity to Imatinib.....	82
3.2.2 Specificity of hLASS1 in Imatinib-Induced Cell Death....	86

3.2.3 Analyses of C ₁₈ -Ceramide Levels in hLASS1 Transfected K562/IMA-1 Cells.....	91
3.2.4 Expression Analyses of hLASS1 in Parental and Resistant Human CML Cells.....	92
3.2.5 Ceramide Synthase Activity in Parental and Resistant Cells	93
3.3 ONE OF THE MECHANISMS OF RESISTANCE TO IMATINIB-INDUCED CELL DEATH INVOLVES THE OVEREXPRESSION OF SPHINGOSINE KINASE 1 (SK-1).....	95
3.3.1 Sphingosine Kinase-1 Activity in Parental and Resistant Cells.....	97
3.3.2 Inhibition of SK-1 by siRNA Increased Sensitivity of Human CML Cells to Imatinib.....	98
3.3.3 Overexpression of SK-1 Resulted in an Increase in the Resistance of Human CML Cells to Imatinib.....	102
3.3.4 Analyses of C ₁₈ -Ceramide and S1P Levels in SK-1 Transfected K562 Cells.....	105
3.4 INVOLVEMENT OF GCS, WHICH CONVERTS PRO-APOPTOTIC CERAMIDE TO GLUCOSYL CERAMIDE, IN RESISTANCE TO IMATINIB-INDUCED APOPTOSIS IN HUMAN CML CELLS.....	106
3.4.1 Percent Viability of Human CML Cells Exposed to PDMP.....	108
3.4.2 Cell Cycle Profiles of Human CML Cells Exposed to PDMP in the Absence or Presence of Imatinib.....	111
3.4.3 MTT Cell Proliferation Assay in Human CML Cells Exposed to PDMP in the Absence or Presence of Imatinib.....	129
3.4.4 Analyses of Ceramide Levels in Human CML Cells in Response to PDMP in the Absence or Presence of Imatinib.....	131
3.4.5 Expression Analyses of GCS in Parental and Resistant Human CML Cells.....	137

3.5 EXPRESSION ANALYSES OF BCR-ABL IN PARENTAL AND RESISTANT HUMAN CML CELLS.....	138
3.5.1 Expression Pattern of BCR-ABL Gene in hLASS1 and hLASS6 transfected K562 cells.....	140
3.5.2 Expression Pattern of BCR-ABL Gene in SK-1 transfected K562 cells.....	141
3.6 THE ROLE OF P-GLYCOPROTEIN, IN IMATINIB RESISTANCE IN HUMAN CML CELLS.....	141
3.7 SEQUENCE ANALYSES OF IMATINIB BINDING SITE OF ABL KINASE REGION IN PARENTAL AND RESISTANT CELLS.....	144
4. CONCLUSION.....	145
REFERENCES.....	153
APPENDICES	
A. BUFFERS AND SOLUTIONS.....	171
B. SEQUENCE ANALYSES.....	174
C. PLASMID VECTORS.....	181
CURRICULUM VITAE.....	183

LIST OF TABLES

Table 1. Possible bases of resistance to imatinib.....	19
Table 2. Primers used in this study.....	43
Table 3. Ingredients of reverse transcription reaction.....	49
Table 4. Ingredients of PCR tubes for MDR1, hLASS1, hLASS2, hLASS5, hLASS6, SK-1, GCS, ABL Kinase and Beta Actin genes.....	51
Table 5. Ingredients of PCR tubes for BCR-ABL gene.....	51
Table 6-Amplification conditions of MDR1 gene.....	52
Table 7. Amplification conditions of BCR-ABL (b3a2, b2a2) genes.....	52
Table 8. Amplification conditions of SK-1, GCS, hLASS2, hLASS5, hLASS6 and ABL Kinase genes.....	53
Table 9. Amplification conditions of hLASS1.....	53
Table 10. Standard Bovine serum albumin curve for the determination of protein concentrations.....	57

LIST OF FIGURES

Figure 1. Structure of the ABL protein.....	4
Figure 2. Structure of the BCR protein.....	6
Figure 3. Locations of the breakpoints in the ABL and BCR genes.....	7
Figure 4. Mechanisms implicated in the pathogenesis of CML.....	8
Figure 5. Signaling pathways with mitogenic potential in BCR-ABL transformed cells.....	9
Figure 6. 2-D structure of Imatinib, also known as STI571, CGP 57148, Gleevec, and Glivec.....	16
Figure 7. Mechanism of action of Imatinib.....	17
Figure 8. Structure of Imatinib bound to the kinase domain of ABL.....	21
Figure 9. Amino acids contacting Imatinib.....	22
Figure 10. Structure of P-glycoprotein.....	24
Figure 11. Structures of key sphingolipids, mimetics and inhibitors.....	27
Figure 12. Major synthetic and metabolic pathways for ceramide.....	29
Figure 13. Predicted structure of LASS1 protein.....	31
Figure 14. Ceramide-regulated targets and pathways.....	32
Figure 15. Targets and pathways regulated by S1P.....	37
Figure 16. Effects of Imatinib on the growth of K562, K562/IMA-0.2 and -1 cells <i>in situ</i>	64
Figure 17. The effect of Imatinib on cell viability of K562, K562/IMA-0.2 and -1 cells.....	65
Figure 18. Effects of Imatinib on the growth of Meg-01, Meg-01/IMA-0.2 and -1 cells <i>in situ</i>	66
Figure 19. The effect of Imatinib on cell viability of Meg-01, Meg-01/IMA-0.2 and -1 cells.	67

Figure 20. Cell cycle profiles of K562 cells in response to 500 nM Imatinib.....	68
Figure 21. Cell cycle profiles of K562/IMA-0.2 cells in response to 500 nM Imatinib.....	79
Figure 22. Cell cycle profiles of Meg-01 cells in response to 500 nM Imatinib.....	71
Figure 23. Cell cycle profiles of Meg-01/IMA-0.2 cells in response to 500 nM Imatinib.....	72
Figure 24. Caspase-3 activity in parental and resistant cells.....	73
Figure 25. Mitochondrial membrane potential in parental and resistant cells.	74
Figure 26. Protein levels of anti-apoptotic and pro-apoptotic genes in parental and resistant K562 cells.....	75
Figure 27. Protein levels of anti-apoptotic and pro-apoptotic genes in parental and resistant Meg-01 cells.....	76
Figure 28. Analysis of ceramide levels in parental and resistant cells in response to Imatinib.....	77
Figure 29. Analysis of C ₁₄ - and C ₁₈ -ceramide levels in K562 cells in different time points in response to Imatinib.....	78
Figure 30. Analysis of sphingomyelin levels in parental and resistant cells in response to Imatinib.	80
Figure 31. The concentrations of C ₁₈ -ceramide in control and hLASS1 siRNA transfected K562 cells.	81
Figure 32. Cell viability of control and hLASS1 siRNA transfected K562 cells.....	82
Figure 33. The role of overexpression of hLASS1 in the inhibition of apoptosis (by fold changes in cell death) in K562/IMA-0.2 cells.....	83
Figure 34. The role of overexpression of hLASS1 in the inhibition of apoptosis (by fold changes in cell death) in K562/IMA-1 cells.	84

Figure 35. The role of overexpression of hLASS1 in the induction of caspase-3 activity in K562/IMA-0.2 cells	85
Figure 36. Expression analyses of hLASS1 in hLASS1 transfected resistant K562 cells	86
Figure 37. The role of overexpression of hLASS1 in the induction of apoptosis (by decrease in MMP) in K562 cells	86
Figure 38. The role of overexpression of hLASS2 in the induction of apoptosis (by decrease in MMP) in K562 cells	87
Figure 39. The role of overexpression of hLASS5 in the induction of apoptosis (by decrease in MMP) in K562 cells	88
Figure 40. The role of overexpression of hLASS6 in the induction of apoptosis (by decrease in MMP) in K562 cells	88
Figure 41. Expression analyses of hLASS1, hLASS2, hLASS5 and hLASS6 in K562 cells transfected with counterpart vectors	89
Figure 42. The role of overexpression of hLASS1 in the induction of apoptosis (by decrease in MMP) in K562/IMA-1 cells	90
Figure 43. The role of overexpression of hLASS5 in the induction of apoptosis (by decrease in MMP) in K562/IMA-1 cells	90
Figure 44. Expression analyses of hLASS1 and hLASS5 in K562/IMA-1 cells transfected with hLASS1 and hLASS5, respectively	91
Figure 45. Concentrations of C ₁₈ -ceramide in control and hLASS1 transfected K562/IMA-1 cells	92
Figure 46. Expression analyses of hLASS1 in parental and resistant human CML cells	93
Figure 47. Ceramide synthase activity in response to Imatinib in parental and resistant K562/IMA-1 cells	94

Figure 48. Analyses of S1P levels in parental and resistant K562/IMA-1 cells in response to Imatinib	95
Figure 49. Expression analyses of SK-1 in parental and resistant human CML cells.....	96
Figure 50. Protein levels of SK-1 in parental and resistant human CML cells.....	96
Figure 51. Endogenous sphingosine kinase enzyme activity in response to Imatinib in parental and resistant K562/IMA-1 cells	97
Figure 52. Percent changes in S1P levels in response to Imatinib in K562/IMA-1 cells.....	98
Figure 53. The role of inhibition of SK-1 in the inhibition of apoptosis (by fold changes in trypan blue positive cells) in K562/IMA-0.2 cells.....	99
Figure 54. The role of inhibition of SK-1 in the inhibition of apoptosis (by fold changes in trypan blue positive cells) in K562/IMA-1 cells.....	99
Figure 55. Expression levels of SK-1 in SK-1 siRNA transfected resistant K562/IMA-0.2 and -1 cells.....	100
Figure 56. The role of inhibition of SK-1 in the induction of apoptosis (by decrease in MMP) in K562 cells.	101
Figure 57. Expression levels of SK-1 in SK-1 siRNA transfected K562 cells.....	101
Figure 58. The role of overexpression of SK-1 in the inhibition of apoptosis (by percent changes in trypan blue positive cells) in K562 cells.....	102
Figure 59. The role of overexpression of SK-1 in the inhibition of apoptosis (by increase in MMP) in K562 cells.....	103
Figure 60. The role of overexpression of SK-1 in the inhibition of apoptosis (by decrease in caspase-3 activity) in K562 cells.....	104

Figure 61. Expression levels of SK-1 in SK-1 transfected K562 cells.....	104
Figure 62. Analysis of C ₁₈ -ceramide and S1P levels in SK-1 transfected K562 cells.....	105
Figure 63. The role of overexpression of GCS in the inhibition of apoptosis (by percent changes in trypan blue negative cells) in K562 cells.....	106
Figure 64. The role of overexpression of GCS in the inhibition of apoptosis (by percent changes in trypan blue negative cells) in Meg-01 cells.....	107
Figure 65. Expression analyses of GCS in GCS transfected human CML cells.....	108
Figure 66. The role of inhibition of GCS by PDMP in the induction of apoptosis (by percent changes in trypan blue negative cells) in K562 cells.....	108
Figure 67. The role of inhibition of GCS by PDMP in the induction of apoptosis (by percent changes in trypan blue negative cells) in K562/IMA-0.2 cells.....	109
Figure 68. The role of inhibition of GCS by PDMP in the induction of apoptosis (by percent changes in trypan blue negative cells) in Meg-01 cells.....	110
Figure 69. The role of inhibition of GCS by PDMP in the induction of apoptosis (by percent changes in trypan blue negative cells) in Meg-01/IMA-0.2 cells.....	111
Figure 70. Cell cycle profiles in K562 cells in response to Imatinib (6 hr).....	112
Figure 71. Cell cycle profiles in K562 cells in response to PDMP (6 hr).....	114
Figure 72. Cell cycle profiles in K562/IMA-0.2 cells in response to Imatinib (6 hr).	115
Figure 73. Cell cycle profiles in K562/IMA-0.2 cells in response to PDMP (6 hr).....	117
Figure 74. Cell cycle profiles in K562 cells in response to Imatinib (24 hr).....	118
Figure 75. Cell cycle profiles in K562 cells in response to PDMP (24 hr).....	120
Figure 76. Cell cycle profiles in K562/IMA-0.2 cells in response to Imatinib (24 hr).....	121
Figure 77. Cell cycle profiles in K562/IMA-0.2 cells in response to PDMP (24	

hr).....	123
Figure 78. Cell cycle profiles in K562 cells in response to Imatinib (48 hr).....	124
Figure 79. Cell cycle profiles in K562 cells in response to PDMP (48 hr).....	126
Figure 80. Cell cycle profiles in K562/IMA-0.2 cells in response to Imatinib (48 hr).....	127
Figure 81. Cell cycle profiles in K562/IMA-0.2 cells in response to PDMP (48 hr).....	129
Figure 82. Effects of PDMP, in the absence or presence of Imatinib, on the growth of K562/IMA-1 cells <i>in situ</i>	130
Figure 83. Effects of PDMP, in the absence or presence of Imatinib, on the growth of Meg-01/IMA-1 cells <i>in situ</i>	131
Figure 84. Relative changes of ceramide levels in K562 cells treated with PDMP in the absence or presence of Imatinib.	132
Figure 85. Relative changes of ceramide levels in K562/IMA-0.2 cells treated with PDMP in the absence or presence of Imatinib.	133
Figure 86. Relative changes of ceramide levels in K562/IMA-1 cells treated with PDMP in the absence or presence of Imatinib.	134
Figure 87. Relative changes of ceramide levels in Meg-01 cells treated with PDMP in the absence or presence of Imatinib.	135
Figure 88. Relative changes of ceramide levels in Meg-01/IMA-0.2 cells treated with PDMP in the absence or presence of Imatinib.....	136
Figure 89. Relative changes of ceramide levels in Meg-01/IMA-1 cells treated with PDMP in the absence or presence of Imatinib.	137
Figure 90. Expression analyses of GCS in parental and resistant human CML cells.....	138
Figure 91. Expression analyses of BCR-ABL in parental and resistant human CML cells.....	138
Figure 92. Protein levels of BCR-ABL in parental and resistant human CML cells.....	139
Figure 93. Expression analyses of BCR-ABL in vector and hLASS1 or hLASS6 transfected K562 cells.	140

Figure 94. Expression analyses of BCR-ABL in vector and SK-1 transfected K562 cells	141
Figure 95 Expression analyses of MDR1 gene parental and resistant human CML cells	142
Figure 96. The effect of P-gp inhibitor, Cyc-A, on cell viability of K562/IMA-1 cells.....	142
Figure 97. The effect of P-gp inhibitor, Cyc-A on cell viability of Meg-01/IMA-1 cells.	143

ABBREVIATIONS

CML	Chronic myeloid leukemia
μ L	micro liter
μ M	micromole
μ mol	micromole
ABL	Ableson leukemia virus oncogene
ALL	Acute lymphoblastic leukemia
ARG	Abelson-related gene product
BCR	Breakpoint cluster region gene
BSA	Bovine serum albumin
cDNA	Complementary deoxyribonucleic acid
CNL	Chronic neutrophilic leukemia
dH ₂ O	Distilled water
DMSO	Dimethyl sulfoxide
DNA	Deoxyribonucleic acid
EDTA	Ethylenediaminetetraacetic
ERK1	Extracellular-regulated kinase 1
FBS	Fetal bovine serum
GCS	Glucosyl ceramide synthase
GlcCer	Glucosylceramide
hLASS1	Human longevity assurance gene 1
hr	hour
IC ₅₀	The concentration of any chemical that inhibits growth by 50%
IMA	Imatinib
K562/IMA-0.2	K562 cells those were able to grow in the presence of 0.2 μ M Imatinib
K562/IMA-1	K562 cells those were able to grow in the presence of 1 μ M Imatinib

KDa	Kilo dalton
<i>LAG1</i>	Longevity-assurance gene 1
LC/MS	Liquid chromatography-mass spectrometry
M	Molar
MDR	Multi drug resistance
Meg-01/IMA-0.2	Meg-01 cells those were able to grow in the presence of 0.2 µM Imatinib
Meg-01/IMA-1	Meg-01 cells those were able to grow in the presence of 1 µM Imatinib
min	minute
mL	milliliter
mM	milimolar
mmol	milimole
MMP	Mitochondrial membrane potential
MTT	3-(4,5-Dimethylthiazol-2-yl)-2,5-diphenyltetrazolium bromide
nM	nanomolar
nmol	nanomole
PBS	Phosphate buffer saline
PDFGR	Platelet-derived growth factor receptors
PDMP	N-(2-hydroxy-1-(4-morpholinylmethyl)-2-phenylethyl)-decanamide, hydrochloride
P-gp	P-glycoprotein
Ph	Philadelphia chromosome
PI3	Phosphatidyl inositol-3
Pi	Inorganic phosphate
PKC	Protein kinase C
pM	Pico molar
pmol	Pico mole
PPPP	1-phenyl-2 palmitoylamino-3-pyrrolidino-1-propanol
RB	Retinoblastoma gene product
RNA	Ribonucleic acid
rpm	Revolution per minute

RT	Room temperature
RT-PCR	Reverse transcriptase-polymerase chain reaction
s	Second
S1P	Sphingosine-1-phosphate
S1PP1	S1P phosphatase 1
SDS	Sodium dodecyl sulphate
siRNA	Small interfering RNA
SK-1	Sphingosine kinase-1
SM	Sphingomyelin
SMase	Sphingomyelinase
Sph	Sphingosine
SPT	Serine palmitoyl transferase
STI	Signal transduction inhibitors
TAE	Tris acetate EDTA
TNF α	Tumor-necrosis factor- α
TRAF2	TNF-associated factor 2
VEGF	Vascular endothelial growth factor

CHAPTER 1

INTRODUCTION

In the past decade, significant progress in chemotherapy to treat leukemia has led to the achievement of 5-year disease-free survival in more than 50% of treated patients. However, even among patients treated with allogeneic bone marrow transplantation after high-dose chemotherapy, a large number of cases are still unable to be completely cured. Resistance to anticancer drugs is a critical mechanism by which the outcome in patients with leukemia is affected (Druker, 2002).

Cells exposed to toxic compounds can develop resistance by a number of mechanisms including decreased uptake, increased detoxification, and alteration of target proteins or increased excretion (Litman *et al*, 2001). Several of these pathways can lead to multidrug resistance (MDR) in which the cell is resistant to several commonly used chemotherapeutic agents. This is a particular limitation to cancer chemotherapy and cells with an MDR phenotype often display other properties, such as genome instability and loss of checkpoint control, that complicate further therapy (Dean *et al*, 2001). MDR is termed 'intrinsic' when the disease is refractory to chemotherapy from the outset, or 'acquired' when the disease becomes insensitive to treatment upon relapse. The ATP-binding cassette (ABC) genes play a role in MDR. These genes represent the largest family of transmembrane proteins that bind ATP and use the energy to drive the transport of various molecules across all cell membranes (Borst *et al*, 2000 and Gottesman *et al*, 2002).

In the classic model of multidrug resistance, a membrane-resident P-glycoprotein (P-gp), the product of MDR1 gene, acts as a drug efflux pump, lowering

intracellular drug levels to sub-lethal concentrations. Other causes of multidrug resistance include overexpression of multidrug resistance-associated protein (MRP), a second drug efflux pump that is similar to P-gp (Krishnamachary *et al*, 1993), changes in topoisomerase II activity (Deffie *et al*, 1989) and modifications in glutathione S-transferase activity (Morrow *et al*, 1990). Chemoresistance may also be related to the expression of important apoptosis-associated proteins, such as the Bcl-2 family of proteins (Bcl-2, Bcl-XL, Bax, and Bak) (Reed, 1995), the tumor suppressor protein p53 (Mueller *et al*, 1996), and the synthesis of vaults (Kickhoefer *et al*, 1998). Recent studies (Ogretmen and Hannun, 2004, Hannun *et al*, 2002) suggest that the dysfunctional metabolism of ceramide, a lipid second messenger, may contribute to multidrug resistance.

The regulation of the pro-apoptotic sphingolipid ceramide might be critical in inherent or acquired mechanisms of cellular drug resistance. Numerous studies have helped define the ceramide signaling pathways that contribute to cell death. Studies also indicate that alterations in these cell death signaling pathways may contribute to resistance to standard chemotherapeutic agents in several *in vitro* cancer models, including breast, prostate and squamous cell cancers. Investigators have demonstrated the efficacy of targeting ceramide synthesis or degradation pharmacologically to enhance the cytotoxic effects of several clinically relevant drugs. Targeting ceramide metabolic and cell death signaling pathways is an attractive clinical treatment strategy for overcoming drug resistance and continues to be studied actively.

1.1 CHRONIC MYELOID LEUKEMIA

Chronic myeloid leukemia (CML) is a hematopoietic stem cell disorder (Druker, 2002). There is an elevated white blood cell count including granulocytes, especially neutrophils. About 40% of the patients are asymptomatic at the time of presentation, and the diagnosis is based upon an abnormal white blood cell count. CML accounts for about 20% of all cases of leukemia. The natural history of CML is

progression from a stable or chronic phase to an accelerated phase or to a rapidly fatal blast crisis within 3–5 years. Blood cells differentiate normally in the stable phase but not in the blast phase (Calabretta *et al*, 2004).

CML is usually diagnosed by finding a specific chromosomal abnormality called the Philadelphia (Ph) chromosome. The Ph chromosome is the result of a translocation between the long arms of chromosomes 9 and 22. This exchange brings together two genes: the BCR (breakpoint cluster region) gene on chromosome 22 and the proto-oncogene ABL (Ableson leukemia virus oncogene) on chromosome 9 (Wong *et al*, 2004). The resulting hybrid gene BCR-ABL, codes for a fusion protein with tyrosine kinase activity, which activates signal transduction pathways, leading to uncontrolled cell growth.

1.2 MOLECULAR BIOLOGY OF CHRONIC MYELOID LEUKEMIA

BCR-ABL is a chimeric oncoprotein generated by reciprocal translocation between chromosomes 9 and 22 and is implicated in the pathogenesis of Philadelphia-positive (Ph) human leukemias (Ramadevi *et al*, 2002). The native ABL kinase is located mainly in the nucleus and has tightly regulated kinase activity, while the BCR-ABL fusion protein is located in the cytoplasm and has a constitutively activated tyrosine kinase (Vigneri *et al*, 2001). Similar to other kinases, BCR-ABL functions by binding to ATP and transfers phosphate from ATP to tyrosine residues, activating multiple signal transduction pathways (Sawyers, 1999). These events cause excessive cellular proliferation, prevent apoptosis, and decrease cellular adhesion. It has been shown that the enhanced tyrosine kinase activity of BCR-ABL is essential for CML pathogenesis and is likely to represent the initiating event (Savage *et al*, 2002). Therefore, BCR-ABL protein is an ideal target for molecular-targeted therapy.

1.2.1 The Physiologic Function of the Translocation Partners

The ABL gene is the human homologue of the v-ABL oncogene carried by the Abelson murine leukemia virus (A-MuLV), and it encodes a nonreceptor tyrosine kinase. Human ABL is a ubiquitously expressed 145-kd protein with 2 isoforms arising from alternative splicing of the first exon (Laneuville, 1995). Several structural domains can be defined within the protein (Figure 1). Three SRC homology domains (SH1-SH3) are located toward the NH₂ terminus. The SH1 domain carries the tyrosine kinase function, whereas the SH2 and SH3 domains allow for interaction with other proteins. Proline-rich sequences in the center of the molecule can, in turn, interact with SH3 domains of other proteins, such as Crk. Toward the 3' end, nuclear localization signals and the DNA-binding and actin-binding motifs are found (Von Bubnoff *et al*, 2002).

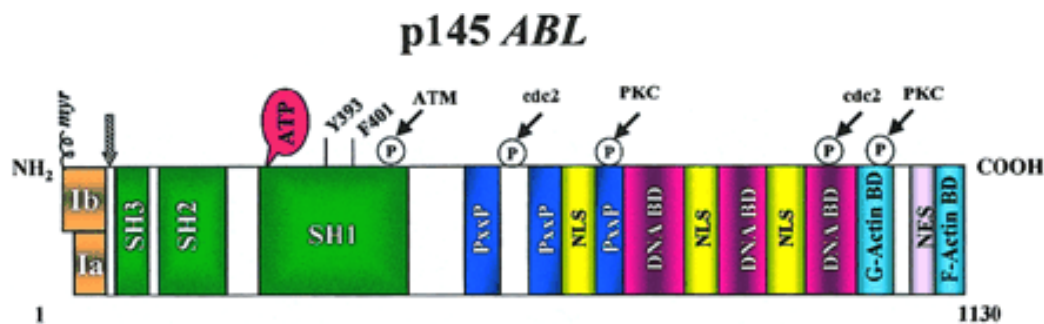


Figure 1. Structure of the ABL protein. Type Ia isoform is slightly shorter than type Ib, which contains a myristoylation (myr) site for attachment to the plasma membrane. Note the 3 SRC-homology (SH) domains situated toward the NH₂ terminus. Y393 is the major site of autophosphorylation within the kinase domain, and phenylalanine 401 (F401) is highly conserved in protein tyrosine kinases (PTK) containing SH3 domains. The middle of each protein is dominated by proline-rich regions (PxxP) capable of binding to SH3 domains, and it harbors 1 of 3 nuclear localization signals (NLS). The carboxy terminus contains DNA as well as G- and F-actin-binding domains. Phosphorylation sites by Atm, cdc2, and PKC are shown. The

arrowhead indicates the position of the breakpoint in the BCR-ABL fusion protein. (From Deininger *et al*, 2000).

Several fairly diverse functions have been attributed to ABL, and the emerging picture is complex. Thus, the normal ABL protein is involved in the regulation of the cell cycle (Calabretta *et al*, 2004), in the cellular response to genotoxic stress, and in the transmission of information about the cellular environment through integrin signaling. Overall, it appears that the ABL protein serves a complex role as a cellular module that integrates signals from various extracellular and intracellular sources and that influences decisions in regard to cell cycle and apoptosis.

The 160-kd BCR protein, like ABL, is ubiquitously expressed. Several structural motifs can be delineated (Figure 2). The first N-terminal exon encodes a serine-threonine kinase. The only substrates of this kinase identified so far are Bap-1, a member of the 14-3-3 family of proteins, and possibly BCR itself (Laneuville, 1995). A coiled-coil domain at the N-terminus of BCR allows dimer formation *in vivo*. The center of the molecule contains a region with dbl-like and pleckstrin-homology (PH) domains that stimulate the exchange of guanidine triphosphate (GTP) for guanidine diphosphate (GDP) on Rho guanidine exchange factors. The C-terminus has GTPase activity for Rac, a small GTPase of the Ras superfamily that regulates actin polymerization and the activity of an NADPH oxidase in phagocytic cells. In addition, BCR can be phosphorylated on several tyrosine residues, especially tyrosine 177, which binds Grb-2, an important adapter molecule involved in the activation of the Ras pathway. Interestingly, ABL has been shown to phosphorylate BCR in COS1 cells, resulting in a reduction of BCR kinase activity.

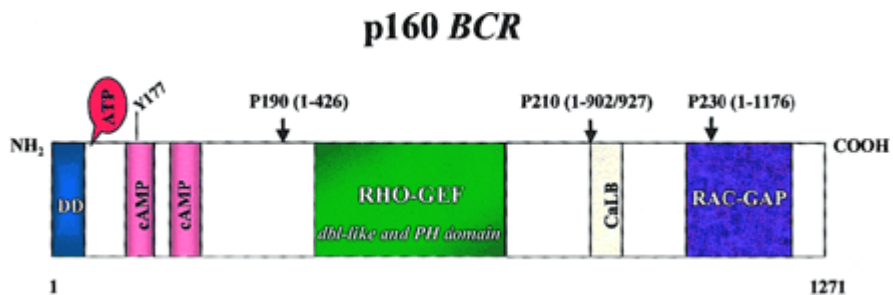


Figure 2. Structure of the BCR protein. Note the dimerization domain (DD) and the 2 cyclic adenosine monophosphate kinase homologous domains at the N terminus. Y177 is the autophosphorylation site crucial for binding to Grb-2. The center of the molecule contains a region homologous to Rho guanine nucleotide exchange factors (Rho-GEF) as well as dbl-like and pleckstrin homology (PH) domains. Toward the C-terminus a putative site for calcium-dependent lipid binding (CaLB) and a domain with activating function for Rac-GTPase (Rac-GAP) are found. Arrowheads indicate the position of the breakpoints in the BCR-ABL fusion proteins. (From Deininger *et al*, 2000).

1.2.2 Molecular Anatomy of the BCR-ABL Translocation

The breakpoints within the ABL gene at 9q34 can occur anywhere over a large (greater than 300 kb) area at its 5' end, either upstream of the first alternative exon Ib, downstream of the second alternative exon Ia, or, more frequently, between the two (Figure 3). Regardless of the exact location of the breakpoint, splicing of the primary hybrid transcript yields an mRNA molecule in which BCR sequences are fused to ABL exon a2. In contrast to ABL, breakpoints within BCR localize to 1 of 3 so-called breakpoint cluster regions. In most patients with CML and in approximately one third of patients with Ph-positive acute lymphoblastic leukemia (ALL), the break occurs within a 5.8-kb area spanning BCR exons 12-16 (originally referred to as exons b1-b5), defined as the major breakpoint cluster region (M-BCR). Because of alternative splicing, fusion transcripts with either b2a2 or b3a2 junctions can be formed. A 210-kd chimeric protein ($P210^{BCR-ABL}$) is derived from this mRNA. In the remaining patients with ALL and rarely in patients with CML (Christoph *et al*,

2006), the breakpoints are further upstream in the 54.4-kb region between the alternative BCR exons e2' and e2, termed the minor breakpoint cluster region (m-BCR). The resultant e1a2 mRNA is translated into a 190-kd protein (P190^{BCR-ABL}). Recently, a third micro breakpoint cluster region (μ -BCR) has been identified downstream of exon 19, giving rise to a 230-kd fusion protein (P230^{BCR-ABL}) associated with the rare Ph-positive chronic neutrophilic leukemia (CNL) (Christoph *et al*, 2006), though not in all cases. If sensitive techniques such as nested reverse transcription-polymerase chain reaction are used, transcripts with the e1a2 fusion are detectable in many patients with classical P210^{BCR-ABL} CML (Eren *et al*, 2000). Occasional cases with other junctions, such as b2a3, b3a3, e1a3, e6a2, or e2a2 (Christoph *et al*, 2006), have been reported in patients with ALL and CML. These "experiments of nature" provide important information as to the function of the various parts of BCR and ABL in the oncogenic fusion protein. Based on the observation that the ABL part in the chimeric protein is almost invariably constant while the BCR portion varies greatly, one may deduce that ABL is likely to carry the transforming principle whereas the different sizes of the BCR sequence may dictate the phenotype of the disease.

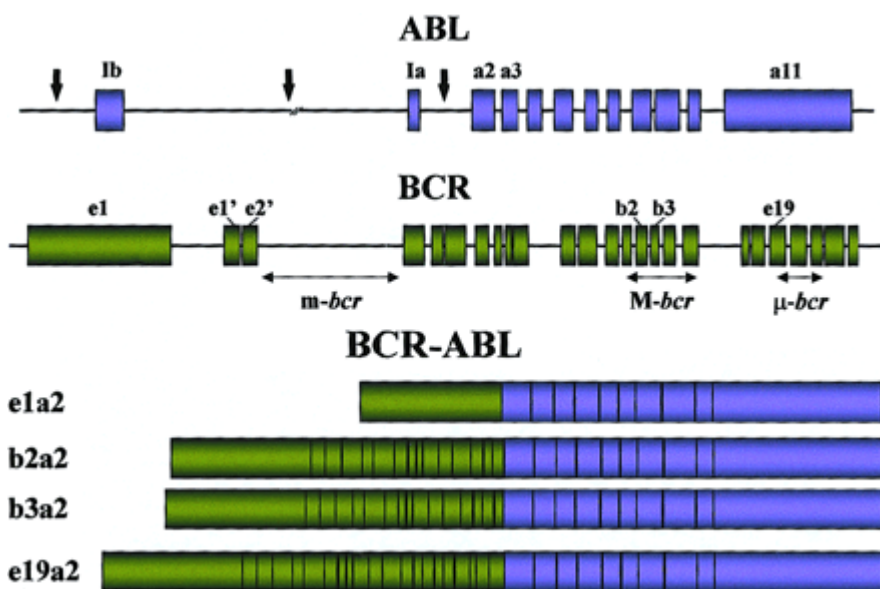


Figure 3. Locations of the breakpoints in the ABL and BCR genes (From Deininger *et al*, 2000).

1.3 ACTIVATED SIGNALING PATHWAYS AND BIOLOGICAL PROPERTIES OF BCR-ABL POSITIVE CELLS

Three major mechanisms have been implicated in the malignant transformation by BCR-ABL, namely altered adhesion to extracellular matrix, constitutively active mitogenic signaling and reduced apoptosis (Figure 4).

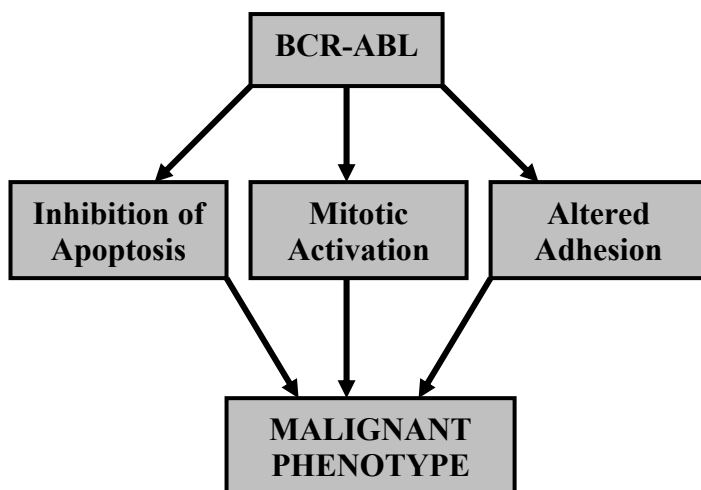


Figure 4. Mechanisms implicated in the pathogenesis of CML.

1.3.1 Activation of Mitogenic Signaling

1.3.1.1 Ras and the MAP Kinase Pathways

Several links between BCR-ABL and Ras have been defined. Autophosphorylation of tyrosine 177 provides a docking site for the adapter molecule Grb-2 (Pendergast *et al*, 1993). Grb-2, after binding to the Sos protein, stabilizes Ras in its active GTP-bound form. Two other adapter molecules, Shc and Crkl, can also activate Ras. Both are substrates of BCR-ABL (Oda *et al*, 1994) and bind BCR-ABL through their SH2 (Shc) or SH3 (Crkl) domains. Circumstantial evidence that Ras activation is important for the pathogenesis of Ph-positive leukemias comes from the observation that activating mutations are uncommon, even in the blastic phase of the disease (Watzinger *et al*, 1994), unlike in most other tumors. This implies that the

Ras pathway is constitutively active and no further activating mutations are required. There is still dispute as to which mitogen-activated protein (MAP) kinase pathway is downstream of Ras in Ph-positive cells. Stimulation of cytokine receptors such as IL-3 leads to the activation of Ras and to the subsequent recruitment of the serine-threonine kinase Raf to the cell membrane (Marais *et al*, 1995). Raf initiates a signaling cascade through the serine-threonine kinases Mek1/Mek2 and Erk, which ultimately leads to the activation of gene transcription (Cahill *et al*, 1996). Moreover, activation of the Jnk/Sapk pathway by BCR-ABL has been demonstrated and is required for malignant transformation (Raitano *et al*, 1995); thus, signaling from Ras may be relayed through the GTP-GDP exchange factor Rac (Skorski *et al*, 1998) to Gckr (germinal center kinase related) and further down to Jnk/Sapk (Figure 5). There is also some evidence that p38, the third pillar of the MAP kinase pathway, is also activated in BCR-ABL-transformed cells (Kabarowski *et al*, 1994), and that there are other pathways with mitogenic potential. In any case, the signal is eventually transduced to the transcriptional machinery of the cell.

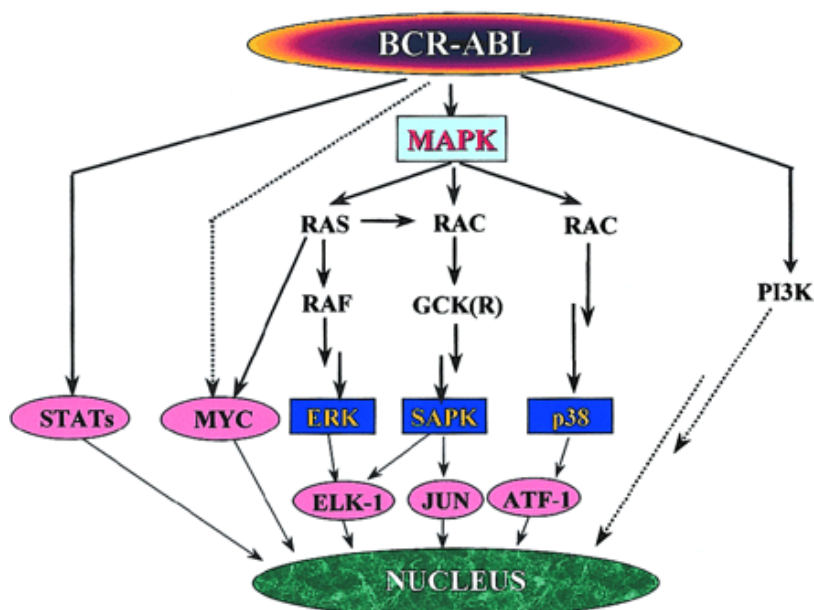


Figure 5. Signaling pathways with mitogenic potential in BCR-ABL-transformed cells. The activation of individual paths depends on the cell type, but the MAP kinase system appears to play a central role. Activation of p38 has been demonstrated only

in v-ABL-transformed cells, whereas data for BCR-ABL-expressing cells are missing. (From Deininger *et al*, 2000).

1.3.1.2 Jak-STAT Pathway

The first evidence for involvement of the Jak-STAT pathway came from studies in v-ABL-transformed B cells (Danial *et al*, 1995). Constitutive phosphorylation of STAT transcription factors (STAT1 and STAT5) has since been reported in several BCR-ABL-positive cell lines (Ilaria *et al*, 1996) and in primary CML cells (Chai *et al*, 1997). STAT5 activation appears to contribute to malignant transformation (De Groot *et al*, 1999). Effect of STAT5 in BCR-ABL transformed cells appears to be primarily anti-apoptotic and involves transcriptional activation of Bcl-XL (Horita *et al*, 2002). In contrast to the activation of the Jak-STAT pathway by physiologic stimuli, BCR-ABL may directly activate STAT1 and STAT5 without prior phosphorylation of Jak proteins. There seems to be specificity for STAT6 activation by P190^{BCR-ABL} proteins as opposed to P210^{BCR-ABL} (Ilaria *et al*, 1996).

The role of the Ras and Jak-STAT pathways in the cellular response to growth factors could explain the observation that BCR-ABL renders a number of growth factor-dependent cell lines factor independent (Kabarowski *et al*, 1994). In some experimental systems, there is evidence for an autocrine loop dependent on the BCR-ABL-induced secretion of growth factors (Sirard *et al*, 1994), and it was recently reported that BCR-ABL induces an IL-3 and G-CSF autocrine loop in early progenitor cells (Jiang *et al*, 1999). Interestingly, BCR-ABL tyrosine kinase activity may induce expression not only of cytokines but also of growth factor receptors. One should bear in mind, however, that during the chronic phase, CML progenitor cells are still dependent on external growth factors for their survival and proliferation (Amos *et al*, 1995), though less than normal progenitors (Jonuleit *et al*, 1998). A recent study sheds fresh light on this issue. FDCP mix cells transduced with a temperature-sensitive mutant of BCR-ABL have a reduced requirement for growth factors at the kinase permissive temperature without differentiation block (Pierce *et*

al, 1998). This situation resembles chronic-phase of CML, in which the malignant clone has a subtle growth advantage while retaining almost normal differentiation capacity.

1.3.1.3 Phosphatidyl Inositol-3 Kinase Pathway

Phosphatidyl Inositol-3 (PI3) kinase activity is required for the proliferation of BCR-ABL-positive cells (Skorski *et al*, 1995). BCR-ABL forms multimeric complexes with PI3 kinase, Cbl, and the adapter molecules Crk and Crkl, where PI3 kinase is activated. The next relevant substrate in this cascade appears to be the serine-threonine kinase Akt (Skorski *et al*, 1997). This kinase had previously been implicated in anti-apoptotic signaling (Franke *et al*, 1997). Another report placed Akt in the downstream cascade of the IL-3 receptor and identified the pro-apoptotic protein Bad as a key substrate of Akt (Del Peso *et al*, 1998). Phosphorylated Bad is inactive because it is no longer able to bind anti-apoptotic proteins such as Bcl-XL and it is trapped by cytoplasmic 14-3-3 proteins. Altogether this indicates that BCR-ABL might be able to mimic the physiological IL-3 survival signal in a PI3 kinase-dependent manner. Thus, BCR-ABL appears to have a profound effect on phosphoinositol metabolism, which might again shift the balance to a pattern similar to physiologic growth factor stimulation.

1.3.1.4 Myc Pathway

Overexpression of Myc has been demonstrated in many human malignancies. It is thought to act as a transcription factor. Activation of Myc by BCR-ABL is dependent on the SH2 domain, and the overexpression of Myc partially rescues transformation-defective SH2 deletion mutants whereas the overexpression of a dominant-negative mutant suppresses transformation (Sawyers *et al*, 1992). The results obtained in v-ABL-transformed cells suggest that the signal is transduced through Ras/Raf, cyclin-dependent kinases (cdks), and E2F transcription factors that

ultimately activate the Myc promoter. Similar results were reported for BCR-ABL-transformed murine myeloid cells (Stewart *et al*, 1995). It seems likely that the effects of Myc in Ph-positive cells are probably not different from those in other tumors. Depending on the cellular context, Myc may constitute a proliferative or an apoptotic signal (Bissonnette *et al*, 1992). It is therefore likely that the apoptotic arm of its dual function is counterbalanced in CML cells by other mechanisms, such as the PI3 kinase pathway.

1.3.2 BCR-ABL Mediated Protection from Apoptosis

The multiple signals initiated by BCR-ABL have proliferative and anti-apoptotic qualities. Thus, BCR-ABL may shift the balance toward the inhibition of apoptosis while simultaneously providing a proliferative stimulus. This is in line with the concept that a proliferative signal leads to apoptosis unless it is counterbalanced by an anti-apoptotic signal, and BCR-ABL fulfills both requirements at the same time.

In response to cellular stress such as DNA damage induced by chemotherapeutic drugs, the cell's mitochondria are triggered to release cytochrome c (a component of the electron transport chain) into the cytosol. Once released, cytochrome c plays a critical role in the formation of a proteolytic cell death machine known as the apoptosome. The formation of the apoptosome results in the activation of a group of zymogenic cysteine proteases (caspases), which carry out the cell death program (Olson *et al*, 2001). Cytosolic cytochrome c initiates apoptosome formation by binding to the adaptor protein Apaf-1 and promoting its oligomerization into a higher-ordered structure. Oligomerization of Apaf-1 then allows binding of the initiator caspase 9, which results in dimerization-induced self-activation (Srinivasula SM, 1998). Once activated, caspase-9 can cleave and activate effectors, caspases 3 and -7, which subsequently cleave a number of cellular substrates. This results in orderly dismantling of the cell and in the hallmark features of apoptosis (Wang *et al*, 2000). The release of cytochrome c from the mitochondria is tightly regulated by

Bcl-2 proteins, a family comprising both pro-apoptotic Bax and Bak and anti-apoptotic Bcl-2 and Bcl-XL family members (Danial *et al*, 2004). These proteins act as mitochondrial gatekeepers and regulate apoptosis by governing the release of cytochrome c. Pro-apoptotic members such as Bak and Bax promote mitochondrial cytochrome c release, while the anti-apoptotic Bcl-2 and Bcl-XL proteins maintain the integrity of the mitochondria to prevent the release of cytochrome c.

Alterations of apoptotic signaling pathways at a number of loci allow malignant cells to evade cell death, a phenomenon thought, in many cases, to be critical for tumor development (Hanahan *et al*, 2000). Although regulation of caspase activation upstream of cytochrome c release has been subject to intense scrutiny, the regulation of apoptosis downstream of mitochondrial cytochrome c release is only beginning to be understood. One mode of caspase regulation post cytochrome c release involves direct binding and inhibition of active caspases by the IAP (inhibitor of apoptosis) family of proteins (Salvesen *et al*, 2002). Kinase signaling pathways have also been shown to impinge upon the proper functioning of the apoptosome. For example, both Akt and ERK, two kinases commonly active in cancer cells, can phosphorylate caspase-9 and subsequently inhibit its enzymatic activity (Allan *et al*, 2003). Furthermore, several additional proteins have been identified which can inhibit apoptosis by binding to either Apaf-1 or caspase-9 (e.g., Hsp70) to prevent proper functioning of the apoptosome (Shiozaki *et al*, 2003).

Prior to cytochrome c release, BCR-ABL can inhibit apoptosis through regulation of Bcl-2 family members. Specifically, BCR-ABL increases expression of antiapoptotic Bcl-2 family members such as Bcl-2 and Bcl-XL through activation of the transcription factor STAT5 (Horita *et al*, 2002). Additionally, BCR-ABL has also been shown to prevent mitochondrial cytochrome c release through a posttranslational mechanism by signaling through the PI3 kinase/Akt pathway to phosphorylate and inhibit Bad (Hoover *et al*, 2001). However, BCR-ABL has recently been reported to be a more effective inhibitor of apoptosis than either Bcl-2 or Bcl-XL. As the Bcl-2 and Bcl-XL proteins can potently suppress mitochondrial

cytochrome c release, these data suggested that BCR-ABL might act at additional sites, perhaps downstream of the mitochondria.

1.4 TREATMENT STRATEGIES FOR CHRONIC MYELOID LEUKEMIA

Until 1990s, the treatment of choice for chronic phase CML was orally administered chemotherapy with either hydroxyurea or busulphan. At that time, interferon was introduced and was found to be better than known cytotoxic chemotherapy in CML. For decades, bone marrow transplantation has been performed in younger CML patients. Related to the bone marrow transplantation procedure are significant risks of morbidity and mortality, but the procedure has up until now been considered the only possible curative treatment in CML. When CML progresses to the accelerated and blastic phase, the available treatments including bone marrow transplantation become less effective.

A major advance in the treatment of CML has the advent of Imatinib which has shown striking activity in the chronic phase, in the accelerated phase, but less so in the blast phase. This drug will be the first of a new series of small organic compounds designed to inhibit specific molecular sites in the cascades of cellular activation pathways.

1.4.1 Imatinib, a Molecular Targeting Approach in CML Treatment

Attempts at designing therapeutic tools for CML based on the current knowledge of the molecular and cell biology of the disease have concentrated on the modulation of protein function by specific signal transduction inhibitors.

Perhaps the most exciting of the molecularly designed therapeutic approaches was brought about by the advent of signal transduction inhibitors (STI), which block or prevent a protein from exerting its role in the oncogenic pathway. Because the

main transforming property of the BCR-ABL protein is affected through its constitutive tyrosine kinase activity, direct inhibition of such activity seems to be the most logical means of silencing the oncprotein. To this effect, several tyrosine kinase inhibitors have been evaluated for their potential to modify the phenotype of CML cells. Synthetic compounds were developed through a rational design of chemical structures capable of competing with the ATP or the protein substrate for the binding site in the catalytic center of the kinase (Deininger *et al*, 2005).

The most promising of these compounds is the 2-phenylaminopyrimidine Imatinib (Figure 6). It is a potent inhibitor of four protein tyrosine kinases, notably inhibits ABL tyrosine kinase at micromolar concentrations, KIT (the receptor for stem cell factor), the platelet-derived growth factor receptors (PDGFR-A and B), and the Abelson-related gene product (ARG) (Deininger *et al*, 2005). Inhibition of the BCR-ABL kinase activity by this compound results in the transcriptional modulation of various genes involved in the control of the cell cycle, cell adhesion, and cytoskeleton organization, leading the Ph-positive cell to an apoptotic death. Its remarkable specificity and efficacy led to consideration of the drug for therapeutic use. Thus, in the spring of 1998, a phase 1 clinical trial was initiated in the United States in which patients with CML in chronic phase resistant to IFN- α were treated with Imatinib in increasing doses. The drug showed little toxicity but proved to be highly effective. All patients treated with 300 mg/d or more entered a complete hematologic remission. Even more striking, many of the patients had cytogenetic responses. This might mean that Imatinib changes the natural course of the disease, though it is far too early to arrive at any definite conclusions. Altogether, the results were convincing enough to justify the initiation of phase 2 studies that included patients with acute Ph-positive leukemias (CML in blast crisis and Ph-positive ALL) and at a later stage, with a large cohort of interferon-intolerant or resistant patients. Clearly, elucidation of the mechanisms underlying the resistance (Mahon *et al*, 2003) will be of critical importance for the development of further treatment strategies, such as a combination of Imatinib with conventional cytotoxic drugs or, perhaps, with other STIs.

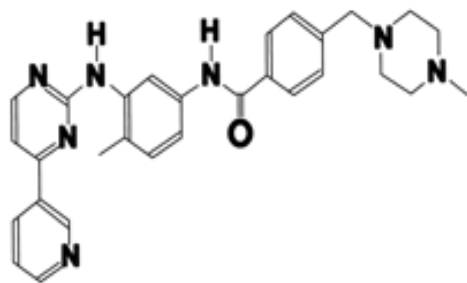


Figure 6. 2-D structure of Imatinib, also known as ST1571, CGP 57148, Gleevec, and Glivec. (From Deininger *et al*, 2003).

A significant advantage of Imatinib is that it is effective when administered orally. In contrast to treatment with antimetabolites and irradiation, side effects from Imatinib are very mild (Kurzrock *et al*, 2003). Imatinib suppresses the proliferation of BCR-ABL expressing cells both *in vitro* and *in vivo*.

Imatinib binds to the amino acids of the BCR-ABL tyrosine kinase ATP-binding site (Figure 7) and stabilizes the inactive, non-ATP-binding form of BCR-ABL, thereby preventing tyrosine autophosphorylation, and in turn, phosphorylation of its substrates (Schindler *et al*, 2000). This process ultimately results in the switching-off of the downstream signaling pathways that promote leukemogenesis. Despite high rates of hematologic and cytogenetic responses to Imatinib therapy, after exposure of drugs, the emergence of resistance to Imatinib has been recognized as a major problem in the treatment of Ph-positive leukemia (Gambacorti-Passerini 2003). Multiple drug resistance (MDR) is responsible for the overall poor efficacy of cancer chemotherapy.

ATP-binding competitors

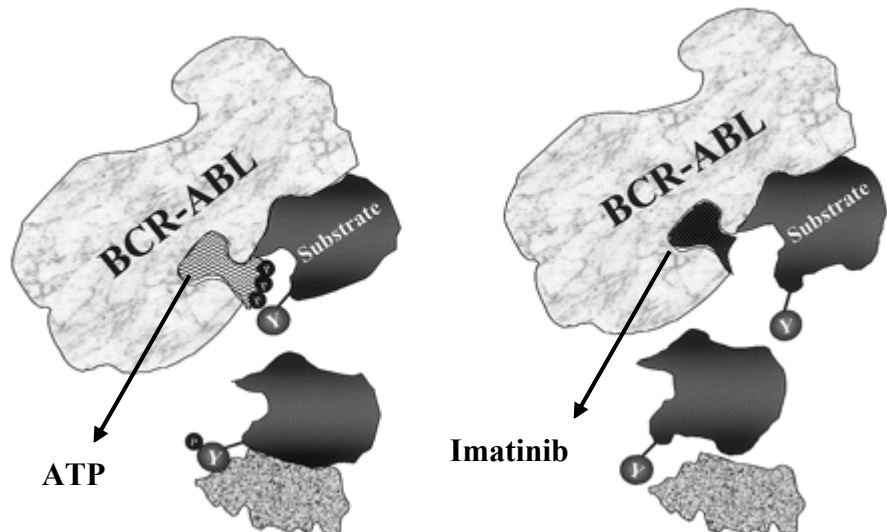


Figure 7. Mechanism of action of Imatinib. The drug competes with ATP for its specific binding site in the kinase domain. Thus, whereas the physiologic binding of ATP to its pocket allows BCR-ABL to phosphorylate selected tyrosine residues on its substrates (left diagram), a synthetic ATP mimic such as Imatinib fits this pocket equally well but does not provide the essential phosphate group to be transferred to the substrate (right diagram). The downstream chain of reactions is then halted because, with its tyrosines in the unphosphorylated form, this protein does not assume the necessary conformation to ensure association with its effector. (From Deininger *et al*, 2000).

1.5 MULTIDRUG RESISTANCE MECHANISMS IN CML

Resistance to Imatinib is multifaceted and is not easily defined. First, it may be inherent, where resistance is identified in cell lines or patients who have not previously been exposed to Imatinib, or acquired, in a situation where resistance occurs after an initial response to the drug. Second, it may be attributable to loss of the ability of Imatinib to inhibit the BCR-ABL kinase or to inability of the Imatinib to reach the intracellular oncprotein at sufficient concentration as a result of

inactivation or degradation. Third, the appearance of resistance to Imatinib in cells from a given patient may or may not be associated with other criteria of resistance or with other evidence of disease progression. It should also be noted that the mechanisms underlying resistance may differ substantially in patients treated in chronic-phase and patients treated in advanced-phase of disease (Goldman, 2004).

1.5.1 Molecular Mechanisms of Resistance to Imatinib

There are two possible categories of Imatinib resistance, which were designated as BCR-ABL independent and BCR-ABL dependent. In the first category, the leukemia cells no longer rely on BCR-ABL for their proliferative drive but grow as a consequence of the secondary oncogenic changes in these cells. In this scenario, BCR-ABL is no longer a relevant Imatinib target; even the most ideal BCR-ABL inhibitor would be ineffective in this setting. Alternatively, something may change in either the patient or the leukemia clone that prevents the drug from effectively shutting down the target BCR-ABL enzyme. Host-mediated resistance could occur through enzymatic modification of Imatinib by a P450 enzyme in the liver or by production of a protein that neutralizes drug activity, such as alpha-1 acid glycoprotein (Marbach *et al*, 2003). Cell-intrinsic resistance may occur by modification of the target BCR-ABL tyrosine kinase through gene amplification or mutation or through a reduction in drug concentration by overexpression of MDR1 (Hegedus *et al*, 2002). Changes in ceramide metabolism, a decrease in the expression of human longevity assurance genes (hLASS) and/or increase in sphingosine kinase-1 (SK-1) and glucosyl ceramide synthase (GCS) may also be responsible for resistance to apoptosis.

Table I. Possible bases of resistance to Imatinib

Resistance dependent on BCR-ABL	
I- Kinase may not be inhibited by Imatinib because of;	<ul style="list-style-type: none"> - BCR-ABL overexpression - ABL kinase domain mutation - Other escape mechanisms
II- Imatinib may not be available intracellularly;	<ul style="list-style-type: none"> - Overexpression of membrane transport proteins - Some drug inactivation mechanisms
Resistance independent of BCR-ABL;	<ul style="list-style-type: none"> - Abarrent ceramide metabolism - Resistance driven by non BCR-ABL dependent mechanisms

1.5.2 BCR-ABL Gene Overexpression

Treatment of CML with Imatinib targets ATP binding site of the BCR-ABL fusion protein. Imatinib competes with ATP to bind to the BCR-ABL fusion protein. By this way, the effects of the BCR-ABL protein are blocked as the phosphorylation ability of the protein is prevented.

Resistance to Imatinib may be result of overexpression of the BCR-ABL protein. This mechanism was initially shown in LAMA84R cell line (Le coutre *et al*, 2002). Studies with Ph-positive cell lines rendered resistance to Imatinib showed that such acquired resistance was associated with increased expression of the BCR-ABL protein, usually associated with gene amplification (Mahon *et al*, 2003, Gambacorti-Passerini *et al*, 2003). The observation that removing Imatinib exposure restored cell line sensitivity to Imatinib was consistent with the notion that resistant cell lines comprise a mixture of relatively resistant and relatively sensitive sub-populations, the former predominating in the presence of Imatinib and the latter predominating in its absence. Subsequently, gene amplification was identified in cells from a significant minority of patients with Ph-positive leukemias who had lost their response to

Imatinib (Gorre *et al*, 2003). Besides, there appears to be no complete correlation between gene amplification and gene overexpression, suggesting that the level of transcription may in some cases be controlled by mechanisms other than gene copy number. However, higher concentrations of Imatinib can inhibit the function of BCR-ABL protein in overexpressing cells.

1.5.3 BCR-ABL Gene Mutations

Imatinib is preferentially binds and stabilizes ABL kinase in its inactive conformation. Since the mutations in the kinase domain of BCR-ABL is crucial for the success of Imatinib treatment, possible mutations in the kinase pocket that might interfere with Imatinib binding were investigated. A number of point mutations in the ABL kinase domain have now been identified, some of which probably impair or prevent Imatinib binding. This disparity between Imatinib binding and ATP binding capacities is explained in part by the discovery that only a portion of the Imatinib molecule occupies the kinase pocket in a manner analogous to the interaction with ATP, while other parts of the molecule may act simply by maintaining ABL to its inactive confirmation (Figure 8).

The crystal structure of the catalytic domain of the ABL kinase in complex with Imatinib (Nagar *et al.*, 2002) has been solved. The most important finding of these studies is that the compound binds to the inactive conformation of ABL, contacting with 21 amino acid residues (Nagar *et al.*, 2002). By exploiting the distinct inactive conformation of the A-loop of ABL, Imatinib is able to achieve its high specificity (Figure 8). No major structural rearrangements are required for Imatinib to bind to the A-loop.

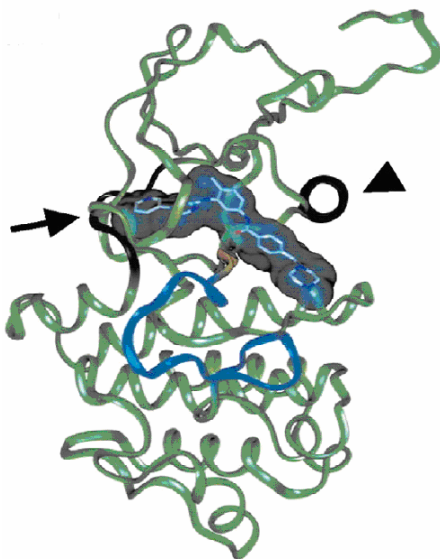


Figure 8. Structure of Imatinib bound to the kinase domain of ABL. Arrow, P-loop; arrowhead, helix α C. The activation loop is shown in blue, with the conserved DFG motif in gold. Imatinib penetrates the center of the kinase, stabilizing the inactive conformation of the activation loop. Binding to the activation loop occurs without major steric clashes, whereas binding to the P-loop involves an induced fit mechanism. (From Nagar *et al*, 2002).

In contrast, there is an induced-fit mechanism for binding to occur in the N-lobe, which normally accommodates the phosphate groups of ATP and is therefore referred to as the P-loop. The P-loop is a glycine-rich and highly flexible structure, which folds down upon binding of Imatinib, resulting in increased surface complementarity. This change in position is stabilized by a newly formed hydrogen bond between Tyr-253 and Asn-322 (Schindler *et al*, 2000). A consequence of the induced fit is the formation of a hydrophobic cage that surrounds Imatinib, engaging van der Waals interactions with residues Tyr-253, Leu-370, and Phe-382 (Figure 9) (Nagar *et al*, 2002). Moreover, Imatinib forms a number of hydrogen bonds with the kinase domain. Methionine 318, threonine 315, methionine 290, glutamine 286, lysine 270, and asparagine 381, together with water molecules, form a network of hydrogen bonds around the Imatinib molecule (Figure 9). Given this extremely tight

fit, it is not surprising that changes of single amino acids can affect the binding of Imatinib.

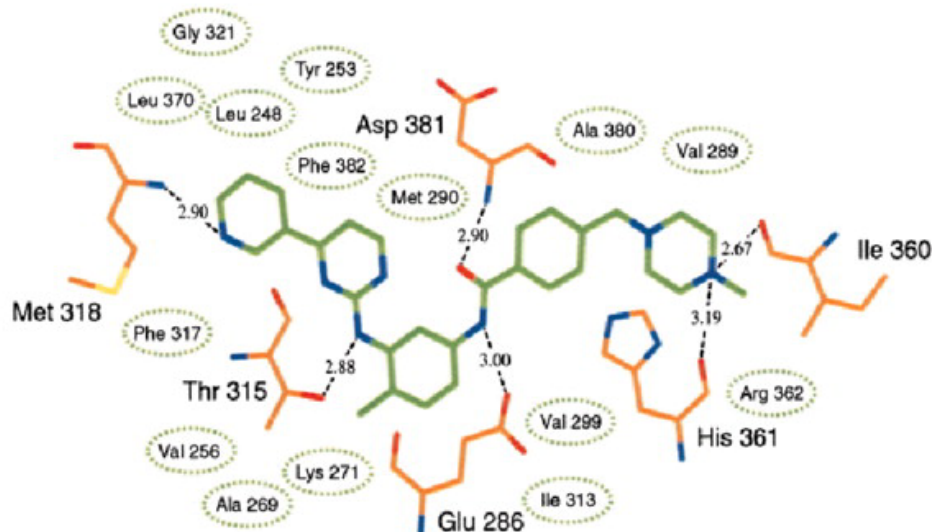


Figure 9. Amino acids contacting with Imatinib. Imatinib: carbon is shown in green, nitrogen in blue, and oxygen in red. Carbons of the protein backbone are shown in orange. Hydrogen bonds are indicated as dashed lines. Numbers represent distances in Angstrom units. Residues that form hydrophobic interactions are circled. Imatinib contacts 21 amino acids within the ABL kinase domain. (From Nagar *et al*, 2002).

Attention has focused on whether these mutations in the ABL kinase domain preceded the administration of Imatinib or were perhaps the direct result of Imatinib treatment. Two groups were able to identify in individual patients point mutations present at low concentrations before starting treatment that were identical to mutations found at increased levels when the patient developed resistance to Imatinib (Roumiantsev *et al*, 2002). These findings are best explained by assuming that mutations that impair the action of Imatinib occur with increasing frequency during the course of chronic-phase CML and either predisposes to or is very likely to be temporally associated with other events that underlie disease progression, either from chronic phase to advanced phase or within advanced phase from accelerated to blastic phase. In most cases they are presumably not the direct cause of such

progression but their presence is revealed when the mutated sub-clone gains a proliferative advantage under the influence of Imatinib.

BCR-ABL gene overexpression/amplification and mutations in ABL kinase region increase the degree of resistance. However, resistance mechanisms to Imatinib have to some extent been explored and include P-gp or may result from decreased ceramide and/or increased sphingosine kinase 1 (SK-1) and glucosylceramide synthase (GCS) levels.

1.5.4 P-glycoprotein (P-gp)

P-gp belongs to the super family of ABC transporters, a family of ATP-dependent transport proteins (Dean *et al*, 2001). The 170 kDa P-gp consists of two structurally homologous halves, each with six transmembrane domains, one ATP-binding site (Figure 10). These two halves are probably derived from internal gene duplication. Several studies have suggested that phosphorylation of P-gp might be essential for drug transport. The glycosylated sites of P-gp at the cellular outside are probably involved in routing and stability of the protein.

P-gp has a wide variety of substrates. All its substrates are large hydrophobic and amphipathic molecules, although they have no structural similarity. These molecules are able to intercalate into the membrane and enter the cytosol by passive diffusion. It is no longer believed that P-gp is a classical pump, which binds substrates from the extracellular fluid and then transports these over the membrane. Hydrophobic compounds that are substrates for P-gp do not fully penetrate into the cytoplasm of cells that express P-gp. Interaction of substrate with P-gp has been shown to take place within the membrane.

The high expression of P-gp and certain other MDR transporters in the epithelia of liver bile ducts, kidney and colon and in the microvasculature comprising blood-organ barriers, suggest that they are normally involved in detoxification and

removal of xenobiotics (Borst *et al*, 2000). Tumors arising from cells that highly express P-gp or other MDR related transporters are often intrinsically resistant to chemotherapy. Other tumor cells acquire high MDR transporter expression upon drug treatment via gene induction or DNA amplification. Based on ample experimental evidence, it is generally believed that these transporters mediate MDR by affecting an energy-dependent export of drugs or drug-conjugates and thus reducing cellular drug levels and efficacy.

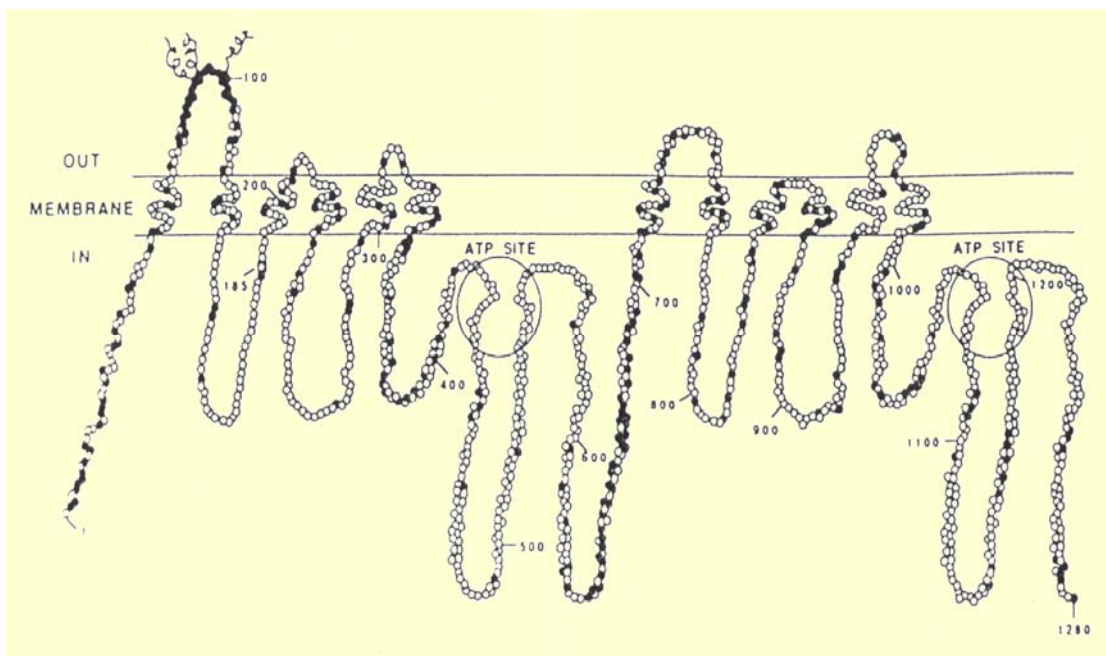


Figure 10. Structure of P-glycoprotein. (From Kleina *et al*, 1999)

The overexpression of P-gp has been thus far shown to occur in the one BCR-ABL positive, Imatinib-resistant cell line, LAMA84-r. In addition, overexpression of the MDR1 gene in the BCR-ABL positive AR230 cell line decreases its sensitivity to Imatinib, whereas verapamil, an inhibitor of P-gp, reverses this effect (Mahon *et al*, 2003). These data suggest a possible role for MDR1 overexpression in Imatinib resistance, although evidence of this phenomenon occurring in patients is thus far lacking.

1.6 INVOLVEMENT OF CERAMIDE IN MULTIDRUG RESISTANCE

Resistance to chemotherapeutic agents is the major reason for the failure of clinical cancer treatment. There is mounting evidence to suggest that cells having aberrant ceramide metabolism acquire resistance to different chemotherapeutic agents. The sphingolipids are a family of membrane lipids with important structural roles in the regulation of the fluidity and sub-domain structure of the lipid bilayer. Unexpectedly, advances in biochemical and molecular studies of sphingolipid metabolism and function during the past two decades revealed that the sphingolipids also act as effector molecules and not as inert precursors and products of sphingolipid metabolism. These molecules have essential roles in many aspects of cell biology, from inflammatory responses through cell proliferation and apoptosis to cell migration and senescence (Ogretmen and Hannun, 2004). Many sphingolipid-regulated functions have significant and specific links to various aspects of cancer initiation, progression and response to anticancer treatments. Ceramide in particular is intimately involved in the regulation of cancer-cell growth, differentiation, senescence and apoptosis (Hannun *et al*, 2002). Many cytokines, anticancer drugs and other stress-causing agonists result in increases in endogenous ceramide levels through *de novo* synthesis and/or the hydrolysis of sphingomyelin (SM) (Ogretmen *et al*, 2001-1).

Several findings suggest that alterations in ceramide metabolism could be, at least in part, responsible for the acquisition of an MDR phenotype in cancer cells. Ceramide is generated either via SM hydrolysis, or *de novo* via ceramide synthase (A.H. Merrill, 2002), and both of these pathways are regulated in cell signaling. Recent studies have demonstrated that *de novo* ceramide synthesis is regulated by members of the mammalian longevity assurance gene (*LASS*) family (Venkataraman *et al*, 2002-1, Winter *et al*, 2002 and Venkataraman *et al*, 2002-2). Surprisingly, overexpression of each of these genes in various mammalian cells leads to an increase in ceramides containing different fatty acids (Mizutani *et al*, 2005, Venkataraman *et al*, 2002-2 and Riebeling *et al*, 2003). The involvement of ceramide in apoptosis was demonstrated by the finding that alterations in ceramide

metabolism, whereby pro-apoptotic ceramide is converted to its non-cytotoxic GlcCer metabolite, contribute to the emergence of MDR (Ogretmen and Hannun, 2004). Several tumor cell lines and clinical samples have been shown to overexpress the GCS enzyme, which transfers glucose from UDP-glucose to ceramide and produces GlcCer. Accumulation of GlcCer is a characteristic of some multidrug-resistant cancer cells of breast, ovarian, colon, and epithelioid carcinomas (Kok *et al*, 2000). These studies demonstrate that ceramide plays important roles in the response of cancer cells to chemotherapeutic drugs.

While ceramide is anti-proliferative and pro-death, S1P has been implicated as a second messenger that promotes cellular differentiation, proliferation, migration, cytoskeletal reorganization, apoptosis and survival (Maceyka *et al*, 2002 and Pyne *et al*, 2000). Many external stimuli, particularly growth and survival factors, activate Sphingosine kinase-1 (SK-1) (Maceyka *et al*, 2002 and Pyne *et al*, 2000), leading to an increase in S1P levels and a concomitant decrease in ceramide levels. The antagonistic effects of these metabolites are regulated by enzymes that interconvert ceramide, sphingosine, and S1P. Thus, conversion of ceramide and sphingosine to S1P simultaneously removes pro-apoptotic signals and creates a survival signal, and vice versa. This led to the proposal of a "sphingolipid rheostat" as a critical factor determining cell fate (Maceyka *et al*, 2002.). According to this hypothesis, it is not the absolute levels but the relative amounts of these antagonistic metabolites that determines cell fate. In agreement, it has been shown that increased S1P protects against ceramide-induced apoptosis, and depletion of S1P enhances ceramide-induced apoptosis (Olivera *et al*, 2003).

1.6.1 Structure and Metabolism of Ceramide

Sphingolipids are structural components of cell membranes and help maintain the integrity and fluidity of the membrane. They are structurally complex lipids composed of a hydrophilic head group conjugated to the lipophilic ceramide backbone, which in turn is composed of a long-chain sphingoid base and an amide-

linked fatty acid (Figure 11). Ceramide serves as the precursor for the synthesis of more complex sphingolipids such as sphingomyelin, ceramide phosphate, cerebroside, a variety of glycolipids and gangliosides (Ogretmen and Hannun, 2004).

Ceramide is generated in cells by multiple pathways (Figure 12). It can be generated via the *de novo* pathway of sphingolipid biosynthesis through the action of serine palmitoyl transferase (SPT). This is followed by the reduction of the product to dihydrosphingosine, followed by the acylation of dihydrosphingosine by dihydroceramide synthetase, which is then followed by the desaturation of dihydroceramide to ceramide through the action of a poorly characterized desaturase, which introduces a 4-5 trans double bond in ceramide (Perry *et al*, 1998). A major discovery in ceramide biology has been the finding that most biochemical and biological effects of ceramide on cell growth and apoptosis are specific to ceramide.

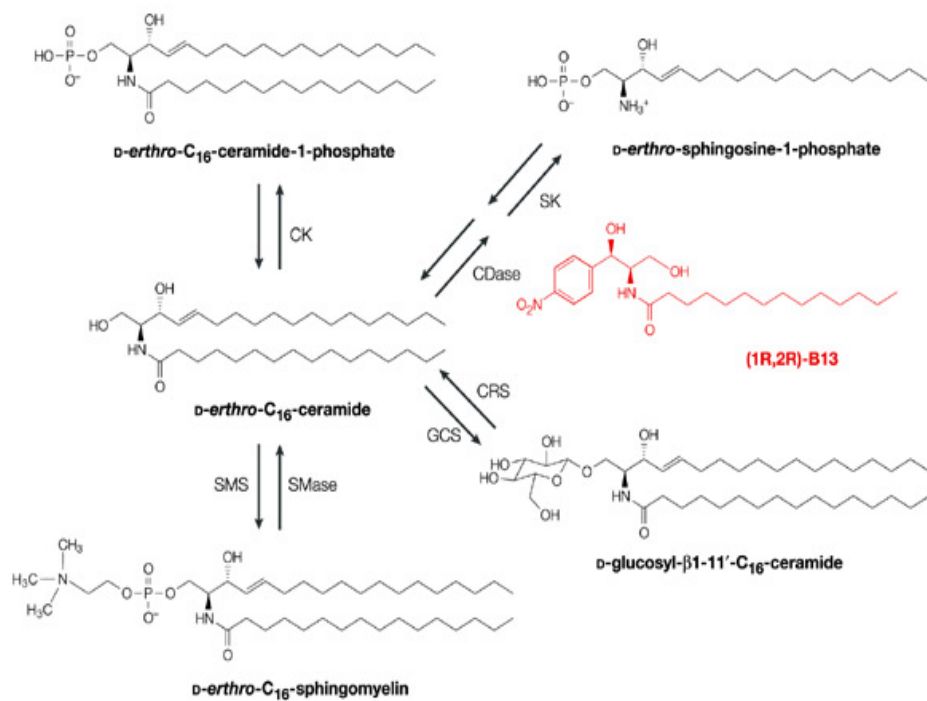


Figure 11. Structures of key sphingolipids, mimetics and inhibitors. Ceramide is composed of an *N*-acylated (14 to 26 carbons) sphingosine (18 carbons). A trans double bond across C4 and C5 of the sphingosine backbone is important for its biological activity, such that dihydroceramide, which lacks this double bond, is

mainly biologically inactive. Complex sphingolipids are composed of a hydrophilic head group attached to the lipophilic ceramide backbone, which in turn is composed of a sphingoid base (usually sphingosine or dihydrosphingosine) and an amide-linked fatty acid. Ceramide then serves as the metabolic and structural precursor for SM, ceramide-1-phosphate and GlcCer, itself the precursor for various complex glycolipids and gangliosides. (From Ogretmen and Hannun, 2004).

Alternatively, ceramide can be generated predominantly by agonist-induced activation of sphingomyelinase (SMase), which catalyses the hydrolysis of sphingomyelin to ceramide and phosphocholine. The re-synthesis of sphingomyelin by sphingomyelin synthase consumes ceramide and phosphatidylcholine, resulting in the formation of sphingomyelin and diacylglycerol; thus completing the sphingomyelin cycle (Hannun *et al*, 2002) Thus, this enzyme not only attenuates ceramide levels, but it also causes an accumulation of diacylglycerol that activates protein kinase C, which often has functions antagonistic to those of ceramide.

As shown in the Figure 12 there are some other enzymes involved in the regulation of ceramide degradation or clearance. These include ceramidases, which catalyze the N-deactylation of ceramide resulting in sphingosine and free fatty acid, and GCS, which catalyzes conversion of ceramide to GlcCer. Inhibitors of ceramide catabolizing enzymes, such as D-MAPP and B13 for ceramidase (Bielawska *et al*, 1996), and PDMP and (1-phenyl-2 palmitoylamino-3-pyrrolidino-1-propanol) PPPP for GCS (Abe *et al*, 1995), result in increased levels of ceramide in cells.

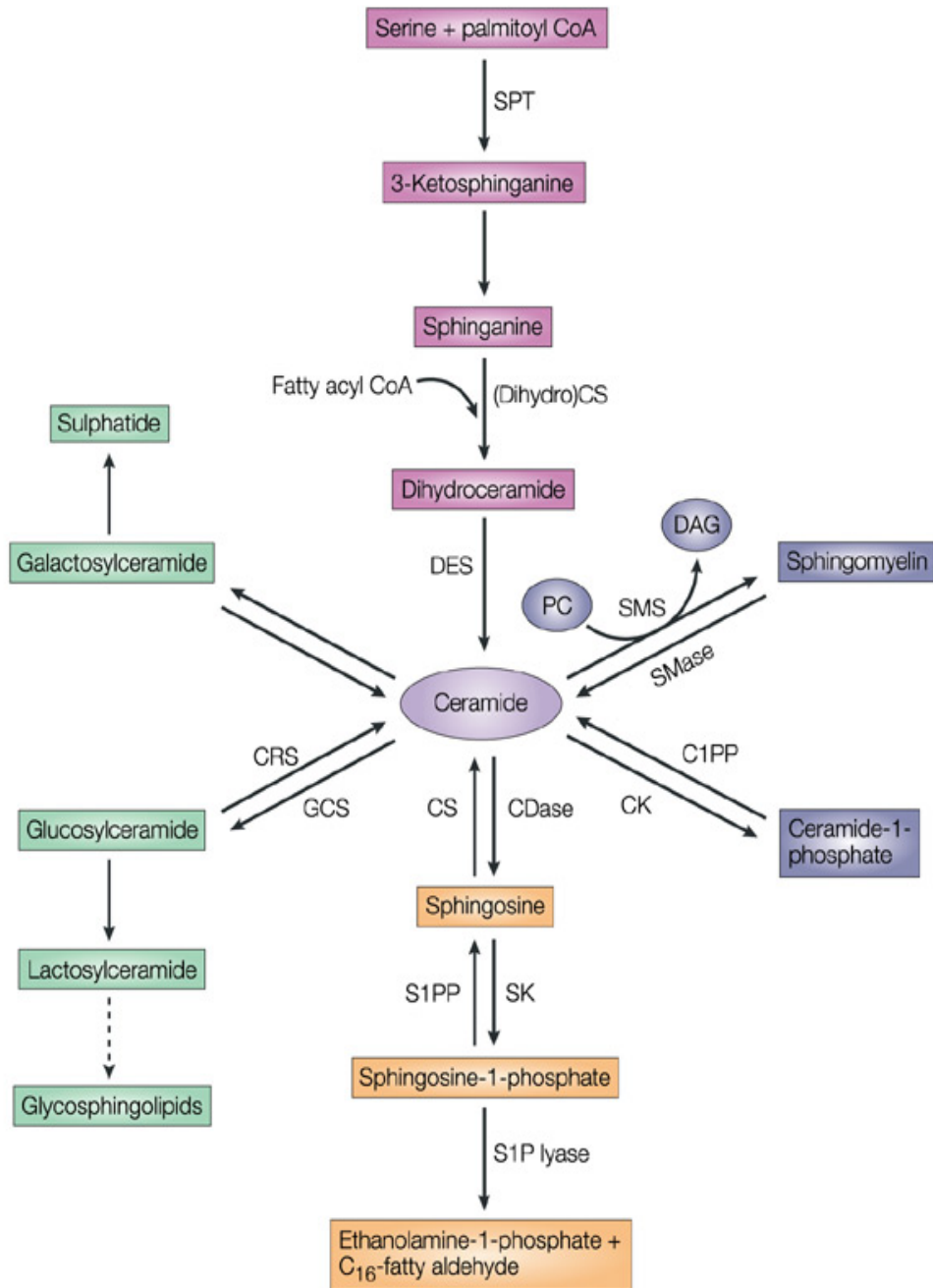


Figure 12. Major synthetic and metabolic pathways for ceramide. Increased ceramide leading to cytotoxicity can come from de novo synthesis due to stimulation of serine palmitoyltransferase and/or dihydroceramide synthase, or by degradation of sphingomyelins via spingomyelinases. Metabolism of ceramide by glycosylation or acylation, appear to ‘shunt’ ceramide into less toxic forms, as does catabolism via ceramidase. Phosphorylation of sphingosine derived from ceramide stimulates pro-

life metabolic pathways and acts to oppose certain cytotoxic actions of ceramides. (From Ogretmen and Hannun, 2004).

1.6.2 hLASS (Human Longevity-Assurance) Genes Regulate Synthesis of Specific Ceramides

Interest in determining the regulatory mechanisms of ceramide metabolism has been stimulated over the past decade by the realization that ceramides formed by turnover of complex sphingolipids, and by *de novo* synthesis, influence key aspects of cell growth, regulation, differentiation, and cell death (Merrill, 2002). Ceramides are formed *de novo* by *N*-acylation of sphinganine to dihydroceramide, which is subsequently desaturated by dihydroceramide desaturase (Pan *et al*, 2001). The *N*-acyltransferase(s), which are referred to herein as (dihydro) ceramide synthase(s), acylate various long chain bases, including sphinganine, sphingosine, and 4-hydroxysphinganine, utilize a wide spectrum of fatty acyl-CoAs.

Among these regulatory mechanisms of ceramide metabolism, a family of mammalian genes that regulates ceramide synthesis has been discovered. Surprisingly, overexpression of each of these genes leads to an increase in ceramides containing different fatty acids.

Longevity-assurance gene 1 (LAG1) was the first of several ceramide synthesising gene discovered in yeast (D'mello *et al*, 1994). Homologues of LAG1 have been identified in several species, including human (Brandwagt *et al*, 2000). The human gene has been renamed hLASS1 to conform to current genetic nomenclature. Recently, an additional human homologue, called LASS2, and 4 different members of LASS family have been discovered named as LASS3, LASS4, LASS5 and finally LASS6.

The LASS family members are highly conserved among eukaryotes. To investigate specific roles for each LASS member in ceramide synthesis, these five proteins were cloned. Overproduction of any LASS protein in cultured cells resulted

in an increase in cellular ceramide, but the ceramide species produced varied. Overproduction of LASS1 increased C18-ceramide levels (Venkataraman, K., 2002), overproduction of LASS2 increased levels of longer ceramides such as C24-ceramides (Mizutani *et al*, 2005) and LASS4 increased C22-ceramides (Riebeling *et al*, 2003). LASS5 and LASS6 produced shorter ceramide species C14- and C16-ceramides (Mizutani *et al*, 2005); however, their substrate preferences towards saturated/unsaturated fatty acyl-CoA differed. In addition to differences in substrate preferences, LASS family members are differentially expressed among tissues. Additionally, it was found that LASS proteins differ with regard to glycosylation. Of the five members, only LASS2, LASS5 and LASS6 were N-glycosylated, each at their N-terminal Asparagines residue. The occurrence of N-glycosylation of some LASS proteins provides topological insight, indicating that the N-termini of LASS family members probably face the luminal side of the endoplasmic reticulum membrane. From these data, a topology for the conserved LAG1 motif in LASS family members has been proposed (Figure 13)

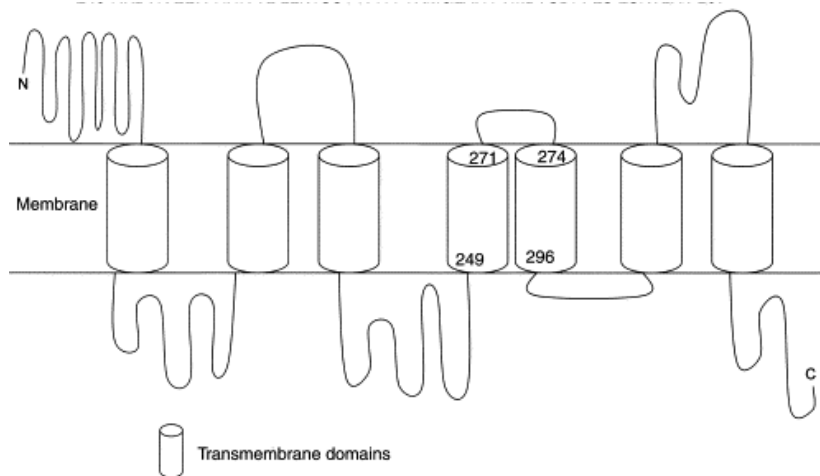


Figure 13. Predicted structure of LASS1 protein. LASS1 is a protein of the ER. Its predicted transmembrane structure is shown. The numbers designate the first and last amino acids of the transmembrane domains containing the Lag1 motif in this 411-amino acid protein. (From Jazwinski SM *et al*, 2002).

1.6.3 Cancer-Suppressing Roles of Ceramide

Ceramide is intimately involved in the regulation of cancer-cell growth, differentiation, senescence and apoptosis (Hannun *et al*, 2002). Ceramide seems to transduce these regulatory pathways predominantly by regulating specific protein targets such as phosphatases and kinases. These protein targets, in turn, modulate the components of various signaling pathways (Ogretmen *et al*, 2001-1); for example, AKT, phospholipase D, protein kinase C (PKC) and mitogen-activated protein kinases (MAPKs; Figure 14). *In vitro*, ceramide also activates specific serine/threonine protein phosphatases (known as ceramide-activated protein phosphatases), protein kinases (for example, c-RAF, PKC α and kinase suppressor of RAS) and cathepsin D (Chalfant *et al*, 2004) (Figure 14).

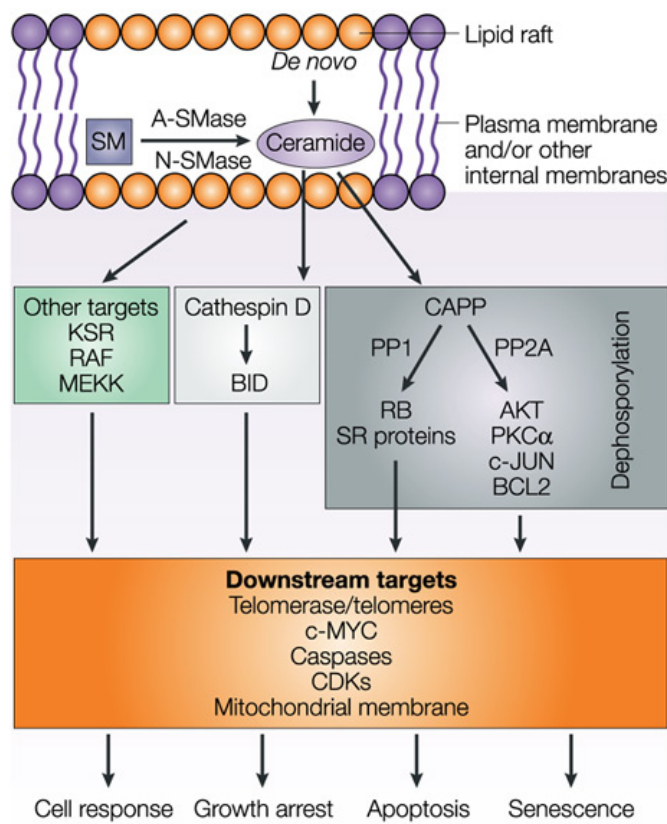


Figure 14. Ceramide-regulated targets and pathways. Several direct targets of ceramide have been identified *in vitro*, including cathepsin D and ceramide-activated

protein phosphatases (CAPPs), which comprise the serine/threonine protein phosphatases PP1 and PP2A. These phosphatases act on several substrates such as the retinoblastoma gene product RB, Bcl-2, c-JUN, protein kinase-C α (PKC α), AKT and SR proteins, which are known regulators of constitutive and alternative splicing. These pathways seem to be compartmentalized. In particular, cathepsin D is activated by ceramide generated in lysosome membranes leading to activation of the pro-apoptotic protein BID. Ceramide also activates the kinase suppressor of RAS (KSR), which in turn can activate mitogen-activated protein kinase (MAPK), RAF1, PKC α and MEKK (MAPK/ERK kinase kinase). Proteins modulated by these pathways include telomerase, c-MYC, caspases and cyclin-dependent kinases (CDKs). Mitochondrial membrane potential can also be altered by these pathways, probably through PP2A-mediated dephosphorylation of Bcl-2. All of these downstream effects can lead to changes in growth arrest, apoptosis and/or senescence. A-SMase, acid sphingomyelinase; N-SMase, neutral sphingomyelinase; SM, sphingomyelin. (From Ogretmen and Hannun, 2004).

1.6.3.1 Ceramide in Apoptosis

Apoptosis defines a set of regulated biochemical processes that lead to organized cell death and it plays an important role in development and many physiological and pathological conditions. Apoptosis can be induced by diverse stimuli including triggering of death receptors (CD95) and tumor necrosis factor, growth factor withdrawal, hypoxia and DNA damage. Defects in apoptosis underlie the pathogenesis of many cancers, such as those overexpressing anti-apoptotic genes (for example, Bcl-2) or those that harbour mutations in pro-apoptotic genes. Apoptotic stimuli initiate signaling events that ultimately activate a class of cysteine proteases known as caspases, which are central elements of the execution machinery of apoptosis. Many of these mediators of apoptosis have been demonstrated as both regulators of ceramide generation and downstream targets of ceramide action (Figure 14), suggesting a role of ceramide in apoptosis (Ogretmen *et al*, 2001-1).

Ceramides have also been shown to exert direct effects on mitochondria, and one mechanism that has been proposed for ceramide-mediated apoptosis is via channel or pore formation in mitochondrial membranes (Figure 14).

1.6.3.2 Ceramide in Quiescence and Senescence

Ceramide regulates several pathways that converge on the induction of G0/G1 cell-cycle arrest. It was shown that in response to TNF α , ceramide induces the dephosphorylation of the retinoblastoma gene product (RB) through the activation of PP1 (Figure 15) (Dbaibo *et al*, 1995). Ceramide also selectively induces the dephosphorylation and inactivation of the cyclin-dependent kinase CDK2, but not CDK4 (Figure 15) (Lee *et al*, 2000). Additional mechanistic studies demonstrate that ceramide induces the up regulation of the CDK inhibitors WAF1 (also known as p21) in Wi-38 human fibroblasts (Lee *et al*, 2000) and KIP1 (also known as p27) in nasopharyngeal carcinoma cells (Zhu *et al*, 2003). Recent studies point to human N-SMase 2 which was the first bone fide mammalian neutral sphingomyelinase to be identified (Marchesini *et al*, 2004-1) as a key regulator of cell growth and cell cycle progression, but not of apoptosis, supporting the functional differentiation of ceramide-regulated pathways of growth suppression (Marchesini *et al*, 2004-2).

The role of ceramide in senescence has also been studied extensively. The inability of cells to undergo indefinite doublings is known as senescence. Obeid and co-workers demonstrated that the levels of ceramide increase significantly in human fibroblasts as they become senescent, and treatment of low-passage-number fibroblasts with short chain ceramides induces the morphological features of senescence and many of the biochemical changes associated with senescence (dephosphorylation of RB, inhibition of CDKs and modulation of growth-factor signalling). A key mechanism of ceramide-induced senescence involves the inhibition of phospholipase D, diacylglycerol generation and protein kinase C activation, leading to a profound suppression of this key mitogenic pathway (Figure 14) (Venable *et al*, 1995).

1.6.4 Cancer-Promoting Roles of Sphingosine 1 Phosphate (S1P)

Ceramide is deacylated by ceramidases, yielding a sphingoid base; the most common of these in mammals is sphingosine. In order for the sphingoid base to be catabolized, it must be phosphorylated on the 1-OH by SK-1. Cells also contain S1P phosphatase and ceramide synthase activities, allowing S1P to be converted back to ceramide. Cells maintain a dynamic equilibrium in the levels of ceramide, sphingosine, and S1P (Figure 12). This is more than a salvage pathway, as ceramide, sphingosine, and S1P have all been demonstrated to be second messengers, conserved from yeast to human.

The sphingolipid metabolite, S1P regulates many important cellular processes including growth, survival, differentiation, cytoskeleton rearrangements, motility, angiogenesis, and immunity (Spiegel *et al*, 2003, Saba *et al*, 2004 and Anliker *et al*, 2004).

1.6.4.1 The Sphingolipid Rheostat: a Conserved Stress Regulator

Stresses increase *de novo* ceramide synthesis or activate sphingomyelinases and ceramidase and elevate levels of ceramide and sphingosine leading to apoptosis, many other stimuli, particularly growth and survival factors, activate SK-1, resulting in accumulation of S1P and consequent suppression of ceramide-mediated apoptosis (Ogretmen and Hannun, 2004). Thus, it has been suggested that the dynamic balance between intracellular S1P and sphingosine and ceramide and the consequent regulation of opposing signaling pathways are important factors that determine whether cells survive or die (Maceyka *et al*, 2002).

Therefore, like other lipid mediators, S1P levels are tightly regulated by the balance between syntheses, catalyzed by SK-1, irreversible cleavage by S1P lyase, and reversible dephosphorylation to sphingosine by specific S1P phosphatases. Diverse external stimuli, particularly growth and survival factors, stimulate SK-1 and

intracellularly generated S1P has been implicated in their mitogenic and anti-apoptotic effects (Edsall *et al*, 2001 and Xia *et al*, 2000). Expression of SK-1 enhanced proliferation and growth in soft agar, promoted the G₁-S transition, protected cells from apoptosis (Figure 15) (Olivera *et al*, 2003 and Xia *et al*, 2000), and induced tumor formation in mice (Nava *et al*, 2002).

The sphingolipid rheostat is evolutionarily conserved, as it also plays a role in regulation of stress responses of yeast cells (Jenkins *et al*, 2001). In these lower eukaryotic cells, the sphingolipid metabolites ceramide and sphingosine have been implicated in heat stress responses as decreased phosphorylated long chain sphingoid bases dramatically enhanced survival upon severe heat shock (Jenkins *et al*, 2001).

1.6.4.2 Cancer-Promoting Roles of S1P

In line with classical models of cell transformation, it was found that overexpression of SK-1, the immediate regulator of S1P, in mouse 3T3 cells results in cellular transformation in tissue culture and tumor formation in SCID mice (Xia *et al*, 2000). The addition of S1P to most cell types promotes proliferation and blocks many forms of apoptosis (Olivera *et al*, 2003). S1P was shown to stimulate invasiveness of human glioblastoma cells and to promote estrogen-dependent tumorigenesis of MCF-7 human breast cancer cells (Van Brocklyn *et al*, 2003 and Nava *et al*, 2002). Reciprocally, using siRNAs, it was shown that inhibition of S1P phosphatase 1 (S1PP1), which converts S1P to sphingosine, results in increased intracellular and extracellular levels of S1P and endows MCF-7 cells with resistance to the cytotoxic actions of TNF α and daunorubicin (Johnson *et al*, 2003). So, the SK-1/S1P pathway exerts significant pro-proliferative activities in cancer cells.

S1P exerts several specific effects on endothelial cells that, overall, promote blood-vessel formation. It promotes endothelial-cell growth and interacts specifically with vascular endothelial growth factor (VEGF) signaling, which is crucial for angiogenesis (Liu *et al*, 2001-1). VEGF was shown to stimulate SK-1 activity in the

T24 bladder tumor cell line and in turn, SK-1 mediated VEGF-induced activation of RAS and MAPKs in these cells (Wu *et al*, 2003). As S1P is also secreted extracellularly (Figure 15), modulation of SK-1 and S1P in tumor cells provides a potential mechanism for recruiting endothelial cells and promoting blood vessel formation/angiogenesis. Indeed, combining S1P with other pro-angiogenic factors, such as basic fibroblast growth factor, stem-cell factor or VEGF, produced synergistic enhancement of vascular sprouting and neovascularization in tissue samples of mouse aortic rings, an *ex vivo* model of angiogenesis. The mechanisms of S1P-mediated neovascularization involve the migration of endothelial cells through the activation of S1P receptors and downstream regulation of the RHO family of small GTPases, which in turn regulate cell motility and remodeling of the cytoskeleton (Kluk *et al*, 2002 and Okamoto *et al*, 2000).

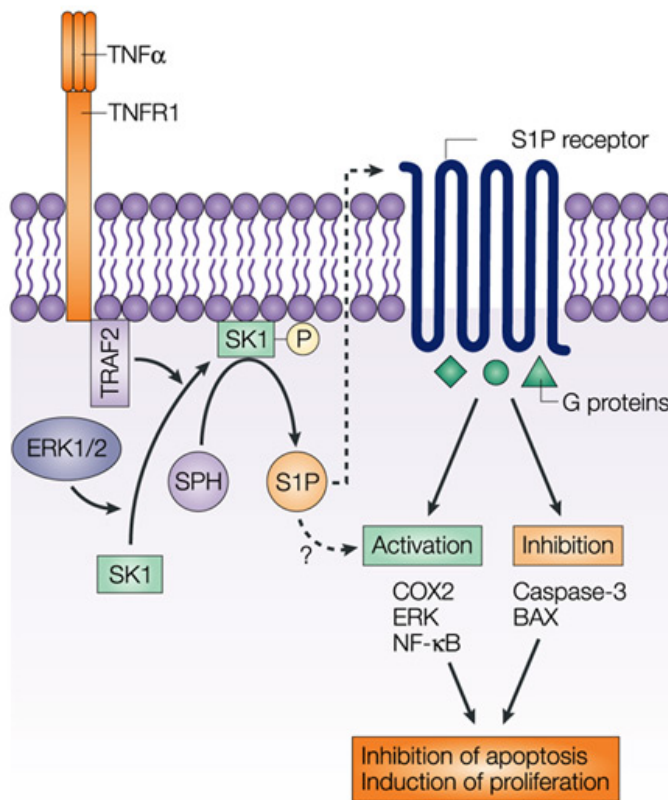


Figure 15. Targets and pathways regulated by S1P. Agonist-induced activation of sphingosine kinase 1 (SK-1) for example, by tumor-necrosis factor- α (TNF α) involves its interaction with TNF-associated factor 2 (TRAF2) and phosphorylation

by extracellular-regulated kinase 1 (ERK1) or ERK2, which then induces translocation of the enzyme from the cytoplasm to the plasma membrane, leading to increased generation of S1P from sphingosine. S1P functions as a specific ligand for the G-protein-coupled S1P receptors. S1P receptors couple to various G proteins, such that S1P can mediate distinct biological responses based on the relative expression levels of S1P receptors and specific G proteins. Primarily, S1P-mediated pathways are proliferative, pro-inflammatory (through cyclooxygenase 2 (COX2) and anti-apoptotic (through inhibition of the pro-apoptotic proteins caspase-3 and BAX). NF- κ B, nuclear factor- κ B. TNFR1, tumour-necrosis factor receptor 1. (From Ogretmen and Hannun 2004).

1.6.5 Targeting Ceramide Metabolism to Overcome Drug Resistance

Cancer cells develop multiple, and often overlapping, mechanisms that allow them to become resistant to chemotherapeutic agents. The dysfunctional metabolism of ceramide is another one of these inherent or acquired mechanisms that contribute to cellular drug resistance. Numerous studies have helped define the ceramide signaling pathways that contribute to cell death. Studies also indicate that alterations in these cell death signaling pathways may contribute to resistance to standard chemotherapeutic agents in several *in vitro* cancer models, including breast, prostate and squamous cell cancers. Investigators have demonstrated the efficacy of targeting ceramide synthesis or degradation pharmacologically to enhance the cytotoxic effects of several clinically relevant drugs. In one study it was shown that multidrug resistance can be increased over baseline and then totally reversed in human breast cancer cells by GCS gene targeting. In adriamycin-resistant MCF-7-AdrR cells, transfection of GCS upgraded multidrug resistance, whereas transfection of GCS antisense markedly restored cellular sensitivity to anthracyclines, Vinca alkaloids, taxanes, and other anticancer drugs. (Liu *et al*, 2001-2).

Targeting ceramide metabolic and cell death signaling pathways (e.g. GCS, SK-1 inhibition and/or LASS induction) is an attractive clinical treatment strategy for overcoming drug resistance and continues to be studied actively.

1.7 AIM OF THE STUDY

Multidrug resistance remains a significant impediment to successful chemotherapy. The ability to determine the possible resistance mechanisms and circumvent the resistance is likely to improve chemotherapy.

Imatinib is a very effective drug in the treatment of chronic myeloid leukemia patients. Although very high hematologic and cytogenetics responses obtained in Imatinib treated patients, in recent years resistance cases were observed. The main objectives of the project are to understand the mechanisms underlying multidrug resistance to Imatinib in order to define new targets for the treatment of chronic myeloid leukemia. The basic idea of this approach is to block steps in the acquired mechanisms of multidrug resistance in chronic myeloid leukemia. Besides expression analyses of MDR1, BCR-ABL, pro-apoptotic and anti-apoptotic genes, sequence analyses of Imatinib binding site of ABL kinase gene was conducted. On the other hand, for the first time in this project, the involvement of sphingolipids in Imatinib induced apoptosis and resistance was examined in chronic myeloid leukemia.

CHAPTER 2

MATERIALS AND METHODS

2.1 MATERIALS

2.1.1 K562 and Meg-01 Cell Lines

The Philadelphia chromosome (Ph) positive K562 and Meg-01 cells were obtained from German Collection of Microorganisms and Cell Cultures, Germany.

2.1.2 Chemicals

The 2-phenylaminopyrimidine derivative Imatinib (MW: 571) was developed and kindly provided by Novartis (Basel, Switzerland). The stock solution of this compound was prepared at 10 mmol/L with sterile distilled water and stored at – 20 °C.

RPMI 1640, fetal bovine serum (FBS), penicilline-streptomycin, phosphate buffer saline (PBS), agarose, propidium iodide and 50X tris acetate EDTA (TAE) were obtained from Invitrogen, USA.

RNeasy RNA isolation kit, QIAquick gel extraction kit, effectene transfection reagent and Taq DNA polymerase were obtained from Qiagen, USA.

DharmaFECT™ siRNA transfection reagent was obtained from Dharmacon, USA.

Bio-Rad protein assay (Bradford dye), 4-15 % SDS polyacrylamide gel, coommasic blue, tween-20, 10X tris-glycine-EDTA and protein markers were obtained from Bio-Rad, USA.

dNTP set, DNA ladder and polyethylene bag were obtained from Fisher Scientific, USA.

Caspase-3 fluorometric assay kit was obtained from R&N Systems, USA.

JC-1 mitochondrial membrane potential detection kit was obtained from T Cell Technology, USA.

Bcl-2, BclXL and Bax primary antibodies were kindly provided by Dr. Hsu Lab, MUSC, USA.

Secondary antibodies were obtained from Jackson Immunoresearch, USA.

Cyclosporin A (Cyc A) was obtained from Calbiochem, Germany.

N-(2-hydroxy-1-(4-morpholinylmethyl)-2-phenylethyl)-decanamide, hydrochloride (PDMP) was obtained from Cayman Chemical, USA.

Reverse-Transcription system and bovine serum albumine (BSA) were obtained from Promega, USA.

Isopropanol, trypan blue solution, β -mercaptoethanol, dimethyl sulfoxide (DMSO), proteinase K and agarose were obtained from Sigma, USA.

Nitrocellulose immobilon transfer membrane was obtained from Millipore, USA.

Developing Solution was obtained from Amersham Biosciences, USA.

25 cm² and 75 cm² tissue culture flasks were obtained from Corning, USA.

2.1.3 PlasmidVectors and siRNAi

pcDNA3.1 (Appendix C-II), pcDNA3.1/GCS, pcDNA3 (Appendix C-I), pcDNA3/SK-1 and pCMVexSVneo plasmids were purchased from Invitrogen, USA.

pCMVexSVneo/hLASS1 plasmid was kindly provided by Dr. S. Michal Jawzwienski, Medical University of South Caroline (MUSC), USA.

pCMVexSVneo/hLASS2, pCMVexSVneo/hLASS5, and pCMVexSVneo/hLASS6 plasmids were kindly provided by Dr. Besim Ogretmen, Medical University of South Caroline (MUSC), USA.

hLASS1 siRNA, SK-1 siRNA, and Scramble siRNA were obtained from Dharmacon, USA.

2.1.4 Primers

BCR-ABL, ABL Kinase gene primers were obtained from Iyontek, Istanbul, Turkey. MDR1, GCS, hLASS1, hLASS2, hLASS5, hLASS6, SK-1 and Beta actin primers were purchased from IDT Technologies, USA.

Table 2. Primers used in this study.

MDR1	5'TACAGTGGATTGGTGCTGGG3'
MDR1	5'CCCATGAAAAATGTTGCCA3'
BCR-ABL (BCR-C)	5'ACCGCATGTTCCGGGACAAAAG3'
BCR-ABL (B2B)	5'ACAGAATTCTGCTGACCATAAAAG3'
BCR-ABL (C5e)	5'ATAGGATCCTTGCAACCGGGTCTGAA3'
BCR-ABL (CA3)	5'TGTTGACTGGCGTGATGTAGTTGCTTGG 3'
ABL Kinase-NTPB	5'AAGCGCAACAAGCCCAGTGTCTAT3'
ABL Kinase-NTPE	5'CTTCGTCTGAGATACTGGATTCCCT 3'
GCS	5'ATGACAGAAAAAGTAGGCT 3'
GCS	5' GGACACCCCTGAGTGGAA 3'
hLASS 1	5' CTATACATGGACACCTGGCGCAA 3'
hLASS 1	5' TCAGAACGCGCTTGTCCCTCACCA 3'
hLASS 2	CCCTCGAGGGATGGATTACAAGGATGACGACGATA AGATGCTCCAGACCTGTATGATT 3'
hLASS 2	5' CGGAATTCCGTCAGTCATTCTACGATGGTT 3'
hLASS 5	5'CCCTCGAGGGATGGATTACAAGGATGACGACGAT AAGATGGCGACAGCAGCGCAGGGA 3'
hLASS 5	5' CGGAATTCCGTTACTCTTCAGCCCAGTAGCT 3'
hLASS 6	5'CCCTCGAGGGATGGATTACAAGGATGACGACGAT AAGATGGCAGGGATCTTAGCCTGG 3'
hLASS 6	5'CGGAATTCCGTTAACATCCATGGAGCAGGA 3'
SK-1	5' CCGACGAGGACTTGTGCTAAT 3'
SK-1	5' GCCTGTCCCCCAAGCATAAC 3'
Beta actin	5' CAGAGCAAGAGAGGCATCCT 3'
Beta actin	5' TTGAAGGTCTAAACATGAT 3'

2.2 METHODS

2.2.1 Cell Line and Culture Conditions

The cells were grown in 5 mL of RPMI 1640 medium containing 15-20% heat-inactivated fetal bovine serum (FBS) and 1% Penicilline-Streptomycin in 25 cm² tissue culture flasks. The cells were incubated in CO₂ incubator (Nuaire, USA) at 37 °C in the presence of 5% CO₂. The medium was refreshed in every five days.

2.2.2 Thawing Frozen Cells

Cells were removed from frozen storage and quickly thawed in a 37 °C water bath to obtain the highest percentage of viable cells. As soon as the ice crystals melted, the content was taken into a sterile Falcon tube and washed with PBS. Then the cells were cultured in 25 cm² tissue culture flask in RPMI 1640 medium.

2.2.3 Maintenance of the K562 and Meg-01 Cell Culture

Cell suspension (0.5 mL) was taken from the tissue culture flask into a sterile Falcon tube. The cells were centrifuged at 1,000 rpm for 2 min. After centrifugation, supernatant was removed and the pellet was resuspended in 1 mL of RPMI 1640. Medium was taken into a sterile 25 cm² tissue culture flask containing 4 mL RPMI 1640 medium. Drug was added at the required concentration to the medium.

2.2.4 Trypan Blue Dye Exclusion Method

The effects of Imatinib and different chemical inhibitors or transfection of different genes and siRNA on cell growth were determined by the trypan blue dye exclusion method as described previously (Zhang *et al*, 1999). In short, cells, seeded as 50×10^3 cells/well in 6-well plates with 2 mL of complete media, were treated in the absence or presence of various concentrations of Imatinib for 48 h. Then, cells (500 μ L) were collected, centrifuged at 1,600 rpm for 3 min and diluted in 1X PBS (100 μ L) buffer. The mixture was incubated in the presence of trypan blue solution at a 1:1 ratio (v/v) (Sigma) for 5 min at room temperature. If cells were exposed to trypan blue for extended periods of time, viable cells may begin to take up dye as well as non-viable cells. The cells were then counted using a hemacytometer under a light microscope (Olympus, USA)

Each square of the hemacytometer (with cover slip in place) represents a total volume of 0.1 mm^3 or 10^{-4} cm^3 . Since 1 cm^3 is equivalent to 1 mL, the subsequent cell concentration per mL (and the total number of cells) will be determined using the following equations:

Cells per mL = the average count per square \times the dilution factor $\times 10^4$.

Total cell number = cells per mL \times the original volume of fluid from which cell sample was removed.

2.2.5 Freezing Cells

Cells were frozen in case they may be needed for further studies. For this purpose high numbers of cells were required. Therefore, cells were cultured in 75 cm^2 tissue culture flask in 20 mL of complete media.

Cells were harvested as usual in 75 cm^2 tissue culture flask and the content of flask was poured in to 50 mL Falcon tube. The cells were centrifuged at 1,000 rpm

for 3 min. After removing supernatant, the pellet was resuspended in 5 mL of 1X PBS and centrifuged at 1,000 rpm for 3 min. During centrifugation, cryogenic vials were taken onto ice. After centrifugation, supernatant was discarded and the tube was taken onto ice. Then the cell pellet was resuspended in 5.4 mL of fetal bovine serum (90%) and 600 μ L of DMSO (10%). The solution was mixed on ice and 1.5 mL from cell suspension was taken into each cryogenic vial. Cryogenic vials were incubated in refrigerator (4 C°) for 30 min before the overnight incubation at -80 C°. Finally, they were stored in liquid nitrogen (-196 C°).

2.2.6 Generation of Resistant Sub-lines

Cells maintained in liquid cultures were exposed to increasing concentrations of Imatinib, starting with a concentration of 0.05 μ M and increasing gradually. After the cells acquired the ability to grow in the presence of a specific concentration of the drug, proportion of cells then were frozen, and the remaining cells were grown at the next highest drug level. In this way, subpopulations of cells with different degrees of resistance were generated for further studies. The level of resistance was defined by the Imatinib concentration at which the growth rate of cells was comparable to that of untreated parental cells.

2.2.7 Total RNA Isolation from Cells

RNeasy Kit (Qiagen) was used for the total RNA isolation from cell lines. Isolation was performed as described by the manufacturer. All steps of the protocol, including centrifugation, were performed at room temperature.

Briefly, the number of cells were determined (The number of cells per prep was 1×10^6). The appropriate number of cells was centrifuged for 3 min at 1,000 rpm in a 15 mL sterile Falcon tube. The supernatant was carefully removed. Buffer RLT

(350 µL) including 10 µL β-Mercaptoethanol per 1 mL of Buffer RLT was added onto the pellet and mixed well by pipetting.

The samples were homogenized by passing of the lysate at least 5 times through a 20-gauge needle (0.9 mm diameter) fitted to an RNase-free syringe.

1 Volume of 70% Ethanol (350 µL) was added to the homogenized lysate and mixed well by pipetting. The sample was then applied to an RNeasy Column in a 2 mL collection tube. The tube was closed gently, and centrifuged for 15 s at 10,000 rpm. The flow-through was discarded and 700 µL Buffer RW1 was added to the RNeasy Column. The tube was closed gently, and centrifuged for 15 s at 10,000 rpm. The flow-through and the collection tube were discarded.

Another 500 µL Buffer RW1 was added into the RNeasy Column and centrifuged for 2 min at 10,000 rpm. The flow through was discarded.

The spin column was transferred to a new 1.5 mL collection tube. RNase-free water (50 µL) was directly added onto the center of the silica-gel membrane. The tube was closed gently, and centrifuged for 1 min at 10,000 rpm.

2.2.8 Quantification of RNA

Quantification of RNA was conducted by spectrophotometer (Shimadzu, Japan). Reading at 260 nm was used to calculate the concentration of nucleic acid in a sample. An OD of 1 corresponds to 40 µg/mL of single-stranded RNA.

Equation Concentration (µg/mL) = (dilution factor) × (40 µg/mL/OD₂₆₀) × (sample's OD)

The ratio between the readings at 260 nm and 280 nm (OD_{260}/OD_{280}) provides an estimate of the purity of the nucleic acid. Pure preparations of RNA have a ratio of 1.8.

2.2.9 Agarose Gel Electrophoresis of RNA

In order to examine the RNA products, 10 μ L of sample was mixed with 2 μ L of loading buffer (6X) and run on 1.2 % agarose gel at 70 V for 60 min.

Agarose (0.42 g) was added to 35 mL 1X TAE buffer and was dissolved by boiling. The solution was cooled down to 50-60 °C. The gel was stained with Ethidium-bromide (0.5 μ g/mL). The comb was placed and agarose solution was poured into electrophoresis apparatus. The gel was left at room temperature for 30 min for solidification and the comb was then removed. The apparatus chamber was filled with 1X TAE and the gel was placed in the chamber. The gel was visualized by UV transilluminator after electrophoresis.

2.2.10 cDNA Preparation from RNA

The following reaction mixture was prepared in a sterile 0.5 mL eppendorf tube.

The samples were vortexed and spun down. The mixture was incubated at room temperature for 10 min, at 42 °C for 50 min and at 95 °C for 5 min. The tube was chilled on ice for 5 min. cDNAs were stored at -20 °C.

Table 3. Ingredients of reverse transcription reaction.

Ingredients	Amount
RNase Free Water	5 µL
Total RNA (5 µg)	5 µL
10X Buffer	2 µL
Random Primers (0.5 µg/µL)	0.7 µL
RNase Inhibitor (50 U/µL)	0.7 µL
MgCl ₂ (25 mM)	4 µL
dNTP (10mM)	2 µL
Moloney Murine Reverse Transcriptase enzyme (200 U/ µL)	0.7 µL
Total	20 µL

2.2.11 Nucleotide Sequence Analyses of Imatinib Binding Site of ABL Kinase Domain in Parental and Resistant Human CML Cells

To determine whether a point mutation in the BCR-ABL ATP-binding domain was responsible for the resistance in K562 and Meg-01 cells to the inhibitory effect of Imatinib, sequencing of the cDNA portion corresponding to the ATP-binding region was performed. Total RNAs, isolated from parental, 0.2 µM and 1 µM Imatinib resistant K562 and Meg-01 cell lines, were converted to cDNA by Reverse Transcriptase enzyme. Imatinib binding region of ABL kinase gene was amplified by using NTPE (exon 9 of ABL gene) and NTPB (exon 4 of the ABL gene) primers (Mahon *et al.*, 2000). The PCR products were run on a 2% agarose gel at 90 V for 1 h and the results were visualized by UV spectrophotometer. After extraction, the fragments were subjected to automated sequencing using the forward primers NTPB and BRN encompassing the ATP-binding domain of the fusion protein. The sequences obtained from parental, 0.2 µM and 1 µM Imatinib resistant K562 and Meg-01 cell lines were aligned and compared to the c-ABL known sequence (Gene Bank accession number: M14752) of the samples were determined (by ABI Prism, 322 DNA Sequencer, USA) in Biotechnology Resource Laboratory

(MUSC, USA). The results were analyzed between parental and Imatinib resistant K562 and Meg-01 cell lines to detect any mutation that occurred in Imatinib binding region of ABL kinase gene.

2.2.11.1 DNA Extraction from Agarose Gel

QIAquick gel extraction Kit (Qiagen) was used for the extraction of DNA from agarose gel. The extraction was performed as described by the manufacturer.

Briefly, the DNA fragments were excised from the agarose gel with a clean and sharp scalpel. The size of the gel slice was minimized by removing extra agarose. The gel slice was weighed and 3 volumes of buffer QG was added to 1 volume of gel (300 µL for each 100 mg of gel). The sample was incubated at 50 °C for 10 min or until the gel slice was completely dissolved. To help dissolve the gel, the tube was mixed by vortexing every 3 min during incubation. 1 Gel volume of Isopropanol was added to the sample and mixed. The sample was applied to the QIAquick column, and centrifuged at 13,000 rpm for 1 min. Flow-through was discarded and QIAquick column was placed back in the same collection tube. To wash, 0.75 mL of Buffer PE was added to QIAquick column and centrifuged at 13,000 rpm for 1 min. The flow-through was discarded and the QIAquick column was centrifuged for an additional 1 min at 13,000 rpm. QIAquick column was placed into a clean 1.5 mL micro centrifuge tube. To elute DNA, 50 µL of Buffer EB (10 mM Tris·Cl, pH 8.5) or H₂O was added to the center of the QIAquick membrane and the column was centrifuged for 1 min.

2.2.12 Polymerase Chain Reaction

The resulting total cDNA was then used in PCR. PCR mixture was prepared in the sterile 0.5 mL PCR-Eppendorf tubes.

Table 4. Ingredients of PCR tubes for MDR1, hLASS1, hLASS2, hLASS5, hLASS6, SK-1, GCS, ABL Kinase and Beta Actin genes.

Reaction Mixture	MDR1, hLASS1, hLASS2, hLASS5, hLASS6, SK-1, GCS, ABL Kinase and Beta Actin (Control)
PCR Grade Water	22.7 µL
Q Solution (5X)	10 µL
Reaction buffer (10X)	5 µL
MgCl ₂ (25 mM)	5 µL
dNTP (10 mM)	4 µL
Primer forward (50 pmol/ µL)	1 µL
Primer reverse (50 pmol/ µL)	1 µL
cDNA	1 µL
Taq DNA Polymerase (5U/µL)	0.3 µL
Total Mixture	50 µL

Table 5. Ingredients of PCR tubes for BCR-ABL gene.

Reaction Mixture	BCR-ABL Gene	Beta actin gene (Control)
PCR Grade Water	20.7 µL	22.7 µL
Q Solution (5X)	10 µL	10 µL
Reaction buffer (10X)	5 µL	5 µL
MgCl ₂ (25 mM)	5 µL	5 µL
dNTP (10 mM)	4 µL	4 µL
Primer BCR-C (50 pmol/ µL)	1 µL	-
Primer B2B (50 pmol/ µL)	1 µL	-
Primer C5E (50 pmol/ µL)	1 µL	-
Primer CA3 (50 pmol/ µL)	1 µL	

Primer β forward (50 pmol/ μL)	-	1 μL
Primer β reverse (50 pmol/ μL)	-	1 μL
cDNA	1 μL	1 μL
Taq DNA Pol.	0.3 μL	0.3 μL
Total Mixture	50 μL	50 μL

2.2.13 Amplification Conditions of PCR

A thermocycler (Bioemtra T3, Germany) was used for the amplification of cDNAs using the following programs;

Table 6. Amplification conditions of MDR1 gene.

Steps	Temperature	Time
Initial Denaturation	94°C	5 min
Denaturation	94°C	30 s
Annealing	55 °C	45 s
Extension	72 °C	1 min
Final Extension	72 °C	5 min

Table 7. Amplification conditions of BCR-ABL (b3a2, b2a2) genes.

Steps	Temperature	Time
Initial Denaturation	95°C	5 min
Denaturation	95°C	45 s
Annealing	58 °C	30 s
Extension	72 °C	45 s
Final Extension	72 °C	5 min

Table 8. Amplification conditions of SK-1, GCS, hLASS2, hLASS5, hLASS6 and ABL Kinase genes.

Steps	Temperature	Time
Initial Denaturation	94 °C	2 min
Denaturation	94 °C	1 min
Annealing	55 °C	2 min
Extension	72 °C	2 min
Final Extension	72 °C	5 min

Table 9. Amplification conditions of hLASS1.

Steps	Temperature	Time
Initial Denaturation	94 °C	2 min
Denaturation	94 °C	1 min
Annealing	68 °C	2.5 min
Extension	72 °C	2 min
Final Extension	72 °C	5 min

In all conditions denaturation, annealing and extension steps were 35 cycles. PCR products were stored at –20 °C.

2.2.14 Agarose Gel Electrophoresis of PCR Products

In order to examine the PCR products, 10 µL of PCR sample was mixed with 2 µL of 6X DNA loading dye. The samples were run on 2% agarose gel at 90 V for 1 h using the method as previously described.

2.2.15 Measurement of Cell Survival by 3-(4, 5-Dimethylthiazol-2-yl)-2-5-diphenyltetrazolium bromide (MTT)

The concentration of Imatinib that inhibited cell growth by 50% (IC_{50}) were determined from cell survival plots obtained by MTT or trypan blue exclusion assays as described (Ogretmen *et al*, 2001-2). In short, cells (2×10^4 cells/well) were plated into 96-well plates containing 100 μ l of the growth medium in the absence or presence of increasing concentrations of Imatinib at 37 °C in 5% CO₂ for 72 h. They were then treated with 5 μ l of MTT (5 mg/ml) for 4 h. After lysing the cells in 50 μ l of the lysis buffer, the plates were read in a microplate reader (Dynatech, Chantilly, USA) at 570 nm. After that, the IC_{50} concentrations of the compound were determined from cell survival plots as described.

2.2.16 Transient Transfection of Suspension Cells in 60 mm Dishes (6 Well Plates)

Transient transfection of K562 and Meg-01 cell lines with different mammalian expression vector system (pcDNA3, pcDNA3/SK-1, pcDNA3.1, pcDNA3.1/GCS, pCMVexSVneo, pCMVexSVneo/hLASS1, pCMVexSVneo/hLASS2, pCMVexSVneo/hLASS5 and pCMVexSVneo/hLASS6) was conducted using Effectene Transfection Reagent (Qiagen). Transfection was performed as described by the manufacturer.

The cells were split the day before transfection to maintain the viability. On the day of transfection, the cells were harvested by centrifugation, the supernatant was removed and the cells were washed once with PBS in a 15 mL Falcon tube. About 3×10^6 cells were seeded per 60 mm dish in 1.6 mL growth medium containing serum and antibiotics.

One μ g of plasmid DNA was diluted with the DNA-condensation buffer, Buffer EC, to a total volume of 100 μ L. The enhancer solution (6.4 μ L) was added on to sample, mixed by vortexing before incubated at room temperature for 5 min.

Effectene reagent (10 µL) was added on to the DNA–Enhancer solution, mixed well by pipetting up and down for 5 times. The samples were incubated for 10 min at room temperature to allow transfection-complex formation.

Growth medium containing serum and antibiotics (600) µL was added into the tube containing the transfection complex. The mixture was mixed by pipetting up and down twice and then added drop-wise onto the cells in the 60 mm dishes containing cells that were dissolved in 1.6 mL of media. The dish was gently swirled to ensure uniform distribution of the complexes.

2.2.17 Transfection of Cell Lines with siRNA

Transfection of different siRNA (hLASS1, SK-1 and scramble siRNA) was conducted using *DharmaFECT™* siRNA Transfection Reagents (Dharmacon, USA). Transfection was performed as described by the manufacturer.

siRNA (10 µL, Tube 1) and of *DharmaFECT* transfection reagent (4 µL, Tube 2) were diluted in 190 µL and 196 µL of serum-free medium, respectively.

The content of each tube was mixed gently by pipetting carefully up and down and was incubated for 5 min at room temperature. The contents of Tube 1 and Tube 2 were mixed well by pipetting and incubated for 20 min at room temperature.

The mixture was added drop-wise on to the 1.6 mL of complete medium including 25×10^4 cells in a 6-well plate. The cells were incubated at 37 °C in 5% CO₂ for 72 h. Total RNA was isolated and the levels of inhibition of gene expression were analyzed by RT-PCR. After 72 h of transfection the cells were treated with different concentrations of Imatinib for an extra 48 h and the effects of inhibition of desired genes on cell growth were determined by Tryphan Blue exclusion method.

2.2.18 Western Blotting Analyses

2.2.18.1 Protein Isolation

The protein levels of BCR-ABL, SK-1, Bcl-2, Bcl-XL, Bax and beta actin were detected by Western blot analysis (Sultan *et al*, 2006). The cells were centrifuged at 1,000 rpm for 2 min and resuspended in 100 µL of Lysis Buffer (Appendix A). The mixture was incubated on ice for 15 min and transferred into prechilled sterile 1.5 mL eppendorf tubes. The samples were homogenized by passing the lysate at least 5 times through a 20-gauge needle (0.9 mm diameter) and centrifuged at 12,000 rpm for 15 min at 4 °C. Then the supernatant was taken into another prechilled and sterile eppendorf tube and the concentration of protein was determined.

2.2.18.2 Determination of Protein Concentration by Bradford Assay

1 µL of each sample was taken into eppendorf tube that contains 200 µL of Bradford Dye and 799 µL of dH₂O. The mixture was vortexed and spun down. 200 µL of mixture was taken into 96 well-plates and read at 595 nm. The concentration of protein was calculated according to standards (Table 10). Protein concentrations in the samples are in µg/µL since the dilution factor is 1:1000 (1 µL + 799 µL H₂O + 200 µL Bradford dye).

Table 10. Standard Bovine serum albumin curve for the determination of protein concentrations.

	Bovine Serum Albumin (1 mg/mL) (Standards)	dH₂O	Bradford Dye
1	0 µL	800 µL	200 µL
2	1 µL	799 µL	200 µL
3	2 µL	798 µL	200 µL
4	4 µL	796 µL	200 µL
5	6 µL	794 µL	200 µL
6	8 µL	792 µL	200 µL
7	10 µL	790 µL	200 µL
8	15 µL	785 µL	200 µL

2.2.18.3 SDS Polyacrylamide Gel Electrophoresis (SDS-PAGE)

The samples were diluted by 1X PBS to a predetermined concentration and volume before mixing with the denaturing buffer.

Denaturation of proteins was achieved by mixing protein samples 1:1 with a 2X concentrate of sample buffer (Appendix B). The protein concentrations of all unknowns were typically adjusted to some standard concentration prior to mixing with sample buffer, so that the final concentration of protein is the same for all samples. The mixture was incubated at 95 °C for 5 min and was loaded into the wells. Both the upper and lower buffer compartments were filled with 1X (Tris/Glycine/SDS) running buffer (Appendix A). The samples and protein markers were loaded into the wells. Bio-Rad Prestained Standards (15 µL) were used in our studies as markers. The samples were run at 120 V until the dye run off bottom of the gel (~ 2 h).

The levels of proteins in polyacrylamide gels were determined by Coomassie Blue Dye staining (Appendix A). Excess dye was washed out by destaining solution (Appendix A) with acetic acid/methanol and agitation at room temperature.

2.2.18.4 Transfer of Proteins from Gel to Membrane

Proteins were transferred from 4-15% SDS-polyacrylamide gel to nitrocellulose membrane. The membrane was wetted with methanol, rinsed with dH₂O and finally washed with Towbin Buffer (Appendix A). Two pieces of filter paper (slightly bigger than gel) were washed with Towbin Buffer. Then the “sandwich” was assembled as 2 pieces of filter paper-gel-membrane-2 pieces of filter paper for Bio-Rad’s Transblot. Proteins were transferred to nitrocellulose membrane for 4 h at 0.12 Amp at room temperature. When the transfer was finished, the membrane was immersed in milk solution (Appendix A) at 4 °C for overnight and the container was sealed with wrap while the gel itself was soaked in coomassie blue stain. The next day the gel was washed with destaining solution for several times until clear bands were observed.

2.2.18.5 Detection of Desired Proteins by Specific Antibodies

After overnight incubation, the milk was removed and the membrane was washed with 1X PBS. Unnecessary parts of the membrane were removed and the membrane was placed in a small tray. 10 mL of 0.1% TBS Buffer (Appendix A) was added onto membrane and incubated for 5 min at room temperature. The buffer was replaced with new milk solution containing primary antibody and incubated for 1 h at room temperature. At the end of the primary antibody binding, the milk was removed and the membrane was washed in 0.1% TBS buffer 3 times total; 20 min, and two 5 min by refreshing the buffer at each time. Then fresh milk including secondary antibody was added onto the membrane and incubated for 1 h.

The membrane was then washed with 0.3% TBS buffer (Appendix A) 3 times; 20 min, 5 min and 5 min by refreshing the buffer at each time followed by 3 times washing in 0.1% TBS buffer (Appendix A) in a similar manner.

After removing all the buffers, the membrane was soaked in Developing Solution (1.5 mL from Solutions A & B, 1:1, Amersham Biosciences) and incubated for 5 min at room temperature. After drying excess liquid, nylon membrane was taken in between polyethylene plastic bags and taped onto autoradiography cassette. A film was exposed for 5 min in the dark room. Then the film was developed by an imaging machine (Konica Minolta Medical and Graphic-SRX-101A, Taiwan).

2.2.18.6 Stripping the Membranes

The membrane was incubated at 50 °C for 30 min in Stripping buffer in hybridization oven. The membrane was washed with 1X PBS for 10 min, two times. The membrane was blocked in milk solution overnight and starting from incubation of membrane in primary antibody, western blotting procedure was repeated.

2.2.19 Analysis of Cell Cycle Profiles

The effects of Imatinib and PDMP on the cell cycle profiles of K562, K562/IMA-0.2, Meg-01 and Meg-01/IMA-0.2 at 6 h, 24 h and 48 h were analyzed in the presence of DNase-free RNase and propidium iodine by flow cytometry as described previously (Ogretmen *et al*, 2001-2). Untreated cells were used as controls.

2.2.19.1 Fixation

After treatment, cells (at least 5×10^5) were harvested and collected. Then the cells were suspended in 1 mL of cold PBS and were fixed by adding 4 mL of -20 °C absolute ethanol. Finally the cells were stored at -20 °C.

2.2.19.2 Staining

Fixed cells were thawed and centrifuged at 1,200 rpm at of 4°C for 5 min and resuspended in 1 mL of PBS. DNase-free RNase A (100 µL, 200 µg/mL) was added and the mixture was incubated at 37 °C for 30 min. Then 100 µL of propidium iodide (1 mg/mL) was added and incubated at room temperature for 10 min. The samples were placed in 12×75 Falcon tubes and read on Becton Dickinson FACStarPLUS in Flow Cytometry Facility (MUSC, USA).

2.2.20 Determination of Caspase-3 Activity

Caspase-3 Fluorometric Assay Kit (R & D Systems) was used for the detection of caspase-3 activity. The activity assay was performed as described by the manufacturer.

Cells that have been induced to undergo apoptosis were collected by centrifugation in a Falcon tube at 1,000 rpm for 3 min. The supernatant was gently removed and discarded while the cell pellet was lysed by the addition of the Lysis Buffer. The amount of Lysis Buffer to be added to the pellet was determined by the number of cells present. Cold Lysis Buffer (100 µL) was added per 1×10^6 cells. The cell lysate was incubated on ice for 10 min before centrifugation at 12,000 rpm for 5 min. The protein content of the cell lysate was determined using a protein determination assay as described previously in 2.2.19-2. The enzymatic reaction for caspase activity was carried out in a 96-well flat bottom microplate that can be read with a microplate reader equipped with fluorescence detection capabilities.

For each reaction 25 µL of cell lysate, 25 µL of 2X Reaction Buffer 3 (Prior to using the 2X Reaction Buffer 3, 10 µL of fresh DTT stock was added per 1 mL of 2X Reaction Buffer 3) and 2.5 µL of Caspase-3 fluorogenic substrate (DEVD-AFC) were added into one of 96 well flat bottom microplate and mixed well. The plate was incubated at 37 °C for 2 h in a 5% CO₂ incubator.

The plate was read on a fluorescent microplate reader using filters that allow light excitation at 400 nm wavelength and can collect emitted light at 505 nm wavelength.

2.2.21 Detection of Mitochondrial Membrane Potential

JC-1 Mitochondrial Membrane Potential Detection Kit™ (Cell Technology) was used for the detection of changes in mitochondrial membrane potential. The detection was performed as described by the manufacturer.

Cells were cultured to a density not to exceed 1×10^6 cells/mL. Apoptosis was induced by application of different concentrations of Imatinib. Cell suspension was transferred into a sterile Falcon tube. The cells in suspension were centrifuged for 5 min at room temperature at 1,000 rpm and supernatant was removed carefully. Cells were resuspended in 0.5 mL 1X JC-1 Reagent solution prepared under Dilution of JC-1 Reagent. The cells were incubated at 37 °C in a 5 % CO₂ incubator for 15 min, centrifuged for 5 min at 1,000 rpm and supernatant was removed. The cell pellet was resuspended in 2 mL cell culture medium followed by centrifugation. The supernatant was removed and once more washed with 2 mL cell culture medium. The cell pellet was resuspended in 0.5 mL fresh cell culture medium and flow cytometry analyses were performed immediately.

2.2.22 Measurement of Total Endogenous Ceramide Levels by LC/MS

Cells were collected by centrifugation at 1,000 rpm for 3 min after treatment. 50 µL of internal standard was added directly onto each sample to monitor extraction efficiency and calculate ceramide concentrations and mixed well by vortex. 2 mL of JB Cell Extraction Mix (Appendix A) was added to each sample and mixed well. The samples were centrifuged at 3,000 rpm for 5 min. The supernatant was transferred to a new glass tube and an additional 2 mL of JB Solvent was added and centrifuged

again at 3,000 rpm for 5 min. After the second centrifugation of the cell pellets/sample, the additional 2 mL of cell extraction was transferred to the previous 2 mL. From the 4 mL of sample/cell extract, 1 mL was transferred to a separate glass tube for sphingomyelin extraction and 0.5 mL aliquot was also removed for Pi determination. The remaining 2.5 mL was concentrated to dryness under nitrogen and then resuspended in Mobile Phase B Solvent (Appendix A) prior to analyses of endogenous sphingosine and ceramides. The samples were analysed by Reverse Phase-Liquid Chromatography-Mass Spectrophotometry (LC-MS) (Agilent, 1100-HPLC, Finnigan, TSQ 7000- Mass Spectrophotometry) in Lipidomics Core Facility (MUSC, USA).

2.2.22.1 Determination of Inorganic Phosphate (Pi) Concentrations

0.5 mL of the 4 mL total extracted lipids was dried. Then 3 mL of Chlorofom: Methanol (1:2), 0.8 mL of dH₂O, 1 mL of chloroform and 1 mL of dH₂O were added onto the samples respectively. After addition of each, the mixture was vortexed well. The mixture was centrifuged at 3,000 rpm for 5 min. Upper phase was removed by aspiration while the bottom phase (~2 mL) was saved.

Each sample (0.5 mL) were taken and dried using a heating block at 80 °C for 30 min. 0.6 mL of Ashing Buffer (Appendix A) was added both on samples and standards. After vortexing well, all the samples were put in heating block and incubated overnight at 160 °C. The samples were always put in a cold heating block and then set to 160 °C. After removal from the heating block, 0.9 mL dH₂O, 0.5 mL of 9% Ammonium Molybdate and 0.2 mL 9% Ascorbic Acid (Always made freshly) were added onto mixture and vortexed well. The samples were put in water bath at 45 °C for 30 min. The samples were read at 600 nm using Spectrophotometer. The Pi values of the samples were calculated according to known standards of NaH₂PO₄ (0-80 nM).

2.2.23 Analysis of the Endogenous Ceramide Synthase and Sphingosine Kinase Activities by LC/MS

Endogenous enzyme activities of (dihydro)ceramide synthase, and sphingosine kinase for the generation of ceramide and sphingosine-1-phosphate were measured by LC/MS after pulsing the cells 17C-dihydrosphingosine that contains 17-carbons, while its natural analogue contains 18-carbons, as described previously (Sultan *et al*, 2006 and Schulz *et al*, 2006). The *in vitro* enzyme activity of ceramide synthase was also measured using microsomal preparations of the cells by monitoring the conversion of [³H]dihydrosphingosine into ceramides in the presence of stearoyl- or palmitoyl CoAs by thin layer chromatography as described previously (Lahir *et al*, 2005).

CHAPTER 3

RESULTS

3.1 LONG-TERM EXPOSURE TO INCREASING CONCENTRATIONS OF IMATINIB RESULTS IN THE DEVELOPMENT OF RESISTANCE TO APOPTOSIS

To explore the mechanisms involved in the development of resistance to Imatinib-induced apoptosis, human K562 and Meg-01 CML cells were exposed to step-wise increasing concentrations of the drug (50- to 1,000 nM) for several months, and the sub-clones that expressed resistance were selected. First, the degree of resistance was determined by measuring the IC₅₀ values of Imatinib at 72 hr using MTT assay.

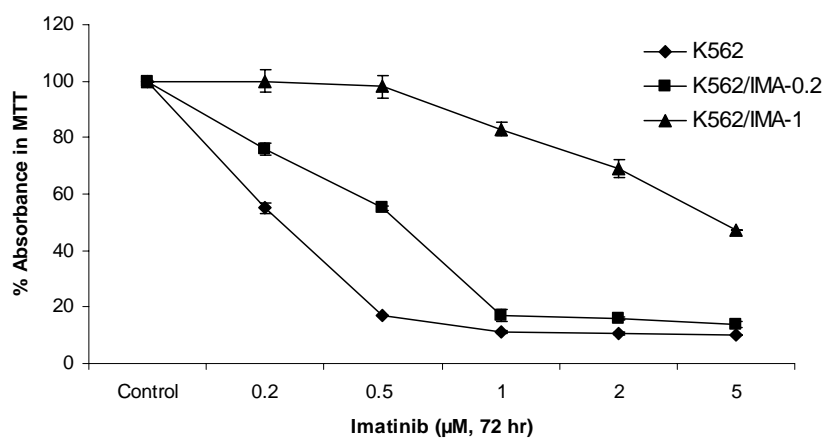


Figure 16. Effects of Imatinib on the growth of K562, K562/IMA-0.2 and -1 cells *in situ*. The IC₅₀ concentration of Imatinib was determined by MTT assay for each cell

line. Experiments were done in triplicate in at least two independent experiments, and statistical analysis was done using two way anova, $p<0.01$ was considered significant. Standard deviations for each point were between 0.5- and 4%. The error bars represent the standard deviations, and when not seen, they are smaller than the thickness of the lines on the graphs.

As shown in Figure 16, K562 cells that survived upon chronic exposure to 200- or 1000 nM Imatinib, which were referred to as K562/IMA-0.2 and -1, respectively, expressed about 2.3- to 19-fold resistance, as compared to their parental sensitive counterparts. The inhibitory concentration (IC_{50}) values of Imatinib that inhibits growth by 50% in these cells were 240-, 565- and 4,600 nM for K562, K562/IMA-0.2, and -1 cells, respectively (Figure 16). Similarly, treatment with 200- and 500 nM Imatinib (48 hr) decreased the viability of K562 cells about 30- and 50%, respectively, whereas there was no significant change in the viability of resistant cells in response to Imatinib at these concentrations as measured by trypan blue exclusion assay (Figure 17).

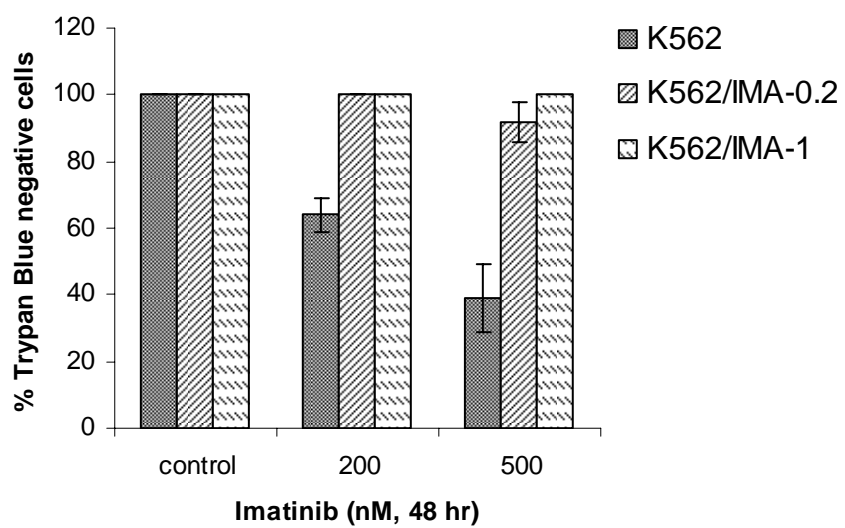


Figure 17. The effect of Imatinib on cell viability of K562, K562/IMA-0.2 and -1 cells. Cells, grown in 6-well plates (5×10^4 cells/well), were treated in the absence or presence of Imatinib (48 hr). Cell viability was determined using trypan blue dye exclusion assay. Experiments were done in duplicates in at least two independent

experiments. Error bars represent standard deviations. Statistical analysis was done Two Way Anova, and $p < 0.01$ was considered significant.

Subpopulations of Meg-01 cells which were able to grow in the presence of 0.2- and 1 μM Imatinib, were also selected, and referred to as Meg-01/IMA-0.2 and -1, respectively. Then, the IC_{50} values of Imatinib in these cells were determined and compared to parental sensitive cells. As shown in Figure 18, Meg-01/IMA-0.2 and -1 cells expressed about 2- to 5-fold resistance, as compared to parental Meg-01 cells. The IC_{50} values of Imatinib were 340-, 650- and 1,500 nM for Meg-01, Meg-01/IMA-0.2, and -1 cells, respectively (Figure 18).

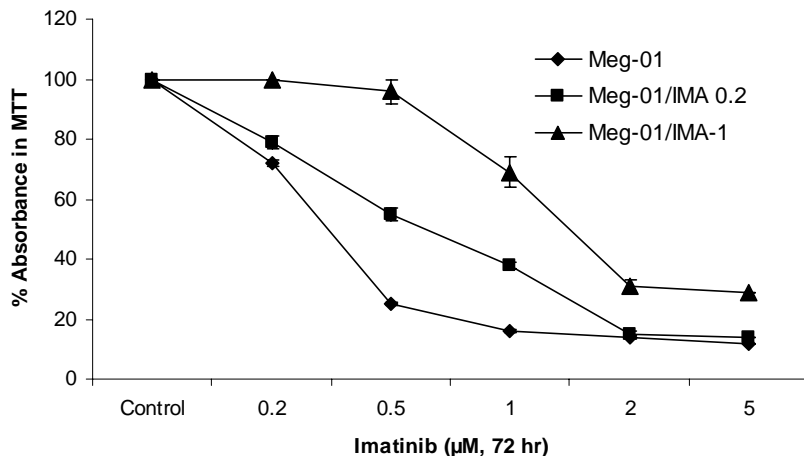


Figure 18. Effects of Imatinib on the growth of Meg-01, Meg-01/IMA-0.2 and -1 cells *in situ*. The IC_{50} concentration of Imatinib was determined by MTT assay for each cell line. Experiments were done in triplicate in at least two independent experiments, and statistical analysis was done using two way anova, $p < 0.01$ was considered significant. Standard deviations for each point were between 0.5- and 4%. The error bars represent the standard deviations, and when not seen, they are smaller than the thickness of the lines on the graphs.

On the other hand, treatment with 200- and 500 nM Imatinib (48 hr) decreased the viability of Meg-01 cells about 20- and 40%, respectively, whereas there was no change in the viability of Meg-01/IMA-1 cells in response to Imatinib at these concentrations. In case of Meg-01/IMA-0.2 cells, there was 2- and 15%

decrease in cell viability comparing the sensitive cells as measured by trypan blue exclusion assay (Figure 19) which is not significant. There were no death K562/IMA-1 cells in response to these concentrations of Imatinib.

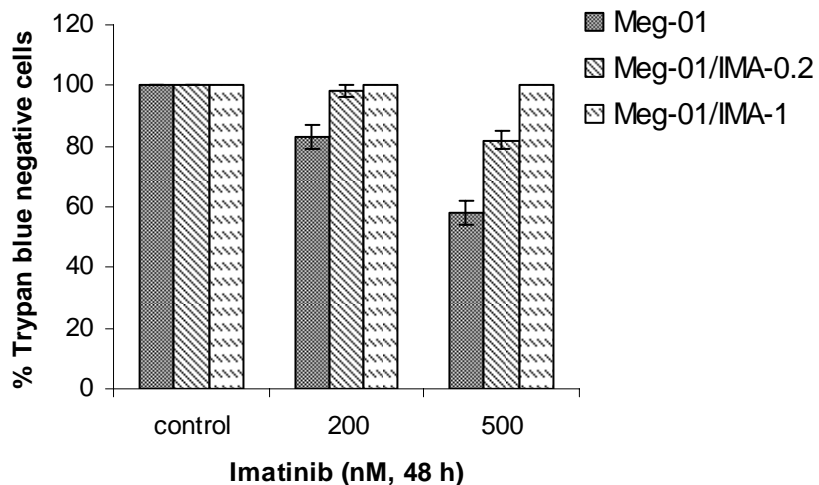


Figure 19. The effect of Imatinib on cell viability of Meg-01, Meg-01/IMA-0.2 and -1 cells. Cells, grown in 6-well plates (5×10^4 cells/well), were treated in the absence or presence of Imatinib (48 hr). Cell viability was determined using trypan blue dye exclusion assay. Experiments were done in duplicates in at least two independent experiments. The error bars represent the standard deviation. Statistical analysis was done using two way anova, $p < 0.01$ was considered significant.

3.1.1 Cell Cycle Profiles in Parental and Resistant Cells

The cell cycle profiles of parental and resistant cells were examined by flow cytometry. The data revealed that while exposure to 500 nM Imatinib (48 hr) caused apoptosis in about 70% of the population in parental K562 cells (Figure 20), there was no detectable apoptosis in resistant K562/IMA-0.2 cells (Figure 21). There were no significant changes in the cell cycle profiles of K562 and K562/IMA-0.2 cells in the absence or presence of Imatinib (Figures 20 and 21).

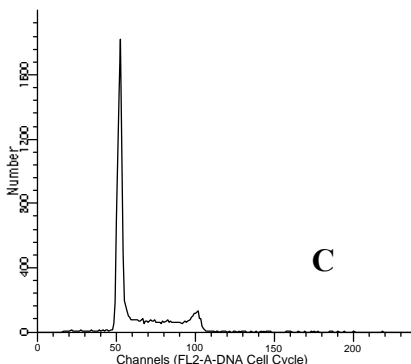
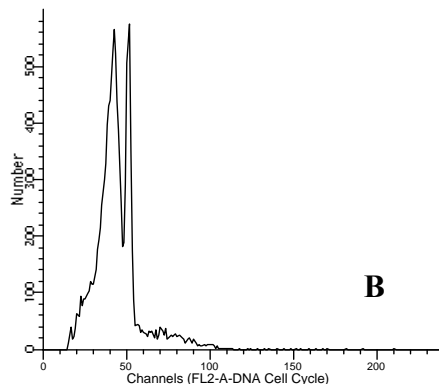
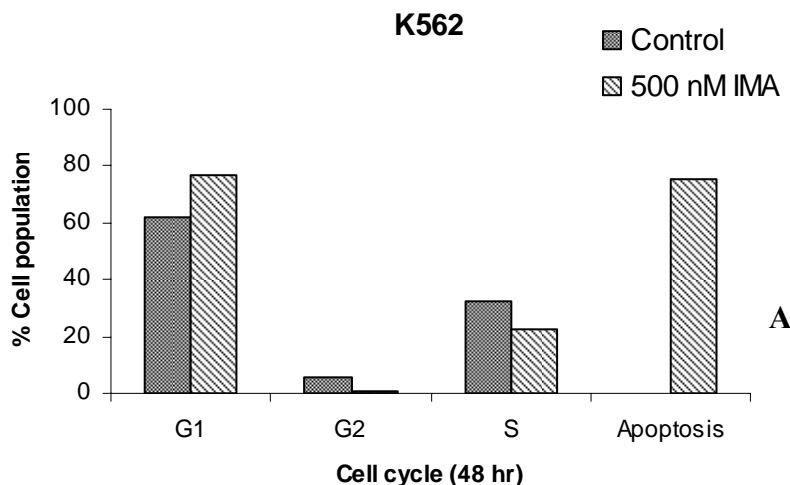


Figure 20. (A) Cell cycle profiles of K562 cells in response to 500 nM Imatinib. The effects of Imatinib (B) on cell cycle profiles of K562 cells were determined and compared to that of untreated cells (C) using flow cytometry. Statistical significance was determined using Two Way Anova, and $p < 0.05$ was considered significant.

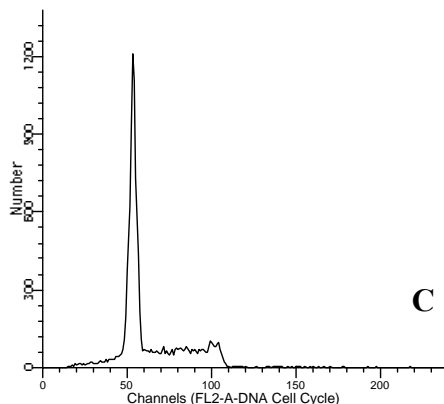
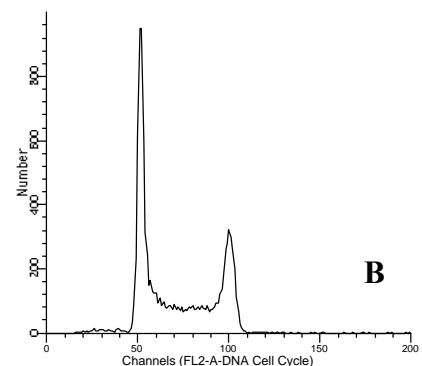
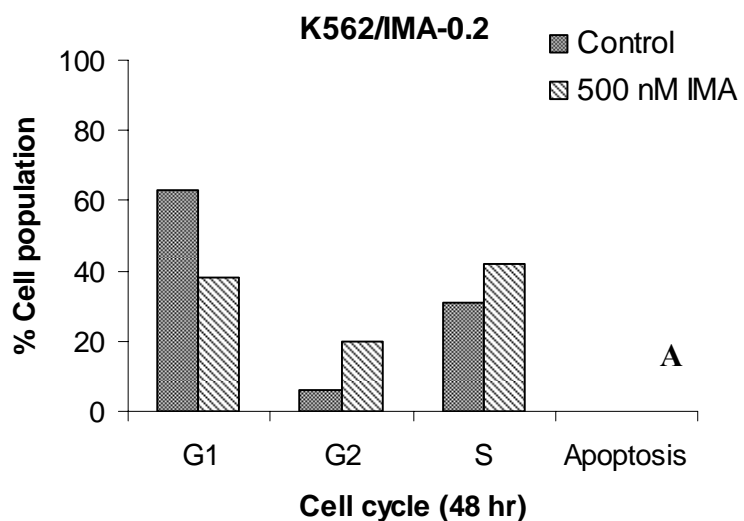
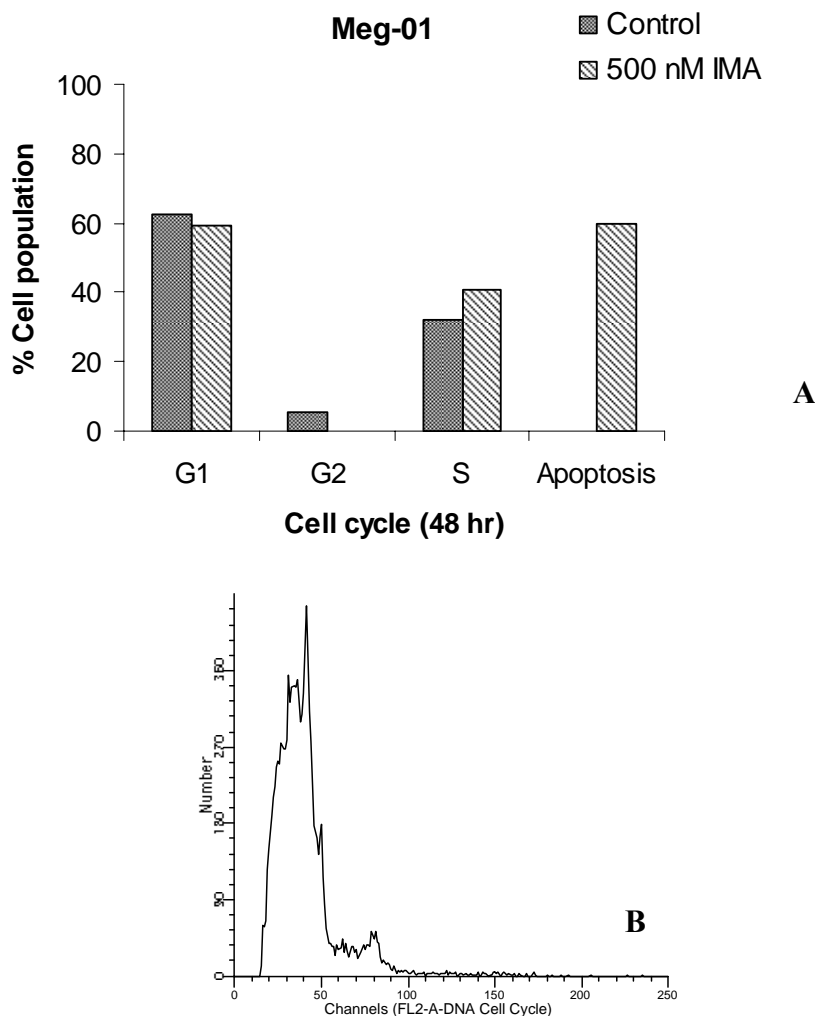


Figure 21. (A) Cell cycle profiles of K562/IMA-0.2 cells in response to 500 nM Imatinib. The effects of Imatinib (B) on cell cycle profiles of K562/IMA-0.2 cells were determined and compared to that of untreated cells (C) using flow cytometry. Statistical significance was determined using Two Way Anova, and $p < 0.05$ was considered significant.

The cell cycle profile studies for Meg-01 cells revealed that while exposure to 500 nM Imatinib (48 hr) caused apoptosis in about 60% of the population in parental Meg-01 cells (Figure 22), there was only 14% apoptosis in resistant Meg-01/IMA-0.2 cells (Figure 23). There were no significant changes in the cell cycle profiles of Meg-01/IMA-0.2 cells as compared to their parental sensitive counterparts (Figures 22 and 23).

These data demonstrate that continuous exposure of Imatinib results in the selection of cells that express resistance to Imatinib-induced cell death in human K562 and Meg-01 cells.



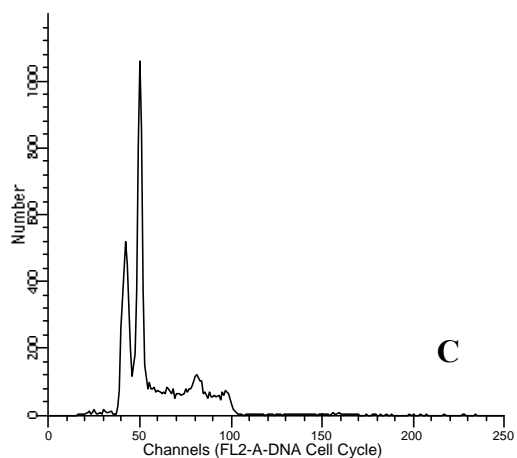
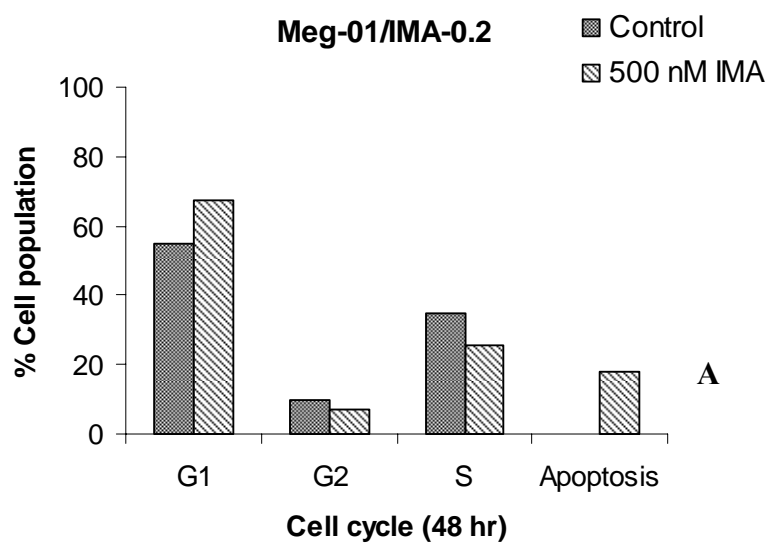


Figure 22. (A) Cell cycle profiles of Meg-01 cells in response to 500 nM Imatinib. The effects of Imatinib (B) on cell cycle profiles of Meg-01 cells were determined and compared to that of untreated cells (C) using flow cytometry. Statistical significance was determined using Two Way Anova, and $p < 0.05$ was considered significant.



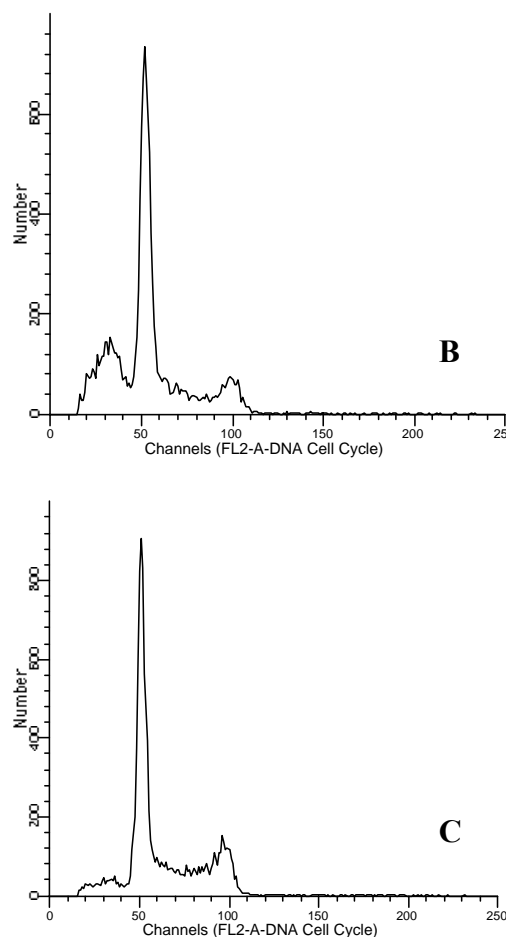


Figure 23. Cell cycle profiles of Meg-01/IMA-0.2 cells in response to 500 nM Imatinib. The effects of Imatinib (500 nM, 48 hr) on cell cycle profiles of Meg-01/IMA-0.2 cells were determined and compared to that of untreated cells using flow cytometry. Statistical significance was determined using Two Way Anova, and $p<0.05$ was considered significant.

3.1.2 Caspase-3 Activity in Parental and Resistant Cells

The activation of pro-caspase-3 of parental and resistant K562 cells was measured using the caspase-3 activity assay by fluorescent spectrophotometer. Treatment of parental K562 cells with Imatinib (200- and 500 nM, 48 hr) resulted in a significant activation of caspase-3 (about 10- and 13-fold, respectively), whereas

treatment of K562/IMA-0.2 and -1 cells at these concentrations did not have any significant effects on the activation of caspase-3 (Figure 24). In untreated controls, there was a parallel decrease in steady state levels of caspase-3 activity with increasing degree of resistance. Thus, these data confirmed that K562/IMA-0.2 and -1 cells exert significant resistance to Imatinib-induced caspase activation.

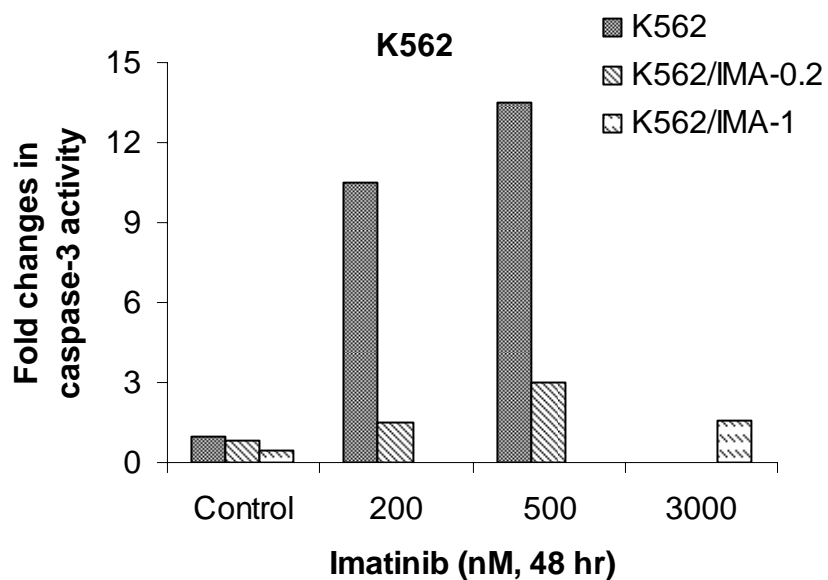


Figure 24. Caspase-3 activity in parental and resistant cells. Caspase-3 activity was measured in K562, K562/IMA-0.2 and -1 cells. The error bars represent the standard deviations. Experiments were done in duplicates in at least two independent experiments, and statistical analysis was done using two way anova, $p<0.01$ was considered significant.

3.1.3 Mitochondrial Membrane Potential in Parental and Resistant Cells

Mitochondrial membrane potential was measured in K562, K562/IMA-0.2 and -1 μM cells using the JC-1 mitochondrial membrane potential detection kit by flow cytometry. Treatment with Imatinib (200- and 500 nM, 48 hr) caused a significant loss of MMP, as measured by increased accumulation of cytoplasmic monomeric form of JC-1, in parental K562, but not in resistant K562/IMA-0.2 cells (Figure 25). Steady state levels of mitochondrial membrane potential were increased

in parallel with increasing the levels of resistance in untreated controls. Thus, these data confirmed that K562/IMA-0.2 and -1 cells exert significant resistance to Imatinib-induced loss of MMP.

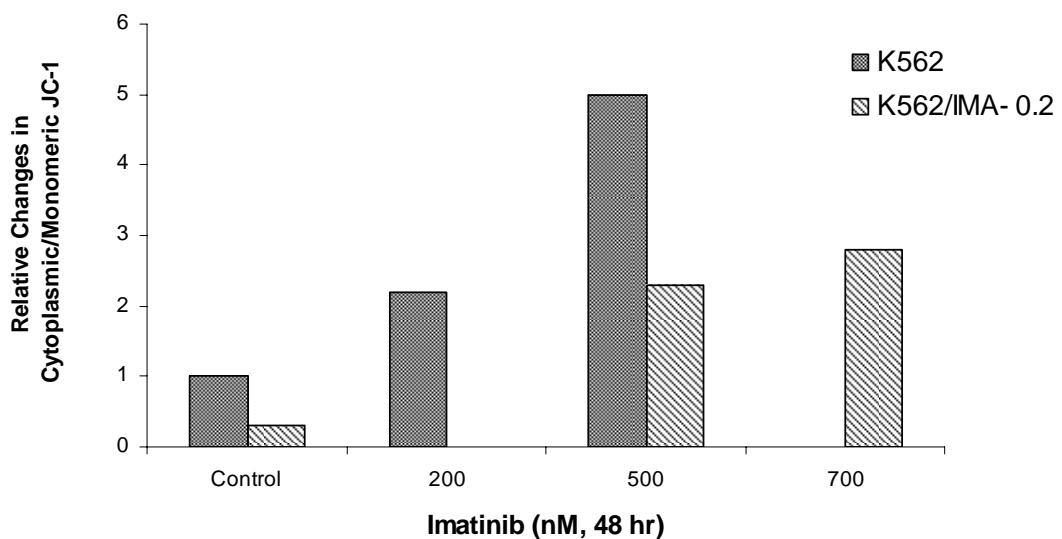


Figure 25. Mitochondrial membrane potential in parental versus resistant cells. Statistical significance was determined using Two Way Anova, and $p < 0.01$ was considered significant.

3.1.4 Protein Levels of Pro-Apoptotic and Anti-Apoptotic Genes in Parental and Resistant Cells

Protein levels of pro-apoptotic Bcl-2 and Bcl-XL in K562 and K562/IMA-1 (Figure 26) and in Meg-01 and Meg-01/IMA-1 (Figure 27) cells were determined. As shown in Figure 26, protein levels of Bcl-2 and Bcl-XL were increased in K562/IMA-1 cells as compared to parental sensitive cells. On the other hand, protein levels of pro-apoptotic Bax was decreased in K562/IMA-1 cells comparing to parental sensitive cells. There was no change in the protein levels of beta actin gene, an internal positive control, in parental and resistant cells indicating that there was no experimental error related to mis-loading. Quantification analyses of Bcl-2, Bcl-XL and Bax protein levels were conducted by Scion Image programme and the results showed that there was around 2-, 1.8- and 0.5-fold increase in protein level of Bcl-2,

Bcl-XL and Bax genes, respectively, in K562/IMA-1 cells as compared to parental K562 cells.

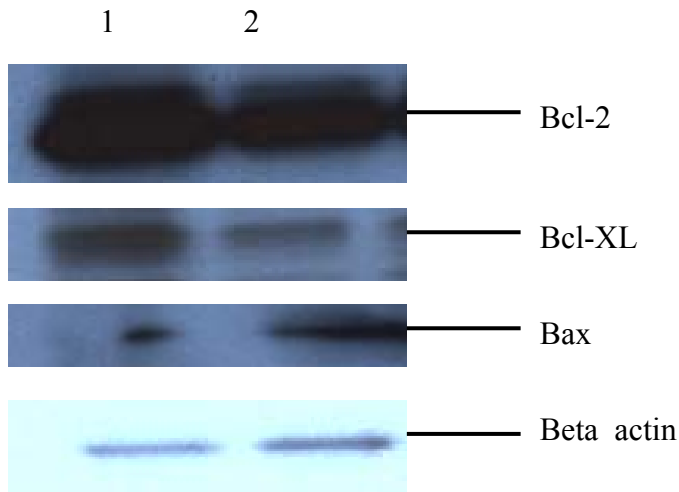


Figure 26. Protein levels of anti-apoptotic and pro-apoptotic genes in parental and resistant K562 cells. Bcl-2, Bcl-XL and Bax protein levels in K562/IMA-1 (lane 1) and K562 (lane 2) cells were measured by western blotting. Beta actin protein levels were detected as an internal positive control (Lanes 1 and 2).

As shown in Figure 27, protein levels of Bcl-2 was increased in Meg-01/IMA-1 cells as compared to parental sensitive cells but there was also a decrease in Bcl-XL in resistant cells. On the other hand, There was no significant changes in protein levels of pro-apoptotic Bax in Meg-01/IMA-1 cells comparing to parental sensitive cells. There was no change in the protein levels of beta actin gene in parental and resistant cells.

Quantification analyses of Bcl-2, Bcl-XL and Bax protein levels were conducted by Scion Image programme and the results showed that there was around 2.5-, 0.8 and 1.3 fold increase in protein level of Bcl-2, Bcl-XL and Bax genes, respectively, in Meg-01/IMA-1 cells as compared to parental K562 cells.

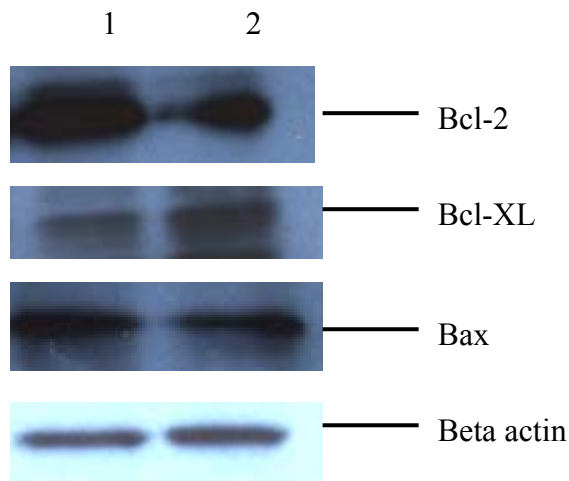


Figure 27. Protein levels of anti-apoptotic and pro-apoptotic genes in parental and resistant Meg-01 cells. Bcl-2, Bcl-XL and Bax protein levels in Meg-01/IMA-1 (lane 1) and Meg-01 (lane 2) cells were measured by western blotting. Beta actin protein levels were detected as an internal positive control (Lanes 1 and 2).

3.1.5 Increased Ceramide Synthesis might be Involved in the Regulation of Imatinib-Induced Apoptosis

To examine whether ceramide synthesis/metabolism is involved in mechanisms responsible for Imatinib resistance, the levels of endogenous ceramide in K562 and K562/IMA-0.2 cells, treated in the absence or presence of Imatinib (500 nM, 48 hr), were measured by LC/MS. Interestingly, the data showed that treatment with Imatinib resulted in a significant increase in the generation of C₁₈-ceramide (about 30-fold), and to a lesser extent, C₁₄-, C₁₆-, and C₂₀-ceramides (around 2- to 8-fold) in parental K562 cells when compared to untreated controls (Figures 28A and 28B). On the other hand, treatment of resistant K562/IMA-0.2 cells with Imatinib (500 nM, 48 hr) did not cause any significant changes in the levels of these ceramides (Figures 28A and 28B). The absolute levels of C₁₈-ceramide were 0.053 and 1.64 in K562 and 0.043 and 0.074 pmol/nmol Pi in K562/IMA-0.2 cells, in the absence or presence of Imatinib, respectively (Figure 28A). It was clearly demonstrated in Figure 28C that the levels of C₁₈-ceramide were increased at most in response to Imatinib comparing to other ceramides.

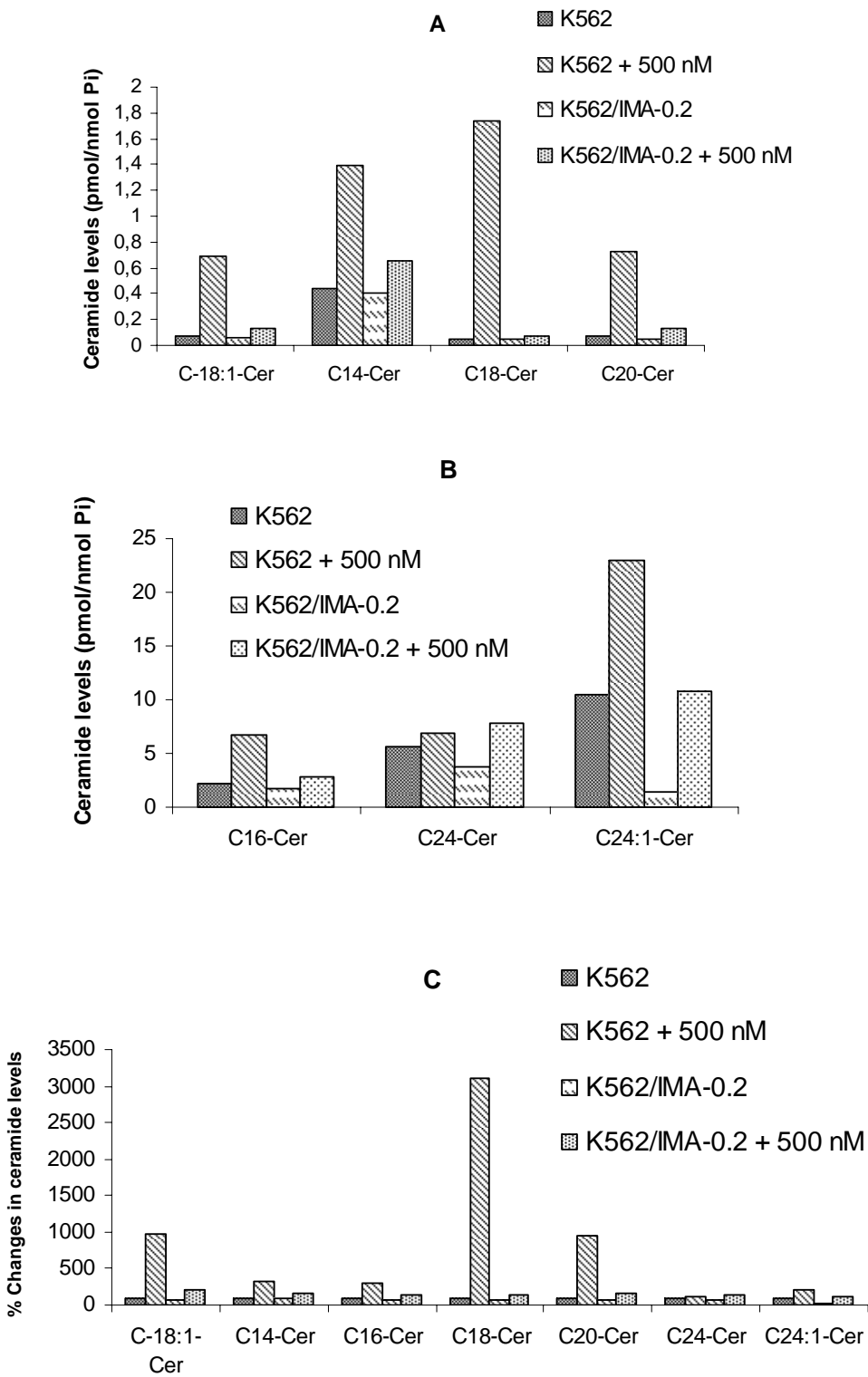


Figure 28. Analysis of ceramide levels in parental and resistant cells in response to Imatinib. The concentrations of C₁₄-, C₁₈-, C_{18:1}-, and C₂₀-ceramides (A), and C₁₆-, C₂₄-, and C_{24:1}- ceramides (B) in K562 and K562/IMA-0.2 cells in the absence or

presence of Imatinib were measured by LC/MS. The levels of ceramide were normalized to Pi concentrations. (C) Percent changes of the levels of ceramide levels were calculated for K562 and K562/IMA-0.2 cells that were exposed to 500 nM Imatinib. The experiments were performed in at least two independent trials. Statistical significance was determined using Two Way Anova, and $p < 0.01$ was considered significant.

Moreover, the effects of Imatinib on the generation of endogenous ceramide was further investigated by measuring the levels of C₁₄- and C₁₈-ceramide after treatment of parental K562 cells with Imatinib (500 nM) for various time points (0-, 12-, 24- and 48 hr). The data showed that C₁₈-ceramide levels increased in a time-dependent manner in response to treatment with Imatinib by about 4-, 10-, and 30-fold at 12-, 24- and 48 hr, respectively, when compared to untreated controls (Figure 29). However, C₁₄-ceramide levels were not increased as much as C₁₈-ceramide in a time-dependent manner in response to treatment with Imatinib. After 48 hr, treatment with 500 nM Imatinib, C₁₄-ceramide levels were increased about only 6-fold, when compared to untreated controls (Figure 29).

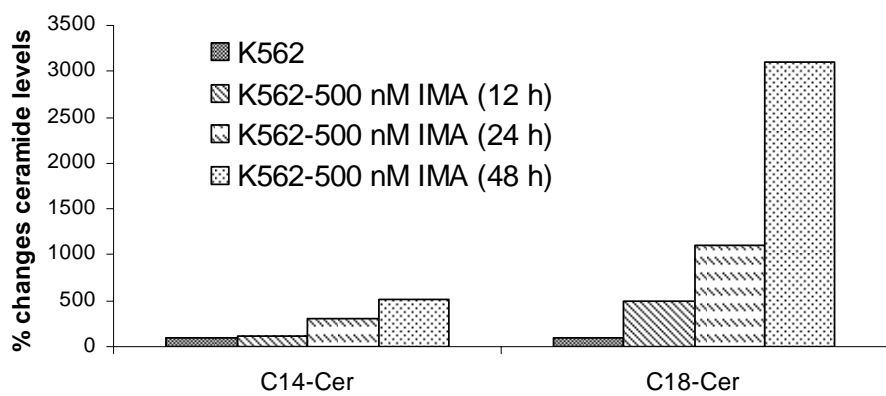
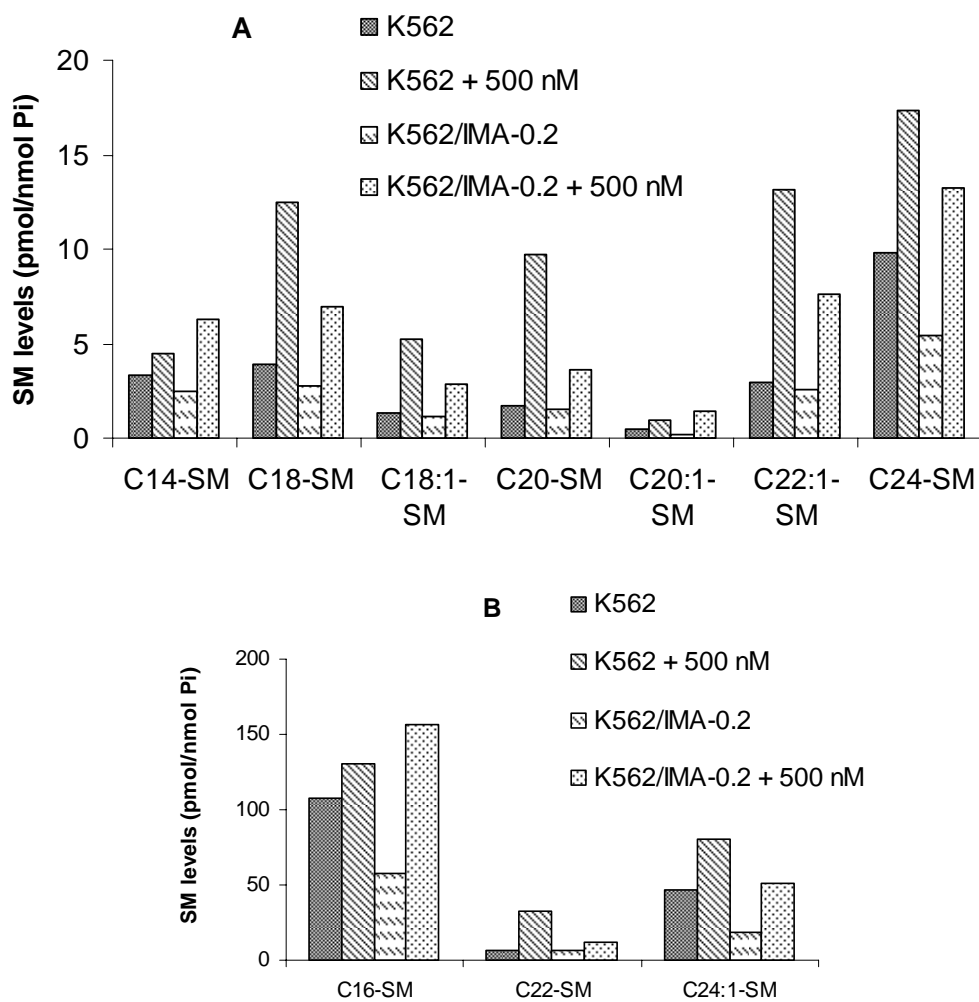


Figure 29. Analysis of C₁₄- and C₁₈-ceramide levels in K562 cells in different time points in response to Imatinib. Percent changes of the levels of C₁₄- and C₁₈-ceramide levels were measured by LC/MS and calculated for K562 cells that were exposed to 500 nM Imatinib for 12-, 24-, and 48 hr. The levels of ceramide were normalized to Pi concentrations. The experiments were done in at least two

independent trials. Statistical significance was determined using Two Way Anova, and $p < 0.01$ was considered significant.

Interestingly, the levels of SMs were also increased in both parental and resistant cells after treatment with Imatinib (500 nM, 48 hr) (Figures 30A and 30B). Besides actual changes in SM concentrations, percent changes in SM levels, as shown in Figure 30C, also clearly showed that there was no decrease in SM levels in response to Imatinib. These results strongly suggest that increased ceramide levels in response to Imatinib are due to *de novo* synthesis, and not due to hydrolysis of sphingomyelin.



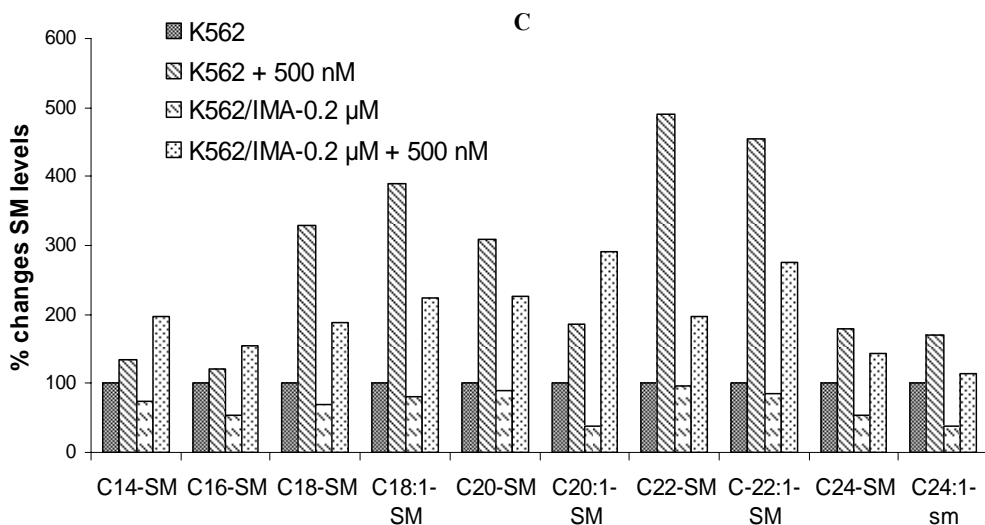


Figure 30. Analysis of sphingomyelin levels in parental and resistant cells in response to Imatinib. The concentrations of C14-, C18-, C18:1-, C20-, C20:1-, C22-, and C22:1-sphingomyelins (A), and C16-, C24-, and C24:1-sphingomyelins (B) in K562 and K562/IMA-0.2 cells in the absence or presence of Imatinib were measured by LC/MS. The levels of sphingomyelin were normalized to Pi concentrations. (C) Percent changes of the levels of sphingomyelins were calculated for K562 and K562/IMA-0.2 cells. The experiments were done in at least two independent trials. Statistical significance was determined using Two Way Anova, and $p<0.01$ was considered significant.

Therefore, these data suggest that increased ceramide generation and/or accumulation might be involved in mediating Imatinib-induced apoptosis, and that defect in C_{18} -ceramide generation and/or metabolism might play a role in increased resistance to Imatinib-induced apoptosis in these cells.

3.2 ROLE OF hLASS1, WHICH SPECIFICALLY INVOLVED IN THE GENERATION OF C₁₈-CERAMIDE, IN IMATINIB-INDUCED CELL DEATH

As shown in Figure 29 and 30, Imatinib treatment elevated the levels of mainly C₁₈-ceramide, and SM levels, which suggested a role for a human homologue of yeast longevity assurance gene 1 (hLASS1), which is known to regulate the generation of specifically C₁₈-ceramide. Therefore, to test any possible roles of hLASS1 and C₁₈-ceramide in Imatinib-induced apoptosis, the expression of hLASS1 was partially inhibited using siRNA, and its effects on cell viability in response to Imatinib (500 nM, 48 hr) were examined by trypan blue assays, and compared to the effects of control (non-targeting, scrambled) siRNA, in parental K562 cells. As seen in Figure 31, partial inhibition of hLASS1 expression resulted in about 35% reduction in steady-state levels of C₁₈-ceramide when compared to controls. More impressively, inhibition of hLASS1 expression by siRNA almost completely prevented the induction of C₁₈-ceramide generation in response to 500 nM Imatinib (48 hr) in these cells, demonstrating a role of Imatinib in the regulation of C₁₈-ceramide generation via hLASS1 activity (Figure 31). The levels of C₁₈-ceramide were 0.038, 1.180 and 0.025 and 0.062 pmol/nmol Pi in cells transfected with control and hLASS1 siRNAs in the absence or presence of Imatinib, respectively.

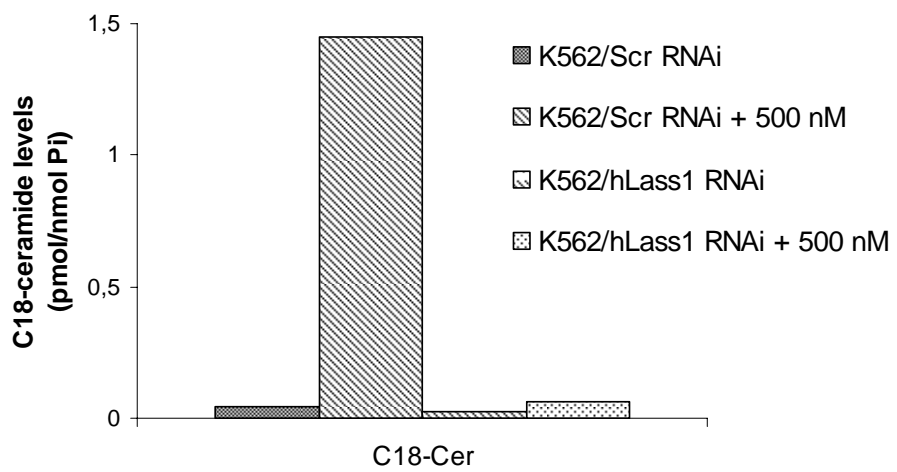


Figure 31. The concentrations of C₁₈-ceramide in control and hLASS1 siRNA transfected K562 cells. Concentrations of C₁₈-ceramide in these cells were examined

by LC/MS. The levels of C₁₈-ceramide were normalized to Pi concentrations. The experiments were done in at least two independent trials. Statistical significance was determined using One Way Anova, and p<0.01 was considered significant.

Importantly, hLASS1 siRNA partially but significantly prevented (about 50%) cell death in response to Imatinib (500 nM, 48 hr) (Figure 32). Specifically, treatment with 500 nM Imatinib resulted in about 45% cell death in response to control siRNA, whereas Imatinib caused around 23% growth inhibition in hLASS1 siRNAs transfected cells, respectively (Figure 32). These data, therefore, demonstrated an important and novel role for hLASS1 via the generation of C₁₈-ceramide in Imatinib-induced cell death in K562 cells.

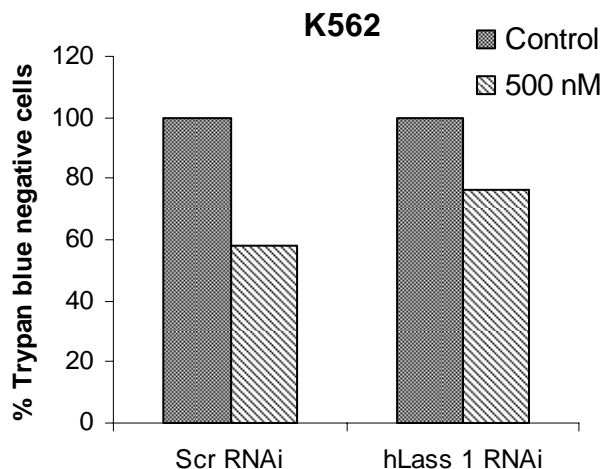


Figure 32. Cell viability of control and hLASS1 siRNA transfected K562 cells. Cell viability was determined by trypan blue dye exclusion assay. Experiments were done in duplicates in at least two independent experiments. Statistical significance was determined using Two Way Anova, and p < 0.01 was considered significant.

3.2.1 Overexpression of hLASS1 in Resistant K562/IMA-0.2 and -1 Cells Increased Sensitivity to Imatinib

The involvement of hLASS1/C₁₈-ceramide pathway in Imatinib-induced cell death were shown in K562/IMA-0.2 and -1 cells, which were transiently transfected

with an expression vector containing the full length hLASS1 cDNA, and then the effects of overexpression of hLASS1 on Imatinib-induced apoptosis were examined by trypan blue dye exclusion assay. As shown in Figure 33, treatment with 1 μ M Imatinib resulted in about 1.5-fold increase in the number of death K562/IMA-0.2 cells, whereas Imatinib caused around 3.5-fold increase in hLASS1 transfected K562/IMA-0.2 cells (Figure 33).

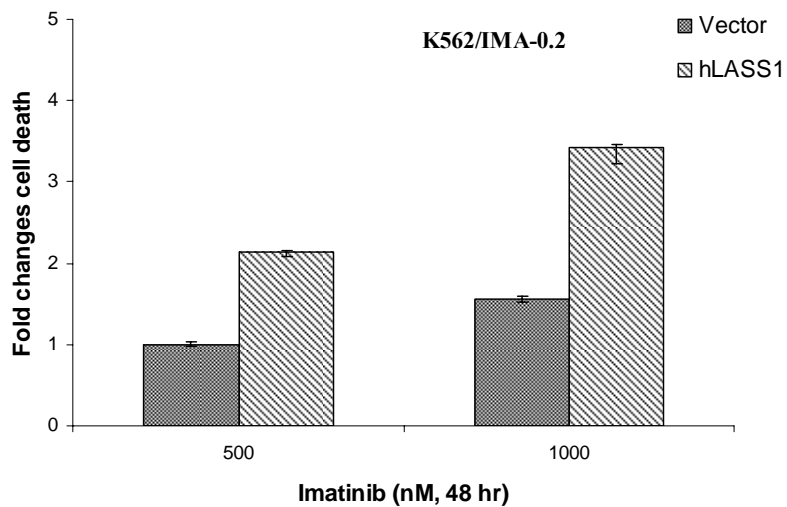


Figure 33. The role of overexpression of hLASS1 in the inhibition of apoptosis (by fold changes in cell death) in K562/IMA-0.2 cells. The effect of Imatinib on cell viability of hLASS1 and vector (control) transfected and Imatinib treated K562/IMA-0.2 cells was determined using trypan blue dye exclusion assay. Cells, grown in 6-well plates (5×10^4 cells/well), were treated in the absence or presence of Imatinib (48 hr). Experiments were done in duplicates in at least two independent experiments, and statistical analysis was done using two way anova, $p < 0.01$ was considered significant.

Similarly, overexpression of hLASS1 in resistant K562/IMA-1 cells further enhanced apoptosis, as determined by trypan blue staining in response to 2- and 5 μ M Imatinib (48 hr) by about 2.5- and 3-fold, when compared to vector transfected cells (Figure 34).

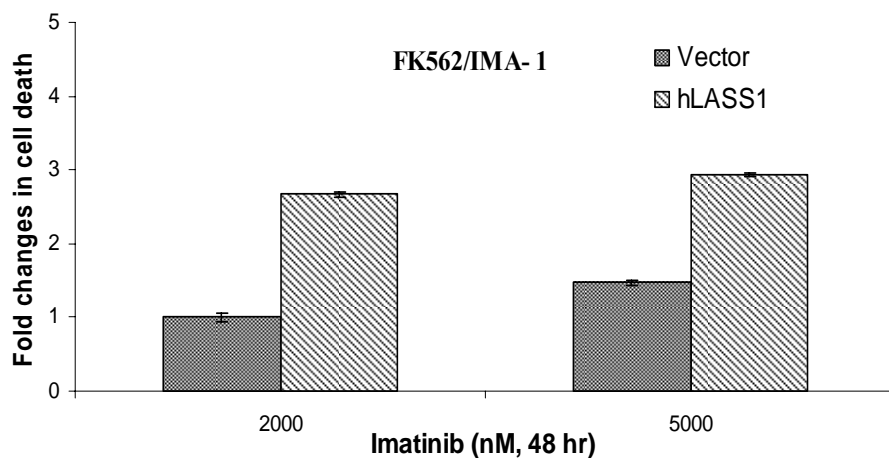


Figure 34. The role of overexpression of hLASS1 in the inhibition of apoptosis (by fold changes in cell death) in K562/IMA-1 cells. The effect of Imatinib on cell viability of vector and hLASS1 transfected and Imatinib treated K562/IMA-1 cells was determined using trypan blue dye exclusion assay. Cells, grown in 6-well plates (5×10^4 cells/well), were treated in the absence or presence of Imatinib (48 hr). Experiments were done in duplicates in at least two independent experiments, and statistical analysis was done using two way anova, $p < 0.01$ was considered significant.

To further assess the role for hLASS1/C₁₈-ceramide pathway in Imatinib-induced cell death, K562/IMA-0.2 cells were transiently transfected by hLASS1, and then the effects of overexpression of hLASS1 on Imatinib-induced apoptosis were examined by measuring the activation of pro-caspase-3, as compared to vector-transfected cells. As shown in Figure 35, while treatment with Imatinib did not have a significant effect on the activation of caspase-3, overexpression of hLASS1 increased caspase-3 activity by about 3.5-fold as compared to controls in response to Imatinib (Figure 35).

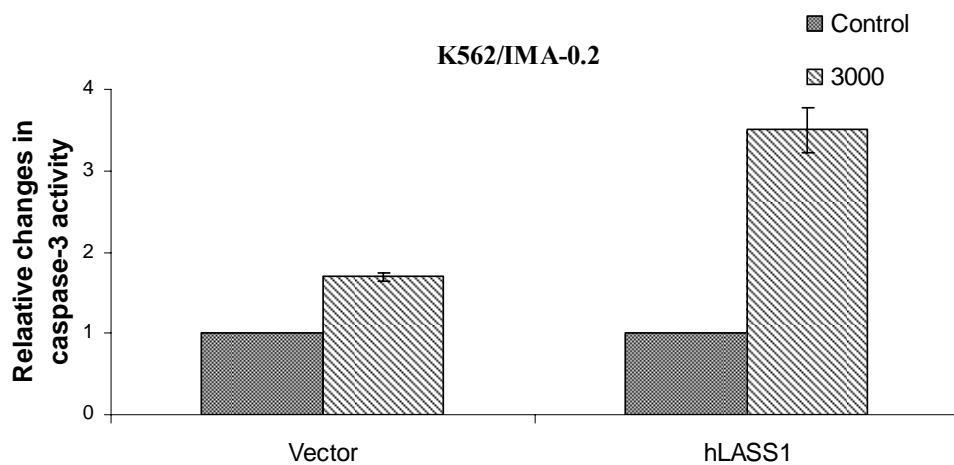


Figure 35. The role of overexpression of hLASS1 in the induction of caspase-3 activity in K562/IMA-0.2 cells. Caspase-3 activity was determined in hLASS1 and vector transfected K562/IMA-0.2 cells, exposed to Imatinib (500 nM, 48 hr), using the caspase-3 fluorometric assay. Experiments were done in duplicates in at least two independent experiments. Error bars represent the standard deviations. Statistical analysis was done using two way anova, $p < 0.01$ was considered significant.

The expression levels of hLASS1 mRNAs in these cells, transiently transfected with hLASS1 and control vector were confirmed by RT-PCR. Beta-actin levels were used as internal positive control (Figure 36). Quantification analyses of hLASS1 gene expression was conducted by Scion Image programme and the results showed that there was around 8- and 7.5-fold increase in expression of hLASS1 gene in hLASS1 transfected K562/IMA-0.2 and -1 cells, respectively, as compared to control transfected ones.

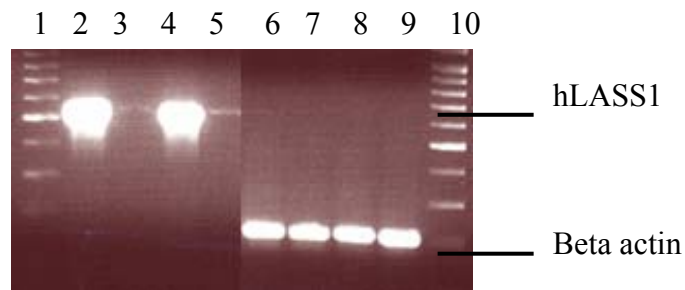


Figure 36. Expression analyses of hLASS1 in hLASS1 transfected resistant K562 cells. hLASS1 mRNA levels in K562/IMA-0.2 (lanes 2 and 3) and -1 (lanes 4 and 5) cells transfected with hLASS1 and vector, respectively, were measured using RT-PCR. Beta-actin levels were used as internal positive controls (lanes 6-9). Lanes 1 and 10 are DNA Ladder.

3.2.2 Specificity of hLASS1 in Imatinib-Induced Cell Death

On the other hand while mitochondrial membrane potential was increased about 1.2-fold in vector transfected K562 cells in response to Imatinib, in hLASS1 overexpressed cells mitochondrial membrane potential was increased to about 1.6-fold as comparing to controls (Figure 37).

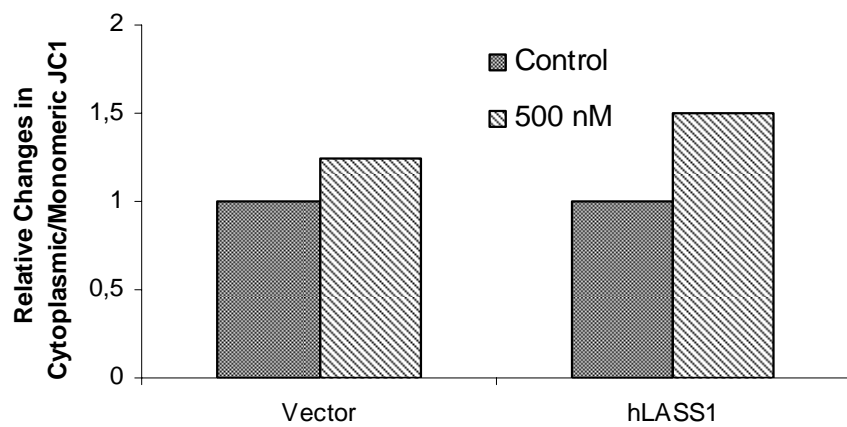


Figure 37. The role of overexpression of hLASS1 in the induction of apoptosis (by decrease in MMP) in K562 cells. Mitochondrial membrane potential was measured in these cells, exposed to 500 nM Imatinib (48 hr) using the JC-1 kit by flow

cytometry. Experiments were done in duplicates in at least two independent experiments. Statistical analysis was done using two way anova, $p<0.05$ was considered significant.

To examine the specificity of hLASS1 in Imatinib-induced cell death, the effects of overexpression of hLASS2 (Figure 38), hLASS5 (Figure 39) and hLASS6 (Figure 40), which are involved in the generation of specifically C₂₄-, C₁₄- and C₁₆-ceramides, on the levels of apoptosis were examined by measuring the loss of MMP in response to Imatinib. While there was a slight decrease in MMP in response to hLASS6 transfection (Figure 40), no significant changes in MMP in hLASS2 and hLASS5 were detected (Figures 38 and 39, respectively).

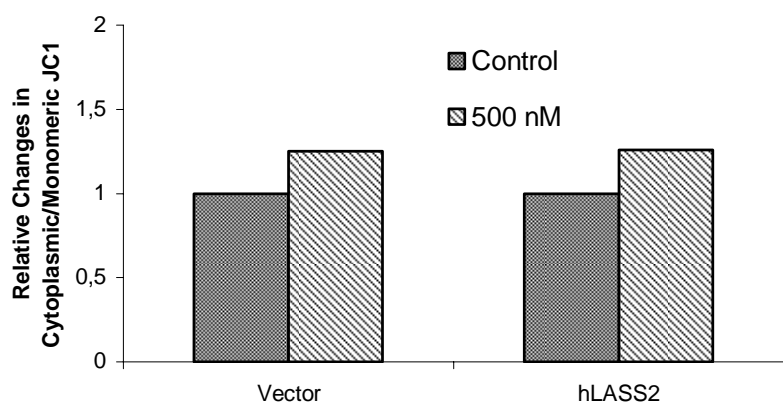


Figure 38. The role of overexpression of hLASS2 in the induction of apoptosis (by decrease in MMP) in K562 cells. Mitochondrial membrane potential was measured in these cells, exposed to 500 nM Imatinib (48 hr) using the JC-1 kit by flow cytometry. Experiments were done in duplicates in at least two independent experiments. Statistical analysis was done using two way anova, $p<0.05$ was considered significant.

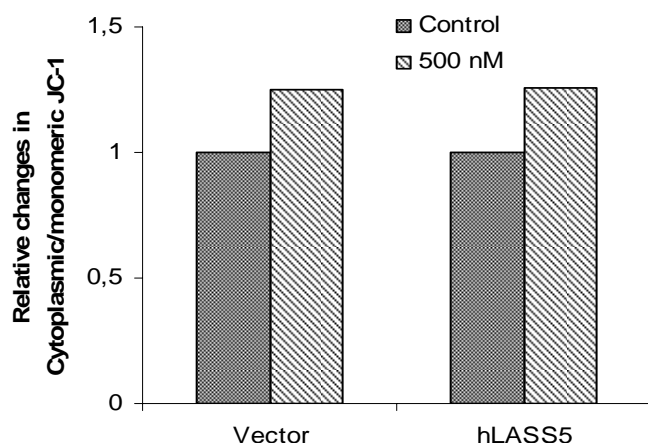


Figure 39. The role of overexpression of hLASS5 in the induction of apoptosis (by decrease in MMP) in K562 cells. Mitochondrial membrane potential was measured in these cells, exposed to 500 nM Imatinib (48 hr) using the JC-1 kit by flow cytometry. Experiments were done in duplicates in at least two independent experiments. Statistical analysis was done two way anova, $p<0.05$ was considered significant.

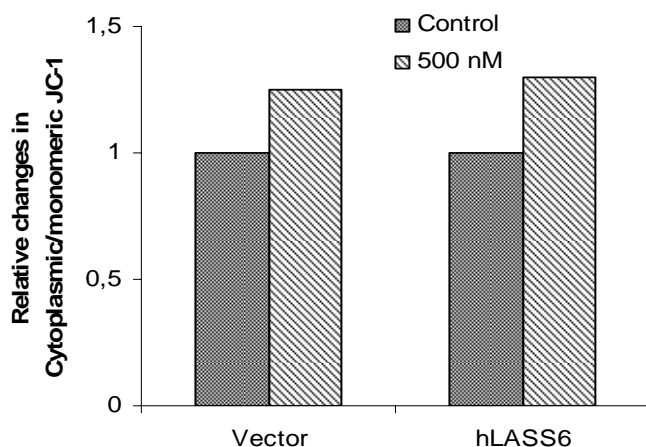


Figure 40. The role of overexpression of hLASS6 in the induction of apoptosis (by decrease in MMP) in K562 cells. Mitochondrial membrane potential was measured in these cells, exposed to 500 nM Imatinib (48 hr) using the JC-1 kit by flow cytometry. Experiments were done in duplicates in at least two independent experiments. Statistical analysis was done using two way anova, $p<0.05$ was considered significant.

The equal overexpression levels of hLASS1, hLASS2, hLASS5 and hLASS6 mRNAs in these cells as compared to their controls were confirmed by RT-PCR. Beta-actin levels were used as internal positive controls (Figure 41). Quantification analyses of hLASS genes expression were conducted by Scion Image programme and the results showed that there was around 8-fold increase in expression of hLASS1, hLASS2, hLASS5 and hLASS6 genes in hLASS1, hLASS2, hLASS5 and hLASS6 transfected K562 cells as compared to control transfected ones.

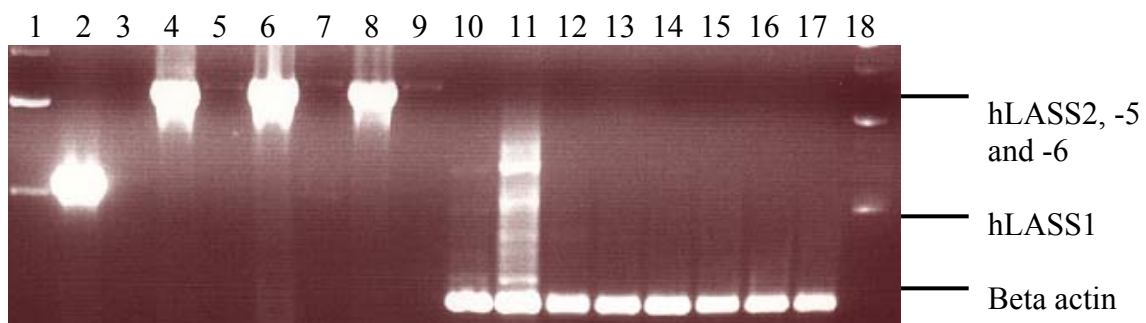


Figure 41. Expression analyses of hLASS1, hLASS2, hLASS5 and hLASS6 in K562 cells transfected with counterpart vectors. hLASS1 (lanes 2 and 3), hLASS2 (lanes 4 and 5), hLASS5 (lanes 6 and 7), and hLASS6 (lanes 8 and 9) mRNA levels in K562 cells transfected with hLASS1, hLASS2, hLASS5, or hLASS6 and vector, respectively, were measured using RT-PCR. Beta-actin levels were used as internal positive controls (lanes 10-17). Lanes 1 and 18 are DNA Ladder.

On the other hand, the specificity of hLASS1 was also investigated in resistant K562/IMA-1 cells. Mitochondrial membrane potential in K562/IMA-1 was increased about 1.2-fold in vector transfected K562 cells in response to Imatinib while in hLASS1 overexpressed cells, mitochondrial membrane potential was increased to about 1.6-fold as comparing to controls (Figure 42).

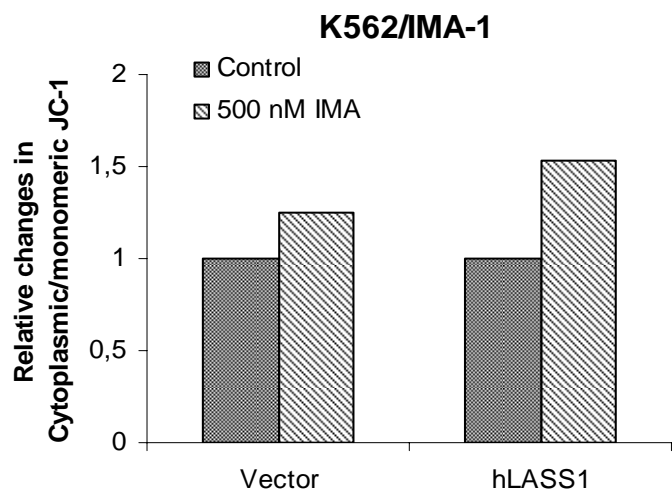


Figure 42. The role of overexpression of hLASS1 in the induction of apoptosis (by decrease in MMP) in K562/IMA-1 cells. Mitochondrial membrane potential was measured in these cells, exposed to 500 nM Imatinib (48 hr) using the JC-1 kit by flow cytometry. Experiments were done in duplicates in at least two independent experiments. Statistical analysis was done using two way anova, $p<0.05$ was considered significant.

The effects of overexpression of hLASS5 on the levels of apoptosis were also examined by measuring the loss of MMP in response to Imatinib in K562/IMA-1 cells, and no significant changes were detected (Figure 43).

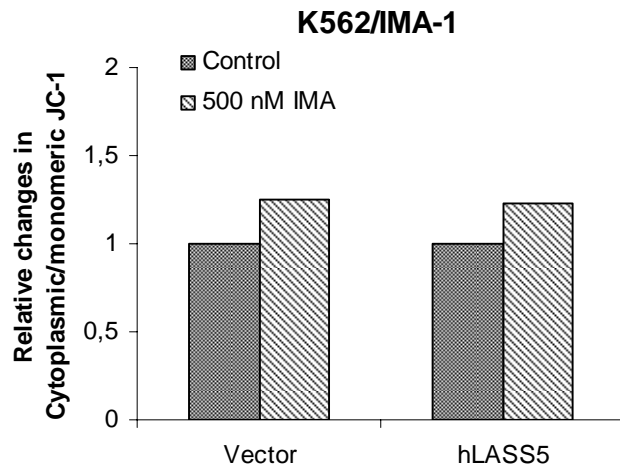


Figure 43. The role of overexpression of hLASS5 in the induction of apoptosis (by decrease in MMP) in K562/IMA-1 cells. Mitochondrial membrane potential was

measured in these cells, exposed to 500 nM Imatinib (48 hr) using the JC-1 kit by flow cytometry. Experiments were done in duplicates in at least two independent experiments. Statistical analysis was done using two way anova, $p<0.05$ was considered significant.

The equal overexpression levels of hLASS1 and hLASS5 mRNAs in K562/IMA-1 cells as compared to their vector controls were confirmed by RT-PCR. Beta-actin levels were used as internal positive control (Figure 44). Quantification analyses of hLASS1 and hLASS5 gene expressions were conducted by Scion Image programme and the results showed that there was around 7-fold increase in expression of hLASS1 and hLASS5 genes in hLASS1 and hLASS5 transfected K562/IMA-1 cells as compared to control transfected ones.

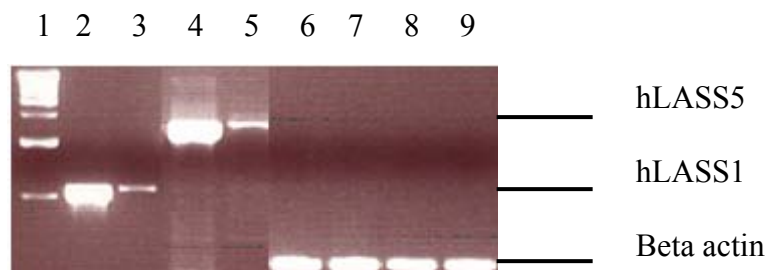


Figure 44. Expression analyses of hLASS1 and hLASS5 in K562/IMA-1 cells transfected with hLASS1 and hLASS5, respectively. hLASS1 (lanes 2 and 3), and hLASS5 (lanes 4 and 5) mRNA levels in K562/IMA-1 cells transfected with hLASS1 or hLASS5, and vector, respectively, were measured using RT-PCR. Beta-actin levels were used as internal positive controls (lanes 6-9). Lane 1 is DNA Ladder.

3.2.3 Analyses of C₁₈-Ceramide Levels in hLASS1 Transfected K562/IMA-1 Cells

In addition, overexpression of hLASS1 was confirmed by measurement of endogenous ceramide levels, and the data showed that hLASS1 overexpression resulted in about 4-fold increase in steady-state levels of C₁₈-ceramide when

compared to vector controls (Figure 45). Moreover, treatment of hLASS1 overexpressing cells with Imatinib induced the generation of C₁₈-ceramide about 16-fold in resistant K562/IMA-1 cells, while its levels in vector transfected resistant cells were increased about 5-fold in response to the drug (Figure 45). The levels of C₁₈-ceramide were 0.045, 0.219, and 0.169, 0.742 pmol/nmol Pi in vector and hLASS1 transfected cells in the absence or presence of 3 μ M Imatinib (48 hr), respectively.

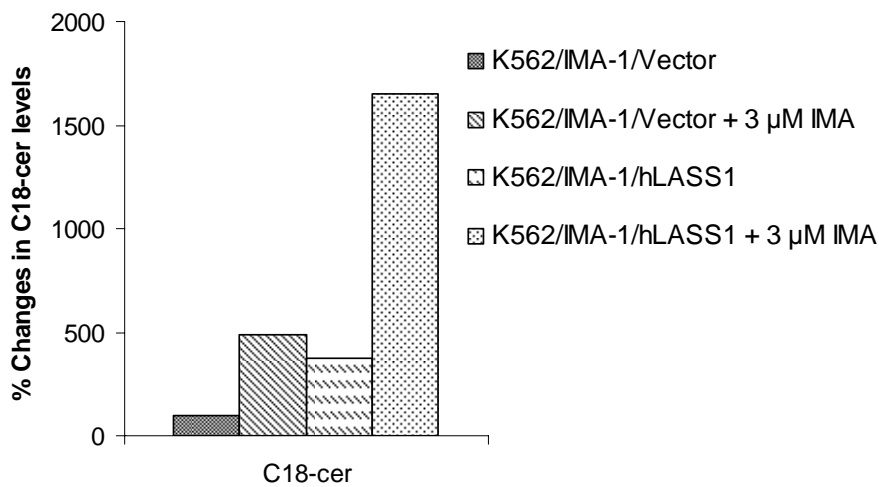


Figure 45. Concentrations of C₁₈-ceramide in control and hLASS1 transfected K562/IMA-1 cells. C₁₈-ceramide in the presence (3000 nM, 48 hr) or absence of Imatinib, were examined by LC/MS. The levels of C₁₈-ceramide were normalized to Pi concentrations. The experiments were done in at least two independent trials. Statistical analysis was done using One Way Anova, p<0.01 was considered significant.

3.2.4 Expression Analyses of hLASS1 in Sensitive and Resistant Human CML Cells

To examine whether mechanisms by which K562/IMA-0.2 and -1 and Meg-01/IMA-0.2 and -1 cells express resistance to Imatinib-induced cell death involve the down-regulation of hLASS1 expression, the mRNA levels of hLASS1 in these cells as compared to their parental sensitive counterparts were examined by semi-quantitative RT-PCR. Interestingly, the data in Figure 46 showed that 0.2 and 1 μ M

Imatinib resistant cells overexpress hLASS1 about 2- and 4-fold compared to their parental sensitive cells. Beta-actin levels were used as internal positive controls (Figure 46). Quantification analyses of hLASS1 gene expression was conducted by Scion Image programme and the results showed that there was around 1.8- and 3.2-fold increase in expression of hLASS1 gene in K562/IMA-0.2 and K562/IMA-1 cells, respectively, as compared to parental K562 cells. On the other hand, quantification analyses of hLASS1 gene expression in Meg-01 cells revealed that there was 1.2- and 3-fold increase in expression of hLASS1 gene in Meg-01/IMA-0.2 and Meg-01/IMA-1 cells, respectively, as compared to parental Meg-01 cells.

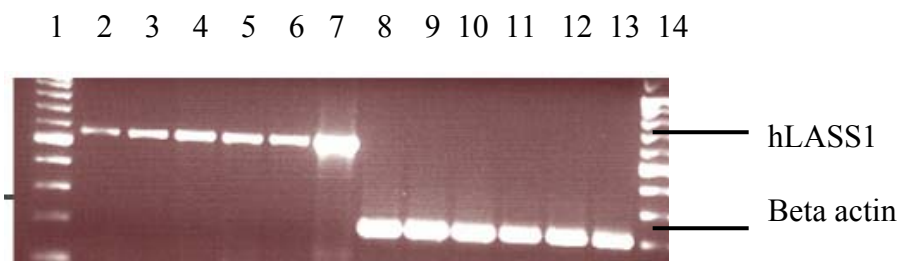


Figure 46. Expression analyses of hLASS1 in parental and resistant human CML cells. hLASS1 mRNA levels in K562, K562/IMA-0.2 and -1 cells (lanes 2-4) and Meg-01, Meg-01/IMA-0.2 and -1 cells (lanes 5-7) were measured by RT-PCR . Beta actin levels were used as internal positive controls (lanes 8-13, respectively). Lanes 1 and 14 are DNA Ladder.

3.2.5 Ceramide Synthase Activity in Parental and Resistant Cells

Next, endogenous ceramide synthase activity in K562 and K562/IMA-1 cells was measured after pulsing the cells with exogenous ¹⁷Cdihydrosphingosine, and monitoring the generation of ¹⁷C-dihydro-C₁₈-ceramides (Figure 47) in the presence or absence of Imatinib. The data showed that resistant K562/IMA-1 cells expressed higher levels of ceramide synthase activity (about 5-fold), when compared to parental K562 cells. Interestingly, Imatinib treatment resulted in about 3-fold increase in ceramide synthase activity for the generation of ¹⁷C-dihydro-C₁₈-

ceramide in parental K562 cells, whereas it did not cause any significant changes in ceramide synthase activity in the resistant cells (Figure 47). These data, therefore, suggested that alterations in the levels of endogenous ceramide in resistant cells in response to Imatinib is not due to decreased levels of hLASS1 mRNA or enzyme activity, but might be due to alterations of ceramide accumulation and/or metabolism.

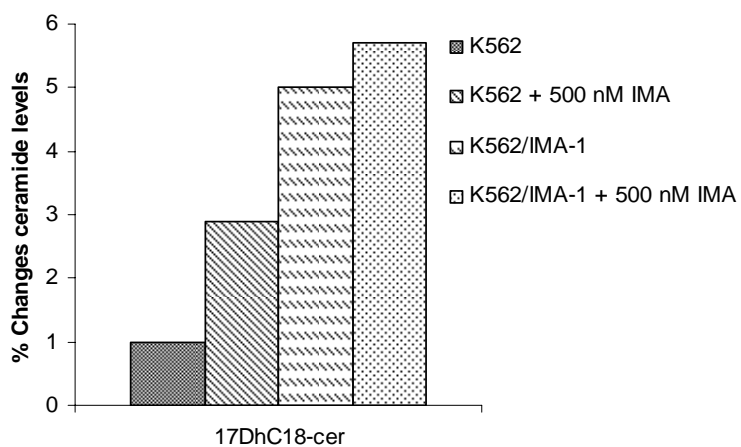


Figure 47. Ceramide synthase activity in response to Imatinib in parental and resistant K562/IMA-1 cells. The endogenous activity of ceramide synthase for the conversion of 17C-dihydrosphingosine to 17C-dihydro-C₁₈-ceramides in K562 and K562/IMA-1 cells in the absence or presence of Imatinib (500 nM, 48 hr) was measured by LC/MS. The levels of C₁₈-ceramide were normalized to Pi concentrations. The experiments were done in at least two independent trials. Statistical analysis was done using One Way Anova, p<0.01 was considered significant.

Taken together, these data show that hLASS1 via the generation of C₁₈-ceramide, plays an important role in Imatinib-induced mitochondrial apoptotic pathway involved in the loss of mitochondrial membrane potential, and the activation of caspase-3/7 in parental K562 cells. Also, these results further suggest that defects in the generation, or accumulation/metabolism of C₁₈-ceramide might result in increased resistance to Imatinib-induced cell death in K562 cells.

3.3 ONE OF THE MECHANISMS OF RESISTANCE TO IMATINIB-INDUCED CELL DEATH INVOLVES THE OVEREXPRESSION OF SPHINGOSINE KINASE 1 (SK-1)

After observing an increase in hLASS1 activity, but a decrease in ceramide levels in resistant cells, the possibility that sphingoid base substrates would be channeled into the SK-1 metabolic pathway was considered. Therefore, the levels of S1P in these cells were measured by LC/MS, and the data showed that S1P levels were significantly higher in resistant K562/IMA-1 cells when compared to sensitive K562 cells (Figure 48). These data also showed that while Imatinib slightly reduced the levels of S1P in sensitive cells, it further increased the levels of S1P about 25% in resistant cells (Figure 48).

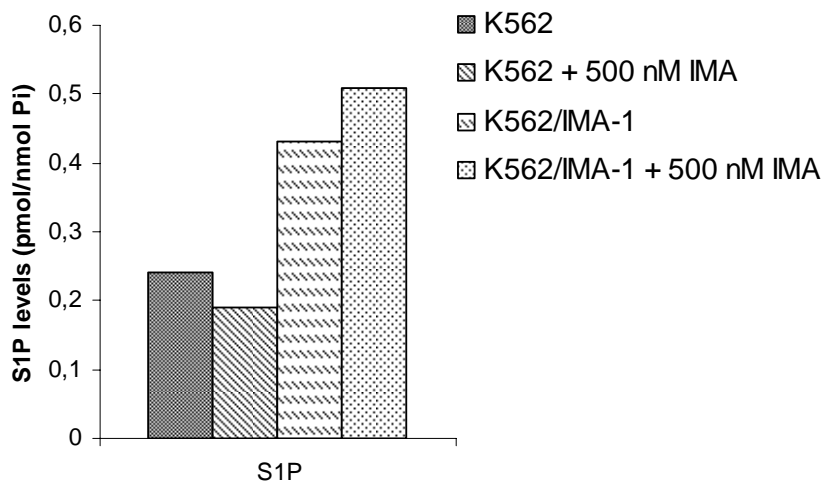


Figure 48. Analyses of S1P levels in parental and resistant K562/IMA-1 cells in response to Imatinib. The levels of S1P in K562/IMA-1 cells transfected with control or SK-1 siRNAs in the absence or presence of Imatinib (3 μ M, 48 hr) were measured by LC/MS. The levels of S1P were normalized to Pi concentrations. The experiments were done in at least two independent trials. Statistical analysis was done using One Way Anova, $p<0.01$ was considered significant.

Then, the levels of SK-1 expression were analyzed in these cells by RT-PCR (Figure 49) and Western blotting (Figure 50). Indeed, the data showed that K562/IMA-0.2 and -1 and Meg-01/IMA-0.2 and -1 cells overexpress SK-1 when compared to parental sensitive counterparts (Figures 49 and 50). Quantification

analyses of SK-1 gene expression was conducted by Scion Image programme and the results showed that there was around 2- and 3.2-fold increase in expression of SK-1 gene in K562/IMA-0.2 and K562/IMA-1 cells, respectively, as compared to parental K562 cells (Figure 49). On the other hand, quantification analyses of SK-1 gene expression was conducted in Meg-01 cells and 1.2- and 1.7-fold increase in expression of SK-1 gene was observed in Meg-01/IMA-0.2 and Meg-01/IMA-1 cells, respectively, as compared to parental Meg-01 cells (Figure 49)

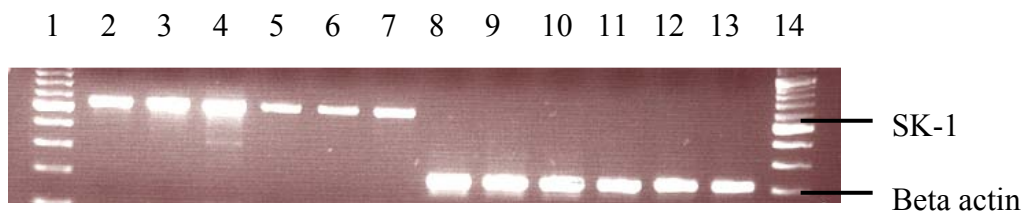


Figure 49. Expression analyses of SK-1 in parental and resistant human CML cells. SK-1 mRNA levels K562, K562/IMA-0.2 and -1 cells (lanes 2-4) and in Meg-01, Meg-01/IMA-0.2 and -1 cells (lanes 5-7) were measured by RT-PCR. Beta actin levels were used as internal positive controls (lanes 8-13, respectively). Lanes 1 and 14 are DNA Ladder.

Quantification analyses of SK-1 protein levels was conducted by Scion Image programme and the results showed that there was around 3.2- and 2.1-fold increase in protein levels of SK-1 in K562/IMA-1 and Meg-01/IMA-1 cells, respectively, cells as compared to their parental sensitive counterparts (Figure 50).

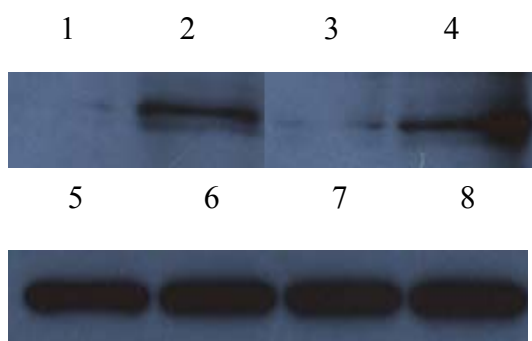


Figure 50. Protein levels of SK-1 in parental and resistant human CML cells. SK-1 protein levels in K562 and K562/IMA-1 cells (lanes 1 and 2, respectively) and in

Meg-01, Meg-01/IMA-1 cells (lanes 3 and 4, respectively) were measured by western blotting. Beta actin levels were used as internal positive controls (lanes 5 to 8, respectively).

3.3.1 Sphingosine Kinase Activity in Sensitive and Resistant Cells

These data were also consistent with increased SK activity in these K562/IMA-1 cells, in which the conversion of 17C-sphingosine to 17C-S1P was about 50% higher as compared to sensitive K562 cells (Figure 51). Also, treatment with Imatinib (500 nM, 48 hr) reduced the activity of SK in sensitive cells, while it slightly increased SK activity in resistant cells (Figure 51). Thus, these data suggested that overexpression of SK-1 might play a role in the development of resistance to Imatinib in these cells.

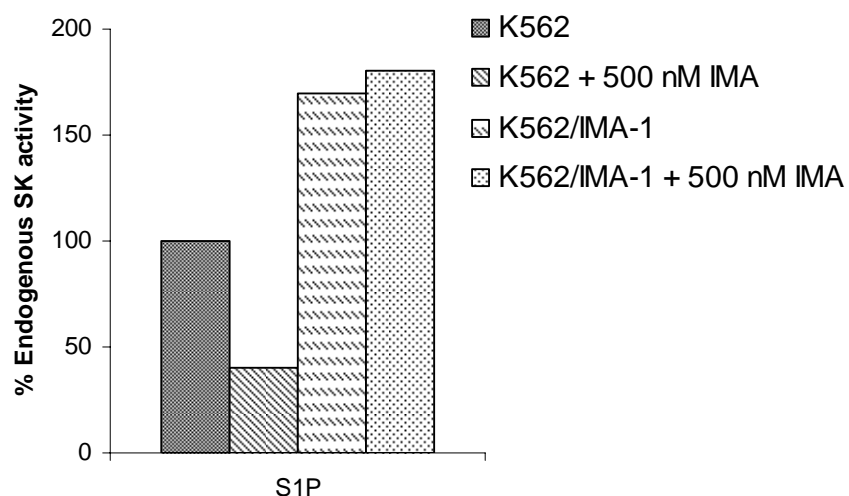


Figure 51. Endogenous sphingosine kinase enzyme activity in response to Imatinib in parental and resistant K562/IMA-1 cells. The endogenous enzyme activity of sphingosine kinase was measured by the analysis of conversion of 17C-sphingosine to 17C-S1P in K562 and K562/IMA-1 cells in the absence or presence of Imatinib (500 nM, 48 hr). Statistical analysis was done using One Way Anova, $p < 0.01$ was considered significant.

3.3.2 Inhibition of SK-1 by siRNA Increased Sensitivity of Human CML Cells to Imatinib

To demonstrate the possible role for SK-1 in the regulation of resistance to apoptosis in response to Imatinib, its expression was partially inhibited by siRNA in K562/IMA-1 cells, which also caused about 50% reduction in the levels of S1P in the absence or presence of Imatinib (Figure 52).

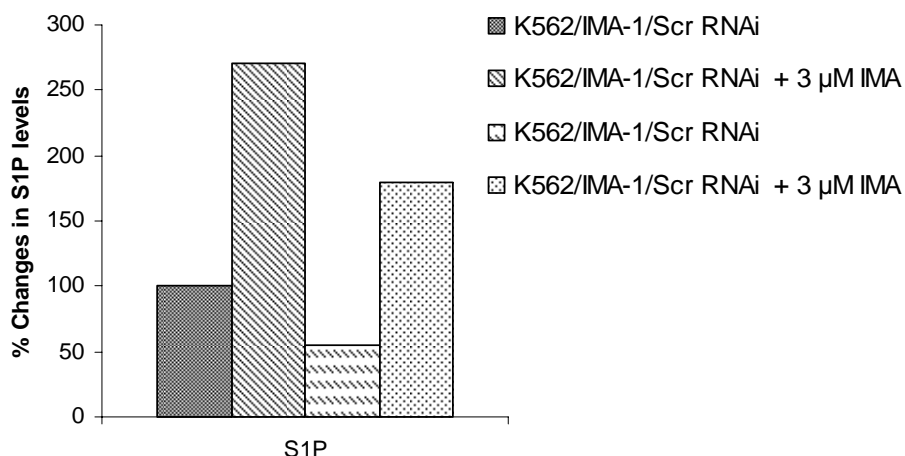


Figure 52. Percent changes in S1P levels in response to Imatinib in K562/IMA-1 cells. The levels of S1P in K562/IMA-1 cells transfected with control or SK-1 siRNAs in the absence or presence of Imatinib (3 μ M, 48 hr) were measured by LC/MS. The levels of S1P were normalized to Pi concentrations. The experiments were done in at least two independent trials. Statistical analysis was done using One Way Anova, $p<0.01$ was considered significant.

Then, its effects on the induction of apoptosis in K562/IMA-1 cells were examined by trypan blue dye exclusion assays. As shown in Figures 53 and -54, SK-1 siRNA increased sensitivity, and resulted in a significant induction of apoptosis, about 3-fold in K562/IMA-0.2 (Figure 53) and 2-fold in K562/IMA-1 cells (Figure 54) in response to 1 μ M Imatinib, suggesting a protective role for SK-1 in Imatinib-induced apoptosis.

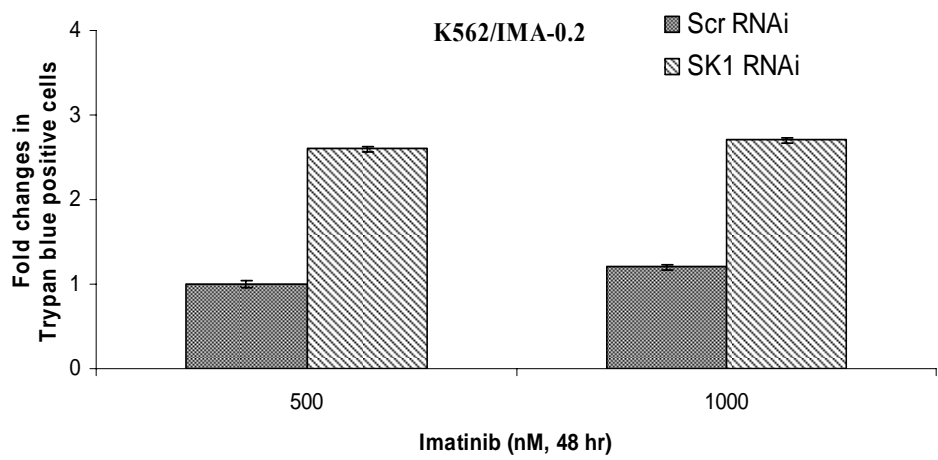


Figure 53. The role of inhibition of SK-1 in the inhibition of apoptosis (by fold changes in trypan blue positive cells) in K562/IMA-0.2 cells. Fold changes of cell death in control and SK-1 siRNA transfected K562/IMA-0.2 cells, exposed to 0.5- and 1 μ M Imatinib (48 hr), was determined using trypan blue dye exclusion assay. Cells, grown in 6-well plates (5×10^4 cells/well), were treated in the absence or presence of Imatinib (48 hr). Experiments were done in duplicates in at least two independent experiments, and statistical analysis was done using two way anova, $p < 0.01$ was considered significant.

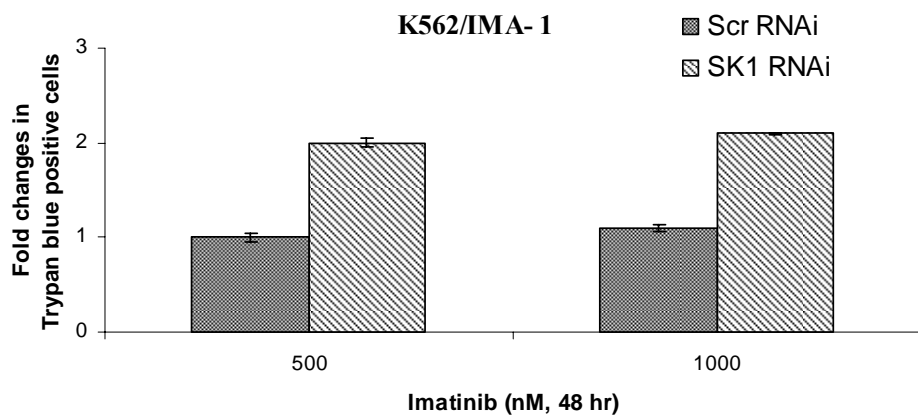


Figure 54. The role of inhibition of SK-1 in the inhibition of apoptosis (by fold changes in trypan blue positive cells) in K562/IMA-1 cells. Fold changes of cell death in control and SK-1 siRNA transfected K562/IMA-1 cells, exposed to 0.5 and 1 μ M Imatinib (48 hr) was determined using trypan blue dye exclusion assay. Cells,

grown in 6-well plates (5×10^4 cells/well), were treated in the absence or presence of Imatinib (48 hr). Experiments were done in duplicates in at least two independent experiments. Error bars represent standard deviations. Statistical analysis was done using two way anova, $p < 0.01$ was considered significant.

The expression levels of SK-1 mRNAs in SK-1 and control siRNA transfected K562/IMA-0.2 and -1 cells as compared to their controls were confirmed by RT-PCR. Beta-actin levels were used as internal positive controls (Figure 55). Quantification analyses of SK-1 gene expression was conducted by Scion Image programme and the results showed that there was around 2.4- and 3.5-fold decrease in expression of SK-1 gene in SK-1 siRNA transfected cells as compared to scramble siRNA transfected K562/IMA-0.2 and -1 cells, respectively.

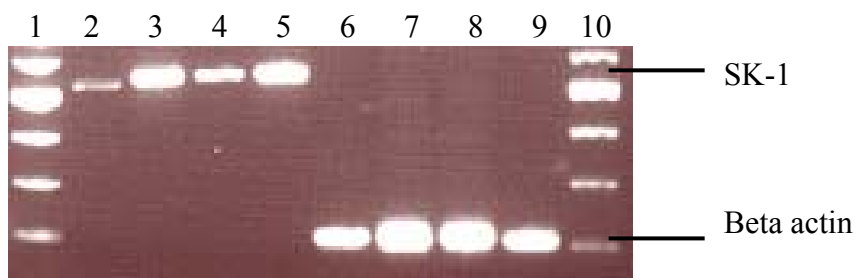


Figure 55. Expression levels of SK-1 in SK-1 siRNA transfected resistant K562/IMA-0.2 and -1 cell. SK-1 mRNA levels transfected with control (lanes 3 and 5) or SK-1 (lanes 2 and 4) siRNAs in K562/IMA-0.2 and -1 cells, respectively, were examined by RT-PCR. Beta actin levels were used as internal positive controls (lanes 6-9 respectively). Lanes 1 and 10 are DNA Ladder.

On the other hand, the involvement of SK-1 in Imatinib-induced cell death was also investigated in parental K562 cells. Mitochondrial membrane potential was increased about 1.2-fold in control siRNA transfected K562 cells in response to 3 μ M Imatinib, while in SK-1 siRNA transfected cells mitochondrial membrane potential was increased to about 1.5-fold as compared to controls (Figure 56).

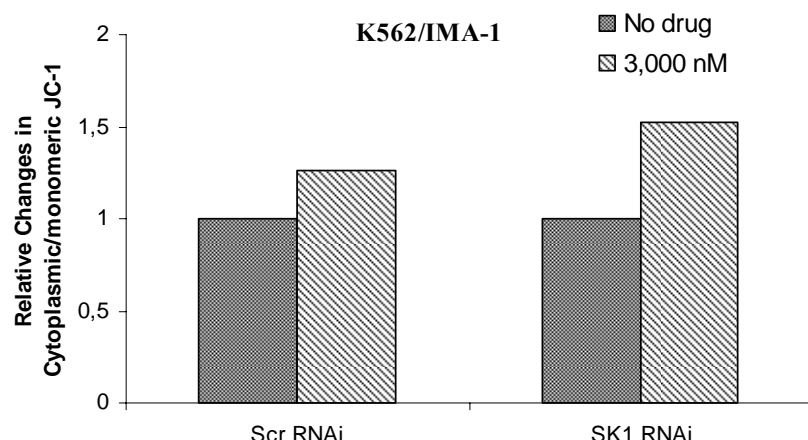


Figure 56. The role of inhibition of SK-1 in the induction of apoptosis (by decrease in MMP) in K562 cells. Mitochondrial membrane potential was measured in control and SK-1 siRNA transfected K562 cells, exposed to 500 nM Imatinib (48 hr) using the JC-1 kit by flow cytometry. Experiments were done in duplicates in at least two independent experiments. Statistical analysis was done using two way anova, $p<0.05$ was considered significant.

The expression levels of SK-1 mRNAs in SK-1 and control siRNA transfected K562 cells as compared to their controls were confirmed by RT-PCR. Beta-actin levels were used as internal positive controls (Figure 57). Quantification analyses of SK-1 gene expression was conducted by Scion Image programme and the results showed that there was around 2.4-fold decrease in expression of SK-1 gene in SK-1 siRNA transfected cells as compared to scramble siRNA transfected K562 cells.

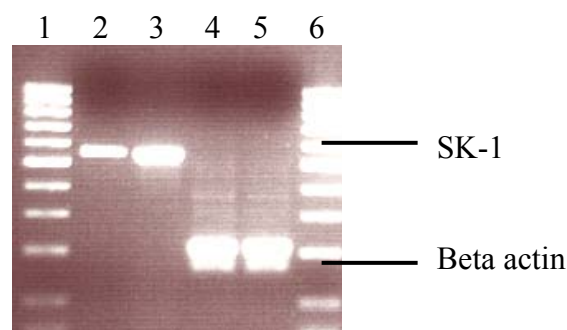


Figure 57. Expression levels of SK-1 in SK-1 siRNA transfected K562 cells. SK-1 mRNA levels in control (lane 3) or SK-1 (lane 2) siRNAs transfected K562 cells

were examined by RT-PCR. Beta actin levels were used as controls (lanes 4 and 5 respectively). Lanes 1 and 6 are DNA Ladder.

3.3.3 Overexpression of SK-1 Resulted in an Increase in the Resistance of Human CML Cells to Imatinib

In reciprocal experiments, overexpression of SK-1 in parental K562 cells significantly prevented cell death, increased mitochondrial membrane potential and also blocked the activation of caspase-3 in response to Imatinib, when compared to vector-transfected controls. As shown in Figure 58, treatment with 0.5- and 1 μ M Imatinib resulted in about 30- and 40% cell death, respectively, in control transfected K562 cells, whereas Imatinib caused only 10- and 15% of cell death in SK-1 transfected K562 cells in response to 0.5- and 1 μ M Imatinib, respectively (Figure 58).

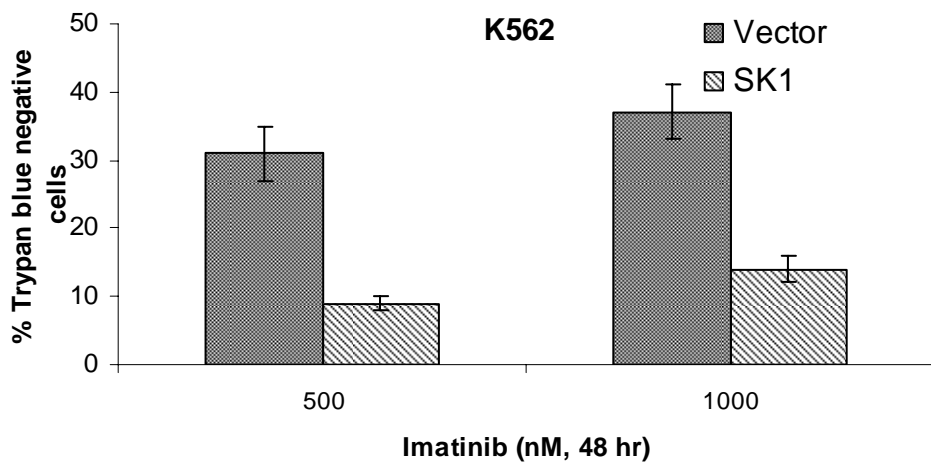


Figure 58. The role of overexpression of SK-1 in the inhibition of apoptosis (by percent changes in trypan blue positive cells) in K562 cells. The effect of Imatinib on cell death of vector and SK-1 transfected and 0.5- and 1 μ M Imatinib treated K562 cells was determined using trypan blue dye exclusion assay. Cells, grown in 6-well plates (5×10^4 cells/well), were treated in the absence or presence of Imatinib (48 hr). Experiments were done in duplicates in at least two independent experiments. Statistical analysis was done using two way anova, $p < 0.01$ was considered significant.

On the other hand, the involvement of SK-1 in Imatinib-induced apoptosis was also investigated in K562 cells. It was observed that mitochondrial membrane potential was increased about 2-fold in vector transfected K562 cells in response to 1 μ M Imatinib, whereas in SK-1 overexpressed cells, mitochondrial membrane potential was about 0.9-fold as compared to controls (Figure 59).

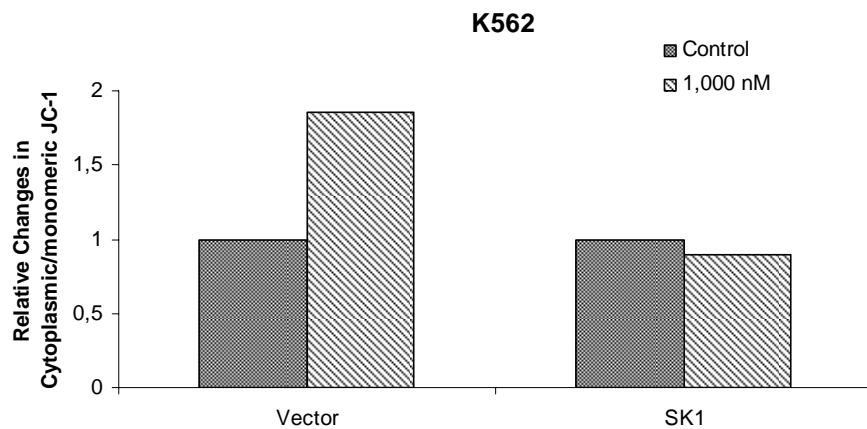


Figure 59. The role of overexpression of SK-1 in the inhibition of apoptosis (by increase in MMP) in K562 cells. Mitochondrial membrane potential was measured in vector and SK-1 transfected K562 cells, exposed to 1,000 nM Imatinib (48 hr) using the JC-1 kit by flow cytometry. Experiments were done in duplicates in at least two independent experiments. Statistical analysis was done using two way anova, $p<0.01$ was considered significant.

The effects of overexpression of SK-1 on Imatinib-induced apoptosis were also examined by measuring the activation of pro-caspase-3, as compared to vector-transfected control cells. As shown in Figure 60, while treatment with 1 μ M Imatinib increased activation of caspase-3 by about 13-fold, in SK-1 overexpressed cells caspase-3 activity was only increased by about 3-fold as compared to controls (Figure 60).

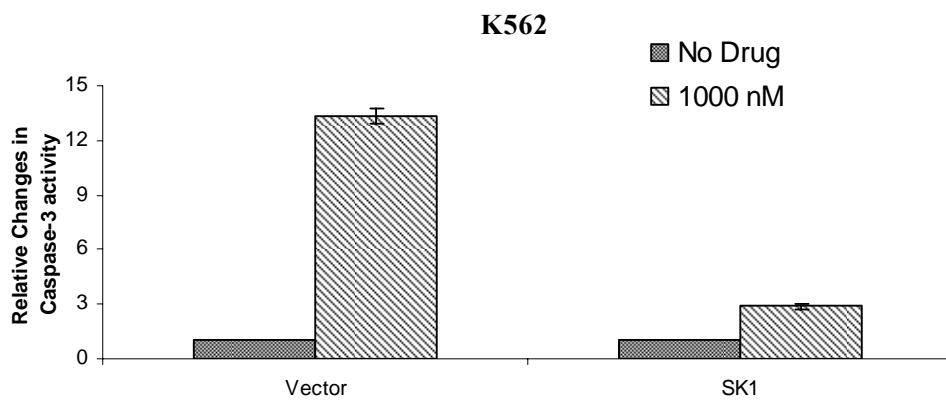


Figure 60. The role of overexpression of SK-1 in the inhibition of apoptosis (by decrease in caspase-3 activity) in K562 cells. Caspase-3 activity was determined in vector and SK-1 transfected K562 cells, exposed to 1 μ M Imatinib (48 hr) using the caspase-3 fluorometric assay. Experiments were done in duplicates in at least two independent experiments. Statistical analysis was done using two way anova, $p<0.01$ was considered significant.

The expression levels of SK-1 mRNAs in SK-1 and control transfected K562 cells as compared to their controls were confirmed by RT-PCR. Beta-actin levels were used as internal positive controls (Figure 61). Quantification analyses of SK-1 gene expression was conducted by Scion Image programme and the results showed that there was around 4.2-fold increase in expression of SK-1 gene in SK-1 transfected cells as compared to control vector transfected K562 cells, respectively.

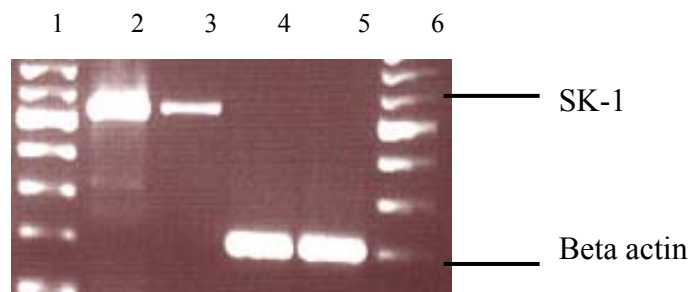


Figure 61. Expression levels of SK-1 in SK-1 transfected K562 cells. SK-1 mRNA levels in SK-1 (lane 2) and vector (lane 3) transfected K562 cells were examined by

RT-PCR. Beta actin levels were used as internal positive controls (lanes 4 and 5 respectively). Lanes 1 and 6 are DNA Ladder.

3.3.4 Analyses of C₁₈-Ceramide and S1P Levels in SK-1 Transfected K562 Cells

These data were in agreement with the measurement of endogenous ceramide and S1P levels by LC/MS, which showed that overexpression of SK-1 resulted in a significant increase in S1P levels, raising its levels above C₁₈-ceramide, while the levels of C₁₈-ceramide was significantly higher than S1P levels in vector transfected cells in response to Imatinib (Figure 62).

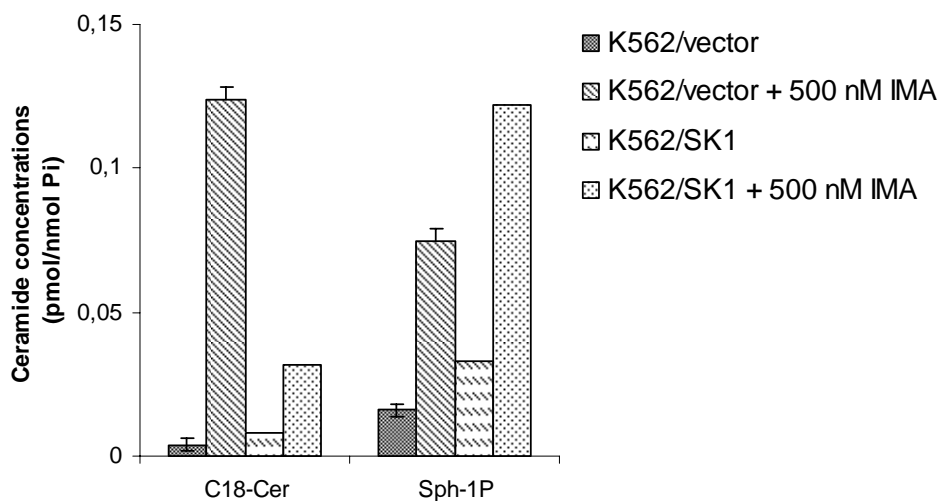


Figure 62. Analysis of C₁₈-ceramide and S1P levels in SK-1 transfected K562 cells. The levels of S1P and C₁₈-ceramide in vector and SK-1 transfected K562 cells, in the presence (1000 nM, 48 hr) or absence of Imatinib, were examined by LC/MS. The levels of C₁₈-ceramide and S1P were normalized to Pi concentrations. The experiments were done in at least two independent trials. Error bars represent standard deviations. Statistical analysis was done using two way anova, p<0.01 was considered significant.

Thus, these data reveal a functional role for SK-1 in the regulation of resistance to Imatinib-induced cell death via altering the balance between pro-apoptotic ceramide and anti-apoptotic S1P levels in these cells

3.4 INVOLVEMENT OF GCS, WHICH CONVERTS PRO-APOPTOTIC CERAMIDE TO GLUCOSYL CERAMIDE, IN RESISTANCE TO IMATINIB-INDUCED APOPTOSIS IN HUMAN CML CELLS

As shown in Figure 63, Imatinib in GCS transfected K562 cells significantly prevented cell death in response to Imatinib (48 hr, Figure 63). Specifically, treatment with 200- and 500 nM Imatinib resulted in about 30- and 55% cell death in response to vector, whereas Imatinib caused only around 10- and 25% growth inhibition in GCS transfected cells, respectively (Figure 63). GCS transfected K562 cells were also exposed to 700 nM Imatinib and showed 50% cell death.

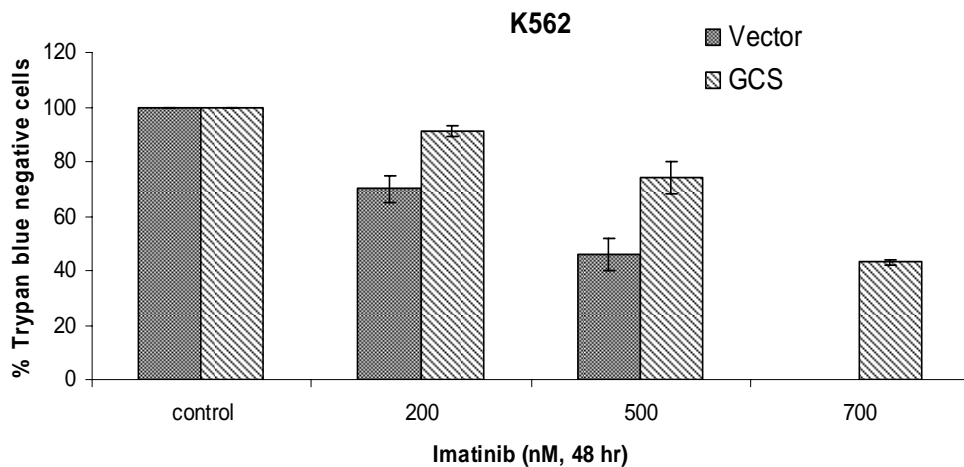


Figure 63. The role of overexpression of GCS in the inhibition of apoptosis (by percent changes in trypan blue negative cells) in K562 cells. Percent changes of cell viability in GCS and vector transfected K562 cells, exposed to Imatinib (48 hr) were determined by trypan blue dye exclusion assay. Experiments were done in duplicates in at least two independent experiments. Error bars represent standard deviations. Statistical analysis was done using two way anova, P<0.01 was considered significant.

Meg-01 cells were also transfected with vector and GCS to see the effects of conversion of ceramide to glucosylceramide in Imatinib treatment. Meg-01 cells, transfected with vector, exposed to 200- and 500 nM Imatinib resulted in about 30- and 60% cell death, while Imatinib caused only around 15- and 30% growth inhibition in GCS transfected cells, respectively (Figure 64). 700 nM Imatinib was also exposed to GCS transfected cells resulted in 50% growth inhibition. These data, therefore, demonstrates an important role for GCS via the conversion of ceramide to glucosylceramide in Imatinib-induced cell death in K562 and Meg-01 cells.

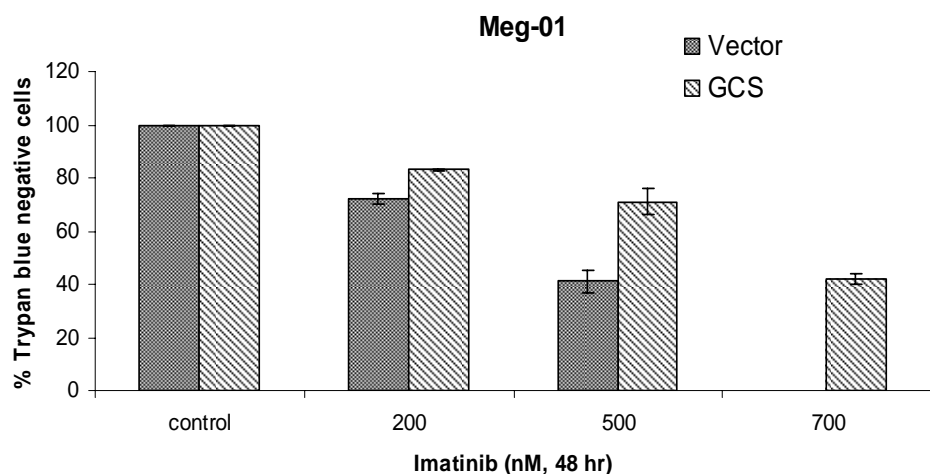


Figure 64. The role of overexpression of GCS in the inhibition of apoptosis (by percent changes in trypan blue negative cells) in Meg-01 cells. Percent changes of cell viability in GCS and vector transfected Meg-01 cells, exposed to Imatinib (48 hr) were determined by trypan blue dye exclusion assay. Experiments were done in duplicates in at least two independent experiments. Error bars represent standard deviations. Statistical analysis was done using two way anova, $P<0.01$ was considered significant.

The expression levels of GCS mRNAs in vector and GCS transfected K562 and Meg-01 cells were confirmed by RT-PCR. Beta-actin levels were used as internal positive controls (Figure 65). Quantification analyses of GCS gene expression was conducted by Scion Image programme and the results showed that

there was around 2.4-fold increase in expression of GCS gene in GCS transfected cells as compared to control vector transfected K562 and Meg-01 cells.

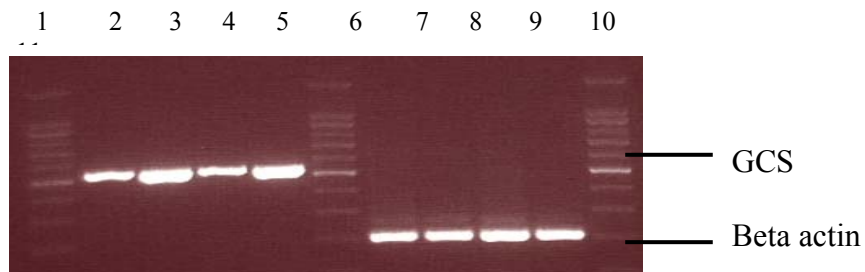


Figure 65. Expression analyses of GCS in GCS transfected human CML cells. GCS mRNA levels in GCS (lane 3 and 5) and vector (lanes 2 and 4) transfected K562 and Meg-01 cells, respectively, were measured using RT-PCR. Beta-actin levels were used as internal positive controls (lanes 7 to 10). Lanes 1, 6 and 11 are DNA Ladder.

3.4.1 Percent Viability of Human CML Cells Exposed to PDMP

To further examine the involvement of GCS in resistance to Imatinib-induced cell death, cells were exposed to PDMP, a strong GCS inhibitor, in the absence or presence of Imatinib. K562 cells, exposed to 10- and 20 μ M PDMP in the presence of 500 nM Imatinib resulted in about 90- and 100% cell death, respectively, while 500 nM Imatinib, by itself, caused around 60% growth inhibition (Figure 66). Treatment of K562 cells with 10- and 20 μ M PDMP resulted in 0- and 5% cell death.

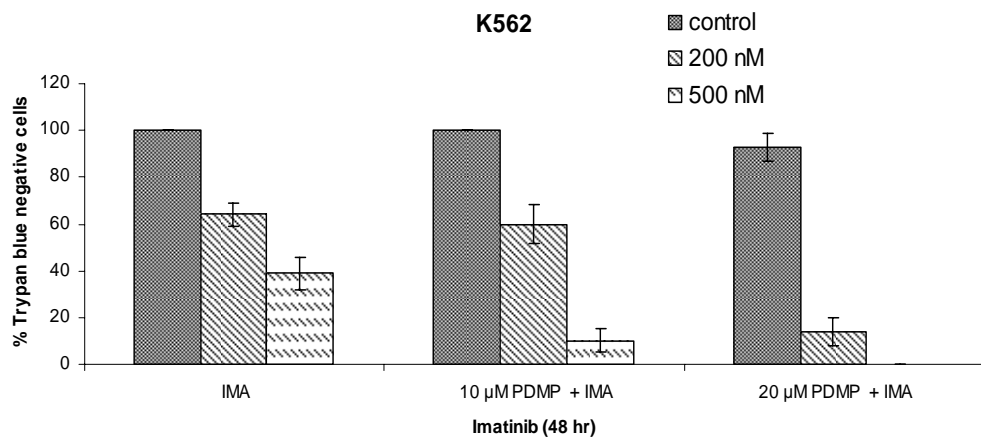


Figure 66. The role of inhibition of GCS by PDMP in the induction of apoptosis (by percent changes in trypan blue negative cells) in K562 cells. Percent changes of cell

viability in K562 cells, exposed to PDMP in the absence or presence of Imatinib (500 nM, 48 hr) were determined by trypan blue dye exclusion assay. Experiments were done in duplicates in at least two independent experiments. Error bars represent standard deviations. Statistical analysis was done using two way anova, P<0.01 was considered significant.

As shown in Figure 67, K562/IMA-0.2 cells, exposed to 10- and 20 μ M PDMP in the presence of 500 nM Imatinib resulted in about 35- and 40% cell death, respectively, while 500 nM Imatinib, by itself, caused around 8% growth inhibition (Figure 67). Treatment of K562/IMA-0.2 cells with 10- and 20 μ M PDMP did not cause cell death by itself.

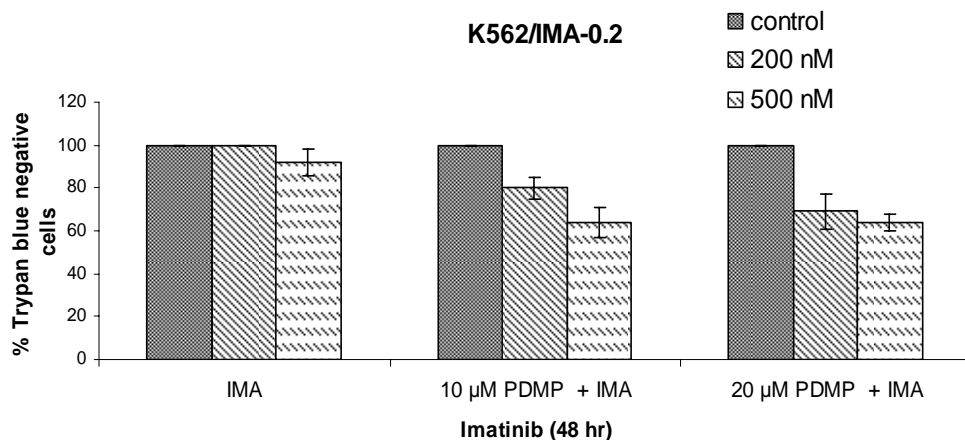


Figure 67. The role of inhibition of GCS by PDMP in the induction of apoptosis (by percent changes in trypan blue negative cells) in K562/IMA-0.2 cells. Percent changes of cell viability in K562/IMA-0.2 cells, exposed to PDMP in the absence or presence of Imatinib (48 hr) were determined by trypan blue dye exclusion assay. Experiments were done in duplicates in at least two independent experiments. Error bars represent standard deviations. Statistical analysis was done using two way anova, P<0.01 was considered significant.

Meg-01 cells were also examined for the effect of GCS inhibition in resistance to Imatinib-induced cell death. Meg-01 cells treated with 10- and 20 μ M PDMP in the presence of 500 nM Imatinib resulted in about 75- and 85% cell death,

respectively, while 500 nM Imatinib, by itself, caused around 40% growth inhibition (Figure 68). Treatment of Meg-01 cells with 10- and 20 μ M PDMP did not cause any cell death.

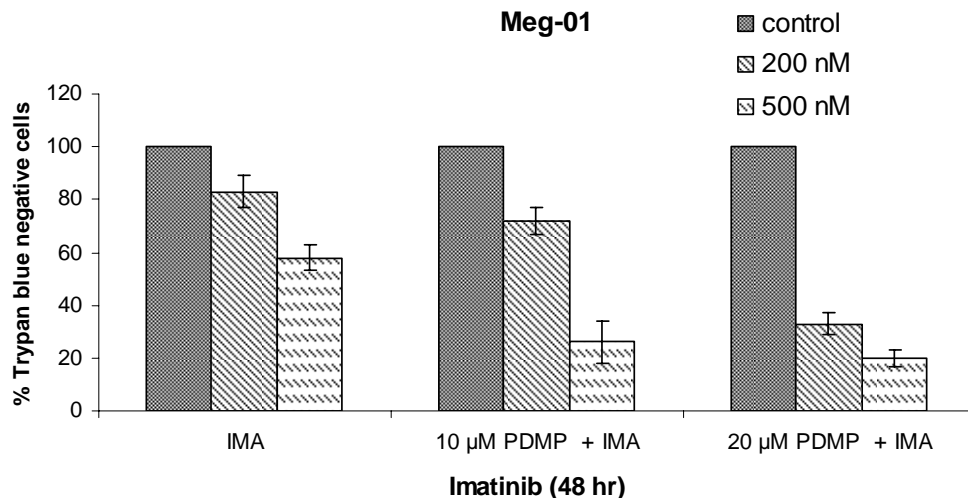


Figure 68. The role of inhibition of GCS by PDMP in the induction of apoptosis (by percent changes in trypan blue negative cells) in Meg-01 cells. Percent changes of cell viability in Meg-01 cells, exposed to PDMP in the absence or presence of Imatinib (48 hr) were determined by trypan blue dye exclusion assay. Experiments were done in duplicates in at least two independent experiments. Error bars represent standard deviations. Statistical analysis was done using two way anova, P<0.01 was considered significant.

As shown in Figure 69, Meg-01/IMA-0.2 cells, exposed to 10- and 20 μ M PDMP in the presence of 500 nM Imatinib resulted in about 45- and 55% cell death, respectively, while 500 nM Imatinib, by itself, caused around 15% growth inhibition (Figure 69). Treatment of K562/IMA-0.2 cells with 10- and 20 μ M PDMP resulted in 0- and 3% cell death.

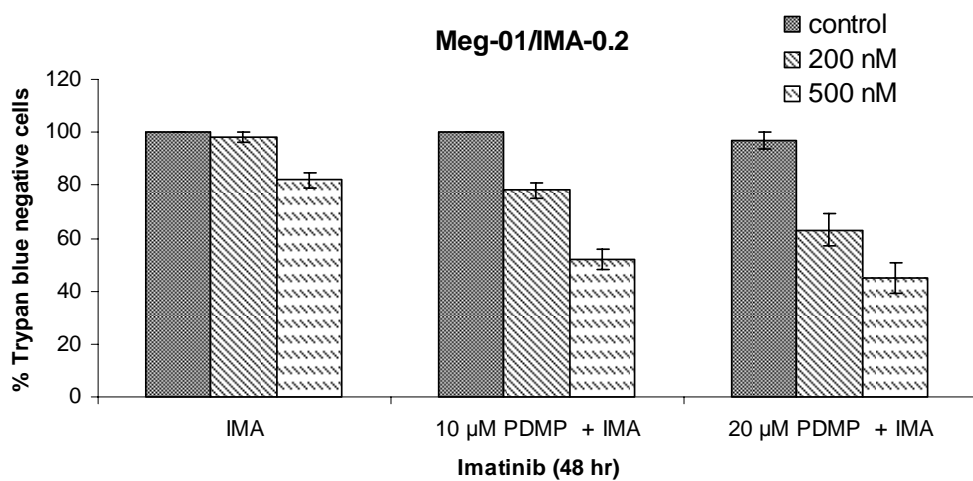


Figure 69. The role of inhibition of GCS by PDMP in the induction of apoptosis (by percent changes in trypan blue negative cells) in Meg-01/IMA-0.2 cells. Percent changes of cell viability in Meg-01/IMA0.2 cells, exposed to PDMP in the absence or presence of Imatinib (48 hr) were determined by trypan blue dye exclusion assay. Experiments were done in duplicates in at least two independent experiments. Error bars represent standard deviations. Statistical analysis was done using two way anova, P<0.01 was considered significant.

3.4.2 Cell Cycle Profiles of Human CML Cells Exposed to PDMP in the Absence or Presence of Imatinib

In addition to cell viability results, the cell cycle profiles of K562 and Meg-01 cells, exposed to PDMP, in the absence or presence of Imatinib, were examined in parental and resistant cells for 6 hr by flow cytometry. The data revealed that exposure to Imatinib (200 nM, 6 hr) did not cause apoptosis in sensitive K562 cells (Figure 70).

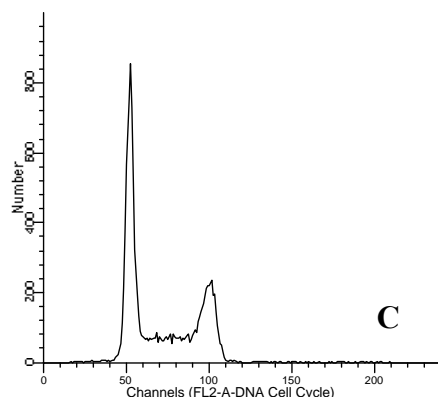
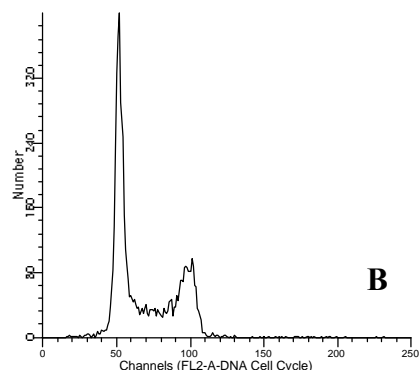
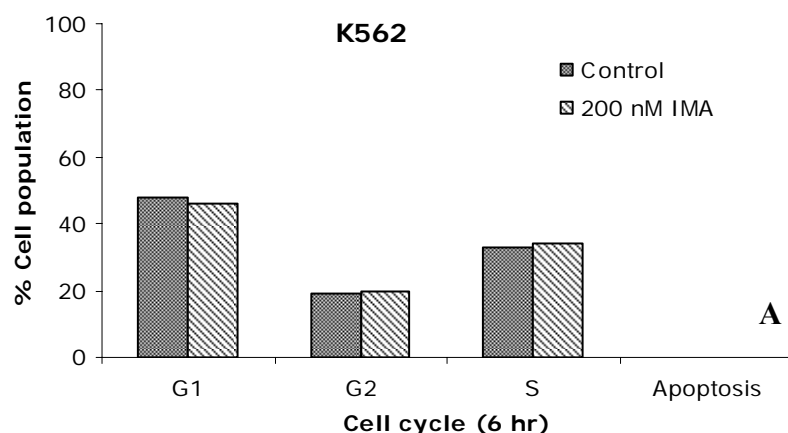
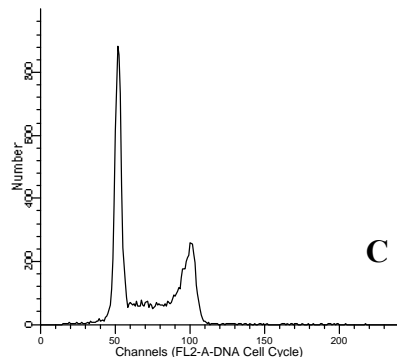
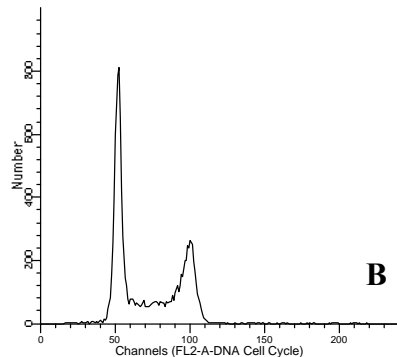
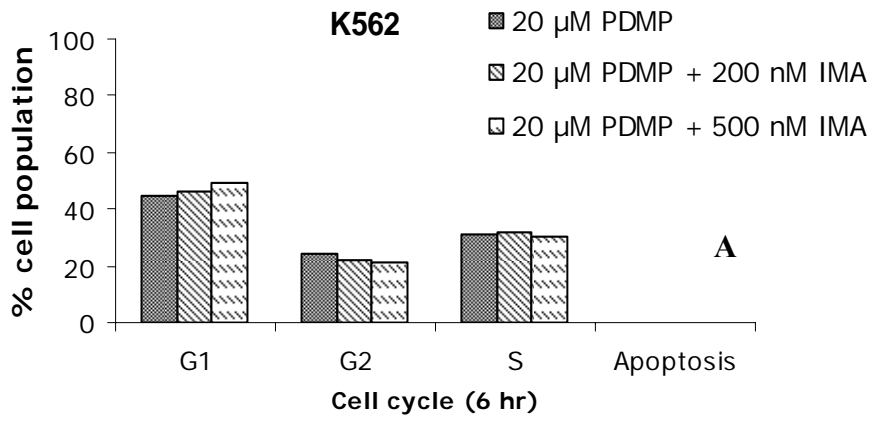


Figure 70. Cell cycle profiles in K562 cells in response to Imatinib (A, 6 hr). The effects of Imatinib (B) on cell cycle profiles of K562 were determined and compared to that of untreated cells (C) using flow cytometry. Statistical analysis was done using two way anova, $P<0.05$ was considered significant.

Treatment of K562 cells with 20 μ M PDMP in the presence of 200- and 500 nM also did not cause any cell death for 6 hr (Figure 71). There were also no significant changes in percent of cells in different cell cycle phases.



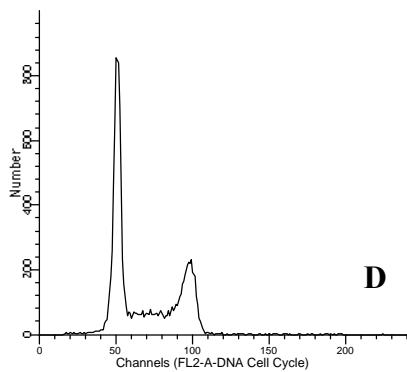
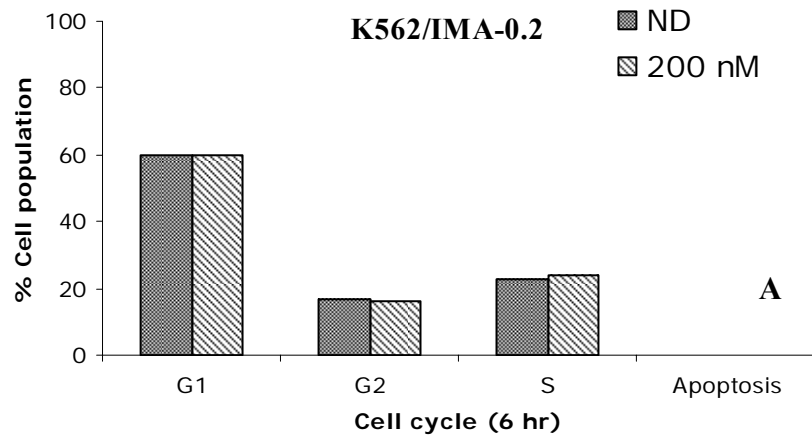


Figure 71. Cell cycle profiles in K562 cells in response to PDMP (A, 6 hr). The effects of PDMP (B) in the absence or presence of 200 nM (C) and 500 nM (D) Imatinib on cell cycle profiles of K562 were determined using flow cytometry. Statistical analysis was done using two way anova, P<0.05 was considered significant.

Cell cycle profiles of K562/IMA-0.2 cells, exposed to PDMP, in the absence or presence of Imatinib, were examined. It was observed that exposure to Imatinib (200 nM, 6 hr) did not cause apoptosis in K562/IMA-0.2 cells (Figure 72). There were also no changes in cell cycle profiles in response to Imatinib in 6 hr.



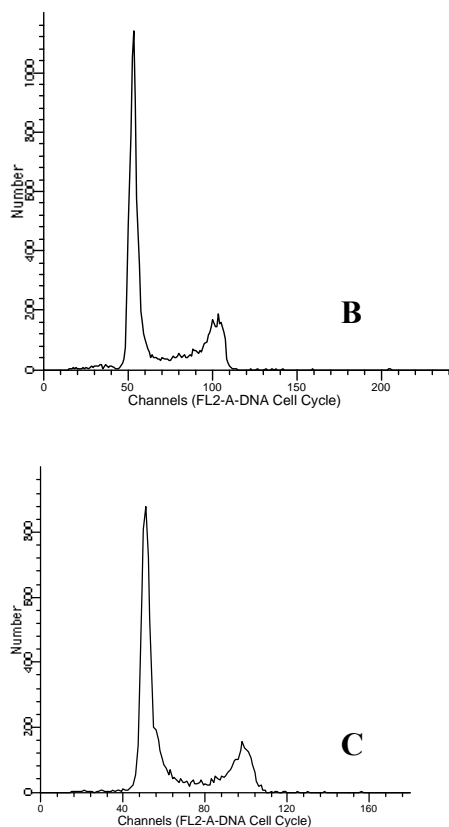
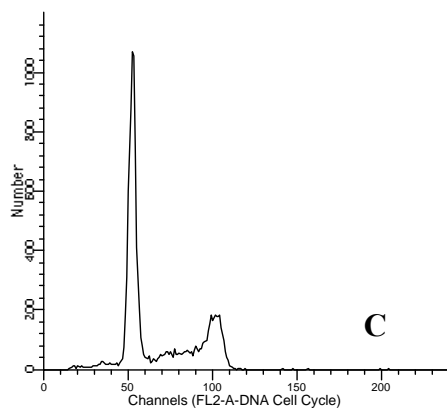
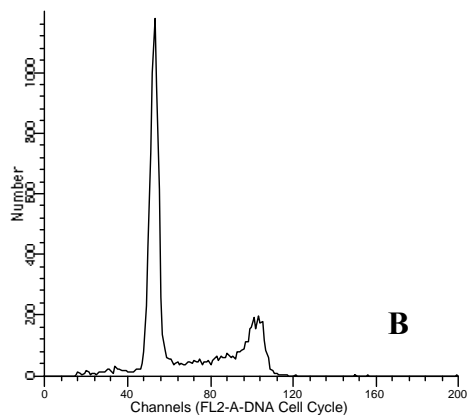
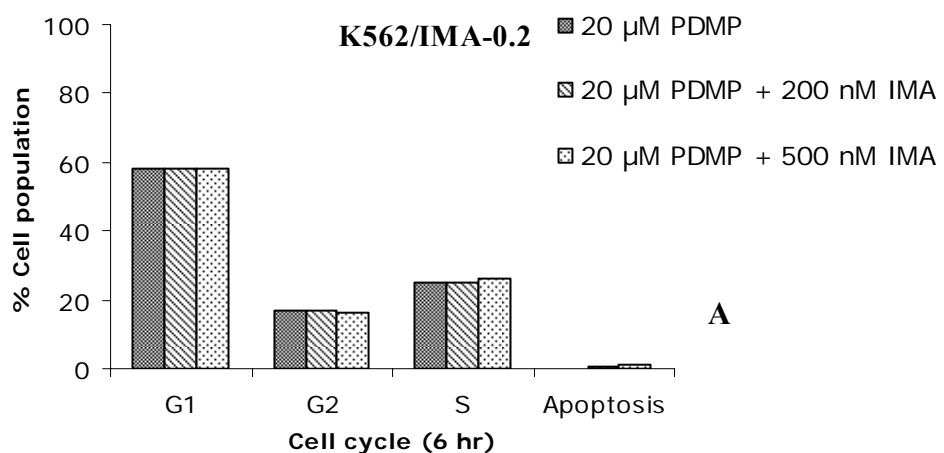


Figure 72. Cell cycle profiles in K562/IMA-0.2 cells in response to Imatinib (A, 6 hr). The effects of Imatinib (B) on cell cycle profiles of K562/IMA-0.2 were determined and compared to that of untreated cells (C) using flow cytometry. Statistical analysis was done using two way anova, $P<0.05$ was considered significant.

Treatment of K562/IMA-0.2 cells with 20 μ M PDMP in the presence of 200- and 500 nM also did not cause any cell death for 6 hr (Figure 73). No changes in cell cycle profiles were observed in response to PDMP and Imatinib together.



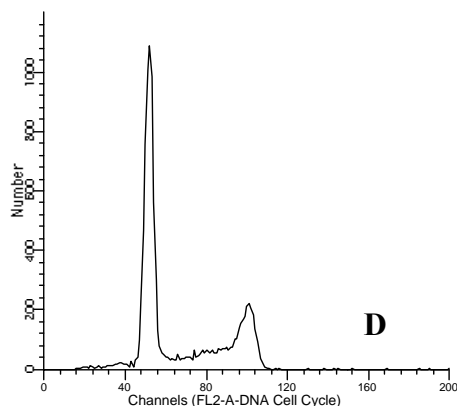
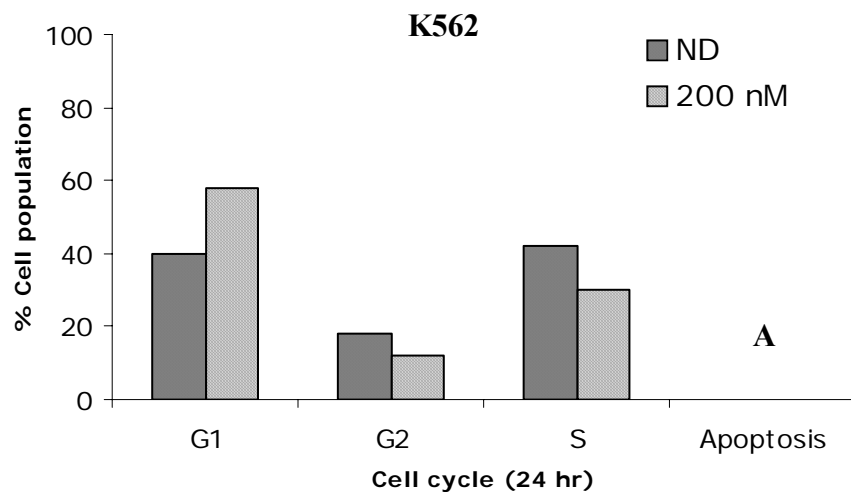


Figure 73. Cell cycle profiles in K562/IMA-0.2 cells in response to PDMP (A, 6 hr). The effects of PDMP (B) in the absence or presence of 200 nM (C) and 500 nM (D) Imatinib on cell cycle profiles of K562/IMA-0.2 were determined using flow cytometry. Statistical analysis was done using two way anova, $P<0.05$ was considered significant.

The cell cycle profiles of PDMP exposed K562 and K562/IMA-0.2 cells were examined, in the absence or presence of Imatinib, for 24 hr by flow cytometry. The data revealed that exposure to Imatinib (200 nM, 24 hr) did not cause apoptosis in parental K562 cells (Figure 74). After 24 hr, in response to Imatinib there were an increase in G1 and a decrease in G2 and S phases indicating that although there were not any cells in apoptosis, cell cycle arrest was observed.



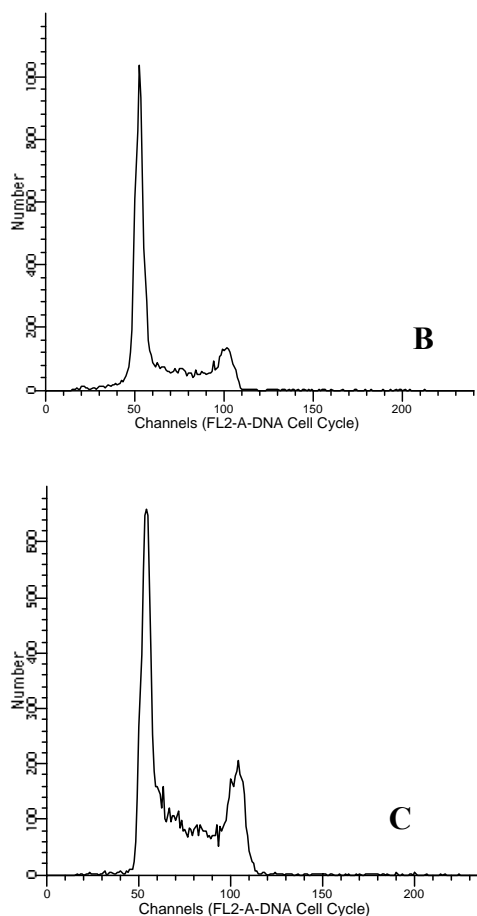
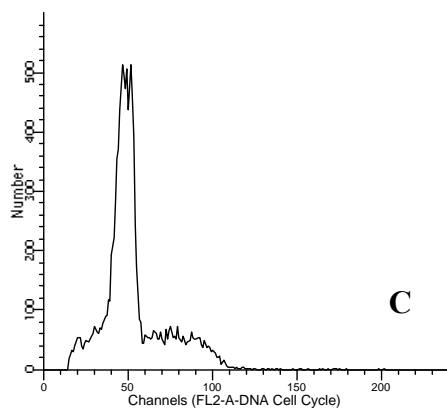
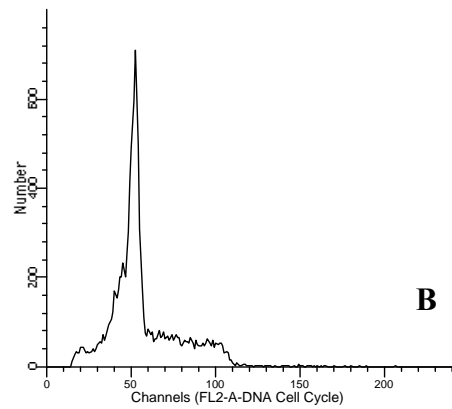
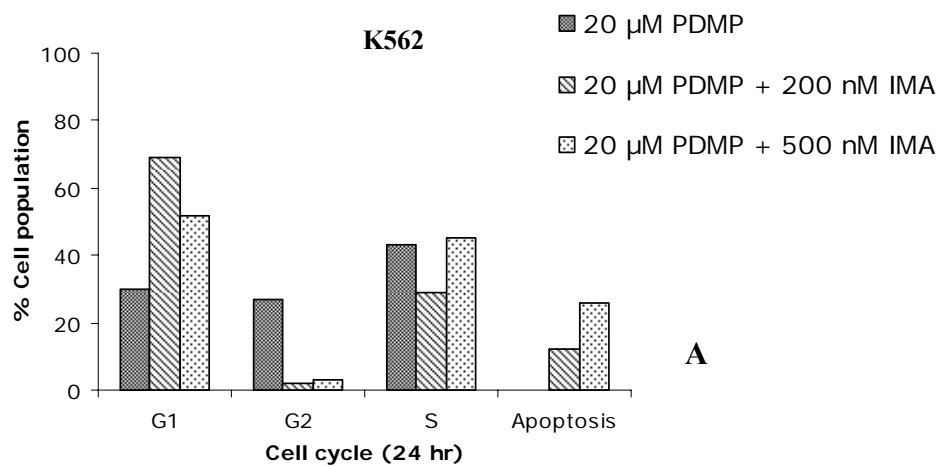


Figure 74. Cell cycle profiles in K562 cells in response to Imatinib (A, 24 hr). The effects of Imatinib (B) on cell cycle profiles of K562 were determined and compared to that of untreated cells (C) using flow cytometry. Statistical analysis was done using two way anova, $P<0.05$ was considered significant.

Treatment of K562 cells with PDMP ($20 \mu\text{M}$, 24 hr) in the presence of 200- and 500 nM Imatinib resulted in 12- and 26% apoptosis, respectively (Figure 75). In response to Imatinib, there was an increase in G1 phase while a decrease in S phase was observed.



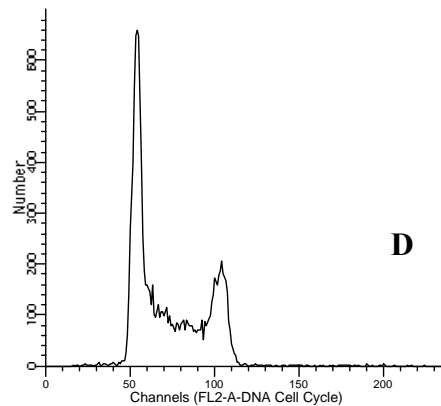
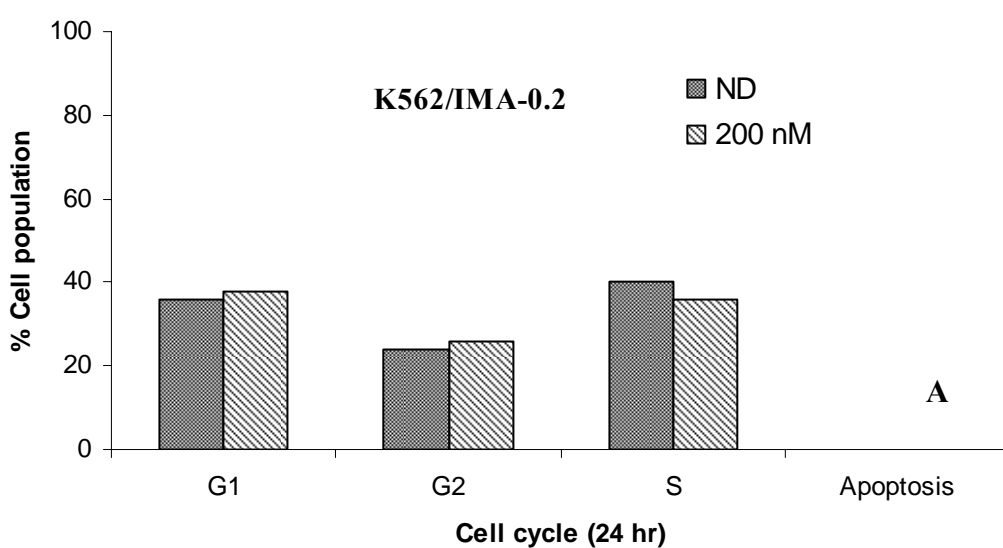


Figure 75. Cell cycle profiles in K562 cells in response to PDMP (A, 24 hr). The effects of PDMP (B) in the absence or presence of 200 nM (C) and 500 nM (D) Imatinib on cell cycle profiles of K562 were determined using flow cytometry. Statistical analysis was done using two way anova, $P<0.05$ was considered significant.

K562/IMA-0.2 cells were treated with PDMP (24 hr), in the absence or presence of Imatinib, and the cell cycle profiles were examined by flow cytometry. The data showed that exposure to Imatinib (200 nM, 24 hr) did not cause apoptosis in K562/IMA-0.2 cells (Figure 76).



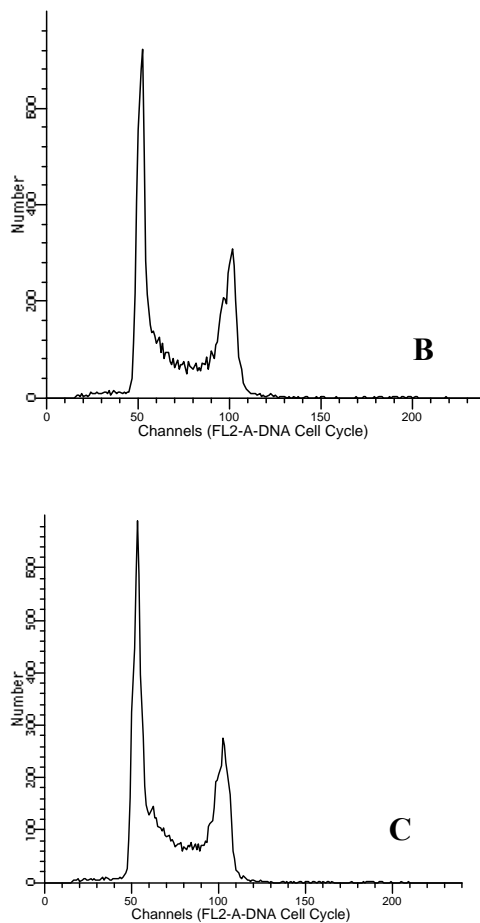
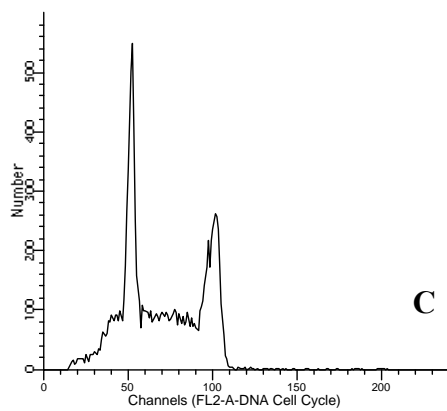
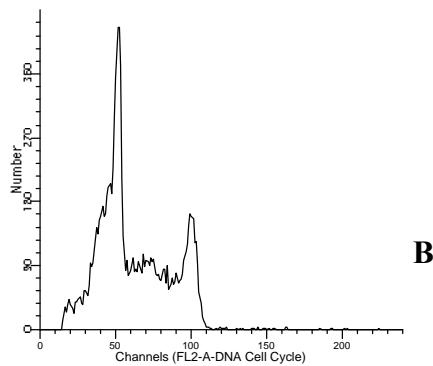
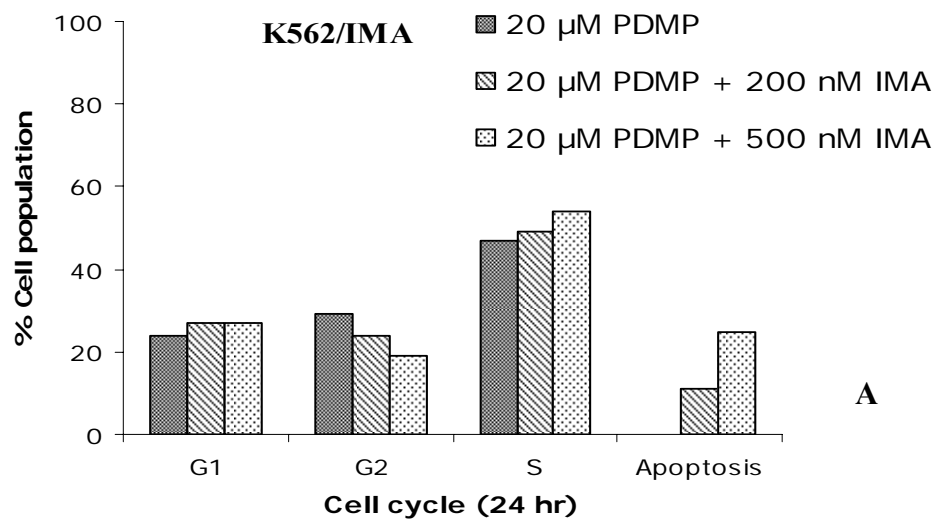


Figure 76. Cell cycle profiles in K562/IMA-0.2 cells in response to Imatinib (A, 24 hr). The effects of Imatinib (B) on cell cycle profiles of K562/IMA-0.2 were determined and compared to that of untreated cells (C) using flow cytometry. Statistical analysis was done using two way anova, $P<0.05$ was considered significant.

Treatment of K562/IMA-0.2 cells with PDMP (20 μ M, 24 hr) in the presence of 200- and 500 nM Imatinib resulted in 8- and 12% apoptosis, respectively (Figure 77). There was also an increase in G1 and S phases and a decrease in G2 phase was observed.



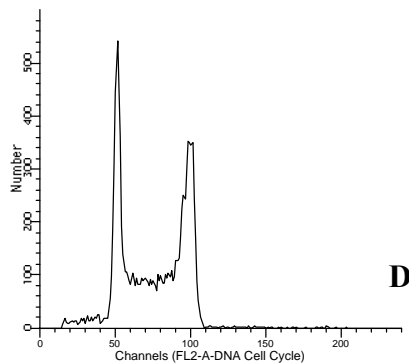
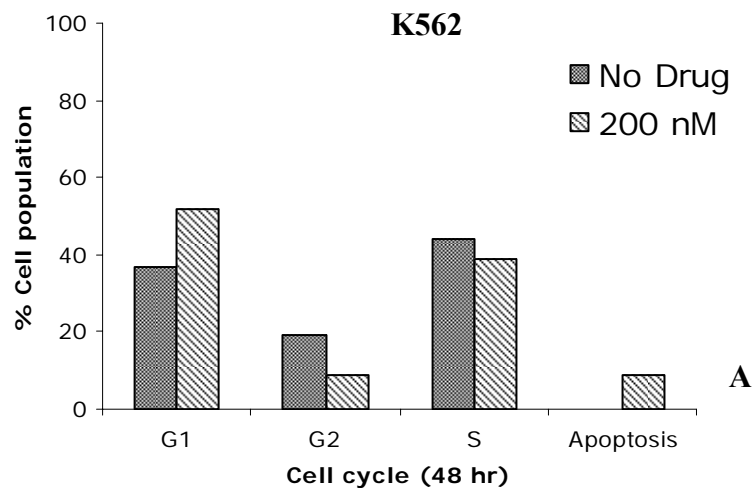


Figure 77. Cell cycle profiles in K562/IMA-0.2 cells in response to PDMP (A, 24 hr). The effects of PDMP (B) in the absence or presence of 200 nM (C) and 500 nM (D) Imatinib on cell cycle profiles of K562/IMA-0.2 were determined using flow cytometry. Statistical analysis was done using two way anova, $P<0.05$ was considered significant.

The cell cycle profiles were examined in PDMP exposed parental and resistant cells (48 hr), in the absence or presence of Imatinib, by flow cytometry. The data revealed that exposure to Imatinib (200 nM, 48 hr) resulted in 9% apoptosis in parental K562 cells (Figure 78). Imatinib treatment resulted in an increase in G1 and a decrease in G2 and S phases.



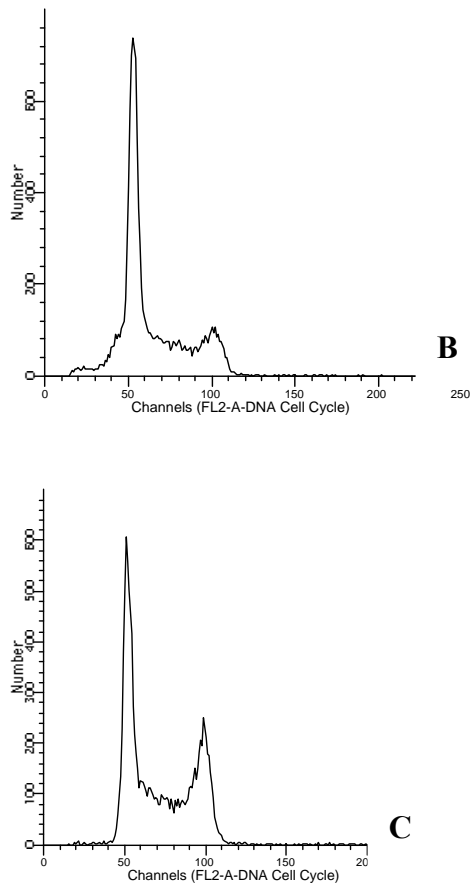
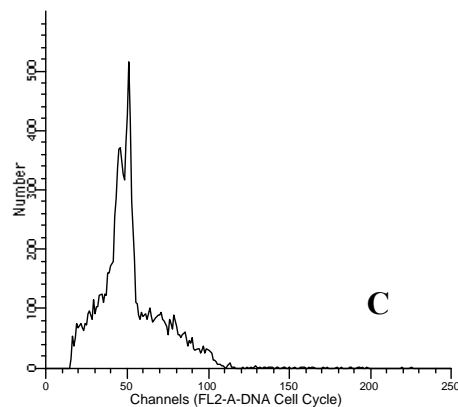
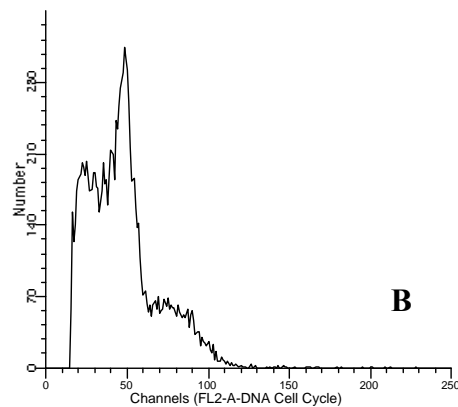
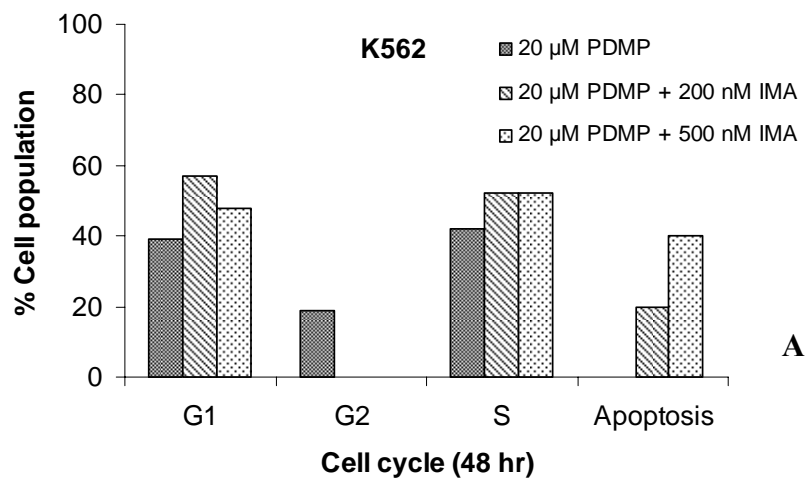


Figure 78. Cell cycle profiles in K562 cells in response to Imatinib (A, 48 hr). The effects of Imatinib (B) on cell cycle profiles of K562 were determined and compared to that of untreated cells (C) using flow cytometry. Statistical analysis was done using two way anova, $P<0.05$ was considered significant.

Treatment of K562 cells with $20 \mu\text{M}$ PDMP in the presence of 200- and 500 nM Imatinib (48 hr) resulted in 20- and 40% apoptosis, respectively (Figure 79). PDMP and Imatinib treatment also revealed that there were an increase in G1, no change in S and a decrease in G2 phases.



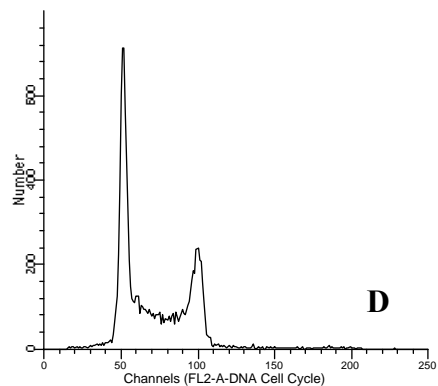
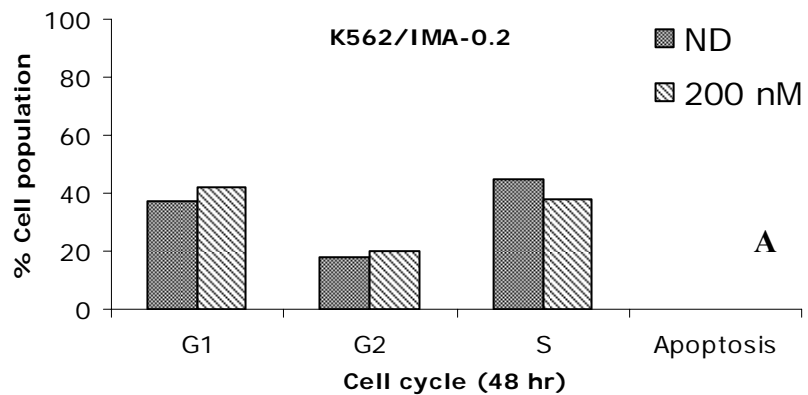


Figure 79. Cell cycle profiles in K562 cells in response to PDMP (A, 48 hr). The effects of PDMP (B) in the absence or presence of 200 nM (C) and 500 nM (D) Imatinib on cell cycle profiles of K562 were determined using flow cytometry. Statistical analysis was done using two way anova, $P<0.05$ was considered significant.

K562/IMA-0.2 cells treated with PDMP (48 hr) in the absence or presence of Imatinib, and cell cycle profiles were examined by flow cytometry. The data showed that exposure to Imatinib (200 nM, 48 hr) did not cause apoptosis in K562/IMA-0.2 cells (Figure 80).



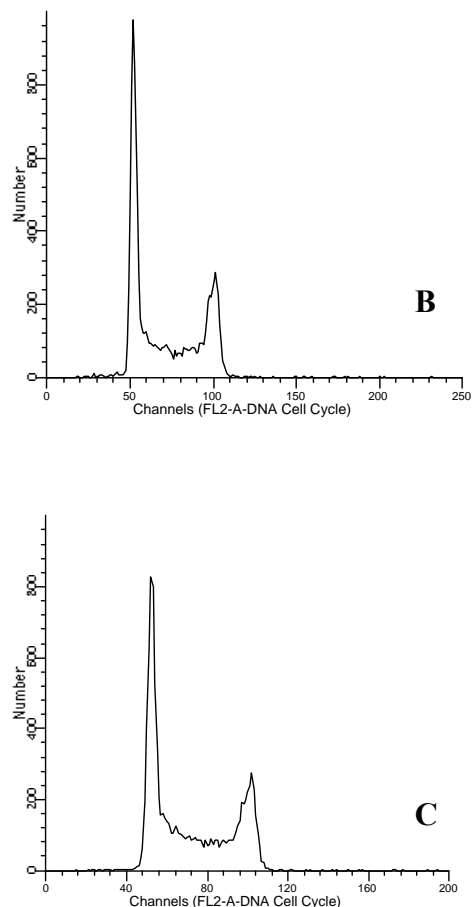
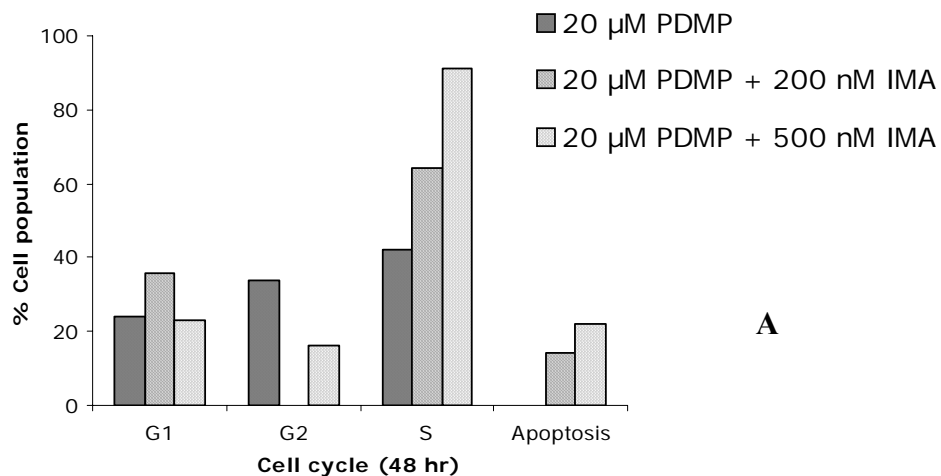


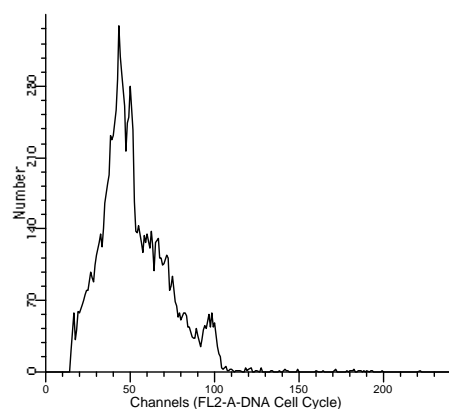
Figure 80. Cell cycle profiles in K562/IMA-0.2 cells in response to Imatinib (A, 48 hr). The effects of Imatinib (B) on cell cycle profiles of K562/IMA-0.2 were determined and compared to that of untreated cells (C) using flow cytometry. Statistical analysis was done using two way anova, $P<0.05$ was considered significant.

Treatment of K562/IMA-0.2 cells with 20 μ M PDMP in the presence of 200- and 500 nM Imatinib (48 hr) resulted in 14- and 22% apoptosis, respectively (Figure 81).

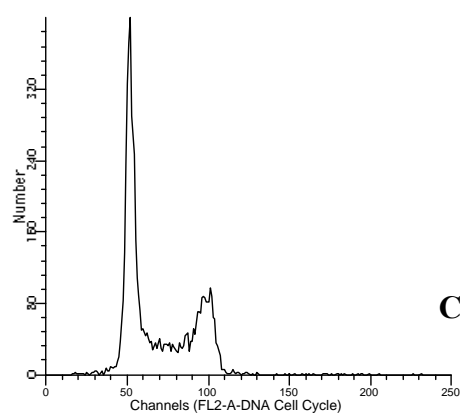
K562/IMA-0.2



A



B



C

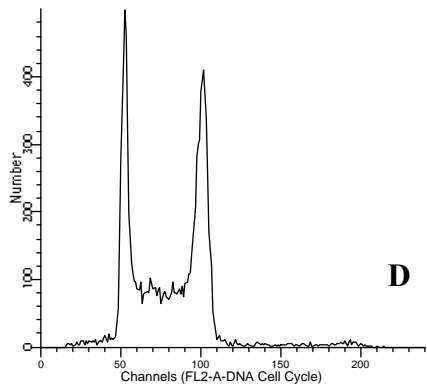


Figure 81. Cell cycle profiles in K562/IMA-0.2 cells in response to PDMP (A, 48 hr). The effects of PDMP (B) in the absence or presence of 200 nM (C) and 500 nM (D) Imatinib on cell cycle profiles of K562/IMA-0.2 were determined using flow cytometry. Statistical analysis was done using two way anova, $P<0.05$ was considered significant.

Taken together all these data showed that PDMP increased apoptotic effect of Imatinib. This combination therapy started to be effective after 24 hr. Besides induction of apoptosis, PDMP and Imatinib treatment also resulted in cell cycle arrest.

3.4.3 MTT Cell Proliferation Assay in Human CML Cells Exposed to PDMP in the Absence or Presence of Imatinib

The IC_{50} values of Imatinib and the combination therapy of PDMP and Imatinib in K562/IMA-1 cells were determined. As shown in Figure 82, K562/IMA-1 cells, exposed to PDMP and Imatinib, expressed about 4-fold more sensitivity, as compared to only Imatinib applied counterparts. The IC_{50} values of Imatinib and combination therapy of PDMP and Imatinib were 4,600- and 1,100 nM for K562/IMA-1 cells, respectively (Figure 82).

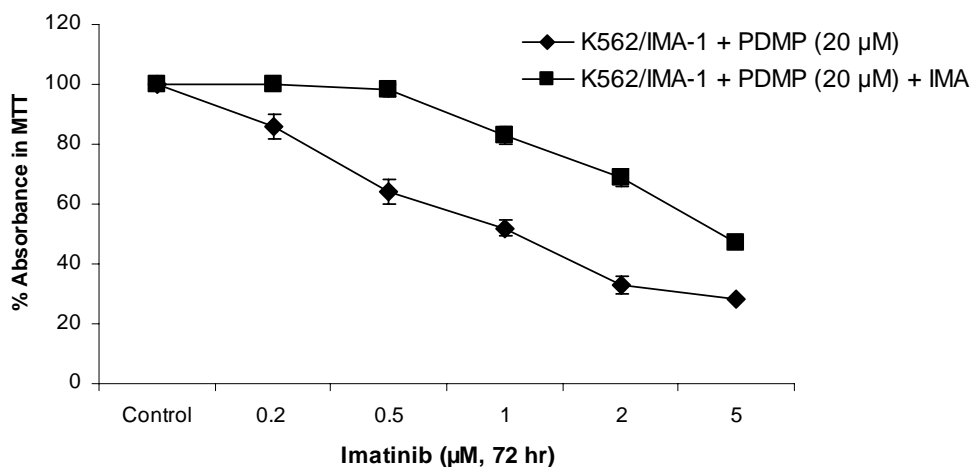


Figure 82. Effects of PDMP, in the absence or presence of Imatinib, on the growth of K562/IMA-1 cells *in situ*. The IC₅₀ concentration of Imatinib was determined by MTT assay for each cell line as described. Experiments were done in triplicate in at least two independent experiments. Statistical analysis was done using two way anova, p<0.01 was considered significant. Standard deviations for each point were between 0.5- and 4%. The error bars represent the standard deviations, and when not seen, they are smaller than the thickness of the lines on the graphs.

The IC₅₀ values of Imatinib and combination therapy of PDMP and Imatinib in Meg-01/IMA-1 cells were also examined. The IC₅₀ values of Imatinib and combination therapy were 1,500- and 1,200 nM for Meg-01/IMA-1 cells, respectively (Figure 83). In Meg-01/IMA-1 cells, PDMP did not result in cell death as much as it did in K562/IMA-1 cells.

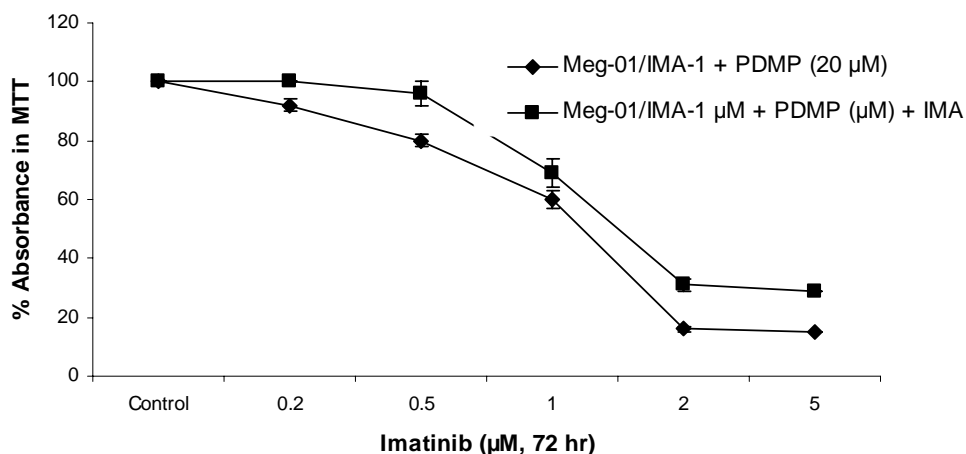


Figure 83. Effects of PDMP, in the absence or presence of Imatinib, on the growth of Meg-01/IMA-1 cells *in situ*. The IC₅₀ concentration of Imatinib was determined by MTT assay for each cell line as described. Experiments were done in triplicate in at least two independent experiments, and statistical analysis was done using two way anova, p<0.01 was considered significant. Standard deviations for each point were between 0.5- and 4%. The error bars represent the standard deviations, and when not seen, they are smaller than the thickness of the lines on the graphs.

3.4.4 Analyses of Ceramide Levels in Human CML Cells in Response to PDMP in the Absence or Presence of Imatinib

The levels of endogenous ceramide in K562, K562/IMA-0.2 and -1 cells, treated with PDMP, in the absence or presence of Imatinib (48 hr), were measured by LC/MS. K562 cells treated with Imatinib (200 nM, 48 hr) showed a slight increase in ceramide levels. In PDMP exposed K562 cells, C₁₄-, C₁₈-, C₂₀-, C₂₄-, and C_{24:1}-ceramides levels were increased above the ceramide levels in Imatinib (200 nM) applied K562 cells. Interestingly, the data showed that treatment with PDMP resulted in a significant increase in the generation of all ceramide especially C₁₈-ceramide (about 35-fold), and to a lesser extent, C₁₄-, C₁₆-, and C₂₀-ceramides (around 7- to 15-fold) in parental K562 cells when compared to untreated controls (Figure 84).

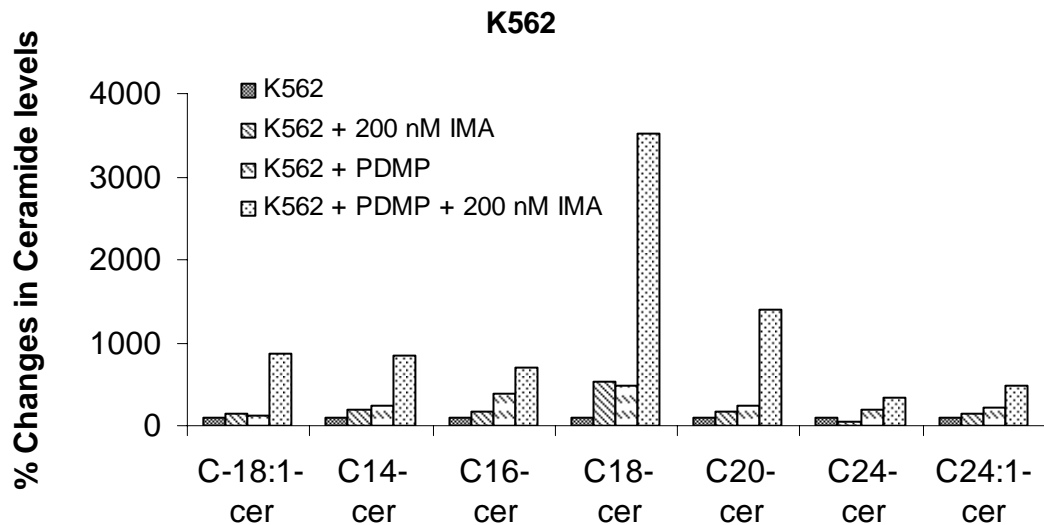


Figure 84. Relative changes of ceramide levels in K562 cells treated with PDMP in the absence or presence of Imatinib. The concentrations of C_{18:1}-, C₁₄-, C₁₆-, C₁₈-, C₂₀-, C₂₄-, and C_{24:1}-ceramides in K562 cells treated with PDMP (20 μ M) in the absence or presence of Imatinib (200 nM, 48 hr) were measured by LC/MS. The levels of ceramide were normalized to Pi concentrations. Percent changes of ceramide levels were calculated. The experiments were done in at least two independent trials. Statistical analysis was done using two way anova, P<0.01 was considered significant.

Treatment of resistant K562/IMA-0.2 cells with Imatinib (500 nM, 48 hr) did not cause any significant changes in the levels of ceramides (Figure 85). In PDMP exposed K562/IMA-0.2 cells, C_{18:1}-, C₁₄-, C₁₆-, C₁₈-, C₂₀-, C₂₄-, and C_{24:1}-ceramides levels were increased above the ceramide levels in Imatinib (500 nM) applied K562/IMA-0.2 cells. The data showed that treatment with PDMP resulted in an increase especially C₁₈-ceramide (about 8-fold), and to a lesser extent, C₁₆-, C₂₀-, C₂₄-ceramides (around 2-fold) in K562/IMA-0.2 cells when compared to untreated controls (Figure 85). Comparing to parental K562 cells, C₁₈-ceramide levels were increased 4 times less in K562/IMA-0.2 cells although higher concentration of Imatinib was applied.

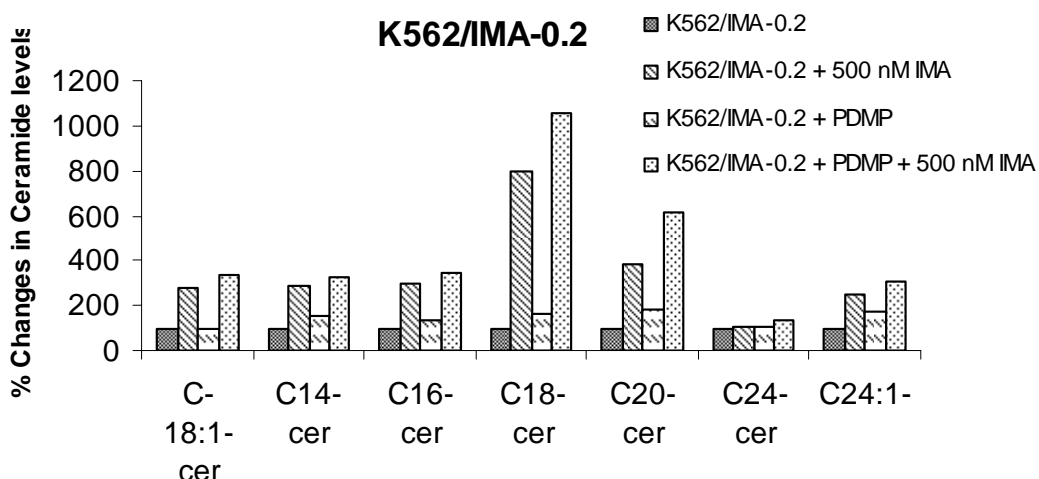


Figure 85. Relative changes of ceramide levels in K562/IMA-0.2 cells treated with PDMP in the absence or presence of Imatinib. The concentrations of C_{18:1}-, C₁₄-, C₁₆, C₁₈-, C₂₀- C₂₄-, and C_{24:1}-ceramides in K562/IMA-0.2 cells treated with PDMP (20 μ M) in the absence or presence of Imatinib (500 nM, 48 hr) were measured by LC/MS. The levels of ceramide were normalized to Pi concentrations. Percent changes of ceramide levels were calculated. The experiments were done in at least two independent trials. Statistical analysis was done using two way anova, P<0.01 was considered significant.

On the other hand, treatment of resistant K562/IMA-1 cells with Imatinib (2 μ M, 48 hr) did not cause any significant changes in the levels of ceramides (Figure 86). Interestingly, there was even a decrease in C₂₄-ceramide levels. In PDMP exposed K562/IMA-1 cells, C₁₄-, C₁₆-, C₁₈-, C₂₀-, and C_{24:1}-ceramides levels were increased comparing to untreated control but below the ceramide levels in Imatinib (2 μ M) applied K562/IMA-1 cells. There were also no changes in C_{18:1}- and C₂₄-ceramide levels in PDMP treated K562/IMA-1 cells. It was also observed that treatment with PDMP and Imatinib (2 μ M) together resulted in an increase in the generation of all ceramide especially C₁₈-ceramide (about 5-fold), and to a lesser extent, C_{18:1}-, C₁₄-, C₁₆-, C₂₀-, C_{24:1}-ceramides (around 2-fold) in K562/IMA-1 cells when compared to untreated controls (Figure 86). Comparing to parental K562 cells, C₁₈-ceramide levels were increased 7 times less in K562/IMA-1 cells although higher

concentration of Imatinib was applied. Taken together all these data suggest that, the more resistant cells are, the less accumulation of ceramides, although higher concentration of Imatinib.

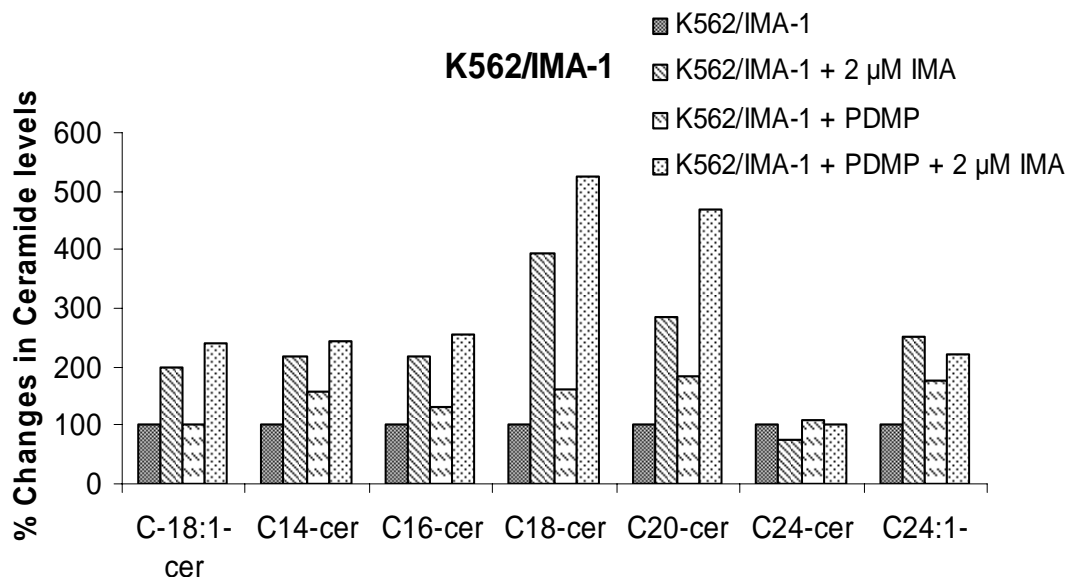


Figure 86. Relative changes of ceramide levels in K562/IMA-1 cells treated with PDMP in the absence or presence of Imatinib. The concentrations of C_{18:1}-, C₁₄-, C₁₆, C₁₈-, C₂₀-, C₂₄-, and C_{24:1}-ceramides in K562/IMA-1 cells treated with PDMP (20 μ M) in the absence or presence of Imatinib (2 μ M, 48 hr) were measured by LC/MS. The levels of ceramide were normalized to Pi concentrations. Percent changes of ceramide levels were calculated. The experiments were done in at least two independent trials. Statistical analysis was done using two way anova, P<0.01 was considered significant.

The levels of endogenous ceramide in Meg-01, Meg-01/IMA-0.2 and -1 cells, treated with PDMP in the absence or presence of Imatinib (48 hr), were also measured by LC/MS. Meg-01 cells treated with Imatinib (200 nM, 48 hr) showed a slight increase in ceramide levels. In PDMP exposed K562 cells, C₁₄-, C₁₆-, C₂₀-, C₂₄-, and C_{24:1}-ceramides levels were increased above the ceramide levels in Imatinib (200 nM) applied Meg-01 cells. Supporting to the previous data, it was observed that treatment with PDMP resulted in a significant increase in the generation of all ceramide especially C₁₈-ceramide (about 8-fold), and to a lesser extent, C_{18:1}-, C₁₄-,

C_{16} -, C_{20} -, C_{24} -, and $C_{24:1}$ -ceramides (around 5-fold) in parental Meg-01 cells when compared to untreated controls (Figure 87).

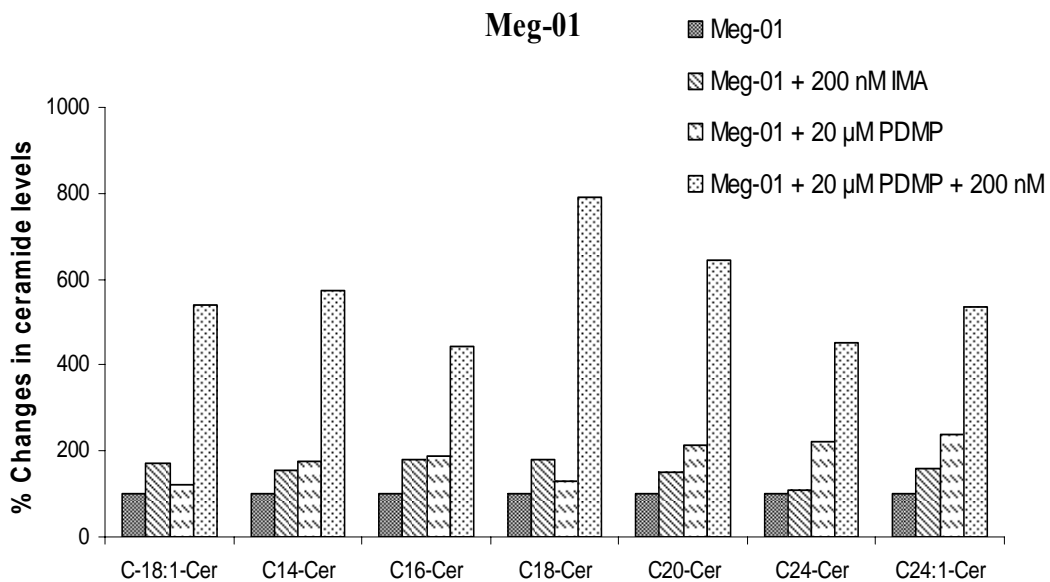


Figure 87. Relative changes of ceramide levels in Meg-01 cells treated with PDMP in the absence or presence of Imatinib. The concentrations of $C_{18:1}$ -, C_{14} -, C_{16} -, C_{18} -, C_{20} -, C_{24} -, and $C_{24:1}$ -ceramides in Meg-01 cells treated with PDMP (20 μ M) in the absence or presence of Imatinib (200 nM, 48 hr) were measured by LC/MS. The levels of ceramide were normalized to Pi concentrations. Percent changes of ceramide levels were calculated. The experiments were done in at least two independent trials. Statistical analysis was done using two way anova, $P<0.01$ was considered significant.

Treatment of resistant Meg-01/IMA-0.2 cells with Imatinib (500 nM, 48 hr) slightly increased the levels of ceramides (Figure 88). In PDMP exposed Meg-01/IMA-0.2 cells, $C_{18:1}$ -, C_{14} -, C_{16} -, C_{18} -, C_{20} -, C_{24} -, and $C_{24:1}$ -ceramides levels were decreased below the ceramide levels in Imatinib (500 nM) applied Meg-01/IMA-0.2 cells. It was also shown that treatment with PDMP resulted in an increase in the generation of all ceramide especially C_{18} -ceramide (about 6-fold), and to a lesser extent, C_{16} -, C_{20} -, C_{24} -ceramides (around 4-fold) in Meg-01/IMA-0.2 cells when compared to untreated controls (Figure 89).

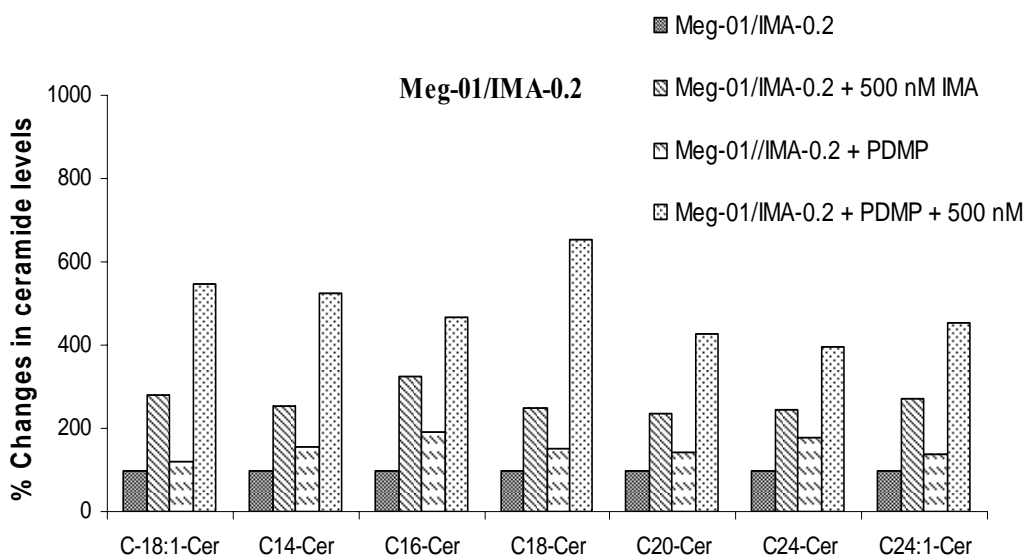


Figure 88. Relative changes of ceramide levels in Meg-01/IMA-0.2 cells treated with PDMP in the absence or presence of Imatinib. The concentrations of C_{18:1}-, C₁₄-, C₁₆-, C₁₈-, C₂₀-, C₂₄-, and C_{24:1}-ceramides in Meg-01/IMA-0.2 cells treated with PDMP (20 μ M) in the absence or presence of Imatinib (500 nM, 48 hr) were measured by LC/MS. The levels of ceramide were normalized to Pi concentrations. Percent changes of the levels of ceramide levels were calculated. The experiments were done in at least two independent trials. Statistical analysis was done using two way anova, P<0.01 was considered significant.

On the other hand, treatment of resistant Meg-01/IMA-1 cells with Imatinib (2 μ M, 48 hr) resulted in a slight increase in the levels of ceramides (Figure 89). In PDMP exposed Meg-01/IMA-1 cells, C₁₄-, C₁₆-, and C₂₄-ceramides levels were increased, while C_{18:1}- C₂₀- and C_{24:1}-ceramide levels were decreased comparing to Imatinib (2 μ M) applied Meg-01/IMA-1 cells. The data also revealed that treatment with PDMP and Imatinib (2 μ M) together resulted in an increase in the generation of all ceramide (about 2- to 5-fold) in Meg-01/IMA-1 cells when compared to untreated controls (Figure 89). Comparing to parental Meg-01 cells, C₁₈-ceramide levels were increased 7 times less in Meg-01/IMA-1 cells although higher concentration of Imatinib was applied. Taken together, all these data suggest that, the more resistant cells, the less accumulated ceramides as compared to parental cells.

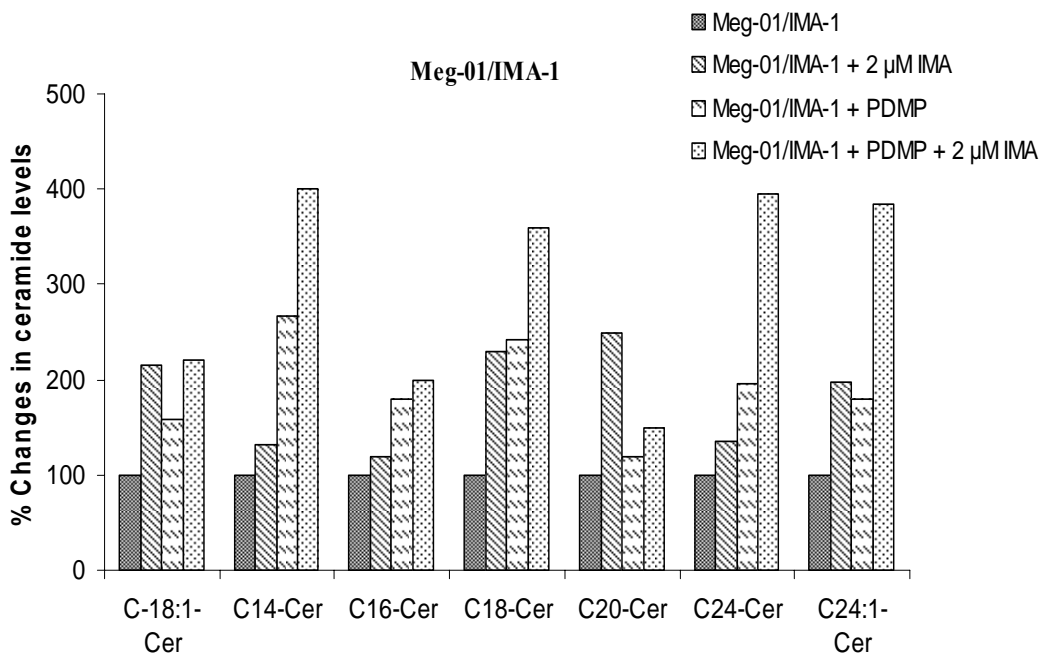


Figure 89. Relative changes of ceramide levels in Meg-01/IMA-1 cells treated with PDMP in the absence or presence of Imatinib. The concentrations of C_{18:1}-, C₁₄-, C₁₆, C₁₈-, C₂₀- C₂₄-, and C_{24:1}-ceramides in Meg-01/IMA-1 cells treated with PDMP (20 μM) in the absence or presence of Imatinib (2 μM, 48 hr) were measured by LC/MS. The levels of ceramide were normalized to Pi concentrations. Percent changes of the levels of ceramide levels were calculated. The experiments were done in at least two independent trials. Statistical analysis was done using two way anova, P<0.01 was considered significant.

3.4.5 Expression Analyses of GCS in Parental and Resistant Human CML Cells

Then, the levels of GCS expression were analyzed in parental and 1 μM Imatinib resistant cells by RT-PCR (Figure 90). The data showed that K562/IMA-1 and Meg-01/IMA-1 cells overexpress GCS when compared to their parental sensitive counterparts (Figures 90). Quantification analyses of GCS gene expression was conducted by Scion Image programme and the results showed that there was around 1.7- and 1.9-fold increase in expression of GCS gene in K562/IMA-1 and Meg-01/IMA-1, respectively, as compared to parental counterparts.

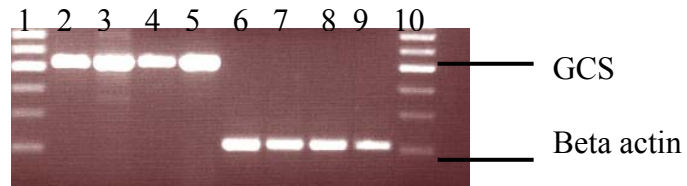


Figure 90. Expression analyses of GCS in parental and resistant human CML cells. GCS mRNA levels in K562 and K562/IMA-1 cells (lanes 2-3) and Meg-01 and Meg-01/IMA-1 cells (lanes 4-5) were measured by RT-PCR. Beta actin levels were used as internal positive controls (lanes 6-9 respectively). Lanes 1 and 10 are DNA Ladder.

3.5 EXPRESSION ANALYSES OF BCR-ABL IN PARENTAL AND RESISTANT HUMAN CML CELLS

Expression levels of BCR-ABL were analyzed in K562, K562/IMA-0.2 and -1 and Meg-01, Meg-01/IMA-0.2 and -1 cells by RT-PCR (Figure 91). Indeed, the data showed that K562/IMA-1 and Meg-01/IMA-1 cells overexpress BCR-ABL gene when compared to their parental sensitive counterparts (Figure 91). Quantification analyses of BCR-ABL gene expression was conducted by Scion Image programme and the results showed that there was around 2.5- and 4.7-fold increase in expression of BCR-ABL gene in K562/IMA-0.2 and K562/IMA-1 cells, respectively, as compared to parental K562 cells. On the other hand, quantification analyses of BCR-ABL was also conducted in Meg-01 cells and 1.2- and 4.4-fold increase in expression of BCR-ABL gene in Meg-01/IMA-0.2 and Meg-01/IMA-1 cells were observed, respectively, as compared to parental Meg-01 cells.

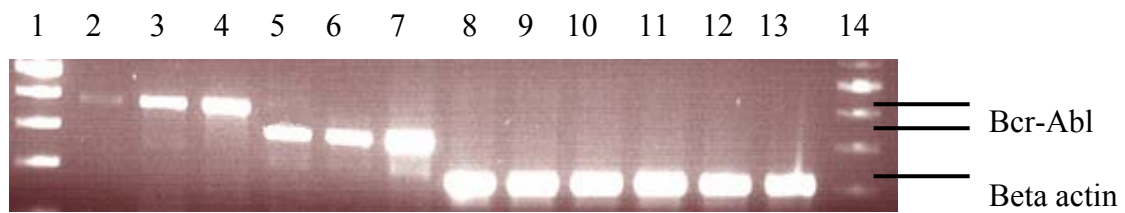


Figure 91. Expression analyses of BCR-ABL in parental and resistant human CML cells. BCR-ABL expression levels in K562, K562/IMA-0.2 and -1 cells (lanes 2, 3,

and 4) and Meg-01, Meg-01/IMA-0.2 and -1 cells (lanes 5, 6, and 7) were measured by RT-PCR. Beta actin levels were used as internal positive controls (lanes 8 to 13, respectively). Lanes 1 and 14 are DNA ladder.

Protein levels of BCR-ABL were also analyzed in parental and resistant K562 and Meg-01 by western blotting (Figure 92). In parallel with previous results, it was observed that 0.2- and 1 μ M Imatinib resistant K562 and Meg-01 cells overexpress BCR-ABL gene when compared to their parental sensitive counterparts (Figure 92). Quantification analyses of BCR-ABL protein levels were conducted by Scion Image programme and the results showed that there was around 1.6- and 2.1-fold increase in protein level of BCR-ABL gene in K562/IMA-0.2 and K562/IMA-1 cells, respectively, as compared to parental K562 cells. On the other hand, quantification analyses of BCR-ABL was also conducted in Meg-01 cells and 1.5- and 2-fold increase in protein level of BCR-ABL gene in Meg-01/IMA-0.2 and Meg-01/IMA-1 cells were observed, respectively, as compared to parental Meg-01 cells.



Figure 92. Protein levels of BCR-ABL in parental and resistant human CML cells. BCR-ABL protein levels were measured in K562, K562/IMA-0.2 and -1 cells (lanes 1, 2, and 3) and in Meg-01, Meg-01/IMA-0.2 and -1 cells (lanes 4, 5, and 6, respectively) by western blotting. Beta actin levels were used as internal positive controls (lanes 7 to 12, respectively).

3.5.1 Expression Pattern of BCR-ABL Gene in hLASS1 and hLASS6 Transfected K562 Cells

To examine if there is any interaction between hLASS1 and hLASS6 genes and BCR-ABL, parental K562 cells were transfected with hLASS1 and hLASS6. The expression analyses of hLASS1 and hLASS6 were shown by RT-PCR (Figure 41) and then BCR-ABL gene expression analyses were conducted. The results revealed that overexpression of hLASS1 in K562 cells resulted in a decrease in expression of BCR-ABL, while there was no change of BCR-ABL expression in hLASS6 transfected cells (Figure 93). Quantification analyses of BCR-ABL gene expression was conducted by Scion Image programme and the results showed that there was around 1.8-fold increase in expression of BCR-ABL gene in hLASS1 transfected K562 cells as compared to control transfected ones. However, there was no change in expression pattern of BCR-ABL gene in hLASS6 transfected cells.

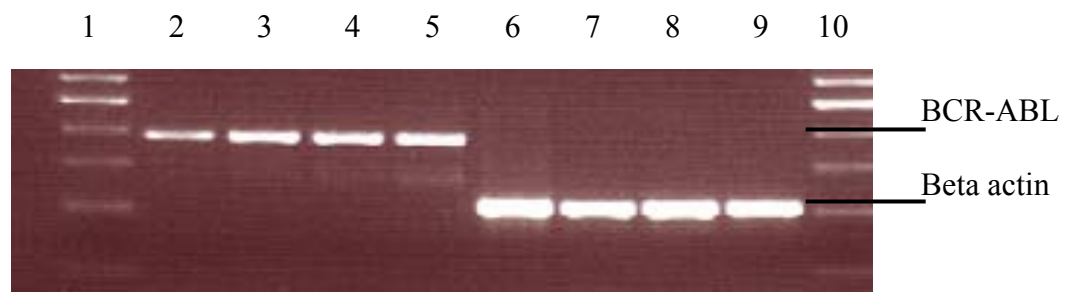


Figure 93. Expression analyses of BCR-ABL in vector and hLASS1 or hLASS6 transfected K562 cells. Expression levels of BCR-ABL in hLASS1 and its vector (lanes 2 and 3) and hLASS6 and its vector (Lanes 4 and 5) transfected K562 cells were measured using RT-PCR. Beta-actin levels were used as internal positive controls (lanes 6-9). Lanes 1 and 10 are DNA Ladder.

3.5.2 Expression Pattern of BCR-ABL Gene in SK-1 Transfected K562 Cells

On the other hand, interaction, if there is, between SK-1 and BCR-ABL genes were examined in parental K562 cells, transfected with SK-1 and control vector. Overexpression of SK-1 was shown by RT-PCR (Figure 94), and the expression analyses of BCR-ABL gene were conducted. Interestingly, the results showed that overexpression of SK-1 in K562 cells resulted in a significant increase in expression of BCR-ABL gene as compared to vector transfected cells (Figure 94). Quantification analyses of BCR-ABL gene expression was conducted by Scion Image programme and the results showed that there was around 2.5-fold increase in expression of BCR-ABL gene in SK-1 transfected K562 cells as compared to control transfected ones.

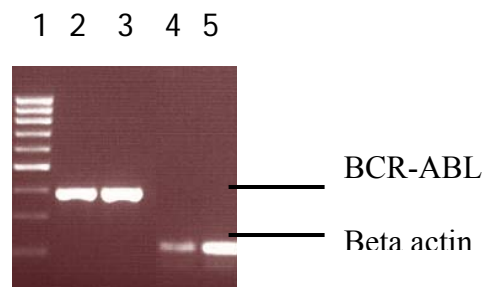


Figure 94. Expression analyses of BCR-ABL in vector and SK-1 transfected K562 cells. Expression levels of BCR-ABL in SK-1 and its vector (lanes 2 and 3) transfected K562 cells were measured using RT-PCR. Beta-actin levels were used as internal positive controls (lanes 4-5). Lane 1 is DNA Ladder.

3.6 THE ROLE OF P-GLYCOPROTEIN IN IMATINIB RESISTANCE IN HUMAN CML CELLS

Expression levels of MDR1 gene were analyzed in K562, K562/IMA-1 and Meg-01, Meg-01/IMA-1 cells by RT-PCR (Figure 95). The data showed that K562/IMA-1 and Meg-01/IMA-1 cells overexpress MDR1 gene when compared to their parental sensitive counterparts (Figure 95). Quantification analyses of MDR1 gene expression was conducted by Scion Image programme and the results showed that there was around 1.9- and 1.6-fold increase in expression of MDR1 gene in

K562/IMA-1 and Meg-01/IMA-1 cells, respectively, as compared to parental counterpart cells.

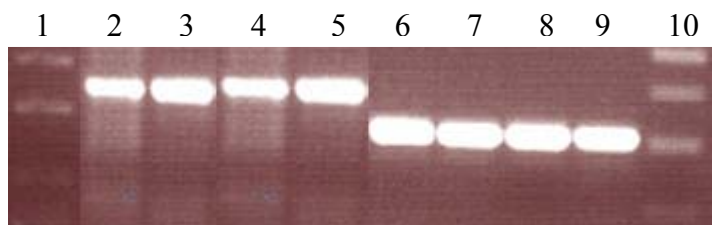


Figure 95. Expression analyses of MDR1 gene parental and resistant human CML cells. MDR1 gene expression levels in K562 and K562/IMA-1 cells (lanes 2 and 3) and Meg-01, and Meg-01/IMA-1 cells (lanes 4 and 5) were measured by RT-PCR. Beta actin levels were used as internal positive controls (lanes 6 to 9, respectively). Lanes 1 and 10 are DNA ladder.

K562/IMA-1 cells were examined to demonstrate the effect of P-glycoprotein inhibition in resistance to Imatinib. K562/IMA-1 cells treated with 10 μ M cyclosporin a (Cyc-A) in the presence of 2- and 5 μ M Imatinib resulted in about 65- and 80% cell death, respectively, while 2- and 5 μ M Imatinib, by itself, caused around 25- and 40% growth inhibition (Figure 96). Treatment of K562/IMA-1 cells only with 10 μ M Cyc-A resulted in 4% cell death.

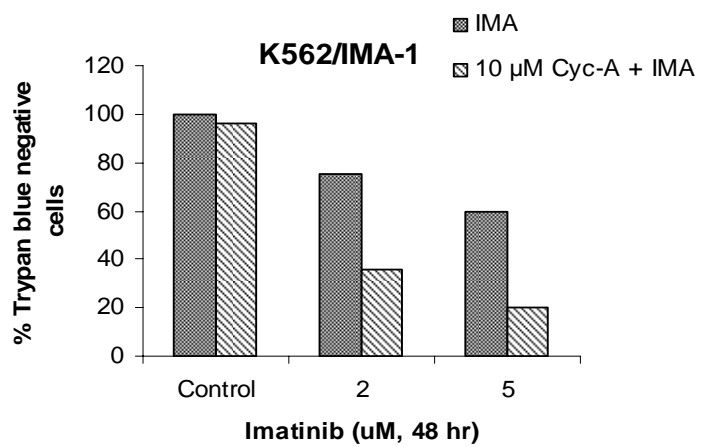


Figure 96. The effect of P-gp inhibitor, Cyc-A, on cell viability of K562/IMA-1 cells. Cells, grown in 6-well plates (5×10^4 cells/well), were treated with Cyc-A, in the absence or presence of Imatinib (48 hr). Cell viability was determined using trypan

blue dye exclusion assay. The experiments were done in at least two independent trials. Statistical analysis was done using two way anova, $P<0.01$ was considered significant.

The effect of P-glycoprotein inhibition in resistance to Imatinib-induced cell death in Meg-01/IMA-1 cells was also examined. Meg-01/IMA-1 cells treated with 10 μM Cyc-A in the presence of 2- and 5 μM Imatinib resulted in about 55- and 75% cell death, respectively, while 2- and 5 μM Imatinib, by itself, caused around 25- and 35% growth inhibition (Figure 97). Treatment of Meg-01/IMA-1 cells only with 10 μM Cyc-A resulted in 4% cell death.

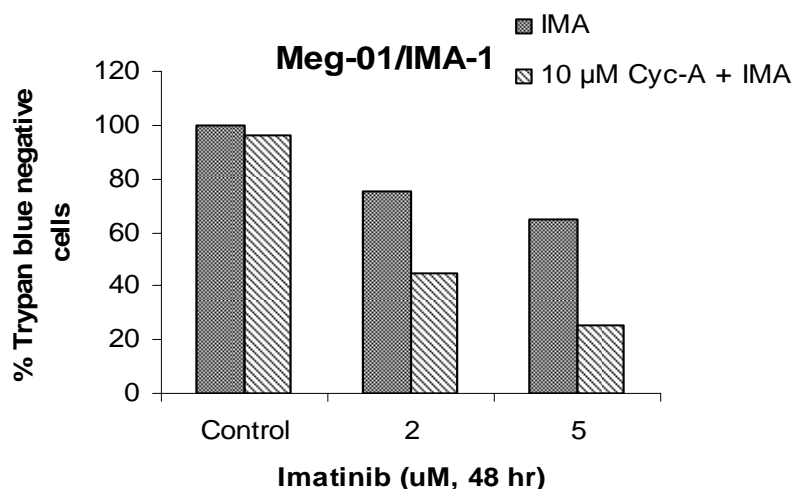


Figure 97. The effect of P-gp inhibitor, Cyc-A on cell viability of Meg-01/IMA-1 cells. Cells, grown in 6-well plates (5×10^4 cells/well), were treated with Cyc-A in the absence or presence of Imatinib (48 hr). Cell viability was determined using trypan blue dye exclusion assay. The experiments were done in at least two independent trials. Statistical analysis was done using two way anova, $P<0.01$ was considered significant.

3.7 SEQUENCE ANALYSES OF IMATINIB BINDING SITE OF ABL KINASE REGION IN SENSITIVE AND RESISTANT CELLS

The sequence analyses of ABL kinase region to which Imatinib specifically recognizes and binds to 21 amino acids were examined in parental and resistant K562 and Meg-01 cells. The data revealed that there were no detectable mutations on this site of BCR-ABL in any of the K562/IMA-0.2 or -1 (Appendix B, II and III, respectively) and Meg-01/IMA-0.2 or -1 cells (Appendix B, V and VI, respectively) comparing to parental K562 (Appendix B, I) and Meg-01 cells (Appendix B, IV), respectively.

CHAPTER IV

DISCUSSION

The tyrosine kinase activity of the BCR-ABL fusion protein is required for transformation of hematopoietic cells. Imatinib was designed based on the structure of the ATP binding site of the ABL kinase domain. Imatinib displays high specificity at the sub-micromolar level for the ABL and selectively kills BCR-ABL expressing cells. Although it is very effective in chronic phase of CML patients, in accelerated and blastic crisis phases it is less effective.

To produce Imatinib-resistant sub-lines of human CML cell lines, K562 and Meg-01 cells, were cultured in the presence of gradually increasing concentrations (0.05 µM to 1 µM) of Imatinib over a period of 12 months. However, rare Ph-positive K562 and Meg-01 cells were observed which were unaffected by concentrations of Imatinib that suppress the proliferation of most CML cells. These sub-lines with differential sensitivity to Imatinib were generated from Imatinib sensitive BCR-ABL positive human CML cells and the possible molecular mechanisms of resistance to Imatinib-induced apoptosis were investigated.

The first remarkable observation from this study was the overall difficulty in generating resistant sub-lines from the parental sensitive cells. Obtaining rare survivors from massive cells, even when subjected to a gradual exposure to Imatinib in liquid culture, suggested that resistant cells arose in response to selective pressure of the inhibitor. These results emphasized the specificity and high efficacy of this drug for the control of proliferation of BCR-ABL positive cells.

Importantly, results presented here demonstrated that continuous exposure of K562 and Meg-01 cells to stepwise increasing concentrations of Imatinib results in the selection of sub-clones expressing resistance to Imatinib-induced apoptosis. It was interesting to observe that although the tyrosine kinase inhibitor did not kill these resistant sub-lines, in the beginning their proliferation was slowed in comparison with the parental cultures, suggesting that a delaying effect over the cell cycle was still elicited by the drug.

Similar approach has been used in various studies to derive Imatinib-resistance starting with Ph-positive cell lines previously, including AR230, LAMA84 and K562 (Mahon *et al*, 2000). Mahon and co-workers were able to grow K562 cells up to presence of 0.6 μ M Imatinib concentrations. In this study, K562 and Meg-01 cells were able to be grown up to 1 μ M. Various diverse mechanisms have been reported for their involvement in the resistance to Imatinib-induced apoptosis. The most common mechanism was the overexpression/amplification of BCR-ABL, and it has been well documented that the degree of BCR-ABL expression appears to be directly proportional to the levels of Imatinib resistance (Mahon *et al*, 2000, Wiesberg *et al*, 2000). In this study, both in mRNA and protein levels it was observed that BCR-ABL expression was higher in 1 μ M Imatinib resistant CML cells (K562/ and Meg-01/IMA-1) than 0.2 μ M Imatinib resistant ones (K562/ and Meg-01/IMA-0.2) in which BCR-ABL expressed more as compared to parental sensitive counterparts.

Another mechanism for the development of resistance was due to selection of cells with mutated BCR-ABL in the Imatinib-binding domain in various CML cell lines (Gorre *et al*, 2003). In investigating the emergence of the mutations, all the sub-lines with intermediate (0.2 μ M) and high levels of resistance (1 μ M) and of course parental sensitive cells were examined. An extensive search for the presence of all 21 mutations in parental and resistant K562 and Meg-01 cells using RT-PCR followed by direct sequencing failed to identify any of these mutations. These findings showed that resistance to Imatinib in these resistant human CML cells did not result from any mutation in Imatinib binding site of ABL kinase domain.

In addition, there has been BCR-ABL independent mechanisms reported for driving resistance against Imatinib in various CML cells. For example, overexpression of MDR1/P-gp, a classical drug efflux protein, decreased the intracellular concentrations of Imatinib to sub-lethal levels that blocks Imatinib effects (Illmer *et al*, 2004). It was demonstrated that cells resistant to Imatinib showed an overexpression of P-gp (Druker *et al*, 2001). It was also shown by Dai and co-workers that Imatinib is not only a substrate of P-gp but also a modulator of P-gp. The P-gp-inhibitory effect of Imatinib is slightly weaker than that of cyclosporin A (Dai *et al*, 2003). In the present study, the expression analyses of P-gp in parental and Imatinib-resistant human K562 and Meg-01 cells were examined. Overexpression of P-gp in Imatinib resistant K562/ and Meg-01/IMA-1 cells was observed as compared to parental sensitive counterparts. In a parallel study it was observed that inhibition of P-gp by Cyc-A significantly restored the sensitivity of human K562/ and Meg-01/IMA-1 cells to Imatinib.

On the other hand, Imatinib resistance can be due to a failure to induce apoptosis. The signals inducing apoptosis could be blocked and/or anti-apoptotic genes' overexpression can be observed in resistant cells. The Bcl-2 protein can block apoptosis induced by most chemotherapeutic agents (Reed, 1995 and Reed *et al*, 1996). Up-regulation of anti-apoptotic Bcl-2 by Lyn-kinase-dependent mechanism (Dai *et al*, 2004) and by BCR-ABL gene in hematopoietic cells (Salomoni *et al*, 2000 and Horita *et al*, 2002) has been shown to be involved in resistance to Imatinib. The Bcl-2 protein family has been suggested to function as pore formers resulting in a decrease in mitochondrial membrane potential which activates proteases (caspase-3, -7 and -9) and nucleases by cytochrome-c release from mitochondria (Zamzami *et al*, 1998).

These data are in agreement with this study which showed that in Imatinib treated parental human CML cells; there were a significant decrease in mitochondrial membrane potential and an increase in caspase-3 activity resulting in higher number of cells in apoptosis. Thus, the pro-apoptotic effect of Imatinib could be explained by

a rapid and sustained inhibition of BCR-ABL, leading to induction of mitochondria-dependent apoptosis in parental cells.

There were an increase in expression of anti-apoptotic Bcl-2 and Bcl-XL and a decrease in expression of pro-apoptotic Bax proteins in Imatinib resistant K562/ and Meg-01/IMA-1 cells as compared to parental sensitive ones. In steady state levels, there were an increase in mitochondrial membrane potential and a decrease in caspase-3 activity in resistant cells as compared to parental sensitive counterparts. Mitochondrial membrane potential and caspase-3 activity analyses revealed that although higher concentrations of Imatinib were exposed, there were almost no decrease in mitochondrial membrane potential and no increase in caspase-3 activity in resistant cells. Increases in expression of Bcl-2 family proteins in resistant cells can be explained by overexpression of BCR-ABL protein, which regulates Bcl-2 family, in resistant cells. It was also shown by Amarante-Mendes and co-workers that Bcl-2 protein family is upregulated in a variety of resistant cell lines and account in part for the resistant phenotype observed in BCR-ABL-positive cells (Amarante-Mendes *et al*, 1998).

In this study, roles and mechanisms of action of ceramide metabolism in the regulation of Imatinib-induced cell death and resistance in human K562 and Meg-01 cells were examined. The data presented here provide a novel and mechanistic information about the role of ceramide/S1P pathway in the regulation of Imatinib-mediated apoptosis, which involves the loss of mitochondrial membrane potential, and the activation of caspase-3 in K562 and Meg-01 cells. The results showed that while treatment with Imatinib mediates the generation of C₁₈-ceramide via hLASS1, which appears to play an important role in Imatinib-induced apoptosis in parental cells, overexpression of SK-1 in resistant cells prevents cell death in response to Imatinib by altering the balance between C₁₈-ceramide and S1P.

Bioactive sphingolipid ceramide is involved in mediating anti-proliferative responses via various distinct mechanisms in human cancer cells (Ogretmen and Hannun, 2004). It has been well documented that treatment with some

chemotherapeutic agents results in increased generation and/or accumulation of endogenous ceramide either via the activation of the *de novo* pathway, or by increased activity of SMases (Ogretmen and Hannun, 2004). However, any role for Imatinib in inducing the generation of ceramide in human CML cells has not been examined previously. Here, the data showed that treatment with Imatinib significantly increased the generation of ceramide, particularly C₁₈-ceramide, in a time-dependent manner, via the action of hLASS1 in parental cells. Importantly, further evaluation of possible roles for hLASS1-generated C₁₈-ceramide by molecular approaches suggested its involvement in Imatinib-induced cell death in parental cells. However, although hLASS1 siRNA completely prevented the generation of C₁₈-ceramide in response to Imatinib in parental cells, it only partially (about 50%) prevented Imatinib-induced apoptosis, indicating that there are other mechanisms and down-stream targets, which are involved in this process. Nevertheless, overexpression of hLASS1 in resistant cells, which induced the generation of C₁₈-ceramide increased the sensitivity to Imatinib, suggesting that up-regulation of ceramide generation might help improve response to Imatinib. The overexpression of hLASS2, hLASS5 and hLASS6 did not cause any change in MMP as compared to vector transfected counterparts. Taken together, these results emphasize the specificity of hLASS1 gene and its product, C₁₈-ceramide, in Imatinib-induced apoptosis.

Koybasi and co-workers showed an important role for C₁₈-ceramide via hLASS1 activity in enhancing chemotherapy-induced cell death by a mechanism involving the activation of mitochondrial apoptotic cascade including the activation of caspase9/3 in squamous cell carcinomas (SCC) of the head and neck both *in vitro* (Koybasi *et al*, 2004), and *in vivo* (Senkal *et al*, unpublished data). These data are also in agreement with the present study showing the role of C₁₈-ceramide in the regulation of caspase-3 activation and loss of mitochondrial membrane potential in parental cells. In a previous study, it was reported that while defects in hLASS1/C₁₈-ceramide pathway plays a role in the pathogenesis and/or progression of SCC of the head and neck, the reduced levels of C₁₆-, C₁₈- and C₂₄-ceramides, products of various LASS proteins, appeared to play important roles in the pathogenesis of non-

squamous head and neck (Koybasi *et al*, 2004), and lung cancers, suggesting that hLASS-dependent generation of ceramide synthesis might be regulated by distinct pathways in a cell line or cell type-dependent manner.

Mechanistically, the data presented here showed that the perturbations of the balance between ceramide and S1P, with opposing functions as pro-apoptotic and anti-apoptotic sphingolipids, respectively, by overexpression of SK-1, and not by altered levels of ceramide synthesis, plays an important role in the regulation of resistance to Imatinib. These results are consistent with previous data, which showed a role for SK-1 via alteration of the ceramide/S1P balance in the regulation of drug-induced apoptosis, and chemotherapy sensor both in culture and in animal models of prostate adenocarcinoma (Pchejetski *et al*, 2005). In parallel with these data, increasing the expression of SK-1 reduced the sensitivity of A-375 melanoma cells to Fas- and ceramide-mediated apoptosis that could be reversed by inhibition of SK-1 expression (Bektas *et al*, 2005). There have been other studies, which showed also that SK-1 expression is up regulated in colon carcinogenesis (Kawamori *et al*, 2006), and in the tumors of the patients with lung cancer (Johnson *et al*, 2005). More importantly, it has been demonstrated previously that modulation of S1P levels increases apoptosis, or abolishes starvation-induced autophagy, which leads to increased cell death (Lavieu *et al*, 2006). Thus, perturbations in the metabolism of ceramide via overexpression of SK-1 may play important roles in the development of resistance to Imatinib. Increased activity/expression of a ceramidase(s), required for the hydrolysis of ceramide to generate sphingosine, which is then converted to S1P by SK-1, might also be involved in the development of resistance to Imatinib, and this needs to be investigated.

In addition, our preliminary data by Western blot analysis showed that BCR-ABL is overexpressed in K562/-, and Meg-01/IMA-0.2 and -1 cells significantly when compared to parental K562 and Meg-01 cells. On the other hand, overexpression of hLASS1 gene, which induces apoptosis, inhibited the expression of BCR-ABL gene while overexpression of SK-1, which inhibits apoptosis and induces cell growth and proliferation, induces the expression of BCR-ABL gene.

There was no effect of hLASS6 on expression levels of BCR-ABL gene. These results suggest that SK-1 and hLASS1 genes are upstream regulators of BCR-ABL gene, resulting in increase and decrease in BCR-ABL gene, respectively.

In addition to its role as a mediator of cell death, recent studies have demonstrated that alterations in ceramide metabolism whereby pro-apoptotic ceramide is converted to the noncytotoxic GlcCer metabolite contribute to the MDR phenomenon (Lucci *et al*, 1998). Elevated levels of GlcCer have been found in a number of multidrug-resistant human cancer cell lines including breast, ovarian, and colon cancer cells and in some patients with melanoma and breast cancer (Kok *et al*, 2000 and Lucci *et al*, 1998). Analysis of human tumor specimens revealed elevated GlcCer levels in patients who failed conventional chemotherapy, but GlcCer levels were low in those who responded to treatment (Lucci *et al*, 1998). Support for involvement of GCS in drug resistance came from transfection experiments, which showed that overexpression of the enzyme resulted in increased resistance to adriamycin in drug sensitive MCF-7 tumor cells (Liu *et al*, 1999). Conversely, when GCS expression was down-regulated with the aid of anti-sense oligonucleotides, this resulted in increased sensitivity of resistant MCF-7-AdrR tumor cells towards adriamycin (Liu *et al*, 2000). These results can be interpreted in the sense that MDR tumor cells display an enhanced activity of GCS, which results in accumulation of GlcCer and metabolic removal of ceramide from the sphingolipid pool. The latter might be beneficial to the survival of tumor cells, especially when under stress of chemotherapy or other stress factors, which induce ceramide formation and accumulation (Hannun *et al*, 2000 and Senchenkov *et al*, 2001). Various works showed also that GCS inhibitors arrest cell division, exhibit anticarcinogenic properties (Kyogashima *et al*, 1996). In agreement with the previous studies, GCS overexpression has been observed in Imatinib resistant human CML cells as compared to parental sensitive counterparts.

The effect of specific GCS inhibitors such as 1-phenyl-2-decanoylamino-3-morpholino-1-propanol PDMP, blocks the conversion of ceramide to GlcCer, was tested. These compounds have been shown to kill multidrug resistant cells besides

drug-sensitive cells. It has previously been demonstrated that PDMP sensitizes murine neuroblastoma cells to Taxol and Vincristine (Sietsma *et al*, 2000). In this study, PDMP-induced chemosensitization was investigated in two Imatinib resistant human CML cells. In parallel with the previous data it was observed that a non-toxic dose of PDMP induced apoptosis in both multidrug-resistant human CML cell lines in response to Imatinib.

Chemosensitization effects of PDMP-altered ceramide metabolism were compared in Imatinib-sensitive and -resistant K562 and Meg-01 cell lines. It is generally assumed that GCS inhibitors exert their chemosensitizing effect by potentiation of drug-induced intracellular ceramide elevation (Kok *et al*, 2004). LC/MS analyses revealed that impairment of ceramide glycosylation by PDMP increased intracellular ceramide levels. On the other hand, cell viability by trypan blue dye exclusion assay and Flow cytometry analyses also showed that PDMP in combination with Imatinib resulted in higher numbers of cells in apoptosis as compared to only Imatinib exposed cells. These findings demonstrated that the ability to modulate ceramide metabolism might provide a new avenue by which drug sensitivity can be increased in multidrug-resistant cells.

Nevertheless, the data presented here have important implication for designing novel therapies for the treatment of CML. For example, in addition to the inhibition of BCR-ABL, targeting ceramide metabolism by increasing its synthesis and/or modulating its metabolism to S1P might provide improved strategies for the treatment of CML.

In conclusion, these results show, for the first time, that the LASS1-dependent generation of endogenous C₁₈-ceramide plays important roles in Imatinib-induced mitochondrial and caspase-3-mediated apoptosis. These data also show that overexpression of SK-1, via alterations of the ceramide/S1P balance, and/or GCS, via conversion of pro-apoptotic ceramide to anti-apoptotic GlcCer, are involved in the regulation of Imatinib resistance in K562 and Meg-01 cells.

REFERENCES

- Abe A, Radin NS, Shayman JA, Wotring LL, Zipkin RE, Sivakumar R, Ruggieri JM, Carson KG, Ganem B. Structural and stereochemical studies of potent inhibitors of glucosylceramide synthase and tumor cell growth. *J. Lipid Res.* (1995) **36**: 611-621.
- Allan LA, Morrice N, Brady S, Magee G, Pathak S, and Clarke PR. Inhibition of caspase 9 through phosphorylation at Thr 125 by ERK MAPK. *Nat. Cell Biol.* (2003) **5**: 647–654.
- Amarante-Mendes GP, McGahon AJ, Nishioka WK, Afar DE, Witte ON and Green DR. Bcl-2-independent Bcr-Abl-mediated resistance to apoptosis: protection is correlated with up regulation of Bcl-xL. *Oncogene* (1998) **16**: 1383–1390.
- Amos TA, Lewis JL, Grand FH, Gooding RP, Goldman JM, and Gordon MY. Apoptosis in chronic myeloid leukaemia: normal responses by progenitor cells to growth factor deprivation, X-irradiation and glucocorticoids. *Br. J. Haematol.* (1995) **91**: 387-393.
- Anliker B, and Chun J. Lysophospholipid G protein-coupled receptors. *J. Biol. Chem.* (2004) **279**: 20555-20558.
- Bektas M, Jolly PS, Muller C, Eberle J, Spiegel S, and Geilen CC. Sphingosine kinase activity counteracts ceramide-mediated cell death in human melanoma cells: role of Bcl-2 expression. *Oncogene* (2005) **24**:178-187.
- Bielawska A, Greenberg MS, Perry D, Jayadev S, Shayman JA, McKay C, and Hannun YA. (IS,’R)-D-erythro-2-(N-myristoyl amino)-1-phenyl-1-propanol as an inhibitor of ceramidase. *J. Biol. Chem.* (1996) **271**: 12646-12654.

Bissonnette RP, Echeverri F, Mahboubi A, and Green DR. Apoptotic cell death induced by c-myc is inhibited by bcl-2. *Nature* (1992) **359**: 552-554.

Borst P, Evers R, Kool M, and Wijnholds J. A family of drug transporters: the multidrug resistance-associated proteins. *J. Natl. Cancer Inst.* (2000) **92(16)**:1295-1302.

Brandwagt BF, Mesbah LA, Takken FL, Laurent PL, Kneppers TJ, Hille J, and Nijkamp HJ. A longevity assurance gene homolog of tomato mediates resistance to *Alternaria alternata* f. sp. *lycopersici* toxins and fumonisin B1. *Proc. Natl. Acad. Sci.* (2000) **97**: 4961–4966.

Cahill MA, Janknecht R, and Nordheim A. Signalling pathways: jack of all cascades. *Curr. Biol.* (1996) **6**: 16-19.

Calabretta B, and Perrotti D. The biology of CML blast crisis. *Blood* (2004) **103**: 4010-4022.

Chai SK, Nichols GL, and Rothman P. Constitutive activation of JAKs and STATs in BCR-Abl-expressing cell lines and peripheral blood cells derived from leukemic patients. *J. Immunol.* (1997) **159**: 4720-4728.

Chalfant CE, Szulc Z, Roddy P, Bielawska A, and Hannun YA. The structural requirements for ceramide activation of serine-threonine protein phosphatases. *J. Lipid Res.* (2004) **45**: 496–506.

Christoph W, and Martin S. Novel targeted therapies to overcome Imatinib mesylate resistance in chronic myeloid leukemia. *Crit. Rev. in Onc/Hem.* (2006) **57(2)**:145-64.

D'mello NP, Childress AM, Franklin DS, Kale SP, Pinswasdi C, and Jazwinski SM. Cloning and characterization of *LAG1*, a longevity-assurance gene in yeast. *J. Biol. Chem.* (1994) **269**: 15451–15459.

Dai H, Marbach P, Lemaire M, Hayes M, and Elmquist WF. Distribution of STI-571 to the brain is limited by P-glycoprotein-mediated efflux. *J. Pharmacol. Exp. Ther.* (2003) **304**:1085–1092.

Dai Y, Rahmani M, Corey SJ, Dent P, and Grant S. A Bcr/Abl-independent, Lyn-dependent form of Imatinib mesylate (STI-571) resistance is associated with altered expression of Bcl-2. *J. Biol. Chem.* (2004) **279**:34227-34239.

Danial NN, and Korsmeyer SJ. Cell death: critical control points. *Cell* (2004) **116**: 205–219.

Danial NN, Pernis A, and Rothman PB. Jak-STAT signaling induced by the v-abl oncogene. *Science* (1995) **269**: 1875-1877.

Dbaibo GS, Pushkareva MY, Jayadev S, Schwarz JK, Horowitz JM, Obeid LM, and Hannun YA. Retinoblastoma gene product as a downstream target for a ceramide-dependent pathway of growth arrest. *Proc. Natl Acad. Sci.* (1995) **92**: 1347–1351.

De Groot RP, Raaijmakers JA, Lammers JW, Jove R, and Koenderman L. STAT5 activation by BCR-Abl contributes to transformation of K562 leukemia cells. *Blood* (1999) **94**: 1108-1112.

Dean M, Hamon Y, and Chimini G. The human ATP-binding cassette (ABC) transporter superfamily. *J. Lipid Res.* (2001) **42**(7):1007-1017.

Deffie AM, Batra JK, and Goldenberg GJ. Direct correlation between DNA topoisomerase II activity and cytotoxicity in adriamycin-sensitive and -resistant P388 leukemia cell lines. *Cancer Res.* (1989) **49**: 58–62.

Deininger MW, Buchdunger E, and Druker BJ. The development of Imatinib as a therapeutic agent for chronic myeloid leukemia. *Blood* (2005) **105**(7): 2640-2653.

Deininger MW, and Druker BJ. Specific Targeted Therapy of Chronic Myelogenous Leukemia with Imatinib. *Pharmacol Rev*(2003) **55**: 401-423

Deininger MW, Goldman JM, and Melo JV. The molecular biology of chronic myeloid leukemia. *Blood*. (2000) **15;(10)**: 3343-3356.

Del Peso L, Gonzalez-Garcia M, Page C, Herrera R, and Nunez G. Interleukin-3-induced phosphorylation of bad through the protein kinase akt. *Science* (1998) **278**: 687-689.

Druker B, Talpaz M, Resta DJ, Peng B, Buchdunger E, Ford JM, Lydon NB, Kantarjian H, Capdeville R, Ohno SJ, and Sawyers CL. Efficacy and safety of a specific inhibitor of the BCR-ABL tyrosine kinase in chronic myeloid leukemia. *N. Engl. J. Med.* (2001) **344**:1031–1037.

Druker BJ. STI571 (Gleevec) as a paradigm for cancer therapy. *Trends Mol. Med.* (2002) **8**: 14-18.

Edsall LC, Cuvillier O, Twitty S, Spiegel S, and Milstien S. Sphingosine kinase expression regulates apoptosis and caspase activation in PC12 cells. *J. Neurochem.* (2001) **76**: 1573-1584.

Eren E, Aytac U, Tetik E, Akman O, Kansu E, Gunduz U. Detection of BCR/ABL gene rearrangement and the elimination of rearranged clone in chronic myelocytic leukemia patients. *Am J Hematol.* (2000) **63**(2): 85-9

Franke TF, Kaplan DR, and Cantley LC. PI3K: downstream AKT ion blocks apoptosis. *Cell* (1997) **88**: 435-437.

Gambacorti-Passerini C, Gunby RH, Piazza R, Galletta A, Rostagno R, and Scapozza L. Molecular mechanisms of resistance to Imatinib in Philadelphia-chromosome-positive leukemias. *Lancet Oncol.* (2003) **4**: 75–85.

Goldman JM. Chronic myeloid leukemia—still a few questions. *Exp. Haematology* (2004) **32**: 2-10.

Gorre ME, Mohammed M, Ellwood K, Hsu N, Paquette R, Rao PN, and Sawyers CL. Clinical resistance to STI571 cancer therapy caused by BCR-ABL gene mutation or amplification. *Science* (2003) **293**: 876–880.

Gottesman MM, Fojo T, and Bates SE. Multidrug resistance in cancer: role of ATP-dependent transporters. *Nat. Rev. Cancer* (2002) **2**: 48–58.

Hanahan D, and Weinberg RA. The hallmarks of cancer. *Cell* (2000) **100**: 57–70.

Hannun YA, and Obeid LM. The ceramide-centric universe of lipid-mediated cell regulation: stress encounters of the lipid kind. *J. Biol. Chem.* (2002) **277**: 25847–25850.

Hannun YA, and Luberto C. Ceramide in the eukaryotic stress response. *Trends. Cell Biol.* (2000) **10**:73– 80.

Hegedus T, Orifi L, Seprodi A, Varadi A, Sarkadi B, and Keri G. Interaction of tyrosine kinase inhibitors with the human multidrug transporter proteins, MDR1 and MRP1. *Biochem. Biophys. Acta* (2002) **1587**: 318–325.

Hoover RR, Gerlach MJ, Koh EY, and Daley GQ. Cooperative and redundant effects of STAT5 and Ras signaling in BCR/ABL transformed hematopoietic cells. *Oncogene* (2001) **20**: 5826–5835.

Horita M, Andreu EJ, Benito A, Arbona C, Sanz C, Benet I, Prosper F, and Fernandez-Luna JL. Blockade of the Bcr-Abl kinase activity induces apoptosis of chronic myelogenous leukemia cells by suppressing signal transducer and activator of transcription 5-dependent expression of Bcl-xL. *J. Exp. Med.* (2002) **191**: 977–984.

Ilaria RL Jr, and Van Etten RA. P210 and P190 (BCR/ABL) induce the tyrosine phosphorylation and DNA binding activity of multiple specific STAT family members. *J. Biol Chem.* (1996) **271**: 31704-31710.

Illmer T, Schaich M, Platzbecker U, Freiberg-Richter J, Oelschlagel U, von Bonin M, Pursche S, Bergemann T, Ehninger G, and Schleyer E. P-glycoprotein-mediated drug efflux is a resistance mechanism of chronic myelogenous leukemia cells to treatment with Imatinib mesylate. *Leukemia* (2004) **18**:401-408.

Jazwinski SM, and Conzelmann A. LAG1 puts the focus on ceramide signaling. *The Int J of Biochem* (2002) **34**: 1491-1495.

Jenkins GM, and Hannun YA. Role for de novo sphingoid base biosynthesis in the heat-induced transient cell cycle arrest of *Saccharomyces cerevisiae*. *J. Biol. Chem.* (2001) **276**: 8574-8581.

Jiang X, Lopez A, Holyoake T, Eaves A, and Eaves C. Autocrine production and action of IL-3 and granulocyte colony-stimulating factor in chronic myeloid leukemia. *Proc. Natl. Acad. Sci.* (1999) **96**: 12804-12809.

Johnson KR, Johnson KY, Becker KP, Bielawski J, Mao C, and Obeid LM. Role of human sphingosine-1-phosphate phosphatase 1 in the regulation of intra- and extracellular sphingosine-1-phosphate levels and cell viability. *J. Biol. Chem.* (2003) **278**: 34541-34547.

Johnson KR, Johnson, KY, Crellin HG, Ogretmen B, Boylan A, Harley RA, Obeid LM. Immunohistochemical distribution of sphingosine kinase 1 in normal and tumor lung tissue. *J. Histochem. Cytochem.* (2005) **53**:1159-1166.

Jonuleit T, Peschel C, Schwab R, Peschel C, Schwab R, Van Der Kuip H, Buchdunger E, Fischer T, Huber C, and Aulitzky WE. Bcr-Abl kinase promotes cell

cycle entry of primary myeloid CML cells in the absence of growth factors. *Br. J. Haematol.* (1998) **100**: 295-303.

Kabarowski JH, Allen PB, and Wiedemann LM. A temperature sensitive p210 BCR-ABL mutant defines the primary consequences of BCR-ABL tyrosine kinase expression in growth factor dependent cells. *EMBO J.* (1994) **13**: 5887-5895.

Kawamori T, Osta W, Johnson KR, Pettus BJ, Bielawski J, Tanaka T, Wargovich MJ, Reddy BS, Hannun YA, Obeid LM, Zhou D. Sphingosine kinase 1 is up-regulated in colon carcinogenesis. *FASEB J.* (2006) **20**:386-388

Kickhoefer VA, Rajavel KS, Scheffer GL, Dalton WS, Scheper RJ, and Rome LH. Vaults are up-regulated in multidrug-resistant cancer cell lines. *J. Biol. Chem.* (1998) **273**: 8971-8974.

Kleina I, Sarkadib B, and Varadia A. An inventory of the human ABC proteins. *Biochimica et Biophysica Acta.* (1999) **1461**: 237-262.

Kluk MJ, and Hla T. Signaling of sphingosine-1-phosphate via the S1P/EDG-family of G-protein-coupled receptors. *Biochim. Biophys. Acta* (2002) **1582**: 72-80.

Kok J.W. and Sietsma H. Sphingolipid metabolism enzymes as targets for anticancer therapy, *Curr. Drug Targets.* (2004) **5**: 375-382.

Kok JW, R. Veldman J, Klappe K, Koning H, Filipeanu CM, and Muller M. Differential expression of sphingolipids in MRP1 overexpressing HT29 cells. *Int. J. Cancer.* (2000) **87**: 172-178.

Koybasi S, Senkal CE, Sundararaj K, Spassieva S, Bielawski J, Osta W, Day TA, Jiang JC, Jazwinski SM, Hannun YA, Obeid LM, Ogretmen B. Defects in cell growth regulation by C18:0-ceramide and longevity assurance gene 1 in human head and neck squamous cell carcinomas. *J. Biol. Chem.* (2004) **279**:44311-44319

Krishnamachary N, and Center MS. The MRP gene associated with a non-P-glycoprotein multidrug resistance encodes a 190-kDa membrane bound glycoprotein. *Cancer Res.* (1993) **53**: 3658–3661.

Kurzrock R, Kantarjian HM, Druker BJ, and Talpaz M, Philadelphia chromosome-positive leukemias: from basic mechanisms to molecular therapeutics. *Ann. Int. Med.* (2003) **138**: 819–830.

Kyogashima M, Inoue M, Seto A, and Inokuchi J. Glucosylceramide synthetase inhibitor, D-threo-1-phenyl-2-decanoylamino-3-morpholino-1-propanol exhibits a novel decarcinogenic activity against Shope carcinoma cells. *Cancer. Lett.* (1996) **101**:25-30.

Lahir S, Futerman AH. LASS5 is a bona fide dihydroceramide synthase that selectively utilizes palmitoyl-CoA as acyl donor. *J. Biol. Chem.* (2005) **280**, 33735–33738.

Laneuville P. Abl tyrosine protein kinase. *Semin Immunol.* (1995) **7**: 255-266.

Liu YY, Han TY, Giuliano AE, Hansen N, Cabot MC. Uncoupling ceramide glycosylation by transfection of glucosylceramide synthase antisense reverses adriamycin resistance. *J. Biol. Chem.* (2000) **275**:7138–7143.

Lavieu G, Scarlatti F, Sala G, Carpentier S, Levade T, Ghidoni R, Botti J, Codogno P. Regulation of autophagy by sphingosine kinase 1 and its role in cell survival during nutrient starvation. *J. Biol. Chem.* (2006) **281**(13):8518-8527.

Le Coutre P, Kruzer K, and Na I. Determination of -1 acid glycoprotein in patients with Ph+ chronic myeloid leukemia during the first 13 weeks of therapy with STI571. *Blood Cells Mol. Dis.* (2002) **28**: 75-85.

Lee JY, Bielawska AE, and Obeid LM. Regulation of cyclin-dependent kinase 2 activity by ceramide. *Exp. Cell Res.* (2000) **261**: 303–311.

Litman T, Druley TE, Stein WD, and Bates SE. From MDR to MXR: new understanding of multidrug resistance systems, their properties and clinical significance. *Cell Mol. Life Sci.* (2001) **58**: 931–959.

Liu F, Verin AD, Wang P, Day R, Wersto RP, Chrest FJ, English DK, and Garcia JG. Differential regulation of sphingosine-1-phosphate- and VEGF-induced endothelial cell chemotaxis. Involvement of G ($\alpha 2$)-linked Rho kinase activity. *Am. J. Respir. Cell Mol. Biol.* (2001-1) **24**: 711–719.

Liu Y, Wada R, Yamashita T, Mi Y, Deng CX, Hobson JP, Rosenfeldt HM, Nava VE, Chae SS, Lee MJ, Liu CH, Hla T Spiegel S, and Proia RL. Edg-1, the G-protein-coupled receptor for sphingosine-1-phosphate, is essential for vascular maturation. *J. Clin. Invest.* (2000) **106**: 951–961.

Liu YY, Han TY, Giuliano AE, and Cabot MC. Ceramide glycosylation potentiates cellular multidrug resistance. *FASEB J.* (2001-2) **15(3)**: 719-730.

Liu YY, Han TY, Giuliano AE, and Cabot MC. Expression of glucosylceramide synthase, converting ceramide to glucosylceramide, confers Adriamycin resistance in human breast cancer cells. *J. Biol. Chem.* (1999) **274**:1140 –1146.

Lucci A, Cho WI, Han TY, Giuliano AE, Morton DL, and Cabot MC. Glucosylceramide: a marker for multiple-drug resistant cancers. *Anticancer Res.* (1998) **18**: 475 –480.

Maceyka M, Payne SG, Milstien S, and Spiegel S. Sphingosine kinase, sphingosine-1-phosphate, and apoptosis. *Biochim. Biophys. Acta* (2002) **1585**: 193–201.

Mahon FX, Belloc F, Lagarde V, Chollet C, Moreau-Gaudry F, Reiffers J, Goldman JM, and Melo JV. MDR1 gene overexpression confers resistance to Imatinib mesylate in leukemia cell line models. *Blood* (2003) **101**: 2368–2373.

Mahon FX, Deininger MW, Schultheis B, Chabrol J, Reiffers J, Goldman JM, and Melo JV. Selection and characterization of BCR-ABL positive cell lines with differential sensitivity to the tyrosine kinase inhibitor STI571: diverse mechanisms of resistance. *Blood* (2000) **96**:1070-1079.

Marais R, Light Y, Paterson HF, and Marshall CJ. Ras recruits Raf-1 to the plasma membrane for activation by tyrosine phosphorylation. *EMBO J.* (1995) **14**: 3136-3145.

Marbach P, Lemaire M, Hayes M, and Elmquist WF. Distribution of STI-571 to the brain is limited by P-glycoprotein-mediated efflux. *J. Pharmacol. Exp. Ther.* (2003) **304**: 1085-1092.

Marchesini N, Luberto C, and Hannun YA. Biochemical properties of mammalian neutral sphingomyelinase 2 and its role in sphingolipid metabolism. *J. Biol. Chem.* (2004-1) **278**: 13775-13783.

Marchesini N, Osta W, Bielawski J, Luberto C, Obeid LM, and Hannun YA. Role for neutral sphingomyelinase 2 in confluence-induced growth arrest of MCF-7 cells. *J. Biol. Chem.* (2004-2) **279**: 25101-25111.

Merrill A.H. *De novo* sphingolipid biosynthesis: a necessary, but dangerous, pathway. *Biol. Chem.* (2002) **277**: 25843-25846.

Mizutani Y, Kihara A, and Igarashi Y. Mammalian Lass6 and its related family members regulate synthesis of specific ceramides. *Biochem J.* (2005) **390**: 263-271.

Morrow CS, and Cowan KH. Glutathione S-transferases and drug resistance. *Cancer Cells* (1990) **2**:15-22.

Mueller H, and Eppenberger U. The dual role of mutant p53 protein in chemosensitivity in human cancers. *Anticancer Res.* (1996) **16**: 3845-3848.

Nagar B, Bornmann WG, Pellicena P, Schindler T, Veach DR, Miller WT, Clarkson B, and Kuriyan J. Crystal structures of the kinase domain of c-Abl in complex with the small molecule inhibitors PD173955 and Imatinib (STI-571). *Cancer Res.* (2002) **62**: 4236-4243.

Nava VE, Hobson JP, Murthy S, Milstien S, and Spiegel S. Sphingosine kinase type 1 promotes estrogen-dependent tumorigenesis of breast cancer MCF-7 cells. *Exp. Cell Res.* (2002) **281**: 115–127.

Oda T, Heaney C, Hagopian JR, Okuda K, Griffin JD, and Druker BJ. Crkl is the major tyrosine-phosphorylated protein in neutrophils from patients with chronic myelogenous leukemia. *J. Biol. Chem.* (1994) **269**: 22925-22928.

Ogretmen B, and Hannun YA. Biologically Active Sphingolipids In Cancer Pathogenesis And Treatment. *Nature* (2004) **4**: 604-615.

Ogretmen B, and Hannun YA. Updates on functions of ceramide in chemotherapy-induced cell death and in multidrug resistance. *Drug Resist. Updat.* (2001-1) **4**: 368–377.

Ogretmen B, Schady D, Usta J, Wood R, Kraveka JM, Luberto C, Birbes H, Hannun YA, and Obeid LM. Role of ceramide in mediating the inhibition of telomerase activity in A549 human lung adenocarcinoma cells. *J. Biol. Chem.* (2001-2) **276**: 24901-24910.

Okamoto H, Takuwa N, Yokomizo T, Sugimoto N, Sakurada S, Shigematsu H, and Takuwa Y. Inhibitory regulation of Rac activation, membrane ruffling, and cell migration by the G protein-coupled sphingosine-1-phosphate receptor EDG5 but not EDG1 or EDG3. *Mol. Cell Biol.* (2000) **20**: 9247–9261.

Olivera A, Rosenfeldt HM, Bektas M, Wang F, Ishii I, Chun J, Milstien S, and Spiegel S. Sphingosine kinase type 1 induces G12/13-mediated stress fiber formation, yet promotes growth and survival independent of G protein-coupled receptors. *J.Biol. Chem.* (2003) **278**: 46452–46460.

Olson M, and Kornbluth S. Mitochondria in apoptosis and human disease. *Curr. Mol. Med.* (2001) **1**: 91–122.

Pan H, Qin WX, Huo KK, Wan DF, Yu Y, Xu ZG, Hu QD, Gu KT, Zhou XM, Jiang HQ, Zhang PP, Huang Y, Li YY, and Gu JR. Cloning, mapping, and characterization of a human homologue of the yeast longevity assurance gene LAG1. *Genomics*. (2001) **77**: 58–64.

Pchejetski D, Golzio M, Bonhoure E, Calvet C, Doumerc N, Garcia V, Mazerolles C, Rischmann P, Teissie J, Malavaud B, Cuvillier O. Sphingosine kinase-1 as a chemotherapy sensor in prostate adenocarcinoma cell and mouse models. *Cancer Res.* (2005) **65**:11667-11675

Pendergast AM, Quilliam LA, Cripe LD, Bassing CH, Dai Z, Li N, Batzer A, Rabun KM, Der CJ, and Schlessinger J. BCR-ABL-induced oncogenesis is mediated by direct interaction with the SH2 domain of the GRB-2 adaptor protein. *Cell* (1993) **75**: 175-185.

Perry DK, and Hannun YA. The role of ceramide in cell signaling. *Biochim. Biophys. Acta* (1998) **1436**: 233-243.

Pierce A, Owen-Lynch PJ, Spooncer E, Dexter TM, and Whetton AD. p210 Bcr-Abl expression in a primitive multipotent haematopoietic cell line models the development of chronic myeloid leukaemia. *Oncogene* (1998) **17**: 667-672.

Pyne S, and Pyne NJ. Sphingosine 1-phosphate signalling in mammalian cells. *Biochem J.* (2000) **349**: 385-402.

Raitano AB, Halpern JR, Hambuch TM, and Sawyers CL. The Bcr-Abl leukemia oncogene activates Jun kinase and requires Jun for transformation. *Proc. Natl. Acad. Sci.* (1995) **92**: 11746-11750.

Ramadevi N, DPhil B, and Kapil B. Mechanisms of resistance to Imatinib mesylate in Bcr-Abl positive leukemias. *Curr. Opin. in Onc.* (2002) **14**: 616-620.

Reed JC, Miyashita T, Takayama S, Wang HG, Sato T, Krajewski S, Aime-Sempe C, Bodrug S, Kitada S, Hanada M. Bcl-2 family proteins: regulators of cell death involved in the pathogenesis of cancer and resistance to therapy. *J. Cell. Biochem.* (1996) **60**: 23-32.

Reed JC. Regulation of apoptosis by bcl-2 family proteins and its role in cancer and chemoresistance. *Curr. Opin. Oncol.* (1995) **5**: 541–546.

Riebeling C, Allegood JC, Wang E, Merrill AH, and Futerman AH. Two mammalian longevity assurance gene (LAG1) family members, trh1 and trh4, regulate dihydroceramide synthesis using different fatty acyl-CoA donors. *J. Biol. Chem.* (2003) **278**: 43452–43459.

Roumiantsev S, Shah NP, Gorre ME, Nicoll J, Brasher BB, Sawyers CL, and Van Etten RA. Clinical resistance to the kinase inhibitor STI-571 in chronic myeloid leukemia by mutation of Tyr-253 in the Abl kinase domain P-loop. *Proc. Natl. Acad. Sci.* (2002) **99**: 10700–10705.

Saba JD, and Hla T. Point-counterpoint of sphingosine 1-phosphate metabolism. *Circ. Res.* (2004) **94**: 724-734.

Salomoni P, Condorelli F, Sweeney SM, Calabretta B. Versatility of BCR-ABL-expressing leukemic cells in circumventing proapoptotic BAD effects. *Blood* (2000) **96**: 676-684.

Salvesen GS, and Duckett CS. IAP proteins: blocking the road to death's door. *Nat. Rev. Mol. Cell. Biol.* (2002) **3**: 401–410.

Savage DG, and Antham KH. Imatinib mesylate: a new oral targeted therapy. *N. Engl. J. Med.* (2002) **346**: 683-693.

Sawyers CL, Callahan W, Witte ON. Dominant negative MYC blocks transformation by ABL oncogenes. *Cell* (1992) **70**: 901-910.

Sawyers CL. Chronic myeloid leukemia. *N. Engl. J. Med.* (1999) **340**: 1330–1340.

Schindler T, Bornmann W, Pellicena P, Miller WT, Clarkson B, and Kuriyan J. Structural mechanism for STI571 inhibition of abelson tyrosine kinase. *Science* (2000) **289**: 1938–1942.

Schulz A, Mousallem T, Venkataramani M, Persaud-Sawin DA, Zucker A, Luberto C, Bielawska A, Bielawski J, Holthuis JC, Jazwinski SM, Kozhaya L, Dbaibo GS, Boustany RM. The CLN9 protein, a regulator of dihydroceramide synthase. *J. Biol. Chem.* (2006) **281**: 2784-2794.

Senchenkov A, Litval DA, Cabot MC. Targeting ceramide metabolism: a strategy for overcoming drug resistance. *J. Natl. Cancer Inst.* (2001) **93**:347–57.

Shiozaki E, Chai NJ, Rigotti DJ, Riedl SJ, Li P, Srinivasula SM, Alnemri ES, Fairman R, and Shi Y. Mechanism of XIAP-mediated inhibition of caspase 9. *Mol. Cell.* (2003) **11**: 519–527.

Sietsma H, Veldman RJ, Kolk D, Ausema B, Nijhof W, Kamps W, Vellenga E, and Kok JW. 1-Phenyl-2-decanoylamino3-morpholino-1-propanol chemosensitizes neuroblastoma cells for Taxol and vincristine. *Clin. Cancer Res.* (2000) **6**:942–948.

Sirard C, Laneuville P, and Dick JE. Expression of bcr-abl abrogates factor-dependent growth of human hematopoietic M07E cells by an autocrine mechanism. *Blood* (1994) **83**: 1575-1585.

Skorski T, Bellacosa A, Nieborowska-Skorska M, Majewski M, Martinez R, Choi JK, Trotta R, Wlodarski P, Perrotti D, Chan TO, Wasik MA, Tsichlis PN, and Calabretta B. Transformation of hematopoietic cells by BCR/ABL requires activation of a PI-3k/Akt-dependent pathway. *EMBO J.* (1997) **16**: 6151-6161.

Skorski T, Kanakaraj P, Nieborowska-Skorska M, Ratajczak MZ, Wen SC, Zon G, Gewirtz AM, Perussia B, and Calabretta B. Phosphatidylinositol-3 kinase activity is regulated by BCR/ABL and is required for the growth of Philadelphia chromosome-positive cells. *Blood* (1995) **86**: 726-736.

Skorski T, Wlodarski P, Daheron L, Salomoni P, Nieborowska-Skorska M, Majewski M, Wasik M, and Calabretta B. BCR/ABL-mediated leukemogenesis requires the activity of the small GTP-binding protein Rac. *Proc. Natl. Acad. Sci.* (1998) **95**: 11858-11862.

Spiegel S, and Milstien S. Sphingosine-1-phosphate: an enigmatic signalling lipid. *Nat. Rev. Mol. Cell. Biol.* (2003) **4**: 397-407.

Srinivasula SM, Ahmad M, Fernandes-Alnemri T, and Alnemri ES. Autoactivation of procaspase 9 by Apaf-1-mediated oligomerization. *Mol. Cell.* (1998) **1**: 949-957.

Stewart MJ, Litz Jackson S, Burgess GS, Williamson EA, Leibowitz DS, and Boswell HS. Role for E2F1 in p210 BCR-ABL downstream regulation of c-myc transcription initiation: studies in murine myeloid cells. *Leukemia* (1995) **9**: 1499-1507.

Sultan I, Senkal CE, Ponnusamy S, Bielawski J, Szulc Z, Bielawska A, Hannun YA, Ogretmen B. Regulation of the sphingosine-recycling pathway for ceramide generation by oxidative stress, and its role in controlling c-Myc/Max function. *Biochem. J.* (2006) **393**: 513-521

Van Brocklyn JR, Young N, and Roof R. Sphingosine-1-phosphate stimulates motility and invasiveness of human glioblastoma multiforme cells. *Cancer Lett.* (2003) **199**: 53–60.

Venable ME, Lee JY, Smyth MJ, Bielawska A, and Obeid LM. Role of ceramide in cellular senescence. *J. Biol. Chem.* (1995) **270**: 30701–30708.

Venkataraman K, and Futerman A. Do longevity assurance genes containing Hox domains regulate cell development via ceramide synthesis? *FEBS Lett.* (2002-2) **528**: 3–4.

Venkataraman K, Riebeling C, Bodennec J, Riezman H, Allegood JC, Sullards MC, Merrill AH, and Futerman AH. Upstream of growth and differentiation factor 1 (uog1), a mammalian homolog of the yeast longevity assurance gene 1 (LAG1), regulates N-stearoyl-sphinganine (C18-(dihydro)ceramide) synthesis in a fumonisin B1-independent manner in mammalian cells. *J. Biol. Chem.* (2002-1) **277**: 35642–35649.

Vigneri P, and Wang J.Y. Induction of apoptosis in chronic myelogenous leukemia cells through nuclear entrapment of BCR-ABL tyrosine kinase. *Nat. Med.* (2001) **7**: 228-234.

Von Bubnoff N, Schneller F, Peschel C, and Duyster J. Bcr-Abl gene mutations in relation to clinical resistance of Philadelphia chromosome- positive leukemia to STI571: a prospective study. *Lancet.* (2002) **359**: 487-491.

Wang X. The expanding role of mitochondria in apoptosis. *Genes Dev.* (2000) **15**: 2922–2933.

Watzinger F, Gaiger A, Karlic H, Becher R, Pillwein K, and Lion T. Absence of N-ras mutations in myeloid and lymphoid blast crisis of chronic myeloid leukemia. *Cancer Res.* (1994) **54**: 3934-3938.

Wiesberg E, and Griffin JD. Mechanism of resistance to the ABL tyrosine kinase inhibitor STI571 in BCR/ABL-transformed hematopoietic cell lines. *Blood* (2000) **95**:3498-3505.

Winter E, and Ponting CP. TRAM, LAG1 and CLN8: members of a novel family of lipid-sensing domains? *Trends Biochem Sci.* (2002) **27**: 381–38.

Wong S, and Witte ON. The Bcr-Abl story:bench to bedside abd back. *Annu Rev Immunol.* (2004) **22**: 247-306.

Wu W, Shu X, Hovsepian H, Mosteller RD, and Broek D. VEGF receptor expression and signaling in human bladder tumors. *Oncogene.* (2003) **22**: 3361–3370.

Xia P, Gamble JR, Wang L, Pitson SM, Moretti PA, Wattenberg BW, D'Andrea RJ, and Vadas MA. An oncogenic role of sphingosine kinase. *Curr Biol.* (2000) **10**: 1527–1530.

Zamzami N, Brenner C, Marzo I, Susin SA, Kroemer G. Subcellular and submitochondrial mode of action of Bcl-2-like oncoproteins. *Oncogene* (1998) **16**: 2265-2282.

Zhang J, Reedy MC, Hannun YA, and Obeid LM. Inhibition of caspases inhibits the release of apoptotic bodies: Bcl-2 inhibits the initiation of formation of apoptotic bodies in chemotherapeutic agent-induced apoptosis. *J. Cell Biol.* (1999) **145**: 99-108.

Zhu XF, Liu ZC, Xie BF, Feng GK, and Zeng YX. Ceramide induces cell cycle arrest and upregulates p27kip in nasopharyngeal carcinoma cells. *Cancer Lett.* (2003) **193**: 149–154.

APPENDIX A (BUFFERS AND SOLUTIONS)

AGAROSE GEL ELECTROPHORESIS

Tris-Acetate-Edta Buffer (TAE) (50X)

Tris Acetate	2 M
EDTA	50 mM

Sample Buffer

dH ₂ O	3 mL
Tris HCl (0.5 M)	1 mL
Glycerol	1.6 mL
SDS (10%)	0.4 mL
β-mercaptoethanol	0.4 mL
Bromophenol Blue (0.5 %, w/v- in water)	0.4 mL

WESTERN BLOTTING

Protein Lysis Buffer

50 mM TrisHcl pH 7.4
150 mM NaCl
1 mM EDTA
1 % TritonX100
1 μl of Protease inhibitor was added per 200 μl of lysis buffer.

2X Sample Buffer

2% SDS
20% glycerol
20 mM Tris-Cl, pH 8
2 mM EDTA
2-mercaptoethanol
0.02 % Bromophenol blue to serve as a tracking dye.

SDS-PAGE Running Buffer (1X)

50 mL 10X Tris/Glycine/SDS (250 mM Tris, 1920 mM Glycine, 1 % w/v SDS)
diluted to 1X by addition of 450 mL dH₂O.

Coomassie Blue Stain

Coomassie Blue R-250	2.5 g
Acetic Acid	92 mL
Methanol	454 mL
dH ₂ O	454 mL

Destaining Solution

Methanol	200 mL
Acetic Acid	75 mL
dH ₂ O	725 mL

Towbin Buffer

50 mL 10X Tris-Glycine
100 mL Methanol
359 mL dH₂O

Milk Solution

10 g milk powder
100 mL 1X PBS
100 µL Tween 20

0.1 % Towbin Buffer

0.5 mL Tween 20

499 mL 1X PBS

0.3% Towbin Buffer

1.5 mL Tween 20

498.5 mL 1XPBS

LIQUID CHROMATOGRAPHY/MASS SPECTROMETRY

JB Cell Extraction Mix

70 % Isopropanol/Ethanol Acetate (2:3)

Mobile Phase B Solvent

1 mM NH₄OCOH : 0.2 % HCOOH dissolved in Methanol

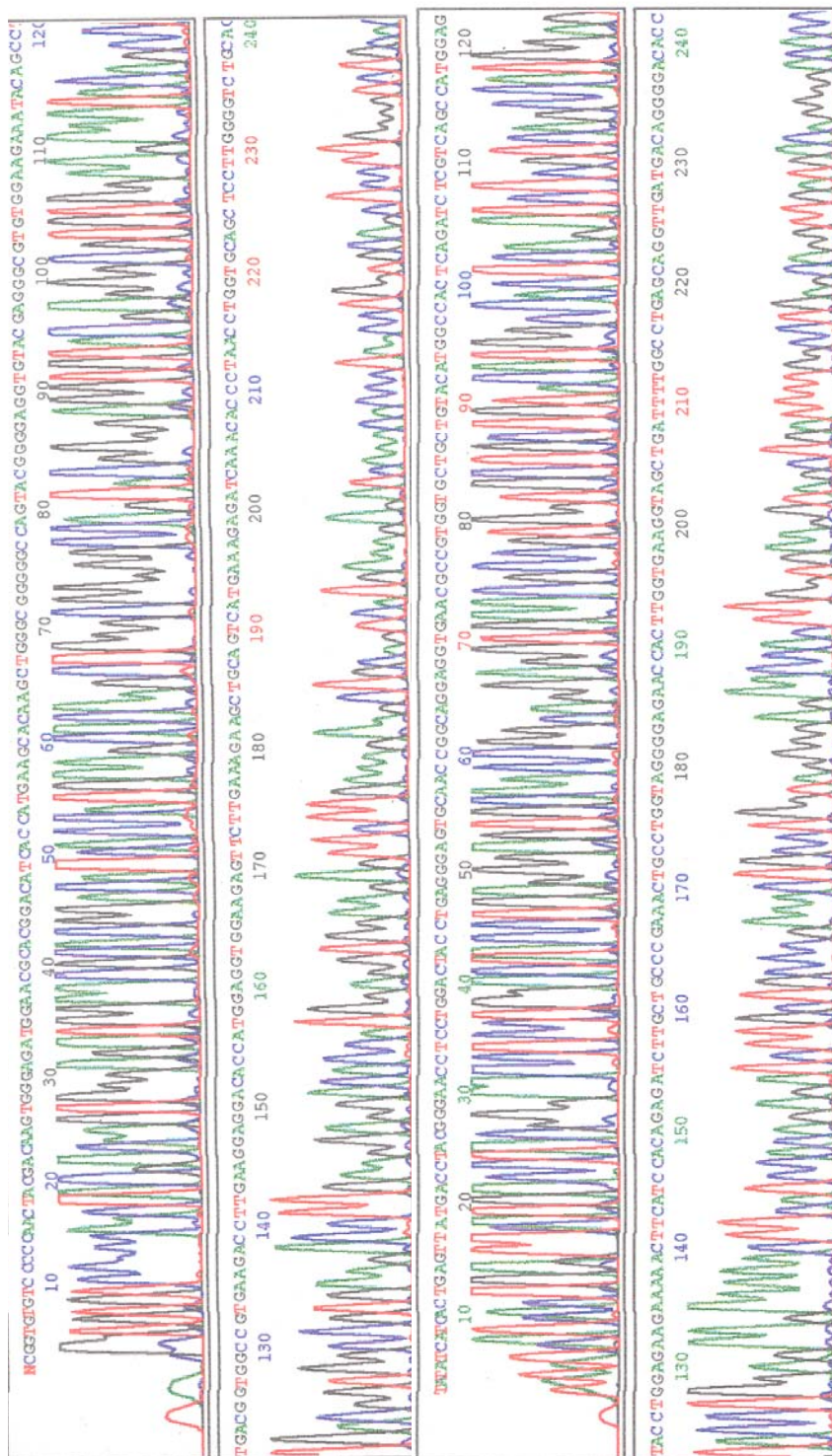
Ashing Buffer

9: 1:40 – 10 N H₂SO₄ : 70 % HClO₄ : H₂O

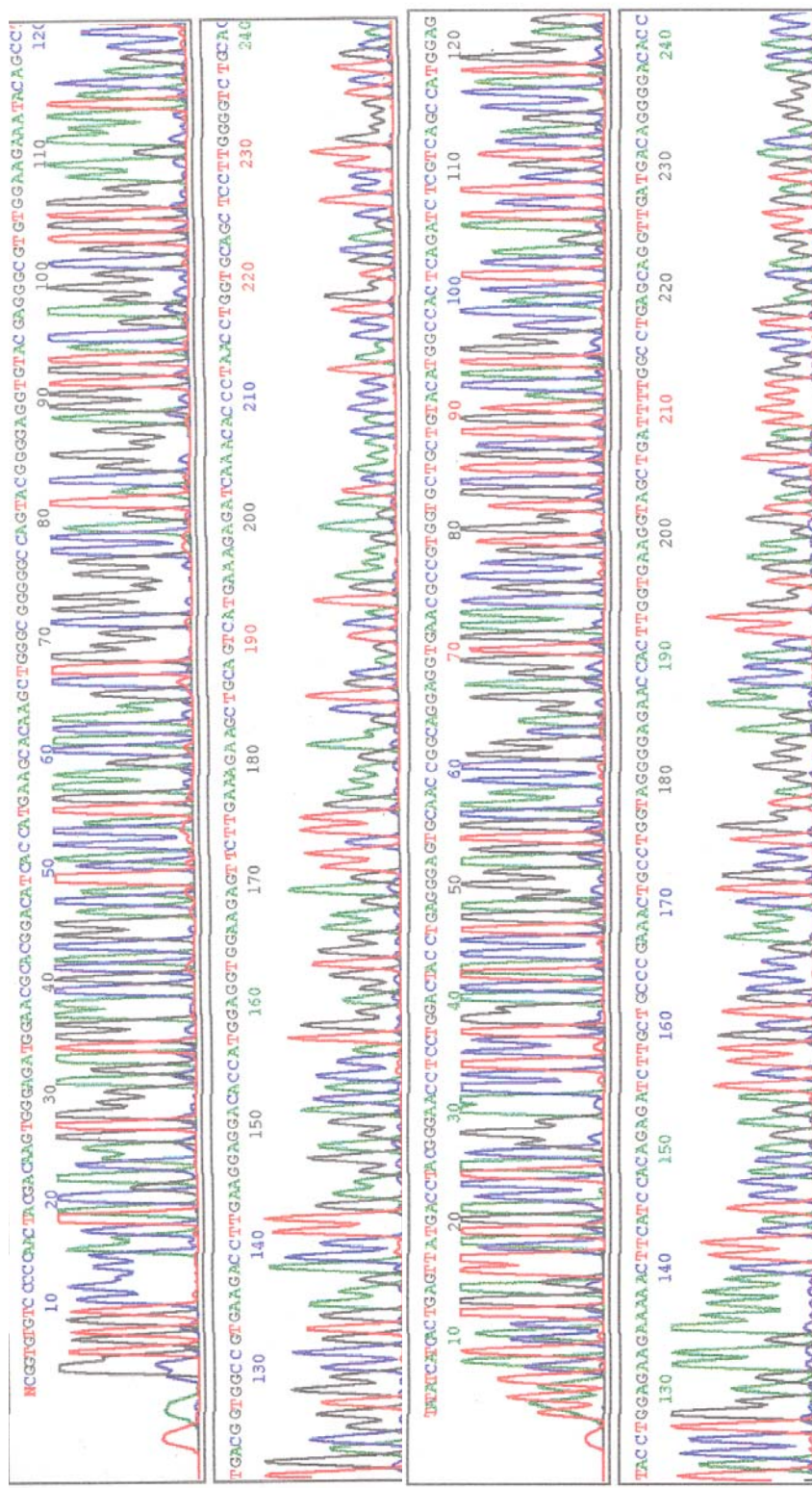
9 % Ascorbic Acid

1.8 g of Ascorbic Acid was dissolved in 20 mL of dH₂O

APPENDIX B (SEQUENCE ANALYSES)



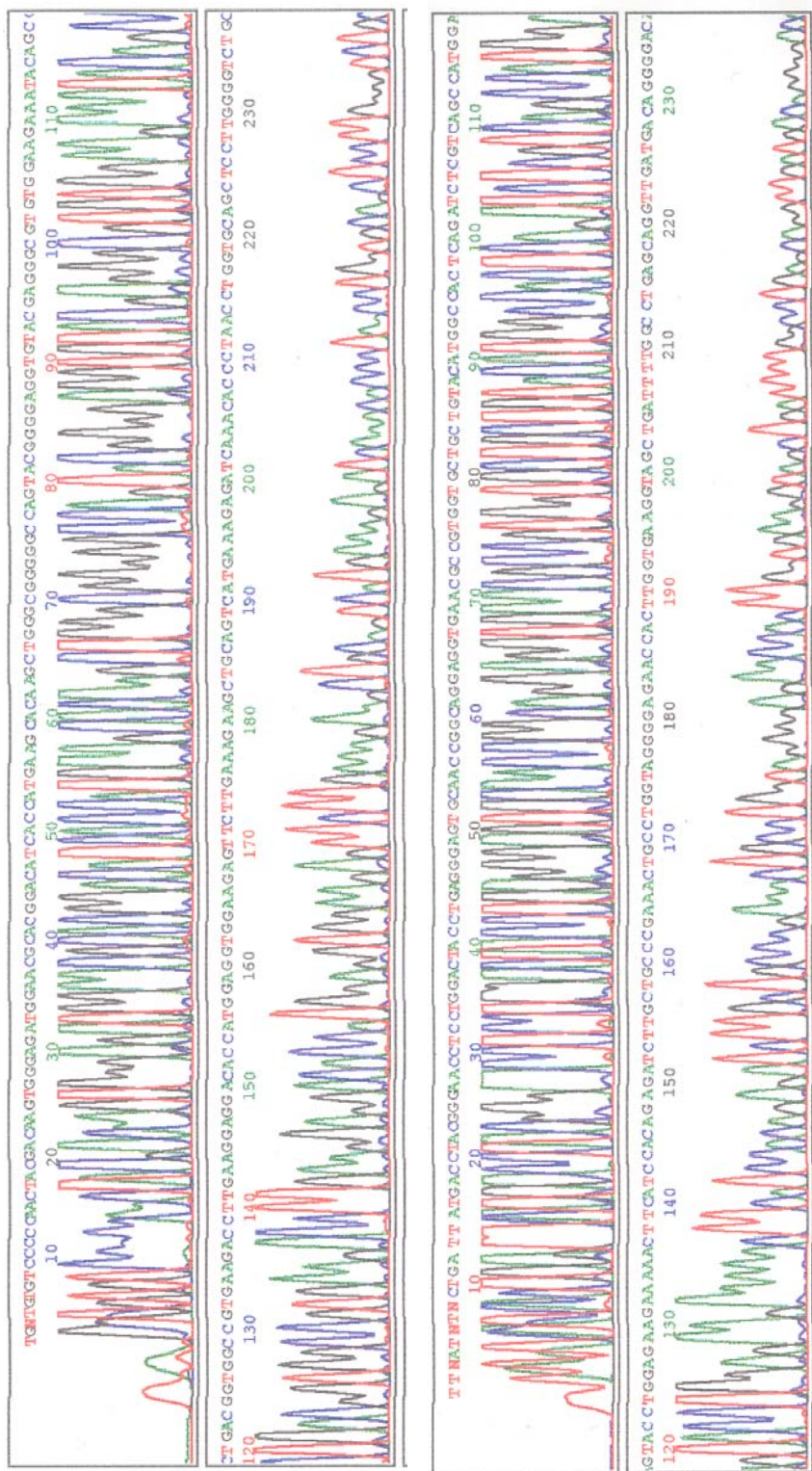
I. Nucleotide sequence analyses of ABL kinase region of parental K562 cells.



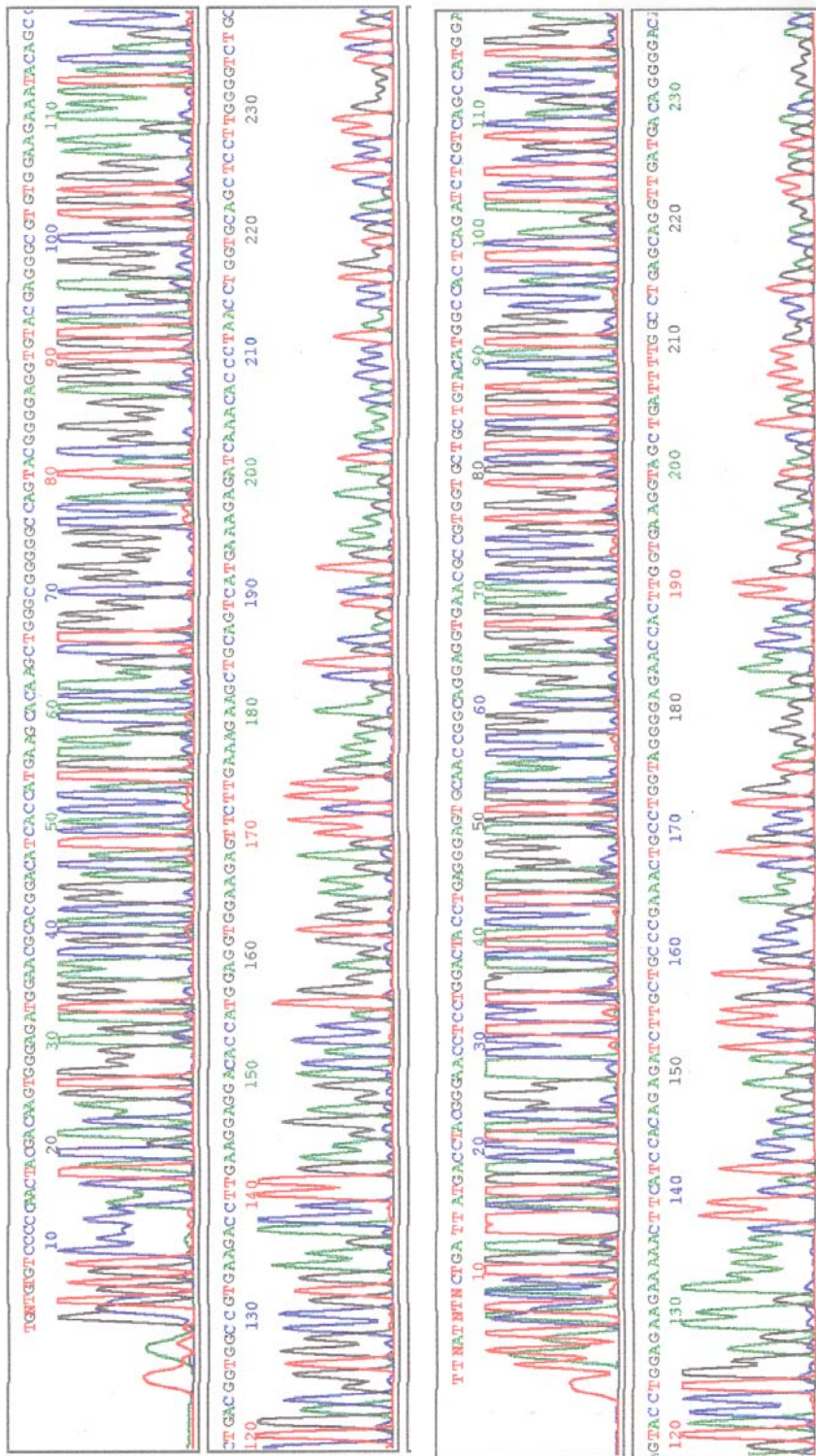
II- Nucleotide sequence analyses of ABL kinase region of parental K562/IMA-0.2 cells.



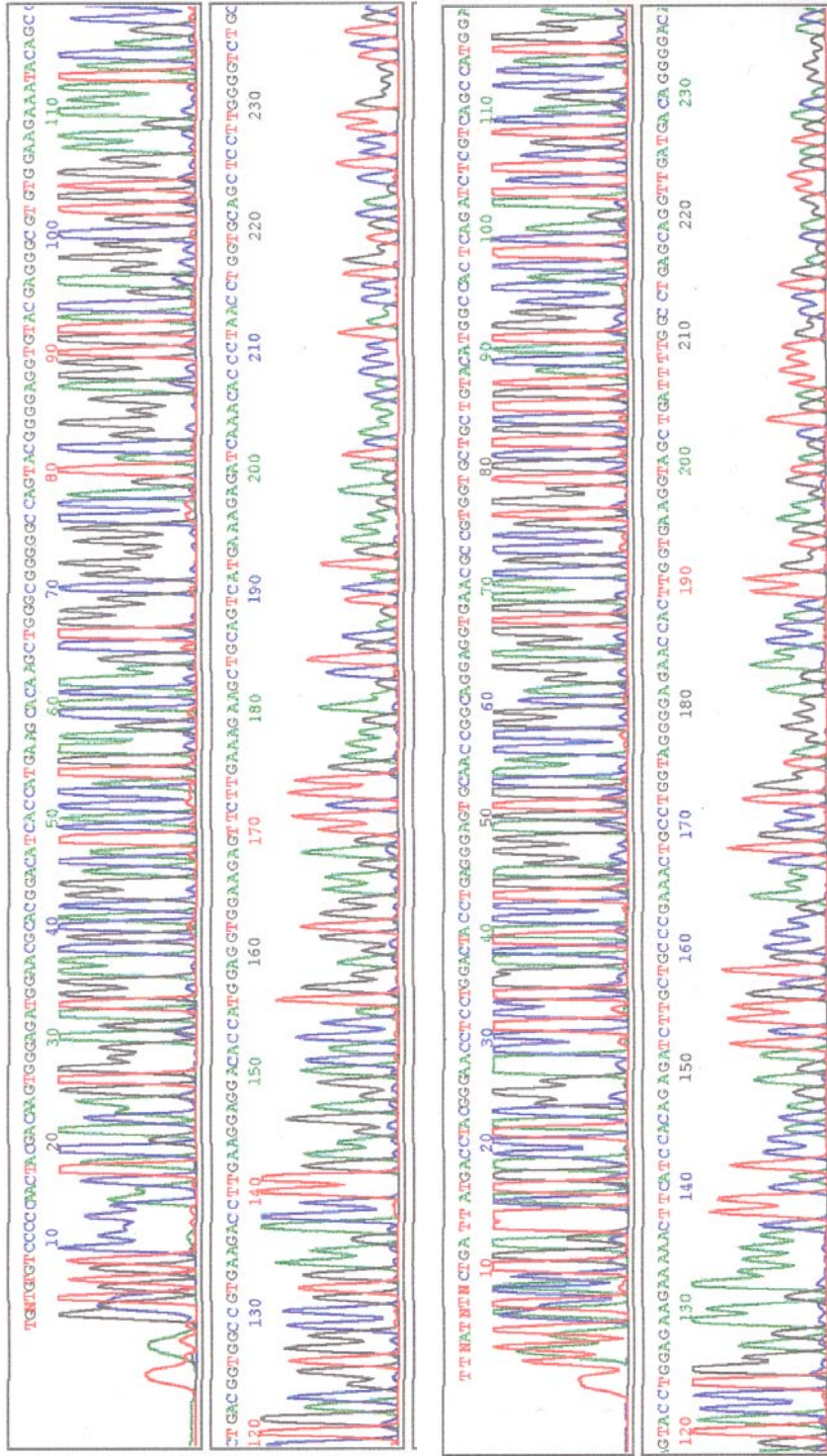
III- Nucleotide sequence analyses of ABL kinase region of parental K562/IMA-1 cells.



IV- Nucleotide sequence analyses of ABL kinase region of parental Meg-01 cells.

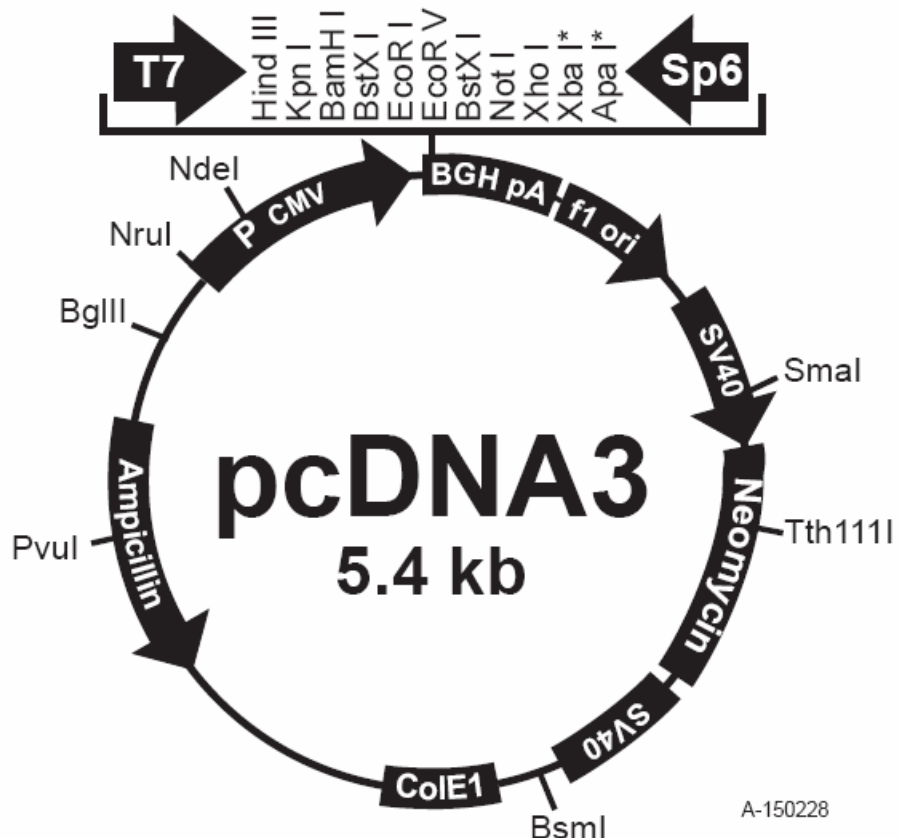


V- Nucleotide sequence analyses of ABL kinase region of parental Meg-01/IMA-0.2 cells.



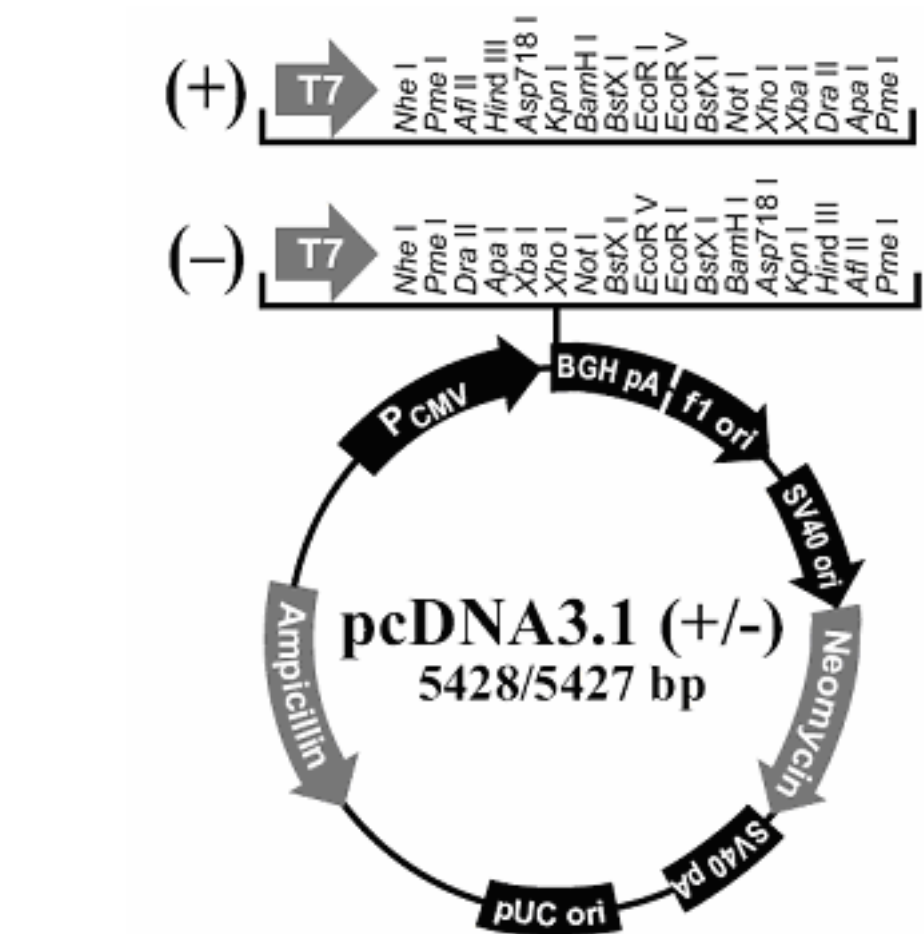
VI- Nucleotide sequence analyses of ABL kinase region of parental Meg-01/IMA-1 cells.

APPENDIX C (PLASMID VECTORS)



pcDNA3: 5446 nucleotides
 CMV promoter: bases 209-863
 T7 promoter: bases 864-882
 Polylinker: bases 889-994
 Sp6 promoter: bases 999-1016
 BGH poly A: bases 1018-1249
 SV40 promoter: bases 1790-2115
 SV40 origin of replication: bases 1984-2069
 Neomycin ORF: bases 2151-2945
 SV40 poly A: bases 3000-3372
 ColE1 origin: bases 3632-4305
 Ampicillin ORF: bases 4450-5310

I- pcDNA3 Plasmid Vector



pcDNA3: 5428 nucleotides

CMV promoter: bases 232-819

T7 promoter/priming site: bases 863-882

pcDNA3.1/BGH reverse priming site: bases 1022-1039

BGH polyadenylation sequence: bases 1028-1252

F1 origin: bases 1298-1726

SV40 early promoter and origin: bases 1731-2074

Neomycin resistance gene (ORF): bases 2136-2930

SV40 early polyadenylation signal: bases 3104-3234

pUC origin: Bases 3617-4287

Ampicillin resistance gene: bases 4432-5428 (complementary strand)

ORF: Bases 4432-5292 (complementary strand)

Ribosome binding site: Bases 5300-5304 (complementary strand)

Bla Promoter (P3): basaes 5327-5333 (complementary strand)

II- pcDNA3 Plasmid Vector

CURRICULUM VITAE

Yusuf BARAN

Department of Biological Sciences
Molecular Biology and Genetics
Molecular Biology & Cancer Research Laboratory
No: 227
METU, ANKARA, TURKEY

Telephone : + 90 533 412 07 24
Fax : + 90 312 210 79 76
E-mail : ybaran@metu.edu.tr
Web-site : www.metu.edu.tr/~ybaran

PROFILE

Skilled Researcher in Molecular Biology and Genetics.

RESEARCH INTERESTS

Molecular Biology of Cancer, Multidrug Resistance Mechanisms in Human Hematological Malignancies, Apoptosis, The Involvement of Ceramides in Apoptosis and Drug Resistance.

EDUCATION

Ph.D. 2002-2006	Middle East Technical University, Ankara, TURKEY Title: Investigation of Multiple Drug Resistance Mechanisms in Imatinib Resistant Human Chronic Myeloid Leukemia Cells <i>Supervisor, Prof. Dr. Ufuk GÜNDÜZ.</i>
M.S. 2000-2002	Middle East Technical University, Ankara, TURKEY Title: Expression of MDR1 gene in Vincristine selected HL60 Cell Line <i>Supervisor, Prof. Dr. Ufuk GÜNDÜZ</i>
B.S. 1994-1998	Dicle University, Diyarbakır, TURKEY

EXPERIENCE

- **Research and Teaching Assistant**, Department of Biological Sciences, Molecular Biology and Genetics, Middle East Technical University, Ankara-Turkey
- **Research and Teaching Assistant**, Department of Molecular Biology and Genetics, Izmir High Institute of Technology, İzmir, Turkey
- **Visiting Scholar**, Department of Biochemistry and Molecular Biology, Holling Cancer Center, Medical University of South Carolina, South Carolina, USA.

TEACHING EXPERIENCE

- Genetics Laboratory
- Microbiology Laboratory
- Animal Cell Culture Techniques
- Experimental Techniques in Molecular Biology
- Molecular And Cellular Biology Laboratory
- General Biology Laboratory

AWARDS

- European Hematology Association. "Travel Grant, 2006"
- The Scientific and Research Council of Turkey. "International Publication Award, 2006"
- North Atlantic Treaty Organisation (NATO). NATO-A2 scholarship (Medical University of South Caroline, SC-USA, 2005-2006)
- Middle East Technical University "Participation to international scientific meetings award, 2006 "
- The Scientific and Research Council of Turkey. "Participation to international scientific meetings award, 2006"
- Middle East Technical University "Publication award, 2005"
- Prime Ministry of Turkey. Full scholarship during B.S. including full tuition, 1994-1998.

PUBLICATIONS

Yusuf Baran, Ufuk Gündüz, Ali Uğur Ural. "Cross-Resistance To Cytosine Arabinoside in Human Acute Myeloid Leukemia Cells Selected for Resistance to Vincristine" Experimental Oncology **2006** 28(2):163-165.

Yusuf Baran, Ufuk Gündüz, Besim Öğretmen. "The Sequence Analyses of Imatinib Mesylate Binding Site of Abl Kinase Domain in Sensitive and Imatinib-Resistant Human CML Cells" 7th Congress of Balkan Meeting on Human Genetics, 31 August-2 September, **2006** (9) Supplement (Balkan Journal of Medical Genetics). Page;128.

Yusuf Baran, Ufuk Gündüz, Jacek Bielawski, Besim Öğretmen. "Circumventing Multi-Drug Resistance by a Combination Therapy of Imatinib and GCS Inhibitor in Imatinib-Resistant Human Chronic Myeloid Leukemia Cells" 7th

Congress of Balkan Meeting on Human Genetics, 31 August-2 September, **2006** (9) Supplement (Balkan Journal of Medical Genetics). Page;127.

Yusuf Baran, Ufuk Gündüz, Ali Uğur Ural, Besim Öğretmen. “Apoptotic Pathways Induced By Imatinib in Sensitive And Imatinib-Resistant K562 Cells” 7th Congress of Balkan Meeting on Human Genetics, 31 August-2 September, **2006** (9) Supplement (Balkan Journal of Medical Genetics). Page;127.

Yusuf Baran, Ufuk Gündüz, Can E. Senkal, Jacek Bielawski, Besim Öğretmen. “The Involvement of Ceramides in Imatinib Induced Apoptosis and Drug Resistance” 7th Congress of Balkan Meeting on Human Genetics, 31 August-2 September, **2006** (9) Supplement (Balkan Journal of Medical Genetics). Page;44.

Yusuf Baran, Ali Uğur Ural, Besim Öğretmen, Ufuk Gündüz. “Multidrug Resistance Mechanisms In Human Chronic Myeloid Leukemia Cells” 11th Congress of European Hematology Association, 15-18 June, **2006**. Page;16. Amsterdam-Netherland.

Yusuf Baran, Can Emre Şenkal, Jacek Bielawski, Besim Öğretmen, Ufuk Gündüz. “The Involvement Of C:18 Ceramide And Human Longevity Assurance Genes In Imatinib Induced Apoptosis”. 11th Congress of European Hematology Association, 15-18 June, **2006**. Page;124. Amsterdam-Netherland.

Yusuf Baran, Can Emre Şenkal, Jacek Bielawski, Besim Öğretmen, Ufuk Gündüz. “Ceramide Glycosylation By Glucosyl Ceramide Synthase Inhibits The Apoptotic Effect Of Imatinib On Human K562 And Meg-01 Cells” 11th Congress of European Hematology Association, 15-18 June, **2006**. Page;125. Amsterdam-Netherland.

Yusuf Baran, Can Emre Şenkal, Jacek Bielawski, Besim Öğretmen, Ufuk Gündüz. “Overcoming Chemoresistance In Human Chronic Myeloid Leukemia K562 Cells By siRNA Inhibition Of Sphingosine Kinase-1” 11th Congress of European Hematology Association, 15-18 June, **2006**. Page;15. Amsterdam-Netherland.

Ferit Avcu, Ali Uğur Ural, **Yusuf Baran**, Güngör Sobacı, Mustafa Deveci, Ahmet Türker Çetin, Aysel Pekel, Meral Sarper, Pınar Elçi, Ufuk Gündüz. “A

Photodynamic Pathway To Apoptosis Induced By Hypericin In Human Myeloma Arh77 Cell Line: Possible Relevance To Photodynamic Therapy” Turkish Journal of Haematology. **2005**; 22(3).

Yusuf Baran, Ufuk Gündüz, Ali Uğur Ural. “Expression of MDR1 gene in HL60 Cells Selected with Vincristine” Turkish Journal of Cancer. **2005**; 35(2); 88-92.

Göğßen Önalan, Belgin Selam, **Yusuf Baran**, Mehmet Cincik, Reside Onalan, Ufuk Gündüz, Ali Uğur Ural, Recai Pabuçcu “ Serum and follicular fluid levels of soluble Fas, soluble Fas ligand and apoptosis in PCOS patients undergoing IVF cycles”. Human Reproduction. **2005**; 20(9); 2391-2395.

Meltem Kars, Özlem İşeri, Can Atalay, **Yusuf Baran**, Pelin Mutlu, Ufuk Gündüz. “Investigation of Molecular Mechanisms of Multiple Drug Resistance in Different Cell Lines and Tissue Types” The European Cost Action B16 Symposium on Multidrug Resistance Reversal (By inhibition of Trans-Membrane Transport), 13-14 May, **2005**. Page;35. Antalya, Turkey.

Yusuf Baran, Ufuk Gündüz, Ali Uğur Ural. “Investigations of cross-resistance to cytarabine in human promyelocytic leukemia cell line selected for resistance to vincristine”. 6th Balkan Meeting on Human Genetics, 28-31 August, **2004**. Page;66. Thessaloniki, Greece.

Yusuf Baran, Ufuk Gündüz, Ali Uğur Ural. “Vinkristine dirençli HL60 hücrelerinin Ara-C’ye karşı çapraz direnci”. II. Klinik Biyokimya ve Kanser Sempozyumu, 16-18 April, **2004**. Page;156. Bursa, Turkey.

Yusuf Baran, Ufuk Gündüz, Ali Uğur Ural. “Vinkristine dirençli HL60 hücreleri sitozin arabinoside çapraz direnç gösterirler” Turkish Journal of Haematology, 10-13 October, **2003**. Page;95. Istanbul, Turkey.

Ali Uğur Ural, Bala Gür, **Yusuf Baran**, Ferit Avcu. İ. Yılmaz, A. Yalçın. “Doksorubisine karşı direnç kazandırılmış HL60 lösemi hattında sitozin-arabinoside karşı gelişen çapraz direnç”. Turkish Journal of Haematology, 25-28 October, **2002**, Page;49. Antalya, Turkey.

Yusuf Baran, Ufuk Gündüz. “Vinkristin ile seçilmiş HL60 hücrelerinde MDR1 geninin ifadesi” 17. Ulusal Biyokimya Kongresi, 24-27 June, **2000**. Page;80. Ankara, Turkey.

Yusuf Baran “Apoptosis, multidrug resistance and sphingolipid metabolism in chronic myeloid leukemia” 32. Congress of Turkish Hematology Association, 8-12 November, **2006**, Antalya, Turkey. (Invited speaker)

IN PROGRESS

Yusuf Baran, Can E. Senkal, Jacek Bielawski, Ufuk Gunduz, Yusuf A. Hannun, Lina M. Obeid, and Besim Ogretmen. “Alterations of Human Longevity Assurance Gene 1 (LASS1)/Sphingosine Kinase-1-Dependent Ceramide Generation and Metabolism Involve in the Regulation of Imatinib-Induced Apoptosis and Resistance in K562 Human Chronic Myeloid Leukemia (CML) Cells”. **2006** Journal of Biological Chemistry, revised to be published.

Yusuf Baran, Ali Uğur Ural, Besim Öğretmen, Ufuk Gündüz. “İmatinib Uygulanan Duyarlı Ve Dirençli K562 Hücrelerinde İlaç Dirençlilik Mekanizmaları” **2006** (Submitted to 32nd National Hematology Congress)

Yusuf Baran, Ufuk Gündüz, Besim Öğretmen. “Kronik Myeloid Lösemi Hücrelerinde İmatinibin Bağlandığı Abl Kinaz Bölgesinin Nükleotid Dizilerinin Belirlenmesi Ve İlaç Dirençliliği” **2006** (Submitted to 32nd National Hematology Congress)

Yusuf Baran, Ufuk Gündüz, Besim Öğretmen. “Glukozil Seramid Sentaz Geninin Pdmp İle Bloke Edilmesi İle Dirençli Kronik Myeloid Lösemi Hücrelerinin İmatinibe Duyarlılığın Arttırılması” **2006** (Submitted to 32nd National Hematology Congress)

Yusuf Baran, Ufuk Gündüz, Besim Öğretmen. “hLASS1 Geninin İmatinib Dirençliliğindeki Rolü” (Submitted to 32nd National Hematology Congress)

Yusuf Baran, Ufuk Gündüz, Besim Öğretmen. “Sfingozin Kinaz 1 Gen İfadesinin İmatinibin Apoptotik Etkisi Üzerine Etkisi”. **2006** (Submitted to 32nd National Hematology Congress)

Yusuf Baran, Jacek Bielawski, Besim Ogretmen and Ufuk Gunduz. “Inhibition of Glucosylceramide Synthas by PDMP Resensitizes Multidrug-Resistant Human Chronic Myeloid Leukemia Cells to Imatinib.” Ready to be submitted.

PROJECTS

1. Title : Investigations and reversal of multidrug resistance mechanisms by molecular approaches in different cell lines. **(2006-)**

Supported by : Prime Ministry, The Scientific and Research Council of Turkey.

2. Title : Investigations of Multiple Drug Resistance Mechanisms in Imatinib Mesylate Applied Chronic Myeloid Cell Lines. **(2004- 2006)**

Supported by : METU Research Fund

3. Title : Expression of MDR1 Gene in HL60 Cell Line Selected for Resistance to Vincristine. **(2000-2002)**

Supported by : METU Research Fund

4. Title : Investigations of Resistance Mechanisms Against Anticancer Drugs in breast Cancer and Drug Targeting. **(2000-2004)**

Supported by: Prime Ministry, State Planning Organization

LANGUAGES

Turkish (Native), English (Advanced)

REFERENCES

Prof. Dr. Ufuk GÜNDÜZ

Middle East Technical University, Department of Biological Sciences/Molecular Biology and Genetics

Phone: + 90 312 2105183

E-Mail: ufukg@metu.edu.tr

Prof. Dr. Ali Uğur URAL

Gulhane Military Medical Academy, Department of Hematology

Phone: + 90 312 3044105

E-mail: aural@gata.edu.tr

Assoc. Prof. Dr. Besim OGRETMEN

Medical University of South Carolina, Holling Cancer Center, Department of Biochemistry and Molecular Biology

Phone: + 1 8437920941

Email: ogretmen@musc.edu

Prof. Dr. Semra KOCABIYIK

Middle East Technical University, Department of Biological Sciences/Molecular Biology and Genetics (Head of the Department)

Phone: + 90 312 2103104

E-Mail: biosemra@metu.edu.tr